1993

An experimental study of the thermal performance of R-134a and refrigerant blends in an air conditioning system

Stephen W. Crown
Iowa State University

Order Number 9334971

An experimental study of the thermal performance of R-134a and refrigerant blends in an air conditioning system

Crown, Stephen W., Ph.D.

Iowa State University, 1993

U·M·I
300 N. Zeeb Rd.
Ann Arbor, MI 48106

An experimental study of the thermal performance of R-134a and refrigerant blends in an air conditioning system

by

Stephen W. Crown

A Dissertation Submitted to the
Graduate Faculty in Partial Fulfillment of the
Requirements for the Degree of
DOCTOR OF PHILOSOPHY

Approved:

Signature was redacted for privacy.

In Charge of Major Work

Signature was redacted for privacy.

For the Major Department

Signature was redacted for privacy.

For the Graduate College

Iowa State University
Ames, Iowa
1993

TABLE OF CONTENTS

LIST OF FIGURES

LIST OF TABLES

ACKNOWLEDGEMENTS

This project was made possible by the funding provided by E.I. DuPont de Numours and Company, the Iowa State University graduate college, and the department of mechanical engineering. Thanks are due to Don Bivens of DuPont, who was patient and supportive throughout the project.

I am grateful for having worked under two very capable and helpful major professors, Dr. Michael B. Pate and Dr. Howard N. Shapiro. My successes and achievements at Iowa State have been directly related to their encouragement and friendship. I hope that as a professor I can give the same support and encouragement to my students.

In everything I give thanks to God who I trust with my life, career, and family. I thank Him for a supportive and loving wife who has put up with long hours and made our home a safe refuge. I am also thankful to Him for our daughter Kayla whose picture by my desk always makes me smile. May God be honored as I make use of the abilities and knowledge that I have gained in my studies.

CHAPTER 1. INTRODUCTION

Environmental Problems

The use of chlorofluorocarbons (CFCs) has become widespread in the second half of this century because they were considered safe, stable and non-toxic chemicals with many applications, including:

- propellants for aerosol sprays
- blowing agents for plastic and foam insulations
- refrigerants for automobile, residential, and commercial applications

However, as early as the mid seventies environmental problems associated with the use CFCs were identified. By the late seventies, the use of CFCs as aerosol propellants in was banned in the United States because of this concern. One advantage of CFCs, namely its chemical stability, is also part of the cause for it being considered an environmental hazard. Many of the stable CFC molecules eventually diffuse into the stratosphere, approximately 6 to 15 miles above the earth's surface. In the stratosphere, the CFCs contribute to two major environmental problems: global warming and ozone depletion. The total impact of these problems is largely unknown, however, many predictions are very unfavorable. Problems such as increased incidence

of skin cancer, death of certain species, and rising coastal waters have all been predicted. Many agree that such problems will occur, however the extent to which they will occur is greatly disputed.

The potential problems associated with the use of CFCs has led to many efforts to eliminate their use, which in turn has required the development of new chemicals that can effectively replace them. In the area of refrigeration, several refrigerants have been developed which are considered safer environmentally. In addition to the development of non-environmentally destructive chemicals, new technologies have been introduced which do not require the use of CFCs. The potential global impact of CFCs on the environment has led to changes in legislation and lifestyle, an international effort and agreement to eliminate production of CFCs, and support of research by government and industry in the area of CFC replacement.

Ozone Depletion

One of the most environmentally harmful effects associated with the release of CFCs into the atmosphere is ozone depletion. Ozone, a molecule made up of three oxygen atoms O_3, exists naturally in the stratosphere and serves as a protective shield against harmful ultraviolet radiation. Ultraviolet radiation from the sun is absorbed by O_3 molecules which break into O_2 and O. The components then reform to give a fairly constant level of ozone. A drop in the amount of ozone in the stratosphere would cause an increase in the amount of ultraviolet radiation which reaches the earth. Such an increase could possibly cause greater incidents of skin cancer, kill many forms of plant life, and upset many of the complex life cycles on earth.

CFCs, in the stratosphere, disrupt the balance of the ozone layer by serving

as a catalyst in the conversion of O_3 to O_2. When ultraviolet rays strike the CFC molecules, chlorine atoms are broken off. These chlorine atoms then react with O_3 to produce ClO and O_2. The ClO then reacts with free oxygen atoms to produce Cl and O_2. This frees the chlorine atoms to react with more ozone in a process that can occur many thousands of times. Each molecule of R-12, one of the common CFCs used in refrigeration, that is released today will continue to affect the ozone for 70 to 300 years [1].

Predicting the destruction of ozone in the atmosphere is difficult for many reasons. Complicated models are required which give varying results depending on the assumptions made. The presence of carbon dioxide and methane in the atmosphere somewhat offsets the effect of the CFCs in that their increased concentrations lead to higher levels of ozone. The effect of ozone depleting gases are not additive in that the actual effect of a number of ozone depleting gases is less than the sum of effects of individual gases on ozone depletion. The destruction of ozone also varies seasonally and geographically. Very cold temperatures and the return of sunlight to the antarctic region in October provide ideal conditions for the ozone destroying reactions to occur. A reduction in the concentration of ozone by as much as 50% from previously measured values has occurred over the past several years in the months of October and November over Antartica [1].

In an effort to reduce the destruction of the ozone layer, representatives of 40 nations met in Montreal Canada in 1987 and made an agreement to reduce the production of CFCs 50% by the year 1998 [2]. The agreement was later revised to include the complete phase out of the production of CFCs by the year 2000.

A scale giving the relative affect of gases in depleting the ozone compared to R-

Table 1.1: Ozone depletion potential for various refrigerants

Refrigerant	ODP
R-12	1.0
R-134a	0.0
R-22	0.05
R-124	0.02
R-152a	0.0

12 is called the ozone depletion potential (ODP). The ODP is defined as the number of pounds of R-12 that would have the same effect as one pound of the particular gas. The ODPs for the different refrigerants used in the study presented here are given in Table 1.1 [3].

Global Warming

The topic of global warming has received much attention because of the possible widespread effects it would have on the world. A change in global temperature of just a few degrees could cause severe problems in coastal regions due to rising seas, in agriculture due to changing climate, and countless other problems. The greatest effect of human activity on global temperature is purported to be the production of CO_2. Carbon dioxide is produced in the burning of fossil fuels. Other gases which lead to global warming are methane, CFCs, and nitrous oxides.

The effects of these gases on climate can be described as follows. The earth receives energy from the sun by short wavelength radiation, the peak being in the visible region [4]. Energy is reradiated back into space as long wavelength infrared radiation. The greenhouse gases let the short wavelength radiation pass through to

the earth but absorb much of the long wavelength radiation that is reradiated from the earth. This intercepting of radiant energy causes a higher equilibrium temperature in the atmosphere and at the surface of the earth. The effect is similar to the action of windows in a greenhouse which allow solar radiation to enter the space but filter long wavelength thermal radiation thus preventing it from leaving. Hence, the effect is often called the greenhouse effect.

The effectiveness of each of the greenhouse gases in absorbing the long wavelength radiation is very different; up to several orders of magnitude greater for the CFCs than for CO_2. The amount of CO_2 in the atmosphere attributed to human activity, however, is much greater than any of the other greenhouse gases. It has been calculated that CO_2 in the atmosphere produced by human activity is the cause of 55% of global warming [5]. CFCs, although hundreds of thousands times more scarce than CO_2, are the cause of 25% of global warming.

The problem of global warming has led to the development of a scale that rates the effect of gases on global warming relative to CO_2. The scale, called the Global Warming Potential (GWP), is defined as the number of pounds of CO_2 that would have the same effect on global warming as one pound of the particular gas. Table 1.2 shows the GWP of the various refrigerants used in the present study [5].

The use of refrigerants to provide cooling has two important effects on global warming. One is the direct effect on global warming due to the release of refrigerants. The other is the introduction of greenhouse gases, primarily CO_2, associated with the production of electricity required to power system compressors. This second effect, which is indirect, contributes to a major portion of the global warming problem associated with the use of refrigerants. Therefore, systems which run on alternative

Table 1.2: Global warming potential of various refrigerants for different periods

Trace gas	GWP 20 yr	100 yr	500 yr
Carbon dioxide	1	1	1
R-12	7100	7300	4500
R-134a	3200	1200	420
R-22	4100	1500	510
R-124	1500	430	150
R-152a	510	140	47

refrigerants must have equal or greater efficiency than with R-12 in order not to increase the global warming problem.

An Experimental Study of Alternative Refrigerants

Many refrigeration and air-conditioning systems currently in operation use CFCs. These systems periodically need to be recharged with new refrigerant due to system leaks or required service. The development of new refrigerants that can effectively work in existing systems, as well as ones that can work with slightly modified systems, is essential to provide a smooth transition in the elimination of CFCs.

An experimental study of three alternative refrigerants developed to replace one CFC, R-12, was conducted to answer questions about the appropriateness of these refrigerants as alternatives. The alternative refrigerants tested were R-134a an HFC (hydrofluorocarbon), and two blends, both HCFCs (hydrochlorofluorocarbons) containing different proportions of R-22, R-124 and R-152a. HFCs, such as R-134a, do not contain any chlorine and therefore have an ODP of zero. The ternary blends, although they contain chlorine, are considered to give an intermediate solution to the phase out of R-12. Both the GWP and the ODP of the blends are lower than for

R-12.

The test system was a fully instrumented 3-ton vapor compression refrigeration system. Tests were run at several different operating conditions and refrigerant charges in order to address a number of questions.

- How does the system performance for an alternative refrigerant compare with that of R-12 when the system is operated over a range of operating conditions?
- What is the effect of refrigerant charge on system performance with the different refrigerants?
- How do the thermodynamic states of the refrigerants in the individual components (i.e. compressor, evaporator and condenser) relate to total system performance?
- How well do models predict the observed behavior of system components and the overall system performance?

The following chapters include a complete description of the experimental setup and process followed in the collection of data. A comparison of the performance characteristics, coefficient of performance (COP) and cooling capacity, are explored in depth since a drop in capacity may give unacceptable system operation and a drop in COP may create a greater environmental global warming problem. Simple models for the compressor and heat exchanger are explored and compared to the experimental data. Comparisons of pressure-enthalpy plots, heat exchanger temperature profiles, and other system parameters (pressures, temperatures, and flow rates) for the different refrigerants are also presented throughout where they provide insight as

to the differences observed in performance. These comparisons are also useful for the purposes of modeling and design in that they show the effects of operating conditions on important refrigerant properties at key points in the system.

Review of Related Literature

The importance of the CFC issue as it relates to the study of alternative refrigerants for R-12 has precipitated much research on this issue. The variety of research with alternative refrigerants ranges from purely theoretical system models to experimental studies that simply measure power input and cooling capacity. The results of the different experimental studies depend on the equipment used, the operating conditions, and system modifications made for different refrigerants. The theoretical models give differing results depending on the simplifying assumptions built into them.

An experimental study conducted at Oak Ridge National Laboratory was presented by Vinyard [6]. A discussion of the preliminary test results of the preceding study are also given by Vinyard [7]. The study compared the performance of R-12, R-134a and a number of other alternative refrigerants in an 18^3ft refrigerator-freezer. The evaporator and condenser were held at constant temperature for all tests. The author noted that a better approach would be to allow these conditions to vary to simulate actual operating conditions. The results showed an increase in energy consumption for all of the alternatives tested.

Another series of experimental tests were conducted at Oak Ridge National Laboratories on a breadboard vapor compression refrigeration test system. The experiment and results were presented by Sand et al. [8]. Nine different alternative refrig-

erants were tested and the performance compared with that of R-12. Four different test conditions were selected according to standard heat pump test conditions. The results showed a higher efficiency with R-134a over R-12 for all but the lowest temperature conditions. No refrigerant blends were tested in the apparatus.

An experimental study of alternative refrigerants in a heat pump test system was conducted by the National Research Council in Canada [9]. The test system was run with R-12, R-134a, and R-152a over a range of evaporator temperatures and degrees of condenser exit subcooling. The condenser temperature and degrees of evaporator exit superheat were held constant for all tests. The subcooling was adjusted by varying the amount of refrigerant charge in the system. The results show increased performance with R-134a over R-12 where significant subcooling existed at the condenser exit. The R-134a performed best at higher evaporator temperatures. The comparisons were all based on equal saturation temperatures in the evaporator. The difference in heat transfer coefficients between refrigerants was not considered.

A study by Domanski [10] considered the merits of different modeling methods in the selection of alternative refrigerants. A simplified model was developed on the merits that it could be used to distinguish refrigerants which would cause large differences in system performance. The good candidates could then be tested experimentally and with more sophisticated models. The model developed is called CYCLE11. The system model used a polytropic compressor model and an average effective temperature difference in the heat exchangers. An assumption of constant overall heat transfer coefficient was also made in modeling the heat exchangers. The model was used to simulate a refrigeration cycle and showed slightly improved efficiency with R-134a and equal performance with two R-22 blends.

The reversed Rankine cycle was used by Devotta [11] to evaluate the performance of several alternative refrigerants for R-12. The purely theoretical analysis was based on the use of equal evaporator and condenser saturation temperatures. The study concluded that R-134a is a logical alternative to R-12 in that its performance is very similar. An analysis of refrigerant blends was not considered. Petersson [12] also used an ideal Rankine cycle to model the performance of R-12 and R-134a. An experimental study of compressor performance was conducted with a swash plate compressor. The saturation temperatures were assumed to be equal for the two refrigerants. The model and experiments showed increased capacity and slightly decreased COP with R-134a.

Modifications in refrigeration equipment and the study of new refrigerant blends are two areas of developing research in the area of alternative refrigerants. Consideration of using different compressor technology to accommodate the different operating pressures and temperatures associated with alternative refrigerants is discussed by Muir [13]. A discussion of possible alternative refrigerants, not typically considered is given by Kopko [14]. The use of new refrigerant blends was examined by Didion [15] where the use of near-azeotropes in existing system was suggested to have the greatest potential. The use of several different non-azeotropic refrigerants were studied by Bare [16] with a computer model of a dual circuit refrigerator-freezer unit. The results showed a 9% increase in the performance with an R-22 blend over the modeled performance with R-12. An experimental study testing the performance of a heat pump was conducted by Galloway [17]. A number of different R-22 blends with varying additional compounds and composition were studied and compared to the performance with R-22.

The selection of alternative refrigerants is a complicated process. Considerations that must be made in the selection process are presented by Boot [18] and include:

- Safety (toxicity and flammability)
- Environment (global warming and ozone depletion)
- Material compatibility and solubility in lubricant (considered in depth in a study by Spauschus [19])
- Compressor modifications
- Performance (COP and capacity)
- Compressor reliability

Several alternative refrigerants, including R-134a and R-22 blends, were tested in a hermetic reciprocating compressor and compared to R-12. The test conditions were based on equal evaporator and condenser temperatures. The test results showed a decrease in performance for all but one of the blends tested.

The present study focuses on the area of system performance. An accurate appraisal of system performance is crucial as it influences operating costs, the environment, and the ability of the system perform the task it was designed for. A variety of conflicting conclusions have been drawn concerning system performance with alternative refrigerants. The present study provides a data base of system performance under controlled experimental conditions. The choice of instrumentation also allows for the comparison of component behavior (compressor and heat exchangers) with theoretical models. An analysis of the data and comparison with models is used to

show the validity of different experimental methods and modeling procedures used by the various researchers.

CHAPTER 2. EXPERIMENTAL SETUP AND TEST PROCEDURES

Introduction

Evaluating the performance of alternative refrigerants with R-12 required an elaborate setup of standard air-conditioning components, instrumentation, a computer controlled data acquisition system, and system controllers. The air-conditioning equipment was incorporated into an existing air flow loop used for control of the air-side conditions of the evaporator. A description of all of the test components and how they were incorporated and used in the study is given below. Following a description of the equipment is an account of the data taking process and the experimental procedure used in the collection of data.

Test Equipment

Air flow loop

The basic test equipment consisted of the refrigeration system being studied, a water flow loop for the condenser, and an air flow loop which supplied air-side conditions to the evaporator. The air flow loop consisted of several controllable heat exchangers, an electric heater, a squirrel cage fan and a spray humidifier as illustrated in Figure 2.1. A picture of the west end of the flow loop and the data acquisition

system is shown in Figure 2.2. The east end of the flow loop is shown in Figure 2.3. The refrigeration system condenser and compressor are located below the evaporator in the duct work shown in Figure 2.3. Several dampers in the air flow loop controlled the flow of outdoor air into the system and the percentage of recirculated air. For the experiment, 100% of the air was recirculated through the system to reduce the humidity of the test air and give best control of the air-side conditions.

Since the recirculated air was cooled by the test system's evaporator, it had to be reheated. This was accomplished with the use of a low-pressure steam coil and an electric heater in series. The steam coil was controlled with a proportional-derivative (PD) pneumatic controller. The controller had a fairly slow response and limited accuracy. The electric heater had a proportional-integral-derivative (PID) silicon controlled rectifier (SCR) controller which could maintain a constant temperature at the evaporator inlet to within a fraction of a degree. The maximum power output (5.2 kW) of the electric heater, however, was only about 50% of that required to reheat the recirculated air. Therefore the steam heater, which was located upstream of the electric heater, was used to meet the base reheating load of about 75%. The electric heater, which made up the final 25% of the load, then allowed for accurate control of the evaporator air inlet temperature.

The air was circulated with the use of a belt driven squirrel cage fan powered by an externally mounted variable speed motor. The motor speed was controlled with a variable speed controller that was set at a specified value to maintain a constant flow rate. The humidity in the flow loop was controlled by the use of a steam spray humidifier. The experiments were all conducted at the lowest possible humidity level such that no condensation occurred at the evaporator coil. The relative humidity of

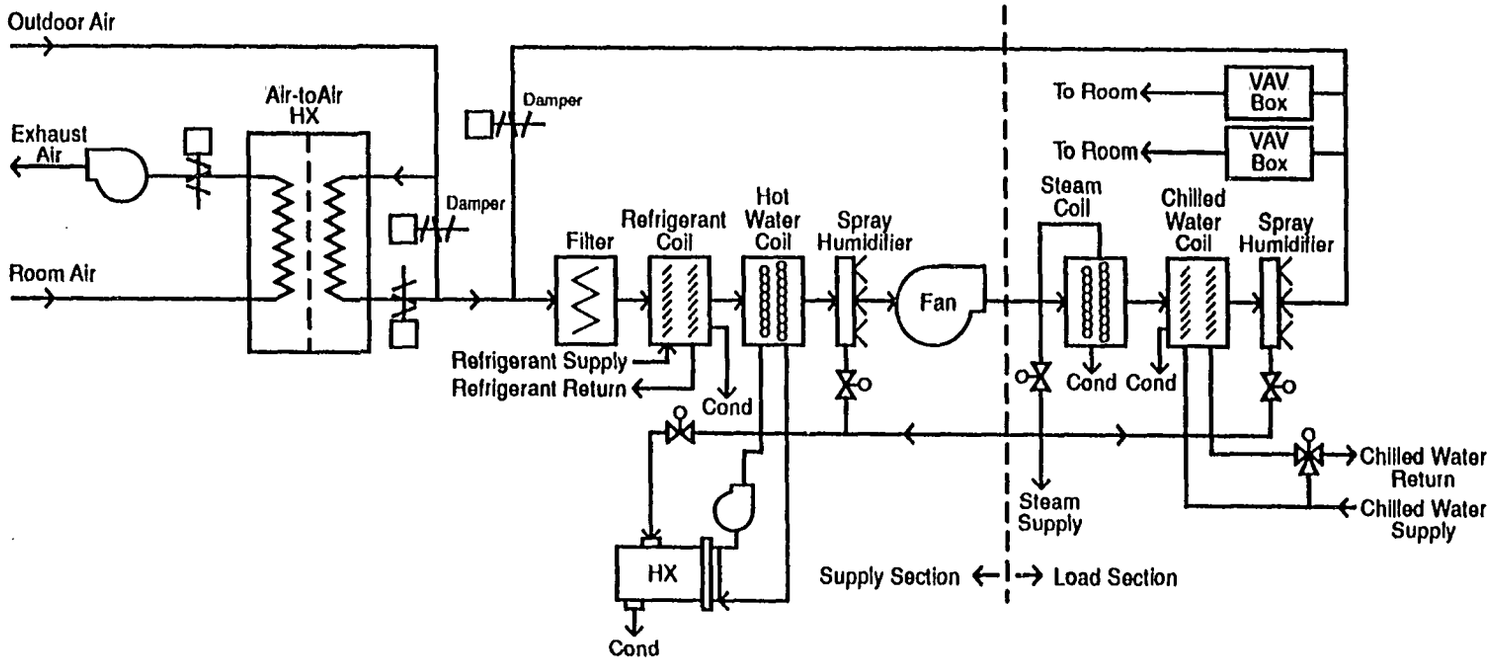

Figure 2.1: Schematic of air flow loop

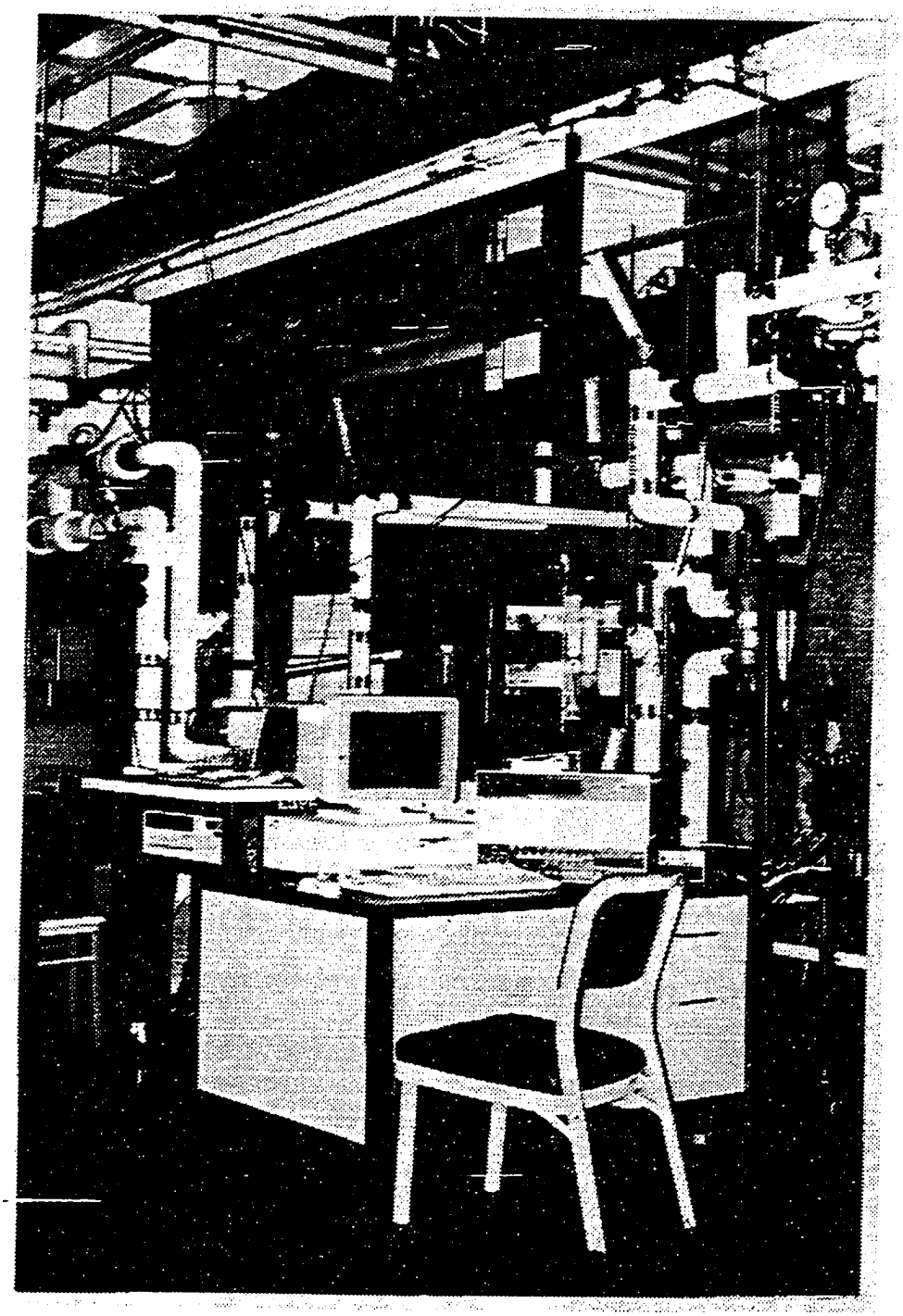

Figure 2.2: West end of air flow loop

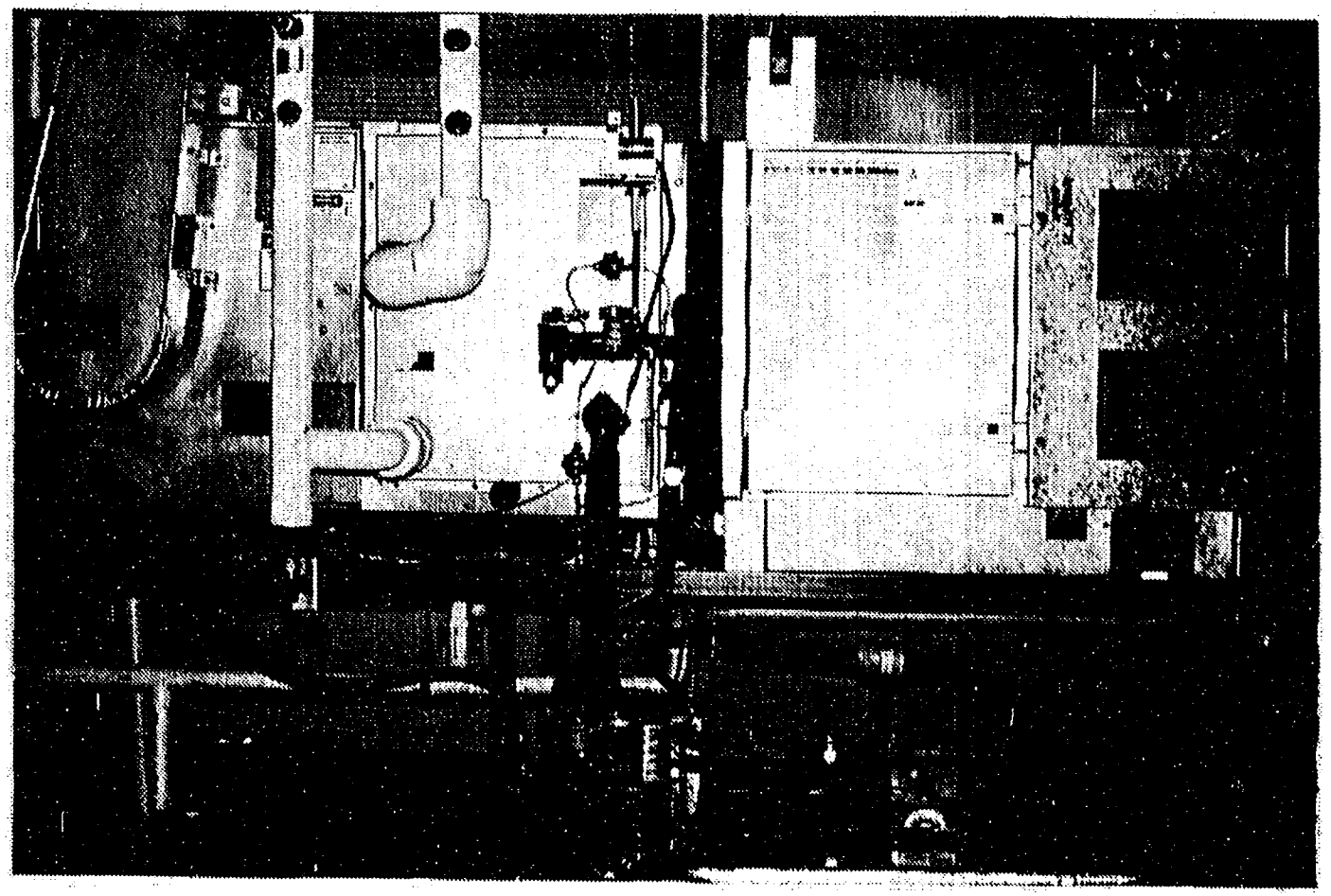

Figure 2.3: East end of air flow loop with refrigeration test system

the evaporator inlet air was typically about 30%. The air flow across the evaporator coil was fairly uniform due to the location of the fan downstream of the coil and a grill diffuser and filter upstream of the coil.

Condenser water flow loop

In order to maintain desired conditions within the condenser, the condenser was supplied with a source of water at a controlled temperature and flow rate. A large water flow rate was desired to reduce the heat transfer coefficient on the water side. Because of these requirements and in an effort to conserve water, the water was recirculated through the condenser with a three-stage centrifugal pump. For the water system pressure drop characteristics, the maximum flow rate achievable through the condenser was 30 gpm. Figure 2.4 shows a schematic of the water flow loop.

The flow rate through the condenser was controlled by adjusting a gate valve at the condenser exit. The water from the condenser exit was pumped into a five gallon holding tank which also supplied the suction line of the pump 6 ft below. The recirculation holding tank was supplied with fresh water through a connecting pipe from a second tank located above. The flow rate from one tank to the other was regulated with a ball valve between the two tanks. A constant head was maintained in the two tanks with the use of two stand pipes. Adjustment of the ball and gate valve gave constant condenser water temperature and flow rate even for significant variations in feed water pressure and temperature.

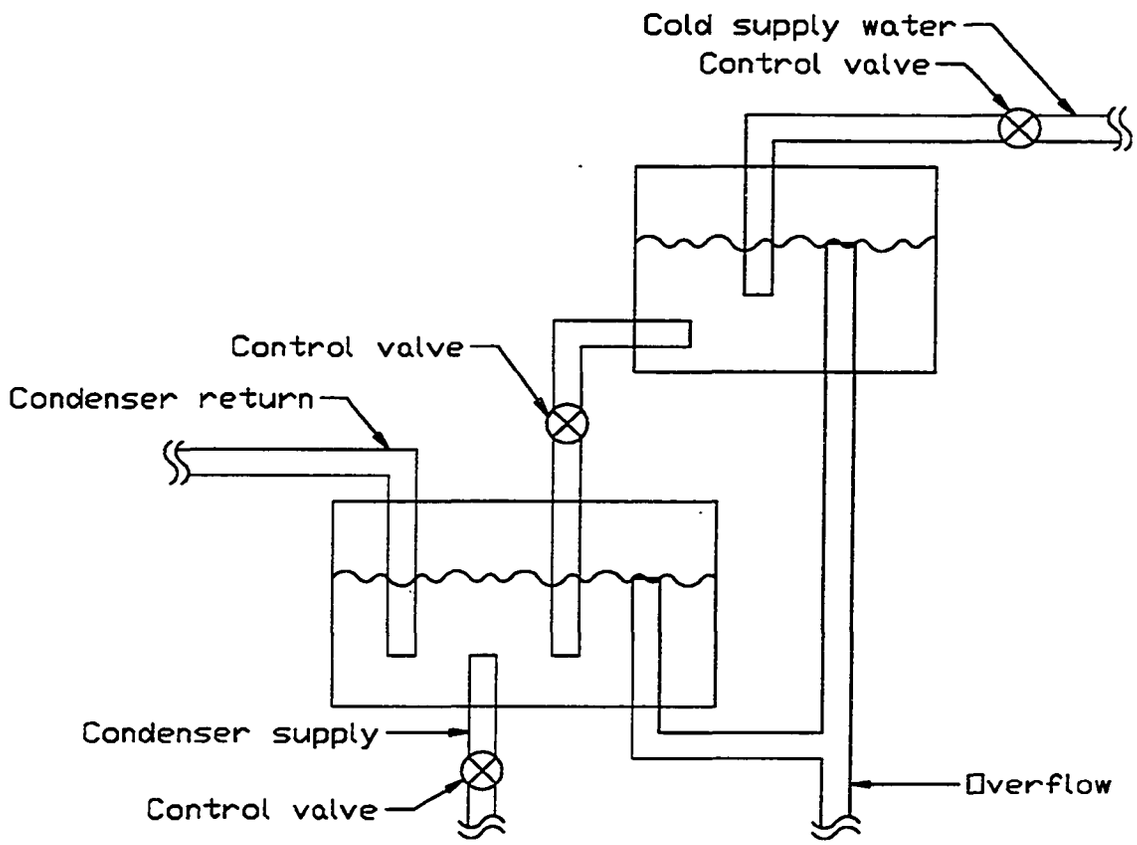

Figure 2.4: Schematic of water flow loop

Refrigeration test system

The refrigeration test system was designed to provide approximately 3 tons of refrigeration. A schematic of the system is shown in Figure 2.5. The figure also shows the locations of sensors used for data acquisition. A picture of the system is shown in Figure 2.6. The condenser is located beneath the board insulation shown. The water-cooled condenser is composed of two helical-coil counter-flow heat exchangers. The water flows in the annulus and refrigerant flows inside the inner tube. Heat transfer is enhanced by dimples made in the surface of the tube separating the water and refrigerant. The refrigerant heat transfer is also enhanced by the addition of a twisted tape. The condenser is well insulated so that the energy rejected by the refrigerant can be estimated by an energy balance calculation for the condenser water.

The evaporator is a five tube, multipass heat exchanger. A flow distribution device at the inlet gives approximately equal flow in each circuit of the evaporator. Heat transfer to the copper tubes is enhanced by the use of closely spaced aluminum fins. Each of the five circuits in the evaporator consists of ten horizontal passes with each pass vertically offset from the previous pass. The first pass is at the downstream side of the evaporator making the heat exchanger perform with counter flow characteristics.

The system can be operated with either of two expansion valves. Figure 2.7 is a picture of the two expansion valves. One is a standard thermostatic expansion valve with an insulated temperature-sensitive gas bulb located on the suction line. The valve was specifically designed to work with R-12. The other expansion device is a needle valve which is adjusted with a DC motor and gearing mechanism. The motor is controlled by the data acquisition system to maintain a set value of superheat.

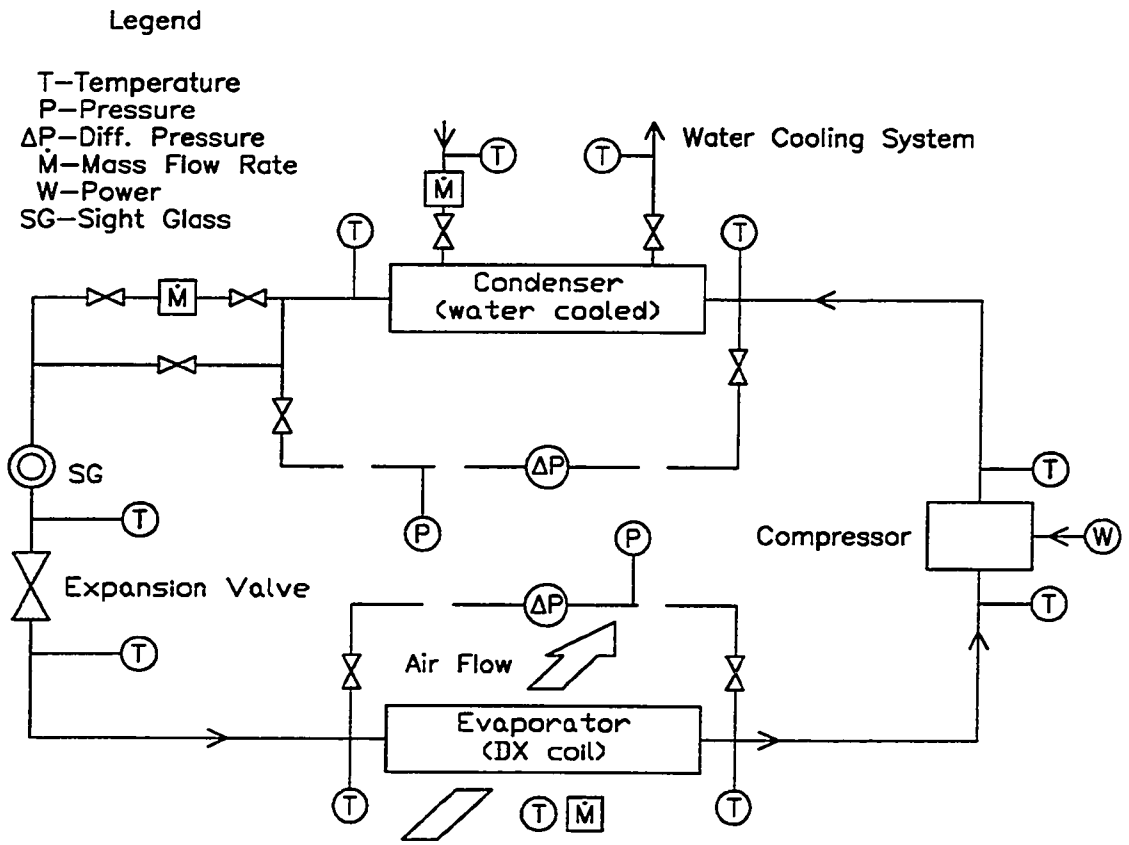

Figure 2.5: Schematic of vapor compression refrigeration system

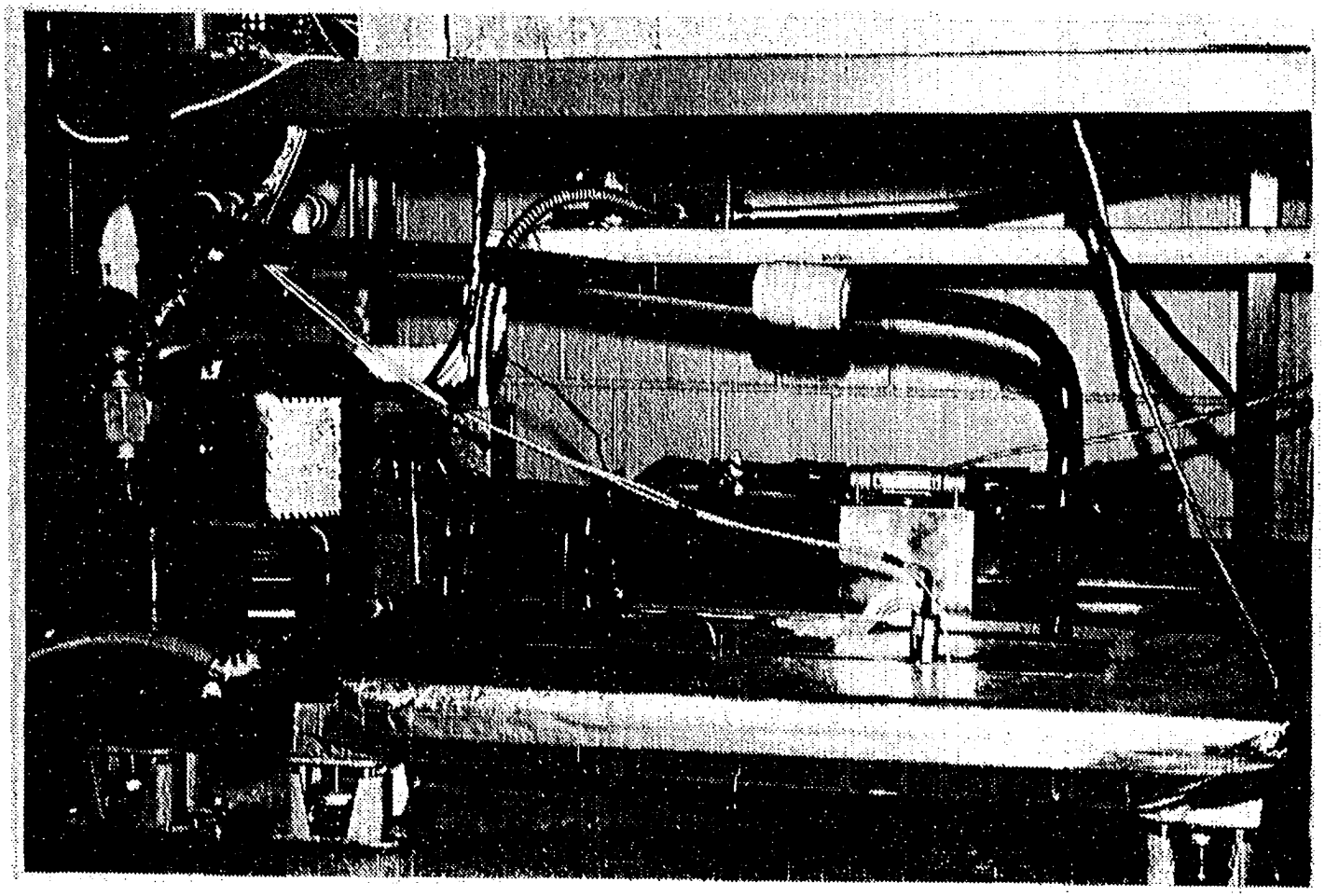

Figure 2.6: Vapor compression refrigeration test system

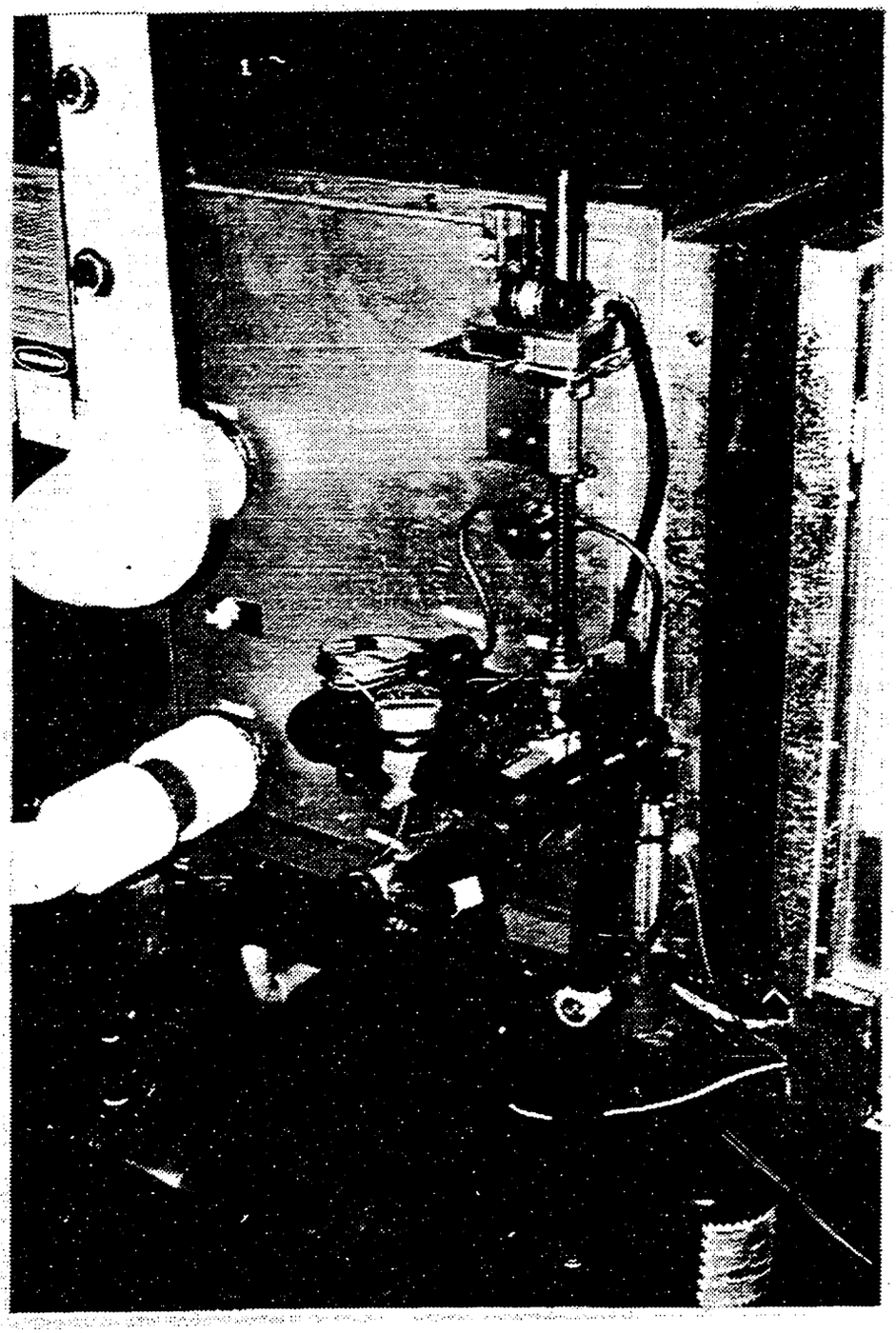

Figure 2.7: Expansion valves and control mechanism

The hermetically sealed compressor was designed specifically for R-12 systems with a capacity of approximately 3 tons of refrigeration. The refrigerant comes into direct contact with the lubricating oil inside the compressor shell and serves to cool the compressor and motor parts. The compressor has three pistons, each with a 1 inch stroke. The displacement volume and motor speed are 7.586 in^3 and 3450 rpm, respectively. A mineral oil was used as the lubricant for the tests with R-12 and the two R-22 blends. An equal viscosity (300 sus) alkylbenzene was used as the compressor lubricant for the R-134a tests.

Instrumentation

The refrigeration system and air flow loop were instrumented so that the performance of the refrigeration system could be evaluated at various operating conditions. Instrumentation was also selected so that the state of the refrigerant at the inlet and exit of each of the components in the system could be determined. This instrumentation includes pressure transducers, thermocouple probes, and flow sensors, as shown in Figure 2.5.

The type T thermocouple probes used to measure temperature in the system were all calibrated over a range of temperatures representative of the operating temperatures. The leads from each probe were shielded to prevent interference due to electrical noise. Calibrations were performed with the same electronic reference junction used during actual testing. The calibration procedure allowed for very accurate and repeatable temperature calculations.

The pressure transducers used in the system consisted of two absolute pressure sensors and two differential pressure transducers. The pressure transducers were all

calibrated over their expected range of operation. The transducers gave repeatable linear voltage outputs with changes in pressure.

The mass flow meter for the refrigerant is a coriolis-type true mass flow meter. This type of flow measuring device measures the mass flow accurately even with changing fluid densities. The density of the fluid in the flow measuring device is also recorded. The flow meter was factory calibrated and can be zeroed under operating conditions with two shut off valves and a by-pass circuit shown in Figure 2.5.

The non-refrigerant side instrumentation consists of two mass flow meters and several thermocouple probes and a watt transducer. This additional instrumentation shown in Figure 2.8 allows for energy balance calculations on each component in the system. The condenser water flow rate was measured with a calibrated drag flow meter located upstream of the water pump. The air flow rate was measured with a calibrated pitot tube arrangement and differential pressure transducer. Noise in the air and water flow rate signals was greatly reduced by the averaging of 500 readings taken over a 4 second interval. The power used by the compressor was measured with a watt transducer.

The temperature drop of the air across the evaporator was measured with two grids of eight type T thermocouples located upstream and downstream of the evaporator. Humidity up and downstream of the evaporator was calculated from dry and wet bulb temperature measurements. The wet bulb measurements were made with thermocouple probes which were constantly wetted by wicks. The temperature change across the electric heater was also measured with two sets of thermocouples across the heater. These were used to verify that the heater was being used to control the air temperature and that it was not overloaded.

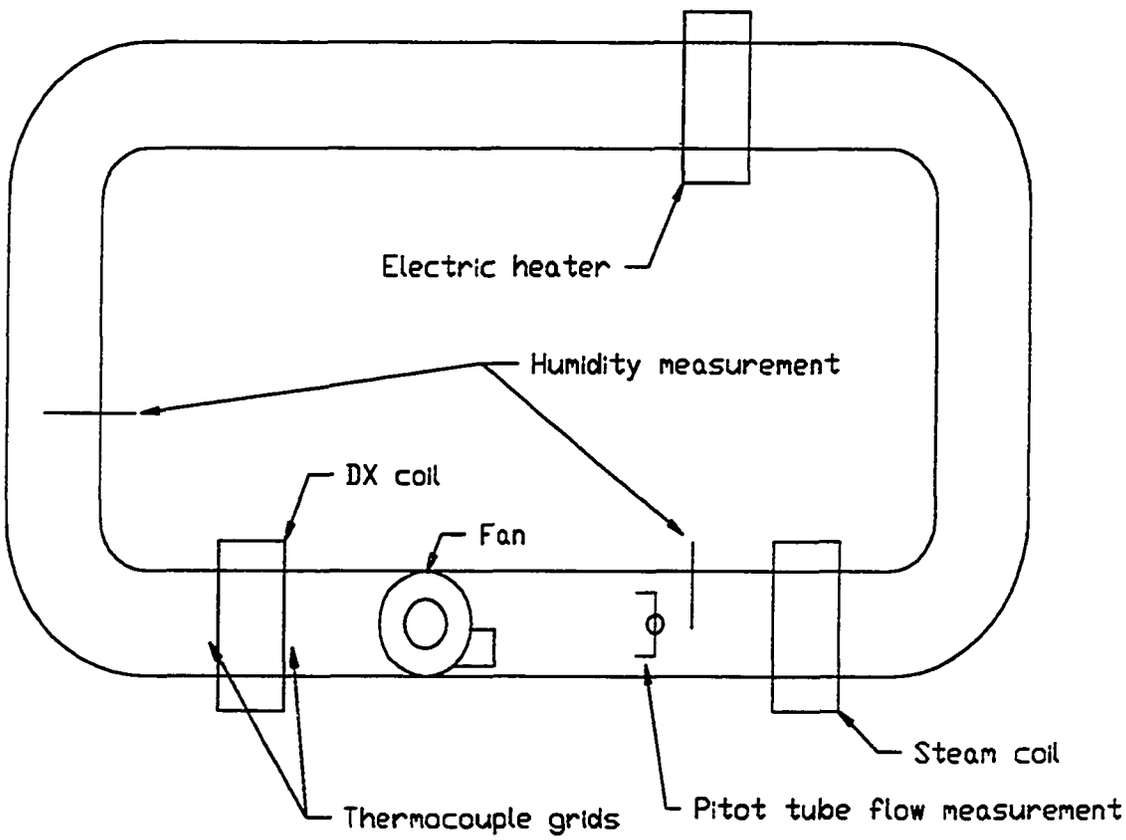

Figure 2.8: Schematic of air flow loop

All of the instrumentation used in the experiment had voltage outputs which were calibrated to the measured variables. Some of the pressure transducers and flow meters gave calibrated current outputs which were converted to voltage outputs with the use of precision resistors. The voltage output of the instrumentation allowed for the use of a computer controlled data acquisition system.

Data Acquisition

The data acquisition system used in the experiment consisted of a computer, a IEEE-488 GPIB (general purpose interface bus) controller card, a computer addressable digital voltmeter and scanner. The data acquisition system was used to channel the voltage output of each piece of instrumentation to the computer for control and recording of data. To make the system interactive and allow for computer control of evaporator exit superheat, the data had to be processed and properties calculated as it was collected.

The GPIB controller card allowed for computer control of the scanner and voltmeter. The card also served as the input path for the digital information received from the voltmeter. The 60 channel scanner was used to connect each of the 40 different input channels from the various instrumentation to the voltmeter, one at a time. The digital voltmeter filtered and averaged several readings, and then converted the analog voltages to digital signals. The digital signals were then transmitted to the computer via the interface bus and eventually stored in computer memory.

The voltages for each piece of instrumentation were first collected and then converted to values representing temperatures, pressures, mass flow rate, etc. using the appropriate stored calibration curves. The refrigerant properties were then calculated

at each state using property calculation subroutines. The property subroutines for R-12 were developed based on the data and equations presented by Downing [20]. The property subroutines for R-134a were based on the data and equations of Wilson and Basu [21]. The properties for the blend were based on the Carnahan-Starling-DeSantis equation of state [22] incorporated with experimental data into a program developed by NIST [23]. With the known states at various points in the system several important control parameters could be output, including:

- superheat at the exit of the evaporator
- subcooling at the exit of the condenser
- coefficient of performance
- capacity of the system

These data were then interpreted by the computer and used for the purpose of control.

Typical output acquired during a test run is shown in Figure 2.9. Key variables are plotted during system operation for the purpose of controlling and monitoring the transient behavior of the system. The property data were also presented on a pressure-enthalpy diagram on the computer monitor as data were taken during system operation. The constant feedback of displayed data and plots during system operation allowed system conditions to be monitored while experiments were in progress so that inputs could be adjusted to obtain the desired conditions.

Control of Superheat

The condition of the refrigerant at the inlet to the compressor must be superheated vapor to prevent droplets from entering the compressor cylinders. Such a

```
REFRIGERANT R134a
Nominal test conditions: 80 F water.  60 F air.
Time: 18:10:45
Elapsed time from start-up: 147.90 minutes

CONDENSER WATER PROPERTIES
Tin (F)      Tout      Mdot(lb/min)    Qdot(BTU/min)
 75.65       80.03       196.03           857.10

COMPRESSOR POWER
Pcmp= 191.47 Btu/min

EVAPORATOR AIR PROPERTIES
Evaporator grid temperatures (F)
Inlet  58.74   58.60   58.57   58.48   58.50   58.47   58.52   58.66
Exit   43.91   43.81   44.07   43.43   38.78   38.74   39.53   39.01
Average inlet = 58.57
Average exit  = 41.41

TDBair in      58.71 F
TWBair in      41.10
TDBair out     44.24
TWBair out     44.42
CFMair       2121.52 ft^3/min
MDOTDair      162.009 lb/min
MDOTcond        0.00
W in            0.0018
QMAX          596.71
QDOTair       564.53 Btu/min
QDOTrefg      567.49

REFRIGERANT PROPETIES
                  Compressor    Condenser   EX - Valve   Evaporator
Temp.in (F)         41.50       163.25       76.54        31.59
Temp.out           164.61        76.63       31.59        41.50
Pres.in (psia)      38.98       117.03      113.72        42.12
Pres.out           117.03       113.72       42.12        38.98
V.in (ft^3/lb)       1.24622      0.50298      0.01330      0.20372
V.out                0.50460      0.01330      0.20372      1.24622
U.in (Btu/lb)       99.754      121.805       35.885       34.575
U.out              122.110       35.918       34.575       99.754
H.in (Btu/lb)      108.750      132.704       36.164       36.164
H.out              133.045       36.197       36.164      108.750
S.in (Btu/lb-F)      0.2260       0.2492       0.0752       0.0769
S.out                0.2497       0.0753       0.0769       0.2260
ATM.in (Btu/lb)     10.088       21.603       18.395       17.512
ATM.out             21.651       18.395       17.512       10.088
X.in                 1.000        1.000        0.000        0.174
X.out                1.000        0.000        0.174        1.000
QDOT (Btu/min)    -189.943      754.505        0.000     -567.483

MDOT = 7.802 lb/min     dTsubcooled    = 10.60 F      S.G.U. = 0.925
COP  = 2.988            dTsuperheated = 13.72 F       Charge = 8.52 lb
```

Figure 2.9: Sample of output data

condition can cause severe damage or failure of the compressor. The thermostatic expansion valve was first used to control evaporator exit superheat but was found to give a significantly underdamped response. With the thermostatic expansion valve, the superheat oscillated over a range of 10 F about the set point value. Since better control of the superheat was required and since the effect of changing refrigerants on valve performance was unknown, a computer controlled expansion valve was added to the system.

The expansion valve was driven by a DC motor through a gearing mechanism that allowed for small adjustments in superheat to be made. The gearing was such that 1/4 turn of the valve required approximately 15 seconds of motor operation. The power to the DC motor was supplied through two channels of the scanner. The polarity of the two channels could be reversed, allowing the motor to rotate in either direction. The amount of valve movement was controlled by the amount of time the motor was powered.

The data acquisition system recorded the refrigerant temperature and pressure at the evaporator exit. The saturation temperature at the given pressure was then calculated and the superheat determined. It was found that using the evaporator exit temperature caused unstable operation since liquid droplets in nonequilibrium caused wetting of the thermocouple probe. Using the temperature probe at the compressor inlet eliminated this instability since the droplets had time to come to equilibrium and vaporize.

The difference in the calculated and desired level of superheat was then used as the control error signal. The amount of valve movement required was calculated using a proportional-derivative control scheme. The motor would then be driven in

the proper direction for the proper amount of time. The control system worked very well for small variations in operating conditions. The superheat could be maintained at the desired value of 13.5 F with less than 0.4 F variation in either direction. For large changes in operating conditions the controller responded slowly and had to be overridden manually.

Experimental Procedure

The final sections of this chapter describe the experimental procedure followed in the collection of data. The choices of variable and fixed parameters for the experimental study are given below and the reasoning behind those choices explained. A description of the experimental process followed is presented as well as a chronology of the experiment. Included is a discussion of data taken with a different set of variable parameters, with a failed compressor valve and with an additional refrigerant.

Determining Operating Conditions

In order to make general comparisons of system performance with different refrigerants, the system must be operated over a range of operating conditions. Using a broad scope of variables makes the data applicable to a variety of conditions. The operating conditions which could have been varied in this study are:

- type of refrigerant
- refrigerant charge
- refrigerant superheat at the evaporator exit

- evaporator air inlet temperature
- evaporator air flow rate
- condenser water inlet temperature
- condenser water flow rate

If it is assumed that all interactive effects could affect system performance then a minimum of 3^7 or 2187 independent tests would be required. This assumes only second order effects of each variable. It is possible to reduce this number if assumptions are made about the interaction between variables. In any case, however, the number of tests required with seven independent variables is prohibitive.

Once the variable parameters are chosen the range over which these variables are to be varied must be determined. The range of operation for the refrigeration system is constrained by the following boundaries that are set for the system.

- The pressure is kept below 250 psia in the system because of limits on the compressor and for safety.
- In order to prevent ice from building up on the coil, the temperature of the refrigerant at the inlet of the evaporator is not allowed to drop much below 32 F.
- The refrigerant is subcooled at the exit of the condenser in order to determine its properties at that point. Subcooling at the condenser exit is also consistent with the operation of actual systems.
- The refrigerant is superheated to a minimum of 10 F at the exit of the evaporator since the system will not reach steady state at conditions below this value.

Superheating at values of 10 F or greater at the evaporator exit is consistent with the operation of actual systems.

These constraints on system operation affect the possible ranges of operating conditions. Limits on the range of operation of the controlling parameters themselves also limits the possible range of operating conditions.

Fixed parameters

Three of the seven possible variable parameters were fixed for the experimental study. The fixed parameters are:

- condenser water flow rate
- evaporator air flow rate
- refrigerant superheat at the evaporator exit

These parameters were fixed because of their limited effect on system performance and because consideration of all parameters was outside the scope of the experiment.

Flow rates The condenser water flow rate was held constant for all tests at 196 lb/min. As the condenser water flow rate is increased, its effect on system performance becomes small. The reason for this is that at high flow rates the thermal resistance between the fluid and the tube wall becomes negligible a nd the temperature profile for the water becomes flat. In other words, further increases in the flow rate do not result in significant changes in either the water-to-wall temperature difference or in the rate of heat transfer to the water. The condenser performance is

then primarily effected by condenser water inlet temperature and refrigerant temperatures. Similarly the effect of evaporator air flow rate becomes increasingly smaller relative to other parameters at high flow rates. Therefore, the maximum achievable air flow rate for the system (2100 cfm) was selected and held constant for all tests.

Superheat Several tests were performed with R-12 and R-134a to determine the effect of varying evaporator superheat on system performance. Four tests were conducted with R-134a at superheats ranging from 5 to 20 F for a fixed evaporator air temperature of 60 F and a fixed condenser water temperature of 74 F. Figure 2.10 shows that the COP increases only slightly with an increase in superheat. The effect on COP of a change in superheat is much smaller than the effect of other independent variables (i.e. condenser water temperature and evaporator air temperature). The variation in COP for all test conditions at a superheat of 13.5 F is shown in Figure 2.10.

The effect of superheat on the cooling capacity is shown in Figure 2.11. The cooling capacity decreases linearly with increasing superheat. The effect of superheat on capacity, as with COP, is smaller than the effect of the other independent variables. Figure 2.11 shows the variation in capacity for all test conditions at a superheat of 13.5 F.

Operation of the system at low superheats (below 13 F) frequently resulted in uncontrollable fluctuations in superheat. Such fluctuations might lead to two-phase conditions at the evaporator exit, thus damaging the compressor. Therefore, operating at low superheats was not practical. In contrast, operating the system with superheats significantly greater than 13 F could cause a drop in capacity, which

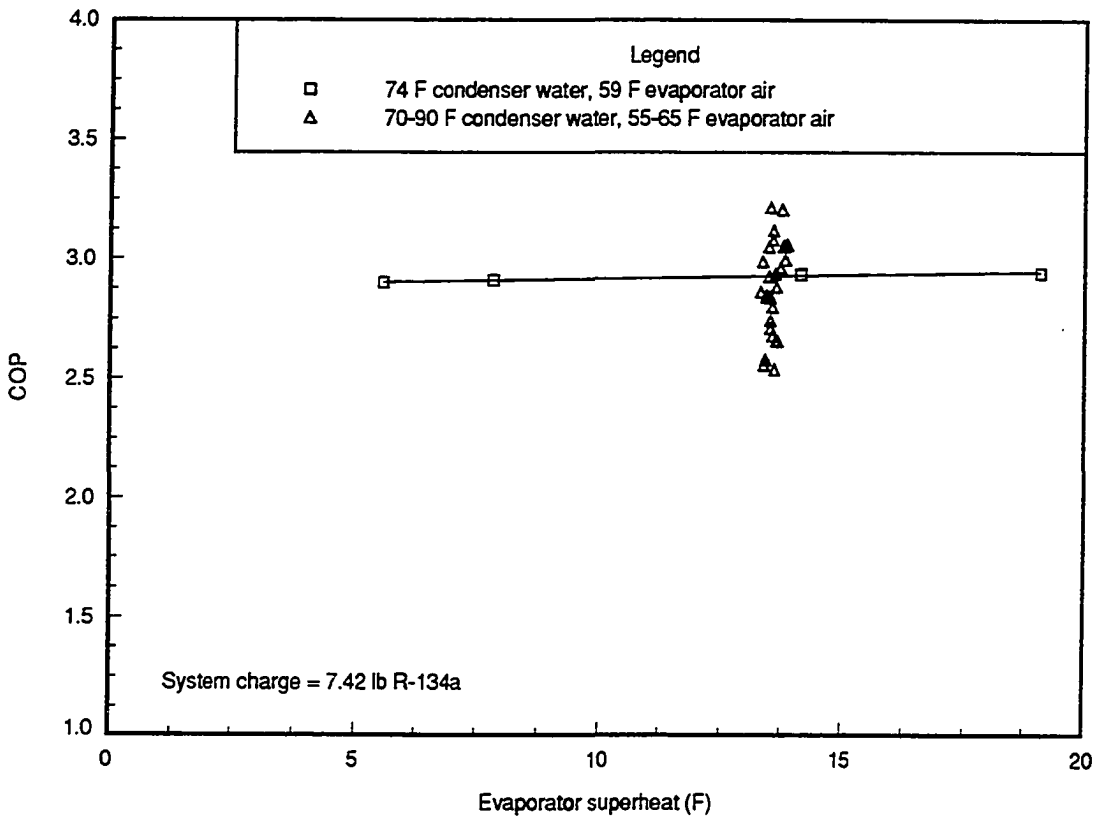

Figure 2.10: Variation of superheat with COP

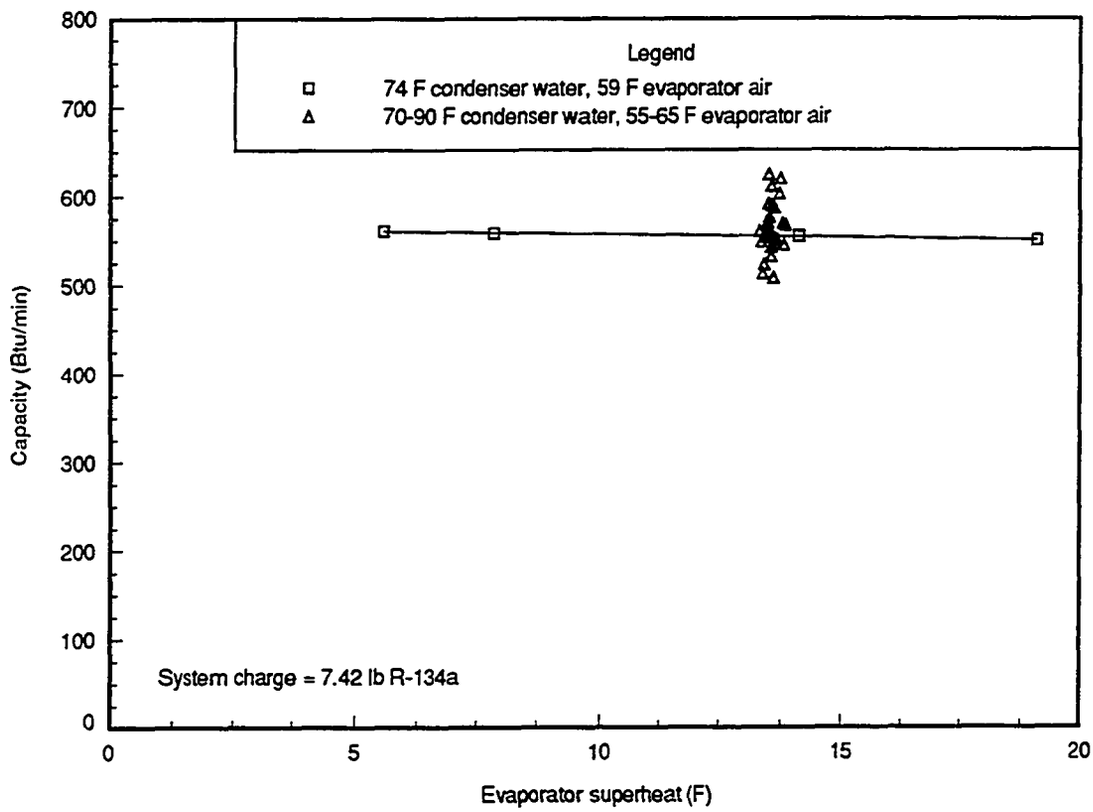

Figure 2.11: Variation of capacity with superheat

might not be offset by the slight increase in COP. A 15 F increase in superheat caused an increase in COP of only 3% and a 2% decrease in capacity for tests with R-134a. Similar behavior was observed with the R-12. Even though the effect of superheat on system performance was measurable, its effect was much smaller than the effect of other independent variables and, therefore, it was held constant at 13.5 F for all tests. This value of superheat is consistent with those found in actual operating refrigeration and air conditioning systems.

Variable parameters

The four parameters which were varied independently are:

- type of refrigerant
- refrigerant charge
- evaporator air inlet temperature
- condenser water inlet temperature

The refrigerants tested in the refrigeration system were R-12 (Dichlorodifluoromethane), R-134a (Tetrafluoroethane), and refrigerant blends: MP-39 (52% R-22, 15% R-152a, 33% R-124) and MP-52 (33% R-22, 15% R-152a, 52% R-124). The chemical names for the blend components are Chlorodifluoromethane (R-22), Difluoroethane (R-152a) and Chlorotetrafluoroethane (R-124). Some test were also conducted with pure R-22, however it was later discovered that one of the compressor inlet valves had failed during these tests.

Changing refrigerants required the complete system to be flushed with R-11 and alternately pressurized with nitrogen and evacuated until traces of the previous test

refrigerant and oil were removed. A different lubricant was required for the tests with R-134a. A sample was taken from the cleaned and recharged system and studied with gas chromatography to determine if contaminants were present in the system. The results showed that the procedure employed in changing refrigerants was effective and that contamination was undetectable.

The minimum refrigerant charge of the system was dictated by the condition that subcooling must occur in the condenser. For the system used in this study, a charge of 8.86 lb was required with R-12 and the blends to give approximately 5 F subcooling. For R-12, the system was also evaluated at charges of 9.27 lb and 9.77 lb to determine the effect of charge on system performance. Since little change in performance was observed no further changes in system charge with R-12 were tested. Five charges were tested with the refrigerant blend, MP-39 (8.20, 8.86, 8.96, 9.72 and 10.52 lb). Changes in system charge had no observable effect on system performance. All of the MP-39 data at refrigerant charges other than 8.86 lb were taken with a failed compressor valve and are therefore not presented. The second refrigerant blend tested, MP-52, was assumed to behave similarly to MP-39, and therefore was only tested at a single refrigerant charge of 8.86 lb. R-134a was tested at five refrigerant charges. The minimum charge which gave subcooling at the condenser exit was 7.42 lb. Additional tests were performed at charges of 7.98 lb, 8.52 lb, 9.05 lb and 9.60 lb. Tests at the highest charge were abbreviated when it was determined that system performance was dropping significantly at this level of charge.

The controller for the air flow loop allowed the evaporator air inlet temperature to be varied from 55 to 90°F. In order to simulate actual air conditioning conditions, the inlet temperature was set at nominal settings of 55, 60 and 65 F for each setting

of the other independent variables.

The condenser water temperature was set at nominal values of 70, 80 and 90 F which represent typical values of heat sinks available for refrigeration and air conditioning systems. Since the air inlet temperature and condenser water temperature are varied over a range of conditions and the data are correlated using multidimensional curve fits, there was no need for these temperatures to be exactly the same for each test.

For a given refrigerant and level of system charge, a minimum of nine tests were required to cover the grid of nominal air and water temperatures. Several additional tests were performed at intermediate conditions and at repeated conditions to give greater certainty to curve fits and to establish repeatability. The tests with the minimum charge of R-134a represented the maximum number of tests at any one charge with 27 independent tests at various levels of air and water temperature.

Achieving Steady State Behavior

All tests of the refrigeration system were to be done under steady state conditions. The transient behavior of the system caused large differences in system performance and required significant time to dampen out. Therefore, in order to achieve steady state operation, the independent or controlled variables had to be held constant. This was not easily accomplished since three of the independent variables were influenced by the system. The interdependence between system performance and the independent variables is summarized as follows:

- The evaporator air inlet temperature is influenced by the heat transfer in the evaporator as the air is recirculated.

- The condenser water inlet temperature is influenced by the heat transfer in the condenser due to the fact that a large portion of the condenser water is recirculated.

- The superheat is a function of the evaporator exit temperature and pressure, which is only indirectly controlled by the expansion valve.

The time required to reach a condition where variations in the independent variables were small was typically 0.5 to 1.0 hour. After one hour, the variations in the dependent variables were also small. Figure 2.12 shows the time variation of the condenser water inlet temperature and the evaporator air inlet temperature for one of the test conditions. The variation is small compared to the range in which these value were varied during the various tests. The other independent variable, evaporator superheat, is shown in Figure 2.13 along with the condenser subcooling. The small variation in subcooling and refrigerant temperatures shown in Figure 2.12 gives evidence that the system does reach a fairly steady operating condition. The system pressures shown in Figure 2.14 also indicate steady state operation. Each variable in the system shows a pattern of small periodic variation, with a period of less than five minutes, about a mean value. Averaging several samples of data taken over a period of at least five minutes gives an accurate representation of the mean value of each variable.

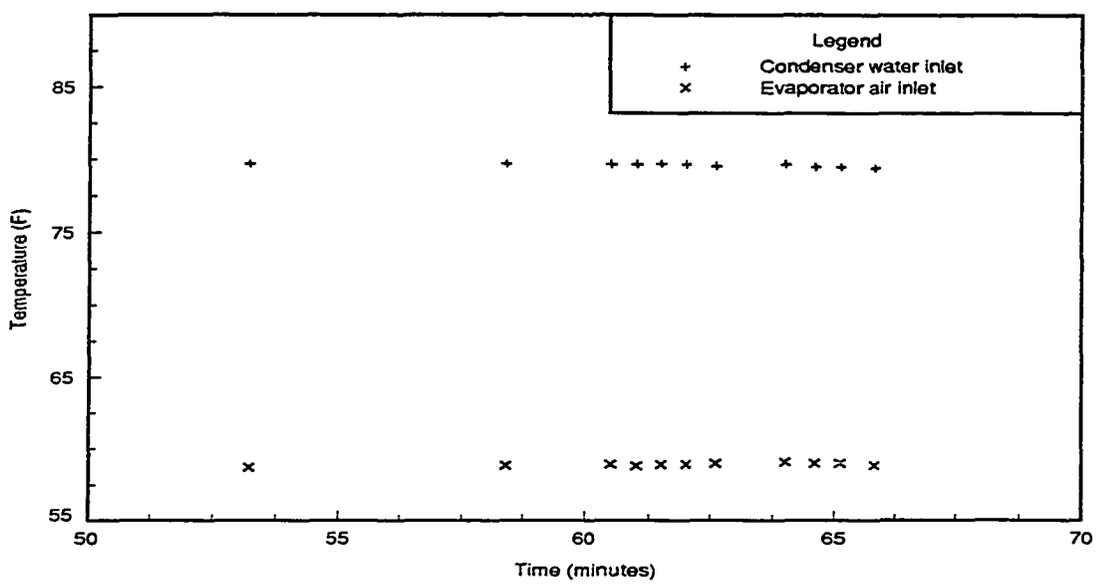

Figure 2.12: Variation of controlled temperatures with time

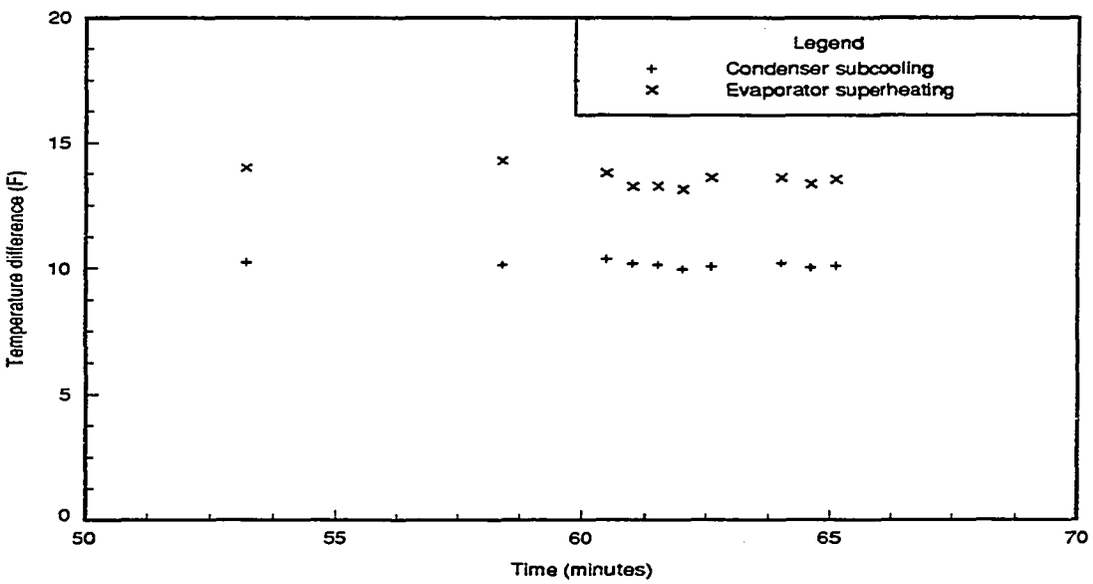

Figure 2.13: Variation of subcooling and superheat with time

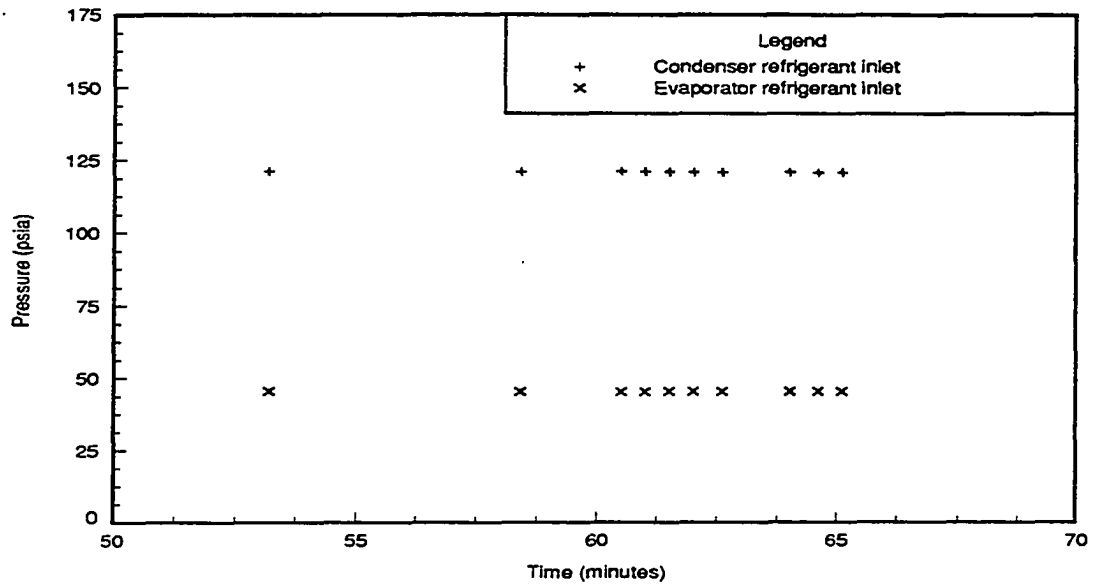

Figure 2.14: Variation of system pressures with time

Error Analysis

Repeatability

The controls used to maintain the independent variables at the desired conditions are effective at bringing the system to steady state quickly and maintaining each variable at a constant mean value. With some care, the operating conditions could be set at repeated conditions which allow the repeatability of experimental results to be determined. Repeating the experiment under the same conditions gives a measure of the error associated with random variations in system performance and in measurements. Several tests were performed at different times with R-12 under the same operating conditions. The system charge was 9.77 lb, the evaporator air temperature was 60 F, and the condenser water was 80 F for all tests. Table 2.1

Table 2.1: Repeatability test (9.77 lb R-12, 60 F evaporator air, 80 F condenser water).

Trial	COP	Capacity (Btu/min)
#1	2.850	555.4
#2	2.856	551.4
#3	2.841	551.3
#4	2.848	554.6

shows the COP and cooling capacity for the four independent tests with constant test conditions. There is a 0.5% and 0.7% difference between extreme values for the COP and cooling capacity, respectively. These values, which also account for some variation in the test conditions, show good repeatability. The repeatability of experimental results was verified with each refrigerant and with each refrigerant charge in a similar fashion.

Experimental uncertainty

The experimental uncertainty of the performance characteristics, coefficient of performance and cooling capacity, is a function of the uncertainty associated in the values of measured variables. The total uncertainty depends on the uncertainty in measurements of temperature, pressure and refrigerant mass flow rate. All of the instruments were calibrated, so the bias may be assumed to be zero for all the instruments. The uncertainty of each instrument is given as follows:

- Temperature $\pm$ 0.5 F for all thermocouple probes
- Condenser inlet pressure $\pm$ 1 psia
- Expansion valve inlet pressure $\pm$ 1.5

- Refrigerant mass flow rate $\pm$ 0.025 lb/min
- Compressor power $\pm$ 0.4 Btu/min

The cooling capacity is calculated from the refrigerant properties as:

$$\text{Capacity} = \dot{m} * (h_{out} - h_{in}) \tag{2.1}$$

where h is the enthalpy at the inlet and exit of the evaporator. The inlet enthalpy is assumed to be equal to the enthalpy at the inlet of the expansion valve. The enthalpies are functions of temperature and pressure. The uncertainty for capacity is then determined as [24]:

$$\begin{aligned} \Delta\text{Capacity} &= \left[(\Delta\dot{m}(h_{out} - h_{in}))^2 + \left(\dot{m}\frac{\delta h_{in}}{\delta T_{in}}\Delta T_{in}\right)^2 + \left(\dot{m}\frac{\delta h_{in}}{\delta P_{in}}\Delta P_{in}\right)^2 \right. \\ &\quad \left. + \left(\dot{m}\frac{\delta h_{out}}{\delta T_{out}}\Delta T_{out}\right)^2 + \left(\dot{m}\frac{\delta h_{out}}{\delta P_{out}}\Delta P_{out}\right)^2\right]^{0.5} \end{aligned} \tag{2.2}$$

where the symbol Δ represents the uncertainly associated with each variable. T_{in} and P_{in} are the temperature and pressure at the inlet to the expansion valve, respectively. T_{out} is the temperature at the exit of the evaporator. P_{out} is the pressure at the evaporator exit.

For a sample condition of 80 F condenser water, 60 F evaporator air and a system charge of 8.52 lb of R-134a, the uncertainty in capacity is calculated using Equation 2.3 as:

$$\begin{aligned} \Delta\text{Capacity} &= [(.025 * (108.75 - 36.16))^2 + (7.8 * .34 * .5)^2 \\ &\quad +(7.8 * 0.0 * 1.5)^2 + (7.8 * .22 * .5)^2 + (7.8 * .086 * 1)]^{0.5} \\ &= 2.5\text{Btu/min} \end{aligned} \tag{2.3}$$

The partial derivatives of enthalpy were determined numerically from property relationships.

The coefficient of performance (COP) is calculated as:

$$\text{COP} = \text{Capacity}/\dot{W}_{compressor} \tag{2.4}$$

The uncertainty in COP is then calculated, based on the value of uncertainty for capacity given above, as:

$$\Delta\text{COP} = \sqrt{\left(\frac{\Delta\text{Capacity}}{\dot{W}_{compressor}}\right)^2 + \left(\frac{\text{Capacity}}{\dot{W}^2_{compressor}}\Delta\dot{W}_{compressor}\right)^2} \tag{2.5}$$

For R-134a at the same condition as above, the uncertainly in COP is:

$$\Delta\text{COP} = \sqrt{\left(\frac{2.5}{191.5}\right)^2 + \left(\frac{567.5}{(191.5)^2} * 0.4\right)^2} = 0.014 \tag{2.6}$$

The relatively small level of uncertainty in COP and capacity calculated above is representative of all the data. The total uncertainties calculated represent all of the error due to the inaccuracies associated with the instrumentation. A major portion of this error is random. Therefore, taking several readings reduces the error associated with random variation. The experimental procedure used to collect data and curve fit system performance with operating conditions also accounts for this random error. The uncertainty in comparisons of performance with different refrigerants is therefore accounted for with statistical methods.

If a bias exists in measurements, it is reasonable to assume that it is a constant error. The uncertainty in measurements listed above is used as the worst case value for a bias of calibrated instrumentation. With these worst case values the uncertainty in a ratio of capacity with R-134a to that with R-12 is only 0.06%. The low level of

uncertainty associated with constant bias errors indicates that the major source of error in comparisons is random error.

Chronology of Experiment

The first set of data with R-12 was taken with different variable parameters than for the data presented here. The condenser water temperature and evaporator air temperature were held constant and the position of the expansion valve adjusted in small increments. This gave conditions of varying superheat at the evaporator exit. The superheat was varied from 7 F to 40 F which corresponded to values of condenser subcooling in the range of 15 to 25 F. The amount of superheat is much greater than what is typical for an evaporator exit, however the data could be used for analyzing the compressor of a system with a suction line heater where significant superheating does occur.

The condenser water inlet temperature was fixed for all tests for this first set of R-12 data. The fixed water temperature was about 60 F. The other variable parameters were condenser water flow rate, system charge, and evaporator air temperature. Four levels of condenser water temperature, three levels of charge and two levels of air temperature were tested at each of 10 to 12 expansion valve positions. A total of 144 independent tests were run following this test procedure. The data were not used in the presentation of results given here, since the test was designed primarily to determine the effect of superheat which was secondary to the primary objectives of the project.

The experimental procedure outlined in the previous sections was adapted following the tests described above. This procedure which varied charge, condenser

water and evaporator air temperatures at fixed superheat represents the data presented in the following chapters. The later procedure used allowed for comparisons of performance at conditions more representative of actual air conditioning systems.

The R-12 data was collected first followed by the R-134a data. The R-12 data required 28 independent tests. Sixty tests were run with R-134a. Following the R-134a tests, the MP-39 blend was tested at four levels of charge (8.20, 8.96, 9.72 and 10.52 lb) for each of the nine nominal operating conditions. Forty one different tests were were conducted with MP-39, with approximately ten tests at each charge. The MP-52 blend was then tested at one level of charge. The performance of the blend data differed significantly from the data with the pure refrigerants.

To answer questions raised about changes in system performance, the system was charged with R-22 and tested at the nine operating conditions. The performance with R-22 was also significantly different than with the other pure refrigerants. In an effort to verify the results the system was charged with R-12 and the R-12 experiments repeated. The data differed significantly from the original set of data, but compared well with the R-22 and blend data. Suspecting some type of compressor failure, the compressor was cut open and examined. It was discovered that one of the compressor intake valves had failed and that the compressor was therefore operating at 2/3 capacity. Accounting for this reduced capacity explained the differences in performance. The data collected are useful experimental data, but are not directly comparable to the original R-12 and R-134a data taken before the valve failure. The blend data was therefore retaken using an identical compressor. The system was also tested with R-12 to verify that the compressor performed identically.

Conclusions

The test procedure used in the experiment provides the data needed to make comparisons of different refrigerants operated over a range of conditions. The procedure involved tests of system performance at three nominal air temperatures (55, 60 and 65 F), three nominal water temperatures (70, 80, and 90 F) and various levels of charge for each refrigerant. A total of 136 tests were performed under this procedure. The results presented in the following chapters are based on those observations. The results were shown to be repeatable with experimental uncertainties of less than 0.5%.

CHAPTER 3. ANALYSIS OF SYSTEM PERFORMANCE

Introduction

One of the primary objectives of this study was to investigate the system performance using various refrigerants under different operating conditions. In order to make direct comparisons, it was necessary to set the operating conditions at exact values for each refrigerant tested. The experiment was designed to give several points of comparison for each variable operating condition. Because of the exponential growth of required experiments with variable operating conditions, three variable conditions were selected. These conditions are the refrigerant charge, the condenser water inlet temperature, and the evaporator air inlet temperature.

This chapter focuses on two performance parameters, the coefficient of performance (COP) and the cooling capacity. Both of these parameters are used to quantify system performance. The capacity is a direct measure of the rate of cooling that a system is capable of providing. The coefficient of performance is a measure of system efficiency. The COP is defined as the ratio of capacity to power input to the compressor.

A useful tool in the study of refrigeration cycles is the pressure enthalpy diagram. Such a diagram shows an approximate value of COP and shows the enthalpy change in the evaporator, which is related to capacity. The pressure enthalpy diagrams are used

to help explain the variation in performance with different operating conditions. An exhaustive analysis of the relationships between COP and capacity and the operating conditions is given, following a discussion of the pressure enthalpy diagrams. In order to make comparisons between refrigerants, curve fits of system performance had to be developed. This was necessary since the operating conditions could not be adjusted exactly to specific test conditions. The results and errors associated with these curve fits are also discussed.

Pressure Enthalpy Diagrams

The pressure enthalpy diagram is particularly helpful in analyzing the system because each component in the system has the same mass flow rate. The enthalpy differences across each component are therefore proportional to the heat transfer rates of the heat exchangers and the power input to the compressor. The ratio of enthalpy difference across the evaporator to that across the compressor is approximately equal the COP. Such a calculation of COP neglects heat transfer through the compressor shell, which is small and relatively constant. The pressure enthalpy diagram clearly shows the system pressures and pressure drop in the condenser and evaporator and the assumption of isenthalpic expansion across the expansion valve.

The data acquisition system was set up to show a pressure enthalpy diagram of the system in real time. It proved to be a useful tool in the collection of data, as the system performance could be analyzed at a glance and necessary adjustments made to the system. Several pressure enthalpy diagrams are shown on the following pages that illustrate the effects of changes in operating conditions. The diagrams provide insight as to cause of variation in COP and unit capacity with operating conditions.

The diagrams also show details of the individual components and show how each is affected by changes in operating conditions and with different refrigerants.

Pressure enthalpy diagrams for R-12

Three pressure enthalpy diagrams are used to show variations in the following parameters with other variables held constant:

- the evaporator air inlet temperature
- the condenser water inlet temperature
- the system charge

The evaporator air and condenser water temperatures given represent the desired set point values. These values were difficult to control during the experiment. The actual data were taken at values near these nominal values. The pressure enthalpy plots are based on actual experimental values and show the trends for variation in the input parameters.

Figure 3.1 shows the effect of variations in evaporator air temperature for the refrigerant charge of 8.86 lb of R-12. The condenser water was held constant at 80 F. An increase in the evaporator air temperature caused a rise in the evaporator pressure, but had little effect on the enthalpy change in the evaporator. The increase in cooling capacity associated with an increase in evaporator air temperature was due to an increase in refrigerant mass flow rate. The enthalpy change in the compressor decreased slightly with increasing evaporator air temperature. This decrease, about 4.5% for the range of air temperatures, caused a rise in the system COP.

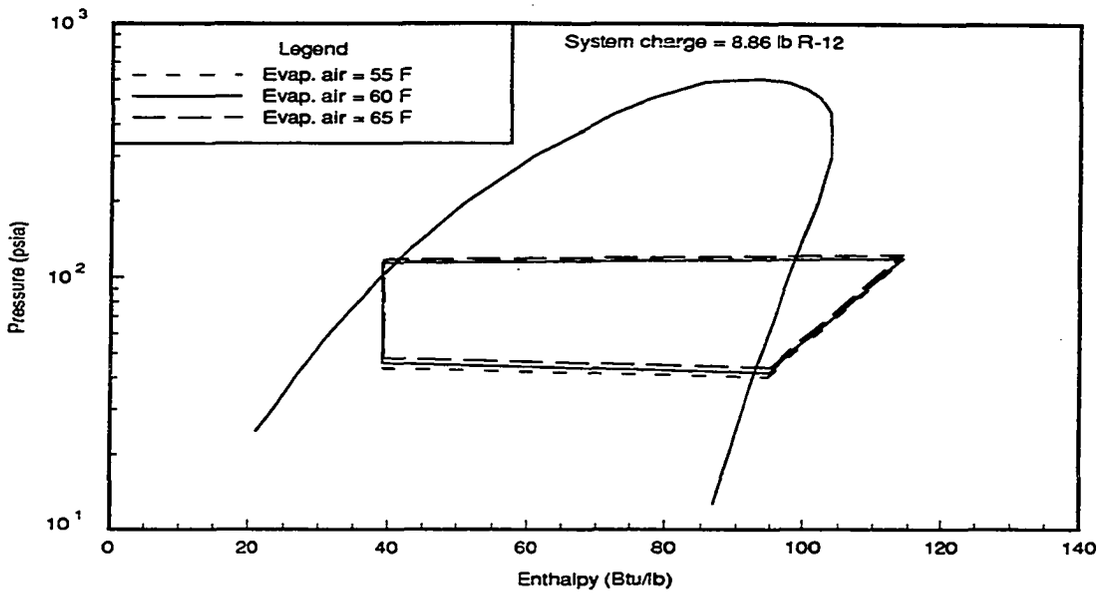

Figure 3.1: Effects of variation in evaporator air temperature for R-12

Changes in condenser water temperature had a significant effect on system performance as seen in the pressure enthalpy plot shown in Figure 3.2. The system charge was held constant at 8.86 of lb R-12. The evaporator air temperature was held constant at 60 F. Three condenser water temperatures (70, 80 and 90 F) are shown. An increase in condenser water temperature caused an increase in the condenser pressure and a decrease in the change in enthalpy in the evaporator because of the higher quality at the inlet. The condenser exit subcooling remained fairly constant. A decrease in the enthalpy change in the evaporator corresponds to a decrease in capacity since the refrigerant mass flow rate was fairly constant with changes in condenser water temperature. The enthalpy change across the compressor remained fairly constant so the COP decreased with increasing condenser water temperature.

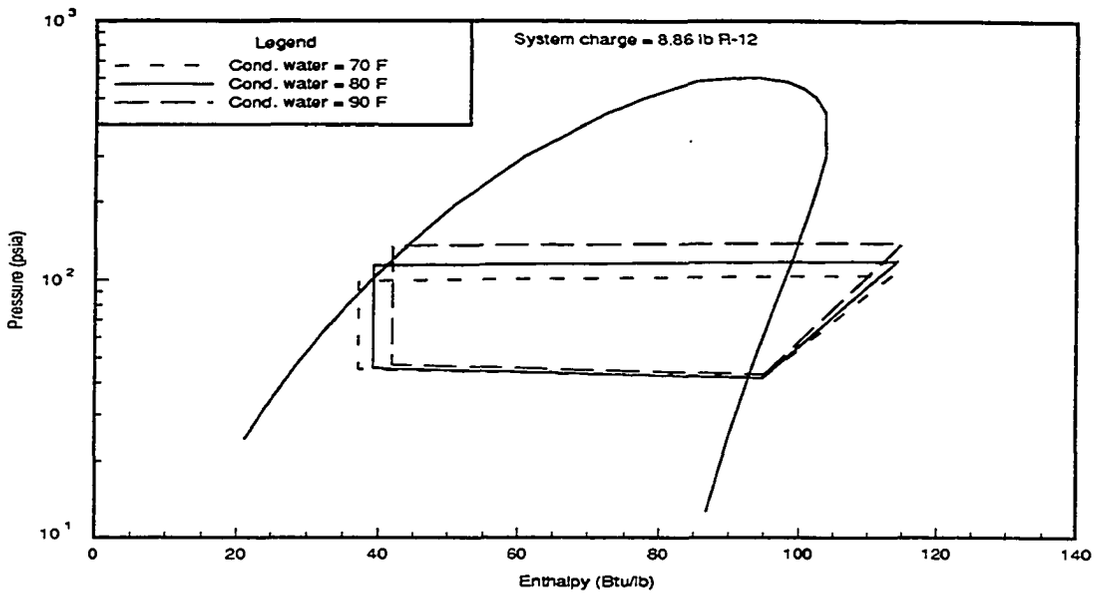

Figure 3.2: Effects of variation in condenser water temperature for R-12

Figure 3.3 shows the effect of changes in refrigerant charge for an evaporator air inlet temperature of 60°F and a condenser water inlet temperature of 80°F. Increasing the charge resulted in slight increases in condenser pressure and the amount of subcooling at the condenser exit. The enthalpy changes across all components, however, were relatively unaffected by the change in charge.

Pressure enthalpy diagrams for R-134a

The pressure enthalpy diagram showing the effect of changes in evaporator air temperature for R-134a is given in Figure 3.4. The same scale was used for the R-134a plots as was used with the R-12 plots in Figures 3.1-3.3. The enthalpy changes for the R-134a data were approximately 35% greater than for the R-134a data. However, the refrigerants had similar cooling capacities since the refrigerant mass flow rate of

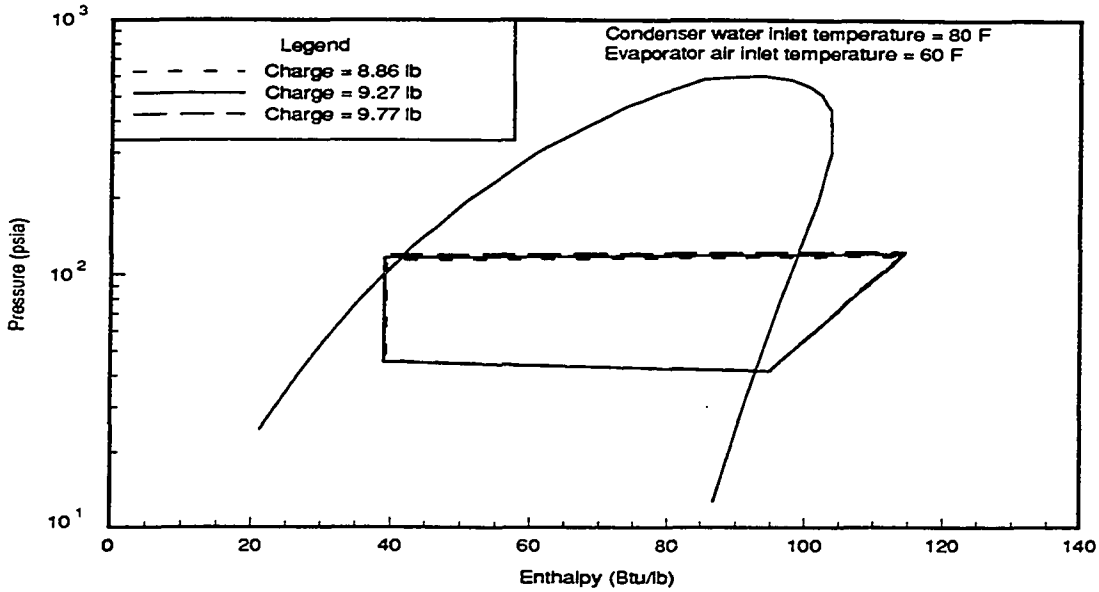

Figure 3.3: Effects of variation in system charge for R-12

the R-134a was lower than that of R-12. The effect of changes in evaporator air temperature was similar to that found with R-12.

The effect of changes in condenser water temperature for the system charged with R-134a was similar to the effect on the system with R-12. Figure 3.5 shows the effect of condenser water temperature for a constant system charge of 8.52 lb and constant evaporator air temperature of 60 F. The effect of greater changes in enthalpy for R-134a were offset somewhat by the greater mass flow rate of R-12.

The effect of changes in system charge for R-134a is shown in Figure 3.6. The condenser water temperature was held constant at 80 F and the evaporator air temperature was held constant at 60 F. Five different system charges are shown ranging from 7.42 lb to 9.60 lb. In general, the greater charges caused higher condenser temperatures and increased condenser exit subcooling. The cooling capacity and COP

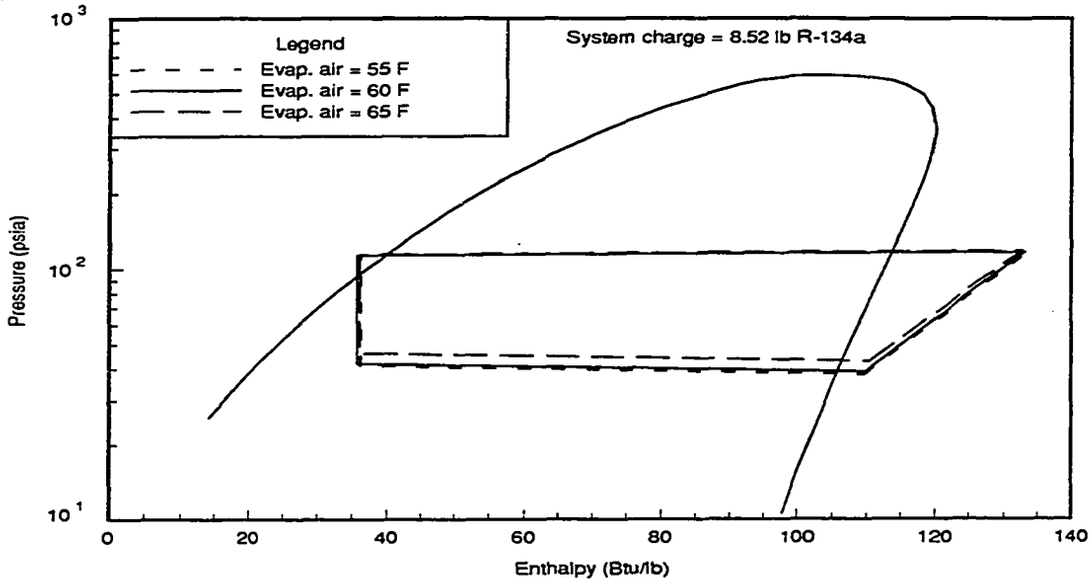

Figure 3.4: Effects of variation in evaporator air temperature for R-134a

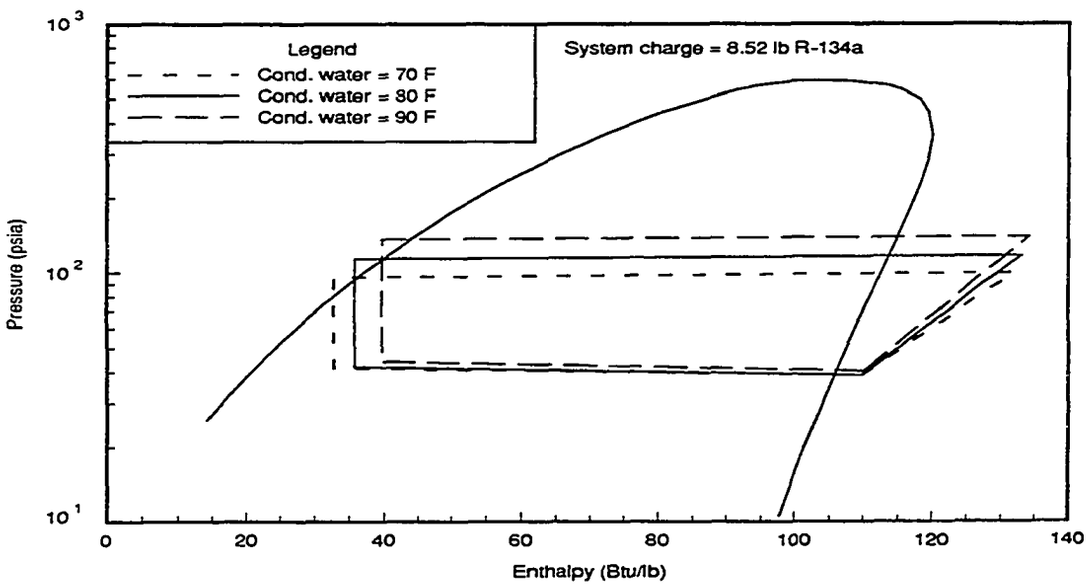

Figure 3.5: Effects of variation in condenser water temperature for R-134a

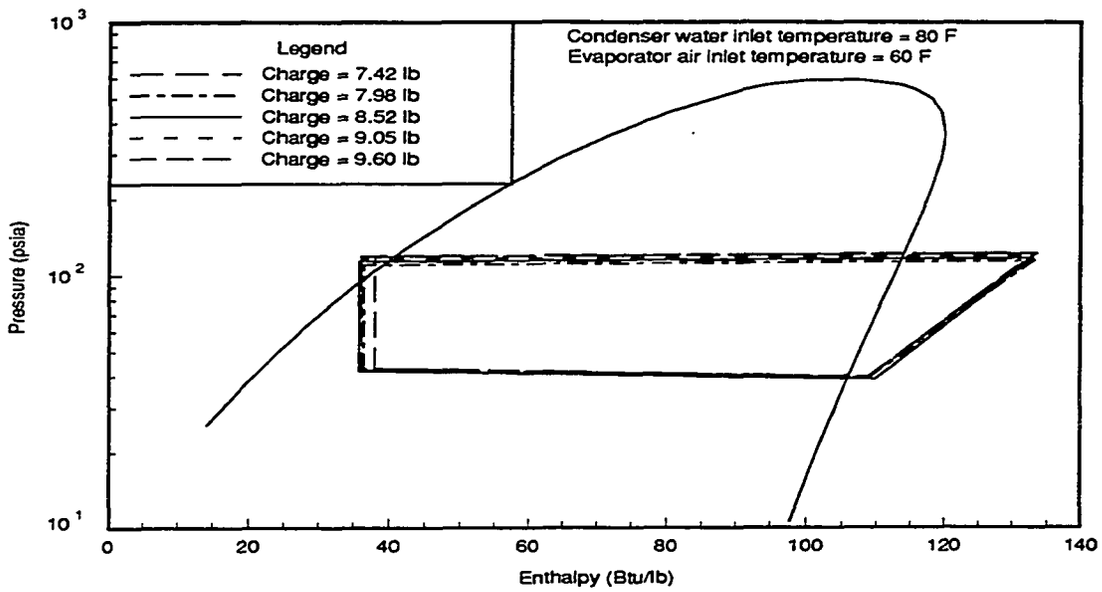

Figure 3.6: Effects of variation in system charge for R-134a

were found to have the greatest overall values near the charge of 8.52 lb. Some of the variation shown in Figure 3.6 is due to the variation in the actual water and air temperatures for each charge. The relative effect of the small variation around the nominal values is significant compared to the effect of system charge. A more accurate comparison would require curve fitting the state points at the inlet and exit of each component to the operating conditions.

Pressure enthalpy diagrams for MP-39

A pressure enthalpy diagram for the MP-39 blend is shown in Figure 3.7. The condenser water and evaporator air inlet temperatures were 80 and 60 F, respectively. The system charge was 8.86 lb. The dashed lines in Figure 3.7 show lines of constant temperature. The slight negative slope of the lines in the two phase region is due

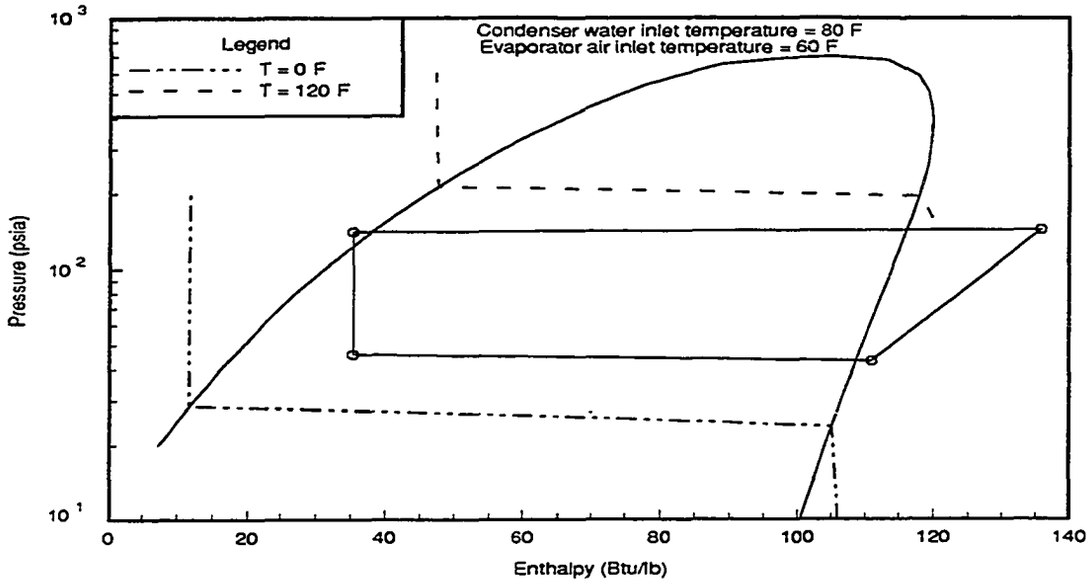

Figure 3.7: Pressure enthalpy diagram for MP-39 with constant temperature lines

to the changing composition of the refrigerant as it boils and condenses. This effect called temperature glide causes an increased temperature drop in the condenser and a temperature rise in the evaporator. The enthalpy changes were close to those observed with the R-134a data. The same scale was used on the pressure enthalpy plots for all the refrigerants.

The effect of changes in evaporator air temperature for a constant condenser water temperature of 80 F is shown in Figure 3.8. Figure 3.9 shows the effect of changes in condenser water temperature. The general effects are similar to those observed with the pure refrigerants. Changes in system charge had little observable effect on system performance.

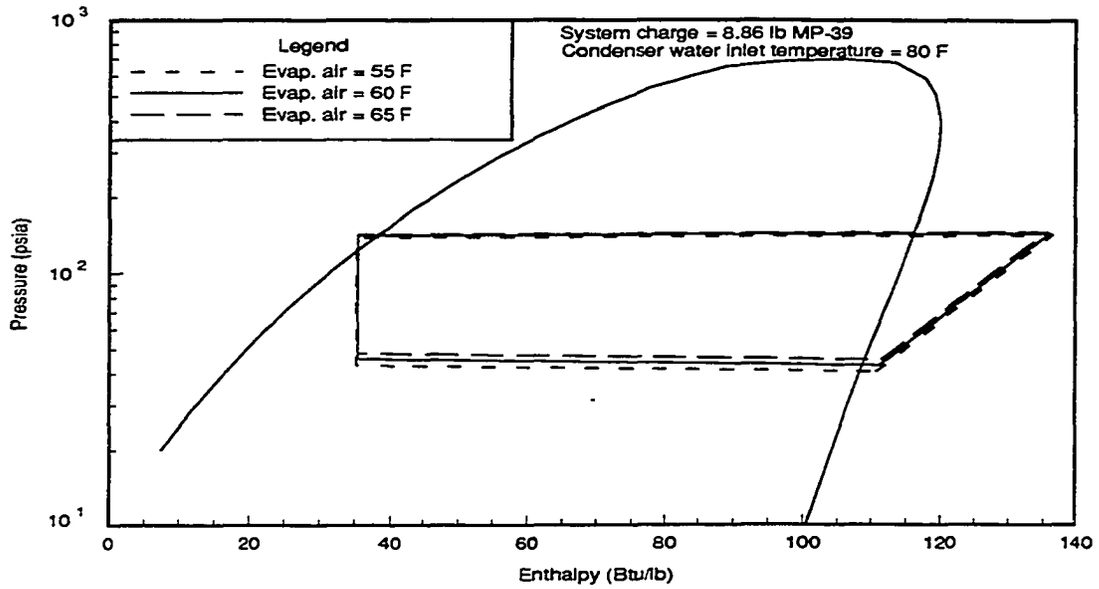

Figure 3.8: Effects of variation in evaporator air temperature for MP-39

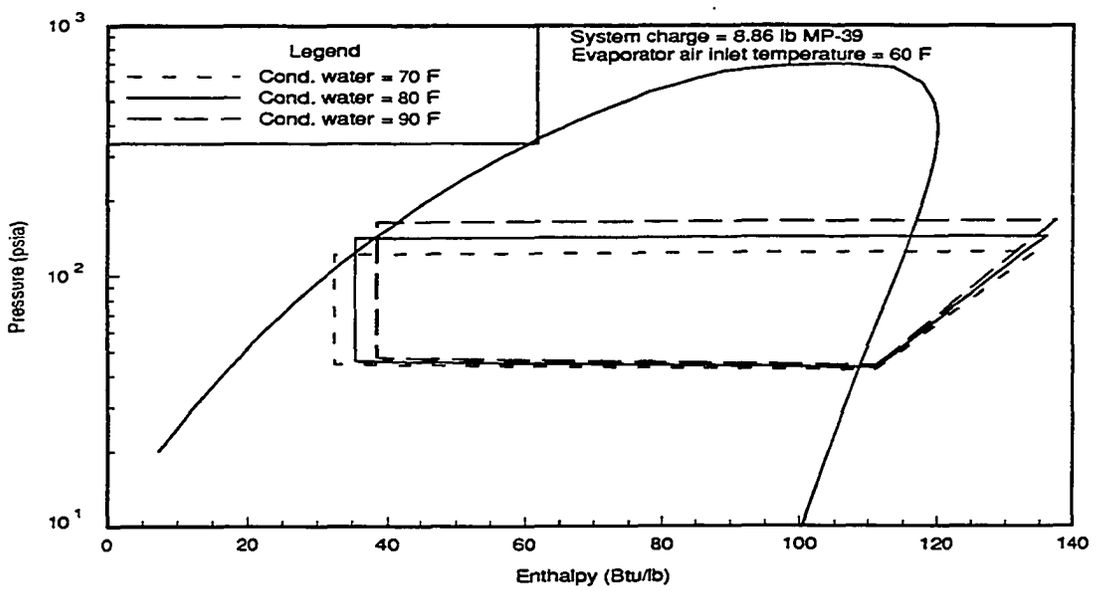

Figure 3.9: Effects of variation in condenser water temperature for MP-39

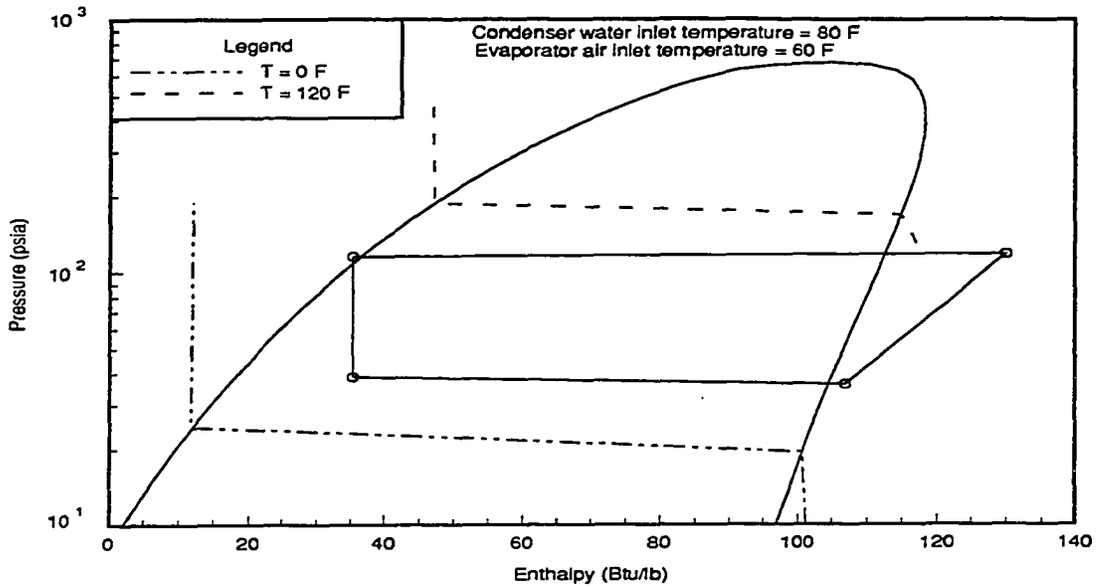

Figure 3.10: Pressure enthalpy diagram for MP-52 with constant temperature lines

Pressure enthalpy diagrams for MP-52

The pressure enthalpy diagrams for the refrigerant blend MP-52 are shown in Figures 3.10, 3.11, and 3.12. The operating pressures were substantially lower for the MP-52 data than for MP-39 under the same operating conditions. The enthalpy change in the evaporator for the MP-52 data was about 7% lower than that of MP-39. The mass flow rate was also lower giving a significantly reduced cooling capacity.

Comparison of Saturation Curves

The differences observed in system performance were due in part to the differences in the enthalpy of vaporization for the different refrigerants. A plot of the saturation curves showing pressure and enthalpy is given in Figure 3.13. Comparing the enthalpy of vaporization at equal pressures would be valid if the system operated

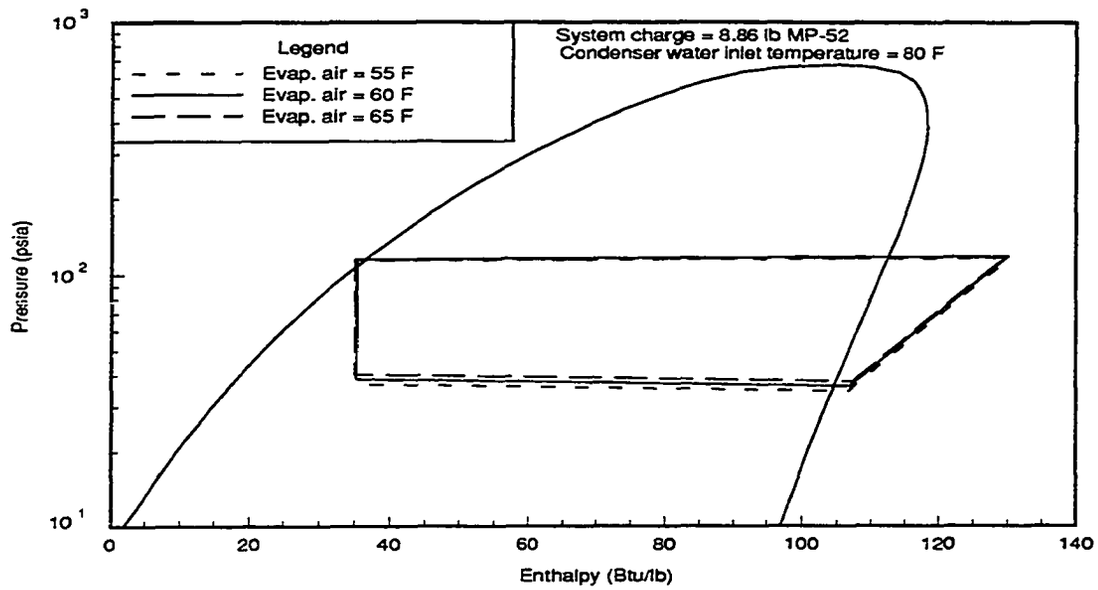

Figure 3.11: Effects of variation in evaporator air temperature for MP-52

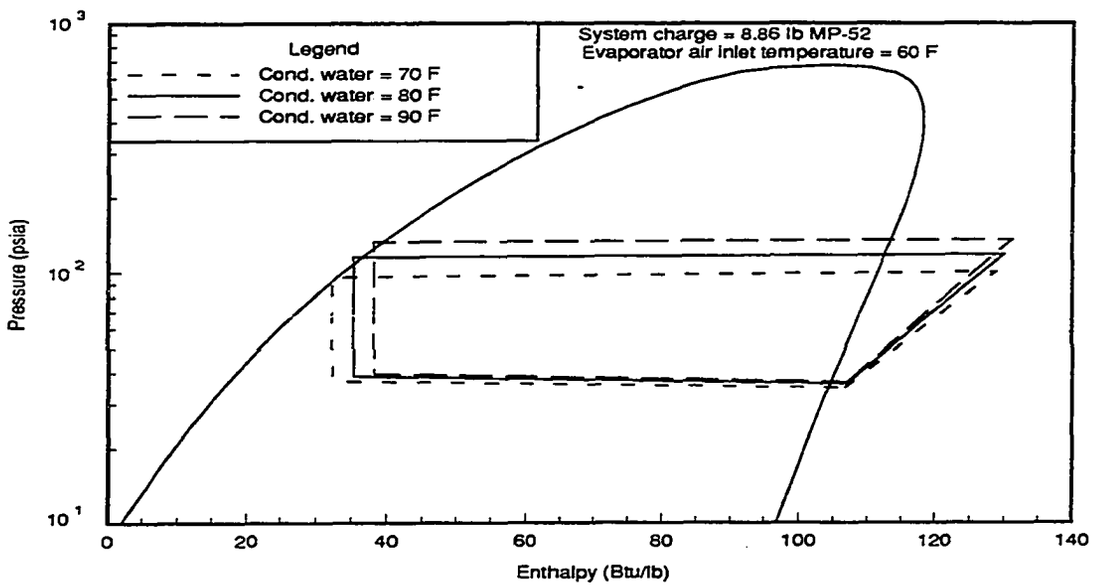

Figure 3.12: Effects of variation in condenser water temperature for MP-52

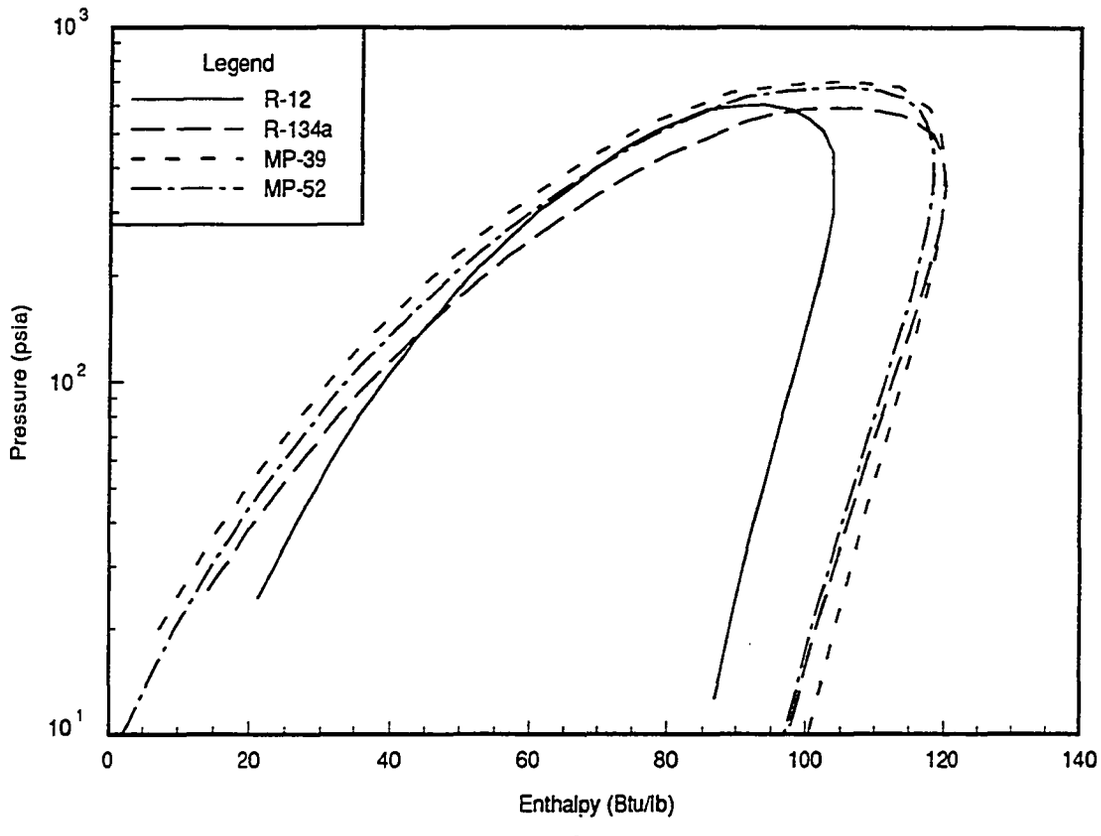

Figure 3.13: Saturation curve on pressure enthalpy coordinates

at similar pressures with different refrigerants. Comparisons at equal saturation temperatures may be more accurate if the temperature differences in the heat exchangers were similar for the different refrigerants. The data show that the condenser temperature differences were similar for the different refrigerants. Therefore, comparisons at equal temperatures would be valid. Figure 3.14 shows the saturation curves for the four refrigerants tested plotted on temperature enthalpy coordinates. The differences between Figures 3.13 and 3.14 lie in the fact that the different refrigerants have different saturation temperature pressure relationships.

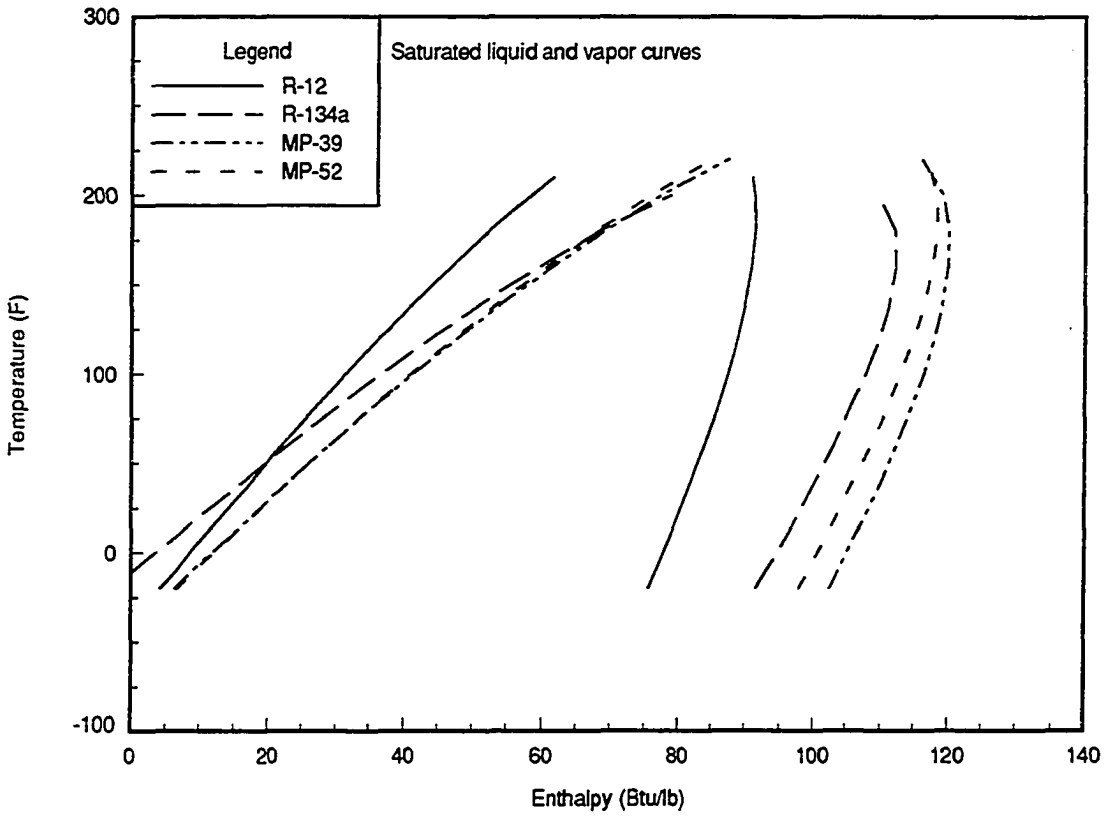

Figure 3.14: Saturation curve on temperature enthalpy coordinates

The saturation temperature enthalpy curves show that the greatest evaporator enthalpy difference occurs with MP-39. The smallest difference occurs with R-12. The capacity, however, for these two refrigerants is about equal since the flow rate of R-12 is larger. The different effect on enthalpy difference across the evaporator with the different refrigerants is due to the different slopes of the saturation curves.

The pressure enthalpy diagrams give insight as to cause of variations in COP and capacity. The pressure enthalpy diagrams, however, did not show the effect of variation in mass flow rate or heat loss through the compressor shell. The exact values of COP and capacity including these effects are presented in the following sections.

Curve Fits of System Performance

The test conditions for each refrigerant charge consisted of three nominal condenser water temperatures at each of three nominal evaporator air temperatures. Because the temperatures could not be set at specific exact values, comparisons of system performance between refrigerants would require the use of curve fits. The curve fits also give some measure of the random error associated with the experiment. With separate curve fits of the data for each refrigerant and refrigerant charge, the system performance can be compared at the nominal values or at any value within the range of operating conditions.

Control of Variable Conditions

The amount of refrigerant charge was the simplest variable to control because it was not affected by system performance. The other system variables, however

were affected by system performance. The amount of refrigerant charge added to the system was measured at the beginning of each set of data where the other conditions were varied.

The condenser water was recirculated and mixed with fresh cold water to maintain a fixed inlet temperature. The water was recirculated to reduce the amount of waste water and because water could not easily be supplied at the required condenser water flow rate. The water flow rate in the condenser was held constant at about 28 gpm. Because of the recirculation, for a fixed rate of fresh cooling water the inlet temperature would vary depending on the energy absorbed in the condenser. The variation in inlet temperature would then effect the system performance. This feedback loop responded like an underdamped second order system. Typically after 15 to 20 minutes of operation the variation would dampen out and some steady state value would be reached. If the steady state value differed from the desired set point the fresh water flow rate would be adjusted and the system would again be allowed to come to equilibrium. This process was time consuming and therefore nominal values of condenser water were used rather than exact set points.

The evaporator air had a feedback problem similar to that of the condenser water. The evaporator air was recirculated and subsequently cooled and reheated. The electric heater which controlled the evaporator air inlet temperature could be set at an exact value with a manual thermostat, but the resolution and accuracy of the dial used to adjust the set point were minimal. The temperature controller on the electric heater helped the system reach steady state faster than the uncontrolled condenser water system. The system, however, took several minutes to come to equilibrium. Therefore nominal values of evaporator air conditions were used rather

than exact set point values.

Development of Curve Fits

Since the input conditions were varied over a range of conditions it was possible to fit the performance data with the variation in the operating conditions. The condenser water temperature and evaporator air temperature were each varied individually at three nominal values (five values for the lowest charge of R-134a). The range of values for the condenser water temperature was 70 F to 90 F. The range of values for the evaporator air inlet temperature was 55 F to 65 F. Several data points were taken at repeated values of the nominal conditions to determine repeatability. Therefore a minimum of nine data points for each refrigerant and refrigerant charge were collected.

Several models were evaluated for each data set where the system COP and cooling capacity were fit with variable operating conditions. The highest order term considered for each variable is a squared term based on the results of the R-134a data where the variables were varied at five levels. The complete second order model for COP including all interactive terms is as follows:

$$COP = C_1+C_2T_w+C_3T_a+C_4T_w^2+C_5T_a^2+C_6T_wT_a+C_7T_w^2T_a+C_8T_wT_a^2+C_9T_w^2T_a^2 \quad (3.1)$$

If a data set had nine values, then the complete model would give an exact fit. The model, however, would provide no means of checking the uncertainty or error associated with the fit. For example, a curve fit of a system that varies linearly with some variable would always be shown to have curvature if the number of constants used equals the number of data. This is because any experimental observation has

some variability and the curve fit will try to fit that variability. Since the data sets have approximately nine observations a reduced model should be used.

Several of the terms of the complete model have little effect on the total error associated with the model. By starting with a simple linear model and adding terms, a simplified model which contains only significant terms may be developed. This procedure was followed for each of the data sets producing curve fits that represent the data well and still leave several degrees of freedom. This gives a check on the goodness of fit and the repeatability of the data. The measure of accuracy for the curve fits is the standard deviation. The constants were all determined based on the values that give the least sum of squares error.

Curve Fits of R-12 Data

The performance of the refrigeration system operating with R-12 must first be characterized before judgements about the alternative refrigerants can be made. Since all of the data for the alternative refrigerants is to be compared to the R-12 data, it is imperative that the curve fits of the R-12 data accurately represent the data. Every possible model up to the complete second-order model was considered and the standard deviations and correlation coefficients were compared. The models that were chosen give minimum standard deviations and are the ones for which all terms have been determined to be statistically significant.

Curve fit of COP

The best curve fit of the COP to the variable parameters (condenser water inlet temperature and evaporator air inlet temperature) requires four constants and gives

a small standard deviation. The curve fit is given as follows:

$$\mathrm{COP} = 0.1 * T_a - 3.56E-6 * T_w^2 T_a - 1.542E-5 * T_w T_a^2 + 1.136E-7 * T_w^2 T_a^2 \quad (3.2)$$

where the air temperature T_a and the condenser water temperature T_w are both given in degrees Fahrenheit. The standard deviation associated with this model is 0.006 which is less than 1% of the observed variation in COP. The standard deviation predicts that 95% of the data is represented by the curve fit plus or minus two standard deviations (0.012), assuming a normal distribution of error.

The curve fit of COP for the R-12 data is shown in Figure 3.15. The lines of lower evaporator air temperature correspond to lower COP. The COP increases approximately 7% for a 10°F increase in evaporator air temperature. A 10°F increase in condenser water temperature causes a decrease in COP of approximately 8%. The amount of refrigerant in the system has a relatively small effect on the COP.

A plot showing the three refrigerant charges of R-12 (8.86, 9.27 and 9.77 lb) is given in Figure 3.16. The variations due to the effect of refrigerant charge are much less than the observed effects of the other variables (condenser water and evaporator air temperature). For the comparisons between refrigerants the data for the minimum refrigerant charge is used since a system would typically be charged only to produce a minimal amount of condenser exit subcooling. This is the case represented by the R-12 charge of 8.86 lb. However, since the R-12 data is very similar at different levels of charge, the comparisons would not be greatly affected by this choice.

Curve fit of cooling capacity

A curve fit of cooling capacity as a function of evaporator air inlet temperature and condenser water inlet temperature is shown in Figure 3.17 for the minimum

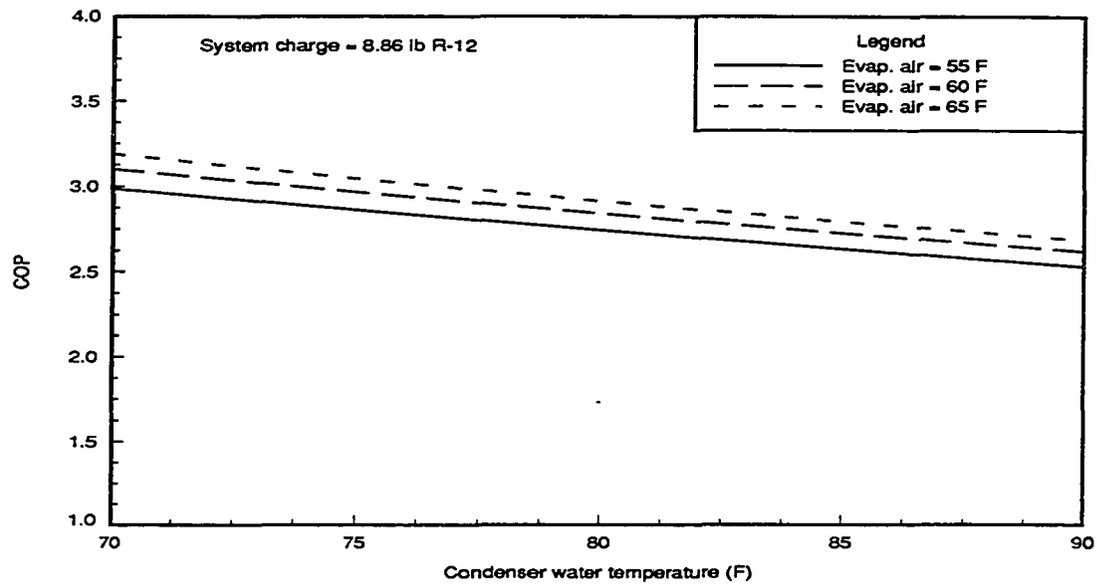

Figure 3.15: COP of R-12 as a function of operating conditions

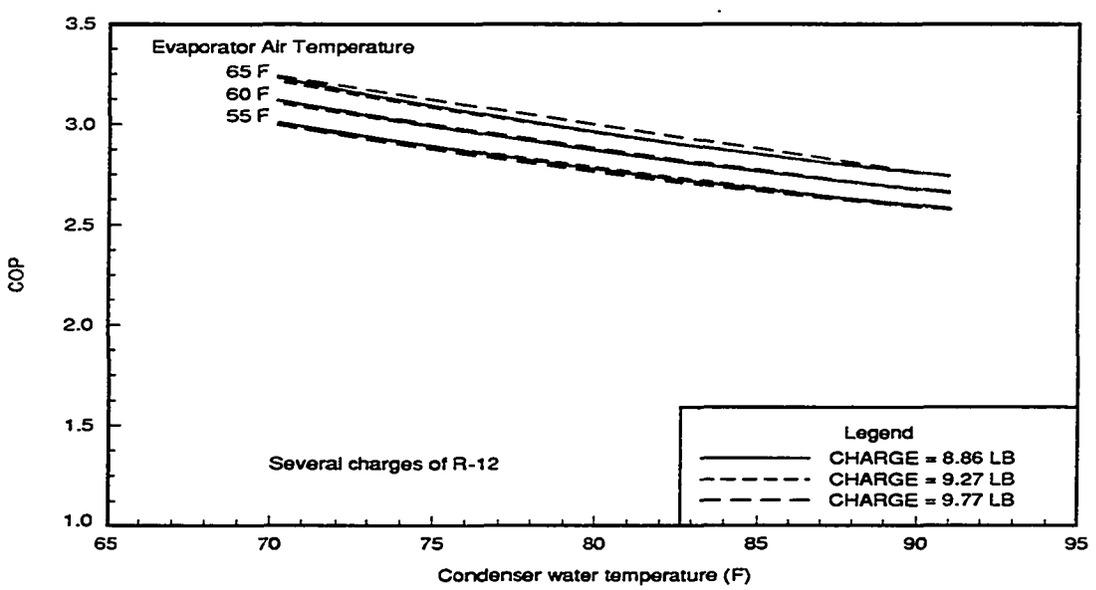

Figure 3.16: Effect of refrigerant charge on COP with R-12

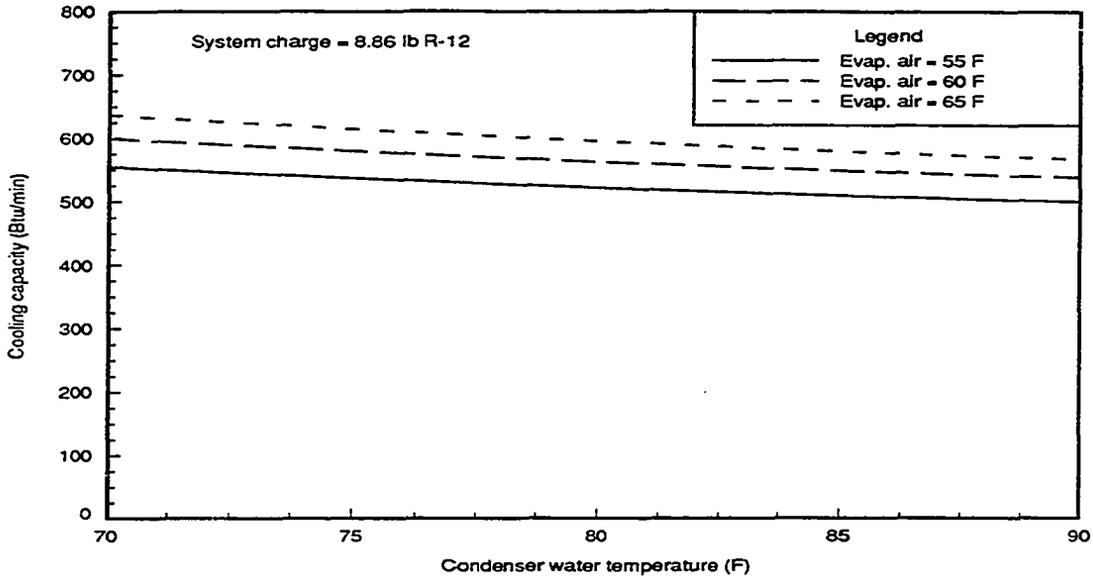

Figure 3.17: Capacity of R-12 as a function of operating conditions

charge of R-12. The curve fit for capacity is given as follows:

$$\text{Capacity} = -5.8 * T_w + 20.18 * T_a + 1.052E-3 * T_w^2 T_a - 2.042E-3 * T_w T_a^2 \quad (3.3)$$

where the capacity is in Btu/min. The standard deviation associated with the curve fit is 2.33 Btu/min which is less than 2% of the total variation observed. The behavior of cooling capacity is similar to that of COP in that the capacity increases with increasing evaporator air temperature and decreases with increasing condenser water temperature. An increase in the evaporator air temperature of 10°F causes an increase in the capacity of approximately 14%. A 10°F increase in the condenser water temperature causes a decrease in the capacity of approximately 5%. The cooling capacity is not significantly affected by the amount of refrigerant charge.

Table 3.1: COP of system with R-12 at nominal values

Condenser water (F)	Evaporator air (F) 55	60	65
70.0	2.99	3.10	3.19
75.0	2.86	2.97	3.04
80.0	2.74	2.84	2.91
85.0	2.63	2.72	2.79
90.0	2.53	2.62	2.68

Table 3.2: Capacity of system with R-12 at nominal values (Btu/min)

Condenser water (F)	Evaporator air (F) 55	60	65
70.0	554.9	599.4	636.7
75.0	536.9	579.4	614.2
80.0	521.9	562.5	595.0
85.0	509.7	548.8	579.3
90.0	500.4	538.3	566.9

Values of COP and capacity at nominal and actual conditions

Several values of COP and capacity, determined from the curve fits, are given in Tables 3.1 and 3.2. The nominal test conditions are represented in the tables along with additional condenser water temperatures of 75 and 85 F. A comparison of the curve fits with the data at actual operating conditions is presented in Tables 3.3 and 3.4 for a system charge of 8.86 lb of R-12. The measured values, predicted values based on the curve fits, and the percent difference between measured and predicted values are given for both capacity and COP.

Table 3.3: Comparison of curve fit to actual COP data

Condenser water (°F)	Evaporator air (°F)	COP		
		Measured	Predicted	% difference
89.9	55.7	2.54	2.54	0.06
80.0	55.6	2.76	2.76	-0.28
70.3	55.6	2.99	2.99	-0.00
91.0	59.3	2.58	2.59	0.23
90.3	59.1	2.60	2.60	-0.21
79.7	58.9	2.82	2.83	0.19
70.2	58.8	3.07	3.07	0.14
70.7	64.0	3.16	3.15	-0.14
80.3	64.1	2.89	2.89	0.11
89.8	64.0	2.68	2.68	-0.10

A linear model

The nearly constant slope and parallel nature of the evaporator air temperature lines shown in Figures 3.15 and 3.17 suggest that the relationship between the capacity and COP and the condenser water temperature could also be adequately represented by first order polynomials with no interactive terms. The linear equations for the complete set of R-12 data including the three system charges are given as follows:

$$\text{COP} = 3.455 + 0.01958T_a - 0.02176T_w \tag{3.4}$$

$$\text{Capacity} = 328.9 + 7.685T_a - 2.812T_w \tag{3.5}$$

The standard deviation and maximum error for the two equations are given in Table 3.5. Although the values for standard deviation of the simplified equations are about double those of the second order models, the maximum error between the measured and calculated values based on the linear equations is less than 2%. However,

Table 3.4: Comparison of curve fit to actual capacity data

Condenser water (°F)	Evaporator air (°F)	Capacity (Btu/min)		
		Measured	Predicted	% difference
89.9	55.7	505.4	506.5	0.21
80.0	55.6	530.0	527.4	-0.50
70.3	55.6	558.2	558.9	0.13
91.0	59.3	530.4	532.0	0.30
90.3	59.1	534.2	531.6	-0.50
79.7	58.9	554.3	555.4	0.20
70.2	58.8	587.1	588.7	0.27
70.7	64.0	628.6	626.1	-0.40
80.3	64.1	586.5	588.6	0.35
89.8	64.0	563.0	562.6	-0.06

Table 3.5: Statistical data for linear curve fit

	COP	Capacity (BTU/min)
Standard Deviation	0.017	4.3
Maximum Error	0.034	9.1

the small differences observed between different refrigerants necessitates that the more accurate model given in equations 3.2 and 3.3 be used for comparison purposes.

R-12 data with new compressor

After running several tests with R-22 and refrigerant blends in the original compressor used for the R-134a test, a change in performance was detected. It was later discovered that at some time during the original blend tests a compressor inlet valve had failed, leaving the compressor functioning at 1/3 capacity. Because of this failure, the compressor was replaced with an identical model and the R-12 data were retaken. Additionally, all of the blend data were rerun with the new compressor. The

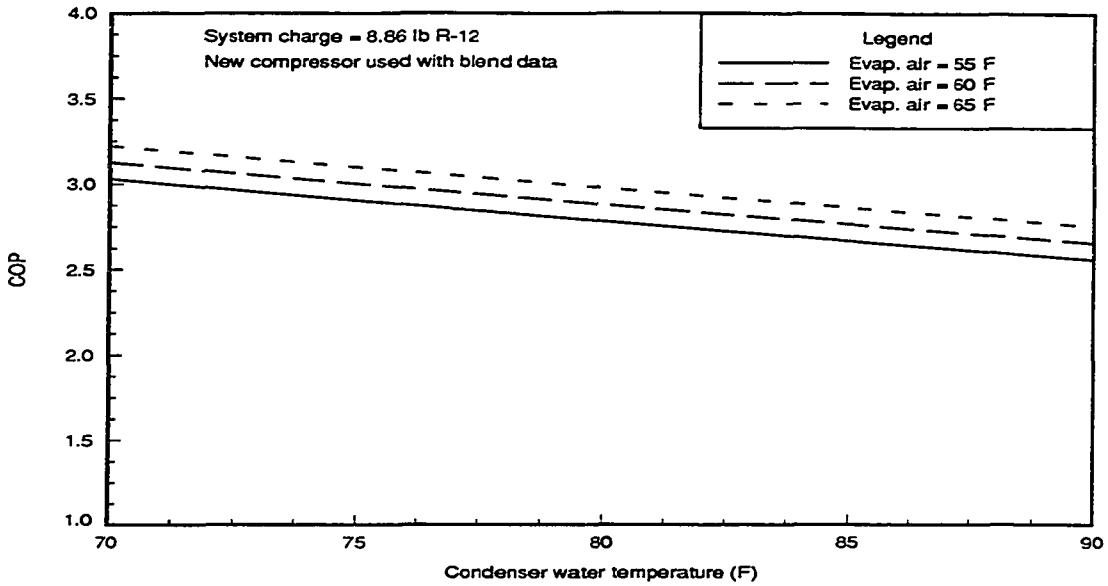

Figure 3.18: COP of R-12 in new compressor as a function of operating conditions

R-134a data is therefore compared to the original R-12 data, and the blend data is compared to the R-12 data taken with the new compressor. Since the compressors were identical, it was expected that the performance would be virtually the same with the two refrigerants. Only small differences in performance were observed between the two R-12 data sets, adding to the reliability of the R-12 results.

The curve fits of COP and capacity are shown for the new compressor in Figures 3.18 and 3.19. The standard deviation associated with the curve fits shown in Figures 3.18 and 3.19 are 0.010 and 3.48 Btu/min for the COP and capacity, respectively. The COP has very slight curvature with water temperature. The capacity was fit well with a linear model with no interactive terms. Values of COP and capacity at the nominal test values are shown in Tables 3.6 and 3.7.

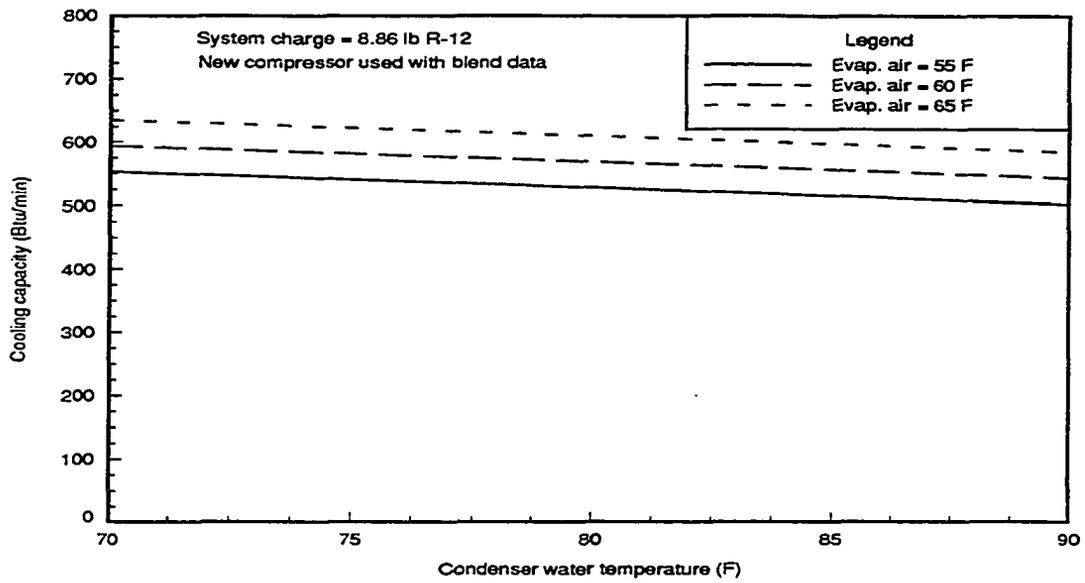

Figure 3.19: Capacity of R-12 in new compressor as a function of operating conditions

Curve Fits of R-134a Data

The R-134a behaved very much like the R-12 under the same operating conditions. Both refrigerants were affected by changes in condenser water and evaporator air temperature in much the same way. Several experiments were conducted at various levels of system charge ranging from 7.42 lb to 9.05 lb. The system charge had a much more noticeable effect with the R-134a than with R-12. The best overall performance was observed at a system charge of 8.52 lb of R-134a. This charge gave approximately 10 to 15 F subcooling at the condenser exit. Increasing the system charge increases the subcooling for operation at constant conditions. The finding that the system performed best at higher degrees of subcooling than the R-12 is consistent with the findings presented by Linton et al. [9] in a similar study. The effect

Table 3.6: COP of system with R-12 at nominal values

Condenser water (F)	Evaporator air (F) 55	60	65
70.0	3.03	3.12	3.22
75.0	2.90	3.00	3.10
80.0	2.78	2.88	2.98
85.0	2.67	2.76	2.86
90.0	2.56	2.65	2.75

Table 3.7: Capacity of system with R-12 at nominal values (Btu/min)

Condenser water (F)	Evaporator air (F) 55	60	65
70.0	553.3	594.1	634.9
75.0	540.6	581.4	622.2
80.0	527.9	568.7	609.5
85.0	515.2	556.0	596.8
90.0	502.5	543.3	584.1

of refrigerant charge on system performance was also studied by Domasceno et al. [25] and Farzad and O'Neal [26].

The performance parameters, COP and capacity, for each complete data set of the four charges of R-134a studied were correlated using a least squares curve fit. Figure 3.20 shows the curve fit of COP at the optimum charge of 8.52 lb. The curve fit of capacity is shown in Figure 3.21. Both plots show slight curvature with condenser water temperature. All of the refrigerant charges for R-134a showed only a linear effect with evaporator air temperature. The standard deviation for the curve fits at a charge of 8.52 lb are 0.016 for COP and 3.71 Btu/lb for capacity. Compared to the total variation observed over the range of test conditions, the standard deviations

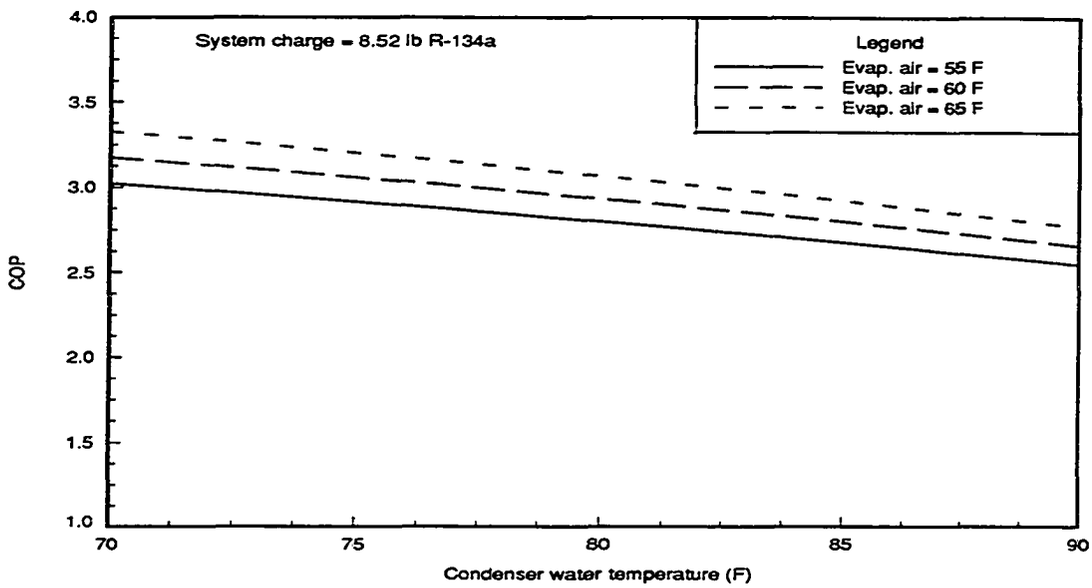

Figure 3.20: COP of R-134a as a function of operating conditions

show that the curve fits accurately represent the data. The values of COP and capacity at the nominal test conditions are shown in Tables 3.8 and 3.9. The other refrigerant charges are not shown individually, but are all compared to the R-12 data in a later section.

Curve Fits of MP-39 Data

The data for the refrigerant blend, MP-39, was also fit using a least squares method. The COP increases approximately 10% for a 10°F increase in evaporator air temperature. A 10°F increase in condenser water temperature causes a decrease in COP of approximately 9%. Compared to the variation observed with R-12, the COP for the blend is more sensitive to changes in the operating conditions. The curve fit of COP for the blend is shown in Figure 3.22. Table 3.10 gives values of COP based

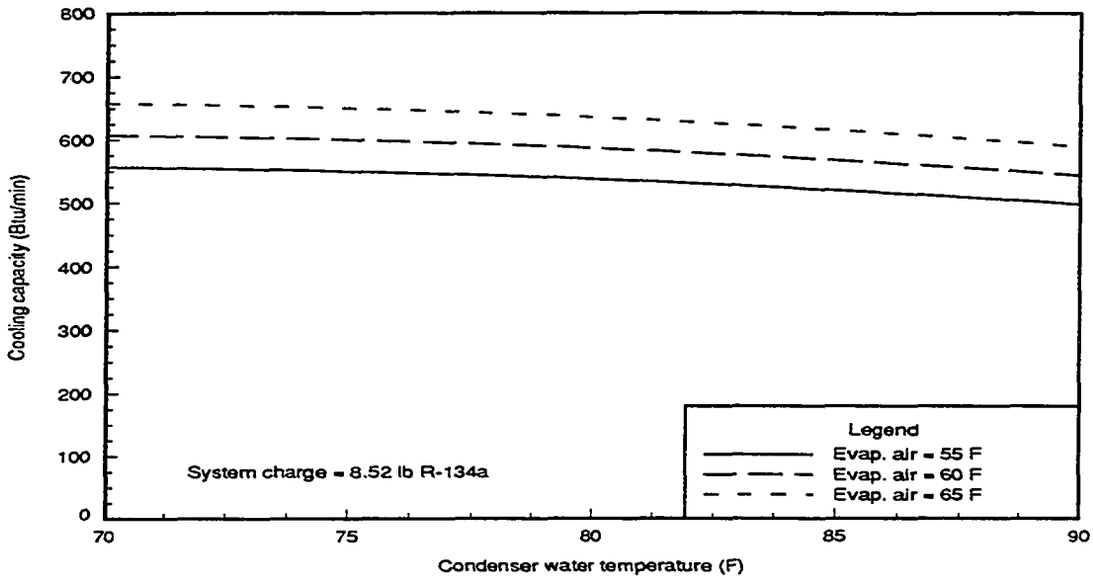

Figure 3.21: Capacity of R-134a as a function of operating conditions

on the curve fit at the nominal test conditions. The standard deviation for the curve fit is 0.009, which is about 1% of the range of values observed.

Figure 3.23 shows the curve fit of cooling capacity data for MP-39. The standard deviation is 4.18 Btu/min which is less than 3% of the total range of values. The capacity is given in tabular form in Table 3.11. The sensitivity of capacity with condenser water temperature is about the same with the blend as with R-12. Changes in evaporator air temperature, however, seem to have a greater effect on the cooling capacity of the blend. An increase in the evaporator air temperature of 10°F causes an increase in the capacity of approximately 20%.

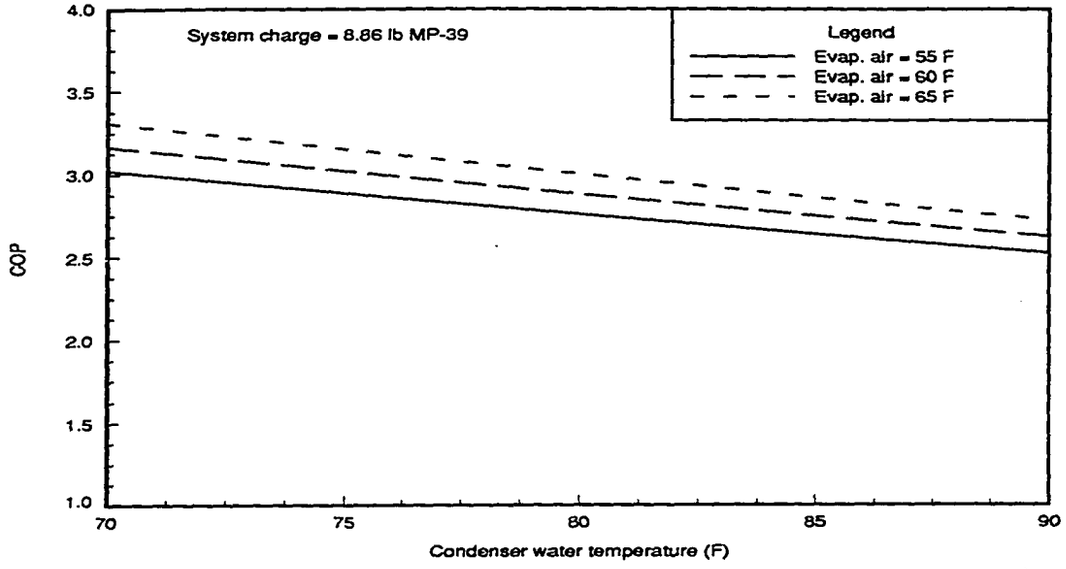

Figure 3.22: COP of MP-39 as a function of operating conditions

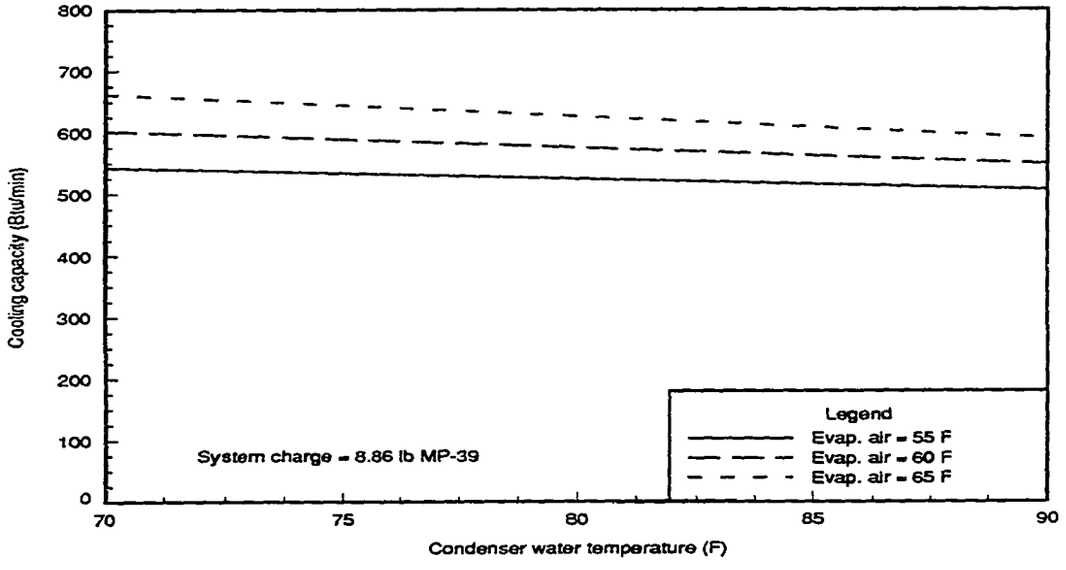

Figure 3.23: Capacity of MP-39 as a function of operating conditions

Table 3.8: COP of system with R-134a at nominal values

Condenser water (F)	Evaporator air (F) 55	60	65
70.0	3.02	3.18	3.33
75.0	2.91	3.06	3.20
80.0	2.80	2.93	3.07
85.0	2.68	2.80	2.92
90.0	2.55	2.66	2.77

Table 3.9: Capacity of system with R-134a at nominal values (Btu/min)

Condenser water (F)	Evaporator air (F) 55	60	65
70.0	556.4	607.0	657.6
75.0	549.2	599.2	649.1
80.0	537.2	586.0	634.9
85.0	520.3	567.5	614.8
90.0	498.4	543.7	589.0

Curve Fits of MP-52 Data

The mass flow rate of the second blend tested, MP-52, is about 9% lower than the flow rate with MP-39. Coupled with the fact that the enthalpy change in the evaporator is smaller, the MP-52 has a significantly lower cooling capacity. However, the COPs of the two refrigerants are about the same. A plot of the COP for MP-52 is given in Figure 3.24. The cooling capacity with MP-52 is less sensitive to changes in evaporator air temperature and has a capacity which is about 14% lower than for MP-39. Figure 3.25 shows the cooling capacity curve fit. The standard deviation for the COP and cooling capacity are 0.019 and 4.99 Btu/min, respectively. Values of the COP and capacity at the nominal test conditions are given in Tables 3.12

Table 3.10: COP of system with MP-39 at nominal values

Condenser water (F)	Evaporator air (F) 55	60	65
70.0	3.02	3.17	3.31
75.0	2.89	3.02	3.15
80.0	2.76	2.88	3.00
85.0	2.64	2.75	2.86
90.0	2.53	2.63	2.73

Table 3.11: Capacity of system with MP-39 at nominal values (Btu/min)

Condenser water (F)	Evaporator air (F) 55	60	65
70.0	542.5	602.0	661.5
75.0	533.4	588.5	643.6
80.0	524.3	575.0	625.7
85.0	515.3	561.5	607.7
90.0	506.2	548.0	589.8

and 3.13.

Confidence Intervals

Another method for determining the accuracy of the curve fits is the use of confidence intervals. Confidence intervals give limits above and below the predicted values which contain a certain percentage of the data, assuming that the error is represented by a normal distribution. Typically, a confidence interval that encloses a large percentage of the data, such as 95%, is selected so that conclusions that are statistically significant can be drawn. Differences in COP or capacity for different operating conditions larger than the 95% confidence intervals are considered statistically

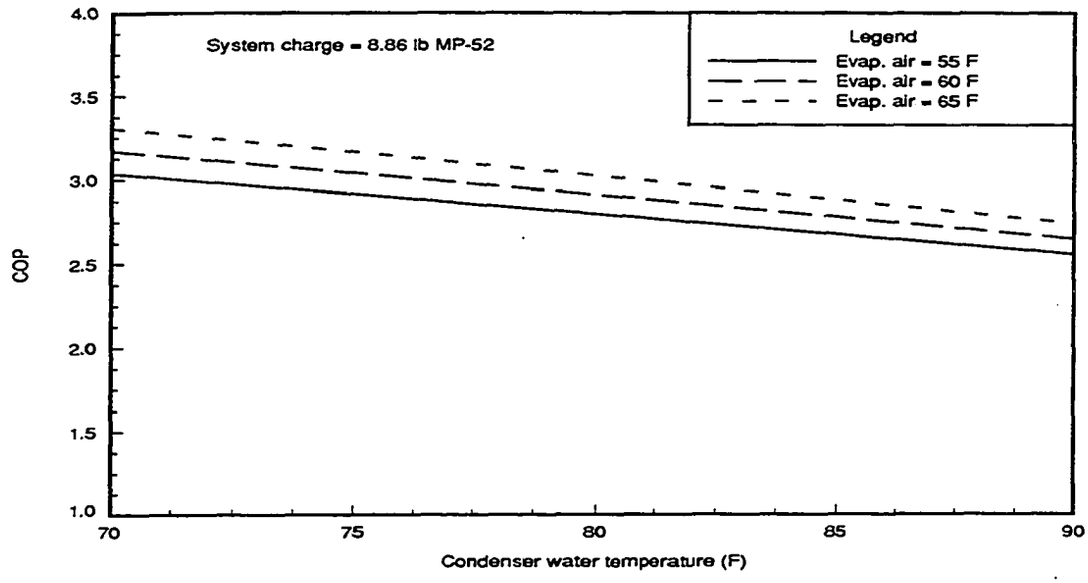

Figure 3.24: COP of MP-52 as a function of operating conditions

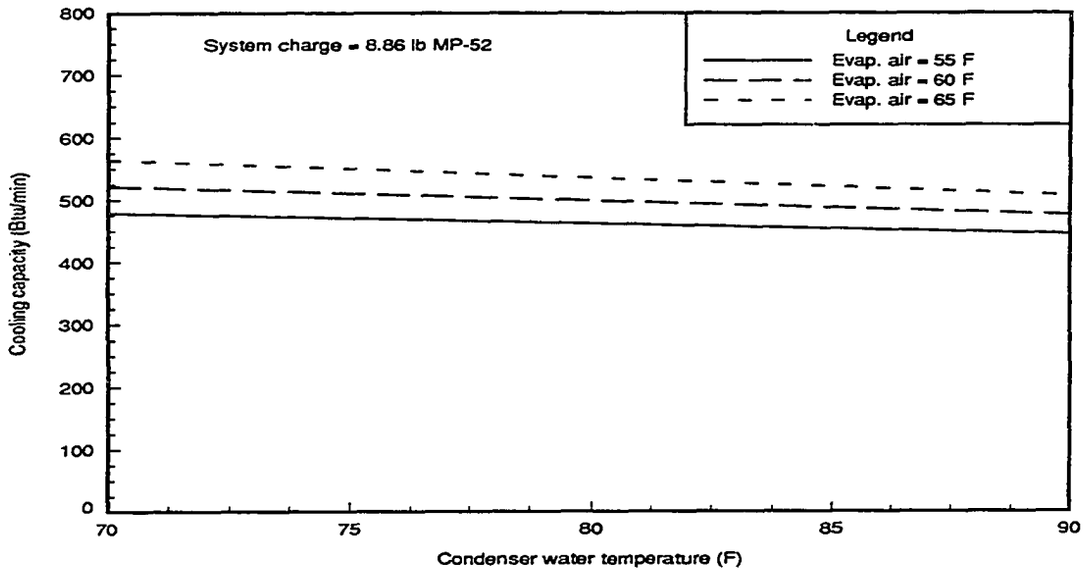

Figure 3.25: Capacity of MP-52 as a function of operating conditions

Table 3.12: COP of system with MP-52 at nominal values

Condenser water (F)	Evaporator air (F) 55	60	65
70.0	3.04	3.17	3.31
75.0	2.92	3.04	3.17
80.0	2.80	2.91	3.02
85.0	2.68	2.78	2.88
90.0	2.56	2.65	2.74

Table 3.13: Capacity of system with MP-52 at nominal values (Btu/min)

Condenser water (F)	Evaporator air (F) 55	60	65
70.0	478.8	521.4	564.1
75.0	470.4	510.1	549.8
80.0	462.0	498.7	535.5
85.0	453.6	487.4	521.2
90.0	445.2	476.0	506.9

significant.

The curve fits and 95% confidence intervals for the experimental data were calculated using a statistical package called SAS. The confidence intervals for the curve fit of COP with the R-12 data are shown in Figure 3.26. The dashed lines about each line of constant evaporator temperature are the 95% confidence interval lines. The confidence intervals show that the variation in COP associated with changes in the test conditions is statistically significant. Figure 3.27 shows a similar plot for the cooling capacity curve of the R-12 data. The curve fits of COP and cooling capacity for R-134a and the 95% confidence intervals are shown in Figures 3.28 and 3.29, respectively. When confidence intervals for the two refrigerants are compared, it

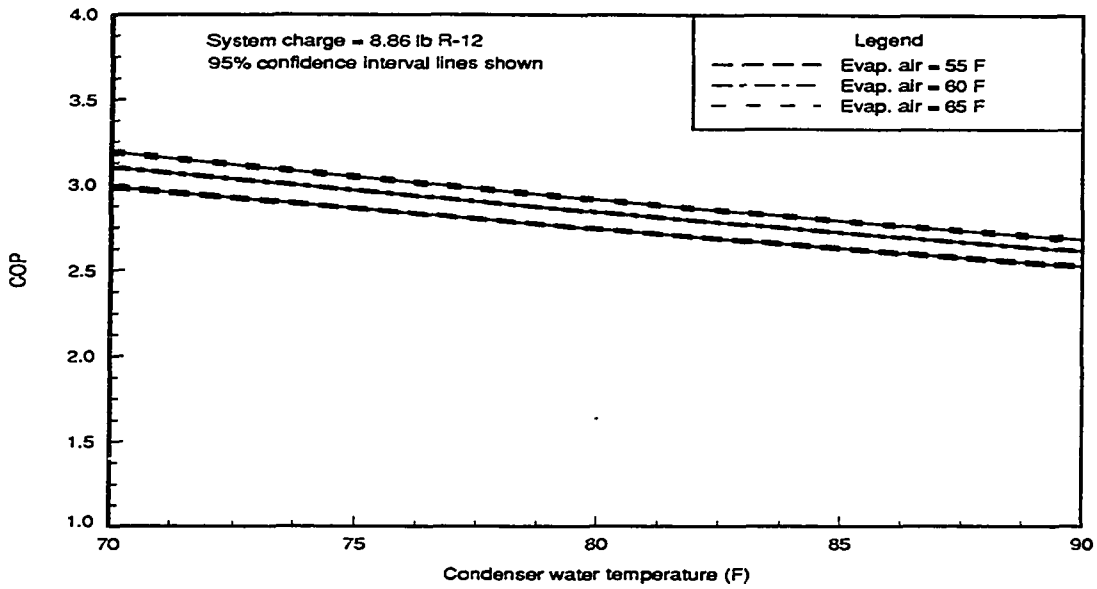

Figure 3.26: COP of R-12 with 95% confidence intervals

can be observed that the difference in performance of the two refrigerants is statistically significant. Therefore, judgements made from the data about the variation in performance due to changes in operating conditions or changes in refrigerant are statistically justified.

Comparison of Experimental Performance With Expected Behavior

The behavior of the experimental COP is consistent with trends observed in a ideal Carnot vapor refrigeration cycle where the COP of a Carnot cycle is defined as:

$$\text{COP} = \frac{T_{cold}}{T_{hot} - T_{cold}} \tag{3.6}$$

For the Carnot cycle, the COP is increased by either an increase in T_{cold} or a decrease in T_{hot}, which is the same behavior that was observed in experiments. The

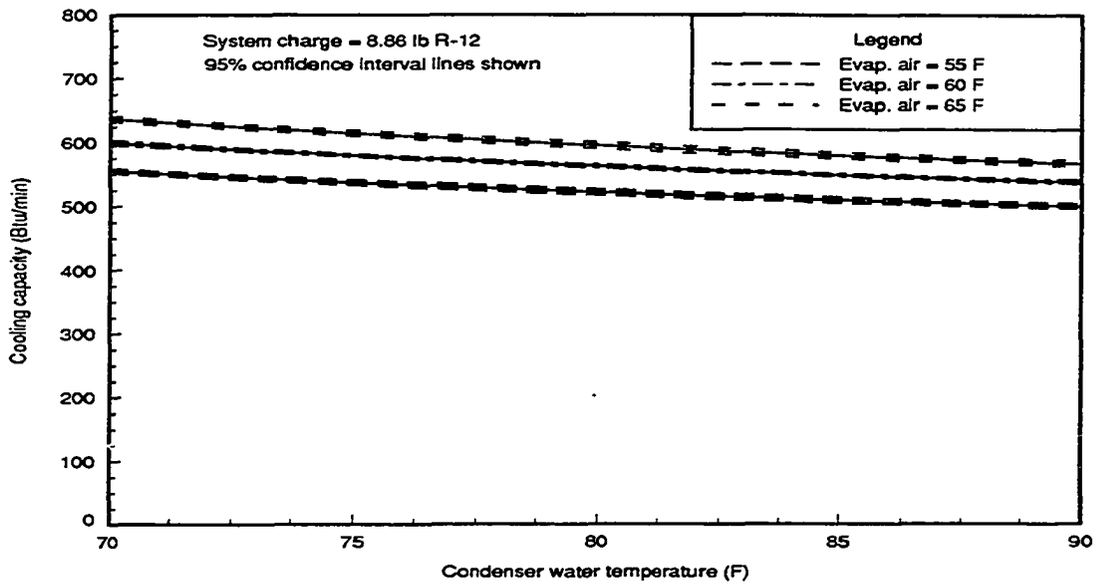

Figure 3.27: Capacity of R-12 with 95% confidence intervals

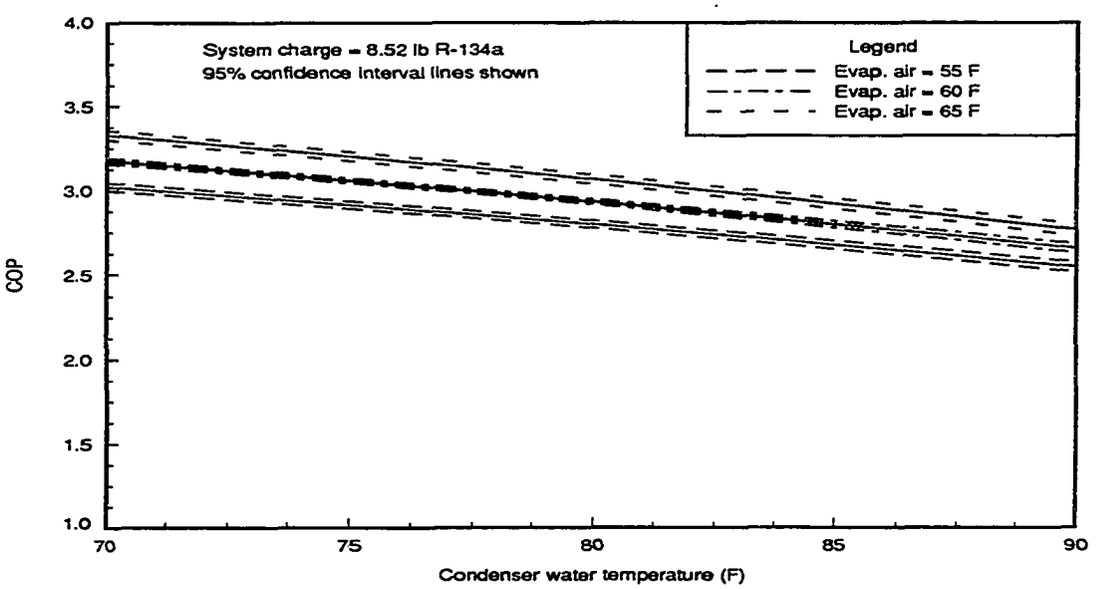

Figure 3.28: COP of R-134a with 95% confidence intervals

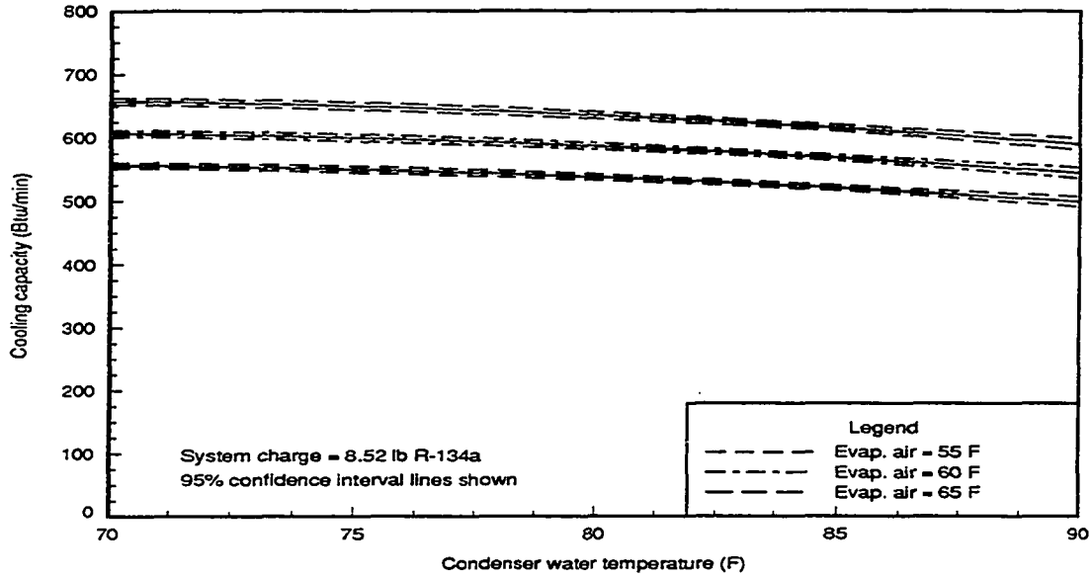

Figure 3.29: Capacity of R-134a with 95% confidence intervals

Carnot cycle COP, however predicts a much higher COP than was observed experimentally. For the nominal test condition of 90 F condenser water temperature and 55 F evaporator air temperature, the Carnot COP is calculated as:

$$\text{COP} = \frac{55 + 460}{(90 + 460) - (55 + 460)} = 14.7 \tag{3.7}$$

This value is about 6 times greater than what was observed experimentally. There are several reasons for the discrepancy. The Carnot cycle assumes that the heat transfer in the condenser and evaporator occurs at constant temperature equal to the corresponding air and water temperature. Both of these conditions are violated in the heat exchangers, especially in regions outside of the two-phase region. The Carnot cycle also assumes isentropic expansion and compression, which do not occur in the real system. However, the ideal Carnot cycle does give limits to system performance and shows that the data follows expected trends.

A simple ideal refrigerant specific model that could also be used to predict trends is sometimes called the reversed Rankine cycle. This model is used by Devotta [11] to predict the efficiency of alternative refrigerants. The reversed Rankine cycle assumes constant pressure processes in the heat exchangers, isentropic compression, and isenthalpic expansion. This model gives results consistent with the observed trends, but does not account for non-ideal conditions of the actual system (i.e. exchanger pressure drops and temperature differences etc.).

The behavior of the cooling capacity as a function of evaporator air temperature and condenser water temperature is also consistent with the ideal models. For the reversed Rankine cycle, the enthalpy change in the evaporator decreases with increasing condenser temperature. This is true because of the positive slope of the saturated liquid line on a temperature enthalpy plot. A plot of the saturation curves on temperature enthalpy axes is shown in Figure 3.14. For a constant displacement compressor the mass flow rate would remain constant since the inlet state is constant. Therefore, the cooling capacity ($\text{Capacity} = \Delta h_{evap} * \dot{m}$) is inversely related to the condenser temperature. Increasing the evaporator temperature increases both the mass flow rate and the evaporator enthalpy change since the saturated vapor line has a positive slope on a temperature enthalpy plot. The cooling capacity is therefore increased by raising the evaporator temperature which is consistent with experimental observations.

Conclusions

As previously discussed, the data could not be taken at precisely repeated test conditions. Therefore, comparisons of performance required the use of curve fits of

the experimental data for each refrigerant. The relatively small changes in system performance between refrigerants require that the curve fits accurately represent the data. Simple curve fits which fit each data set very well were found using various terms of a second order model. The standard deviation associated with the curve fits were generally less than 2% of the total range of values observed. The response of system behavior to the operating conditions was similar among the different refrigerants, but not exactly the same. These differences in response are the primary reason for testing the refrigerants under a variety of test conditions. Comparisons of refrigerants depend in part on the operating conditions selected.

The observed trends in system performance were consistent with ideal refrigeration models. The pressure enthalpy diagrams also provide insight as to variation in system performance with changes in operating conditions. Several observations were made from an analysis of the pressure enthalpy diagrams which are summarized as follows:

- Increases in the evaporator air temperature caused little change in the condenser but raised the evaporator pressure and increased the COP and the refrigerant mass flow rate. The increase in mass flow rate was due to the increased density at the compressor inlet associated with the rise in pressure.

- Changes in the condenser water temperature greatly affected the condenser pressure and the evaporator inlet quality. The condenser exit subcooling remained fairly constant.

- The significant differences in enthalpy change across the evaporator and their effect on performance were made evident in the diagrams.

- The effect of temperature glide for the refrigerant blends was illustrated with lines of constant temperature superimposed on pressure enthalpy diagrams.

The models of system performance and observations made from the pressure enthalpy diagrams help to validate the experimental data presented. The models and trends observed are also helpful in that they allow for general assertions to be made about performance under different operating conditions or with different refrigerants.

CHAPTER 4. COMPARISONS OF SYSTEM PERFORMANCE AMONG ALTERNATIVE REFRIGERANTS

Introduction

The curve fits of the experimental data given in Chapter 3 allow comparisons in system performance to be made with regard to choice of refrigerant. Although there are several possible ways to compare system performance, an obvious choice is to compare the performance of different refrigerants based on the same evaporator air inlet temperature and condenser water inlet temperature. This approach has validity because in an actual system the sink temperatures would be fixed.

Comparisons based on equivalent refrigerant temperatures, as is often done in theoretical analyses, would not be useful. This is because the temperature differences in the condenser and evaporator vary with the choice of refrigerant based on the differing flow rates and heat transfer coefficients [27]. For the R-12 data, the average temperature difference in the condenser between the two phase refrigerant and the condenser water was about 10 F, and the average temperature difference between the two phase refrigerant in the evaporator and the evaporator air was about 23 F. The temperature differences vary depending on operating conditions and choice of refrigerant. This is especially true for the refrigerant blends where the temperature profiles are very different than for the pure refrigerants because of temperature glide.

The objective of an air conditioning or refrigeration system is to provide a desired rate of cooling at an acceptable efficiency. Optimum performance is therefore based on both the cooling capacity and COP. Mapping the performance of each refrigerant over a range of operating conditions (e.g. refrigerant charge, evaporator sink temperature, condenser sink temperature, etc.) is crucial for the following reasons:

- Since the capacity and COP cannot both be optimized simultaneously, their values must be determined for all possible operating conditions in order to make accurate comparisons.
- Changing seasons and load conditions cause the evaporator and condenser temperatures to vary, which in turn affect system performance. Varying the evaporator and condenser inlet temperatures, as was done for the data presented, accounts for these changes in operating conditions.

In short, it is more useful and accurate to make comparisons that take all system variables into account. The system variables which were held constant for all tests (evaporator air flow rate, condenser water flow rate, and evaporator exit superheat) were shown to have little effect on system performance.

Calculation of COP and Capacity Ratios

The coefficient of performance for each refrigerant is compared to that of R-12 under the same operating conditions. The ratio of values are used in the comparisons to show the fractional change in performance. For example, the COP ratio for R-134a is calculated as:

$$\text{COP Ratio} = \frac{\text{COP}_{\text{R-134a}}}{\text{COP}_{\text{R-12}}} \tag{4.1}$$

where the the COPs are evaluated at the same test conditions using the curve fits for COP. The cooling capacities of the two refrigerants were compared in the same manner as the COPs, where ratios are used to evaluate differences in performance. The cooling capacity ratio for R-134a is calculated as:

$$\text{Capacity Ratio} = \frac{\text{Capacity}_{\text{R-134a}}}{\text{Capacity}_{\text{R-12}}} \tag{4.2}$$

Values greater than unity represent an increase in performance by using R-134a in the system. Values less than unity represent a decrease in performance with R-134a. These ratios are calculated at the nominal evaporator air temperatures of 55, 60 and 65 F for a range of condenser water temperatures. The ratios, showing the relative performance of each refrigerant compared to R-12, can then be plotted as functions of operating conditions.

Since identical operating conditions were difficult to achieve, the ratios are calculated based on the curve fits for each refrigerant. The uncertainty in the original curve fits, which accounts for all random error and any lack of fit, must then be carried over to the uncertainty in the calculation of ratios. By representing the ratio with a Taylor series expansion and neglecting second order and higher terms, the variance of the ratio may be determined. By this method of analysis it was determined that the differences in system performance for the various nominal test conditions were valid statistically. The variance for a difference is defined as [28]:

$$\text{Variance for a difference} = \sigma_1^2 + \sigma_2^2 \tag{4.3}$$

where σ^2 is the local variance which may be determined from the confidence intervals. The variance for a ratio is calculated as:

$$\text{Variance for a ratio} = \sigma_1^2/E_2^2 + \sigma_2^2 * E_1^2/E_2^4 \tag{4.4}$$

where E is the expected value for each refrigerant given by the curve fit.

The variance for the COP ratio with R-134a at a condenser water temperature of 80 F and a evaporator air temperature of 60 F is calculated as:

$$\text{Variance for COP ratio} = 0.006^2/2.84^2 + 0.0025^2 * 2.93^2/2.84^4 = 5.3E-5 \quad (4.5)$$

The variance for the ratio of cooling capacity with R-134a under the same test conditions is calculated similarly as:

$$\text{Variance for Capacity ratio} = 1.98^2/562.5^2 + 1.03^2 * 586^2/562.5^4 = 1.6E-5 \quad (4.6)$$

The standard deviation is defined as the square root of the variance. The standard deviations for the COP and capacity ratio at the test condition given are then 0.0023 and 0.004 respectively. Larger values are obtained at the boundaries of the test conditions because of the larger variance in those regions. With this method, confidence intervals were calculated for the ratios with R-134a. The variation in performance observed with changes in the operating conditions was determined to be statistically significant.

Comparison Ratios for R-134a

Plots of the COP ratio at four different levels of refrigerant charge of R-134a are shown in Figures 4.1-4.4. Values of the COP ratio are given at the nominal test conditions for the different charges of R-134a in Tables 4.1- 4.4. At the lower refrigerant charges the greatest difference in performance occurs at the higher condenser water temperatures. This peak shifts to the lower water temperatures for increased levels of charge. Increasing the evaporator air temperature caused a relative increase in COP

Table 4.1: COP ratios of system with 7.42 lb of R-134a

Condenser water (F)	Evaporator air (F) 55	60	65
70.0	0.994	1.001	1.015
75.0	1.006	1.012	1.027
80.0	1.013	1.019	1.034
85.0	1.016	1.021	1.034
90.0	1.013	1.015	1.026

Table 4.2: COP ratios of system with 7.98 lb of R-134a

Condenser water (F)	Evaporator air (F) 55	60	65
70.0	0.999	1.008	1.024
75.0	1.007	1.016	1.032
80.0	1.013	1.021	1.037
85.0	1.016	1.023	1.038
90.0	1.017	1.021	1.034

for all the refrigerant charges. In all cases, the COP with R-134a was greater than that of R-12 for the majority of test conditions. The lowest COP ratio observed with R-134a was only 0.99. This value occurred at the highest condenser water temperature, the lowest evaporator air temperature and the highest charge. The data show that for the operating conditions tested one could expect to see increased system efficiency with R-134a especially if charge is optimized. Several researchers have observed a "crossover point" in efficiency at low evaporator temperatures [8] [9]. This is consistent with the experimental findings presented here. The curvature of the COP ratios suggest lower efficiency with R-134a at low evaporator temperatures.

A comparison of the performance of different charges shows that the charge of 8.52 lb of R-134a displayed the greatest improvement in COP over the range of

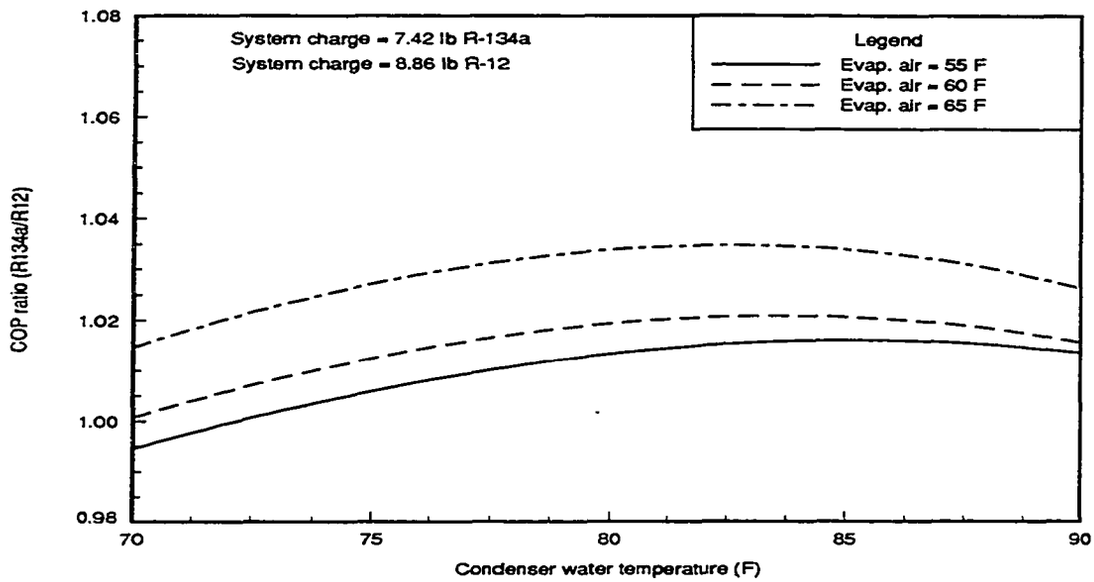

Figure 4.1: COP ratio as a function of operating conditions for a system charge of 7.42 lb of R-134a

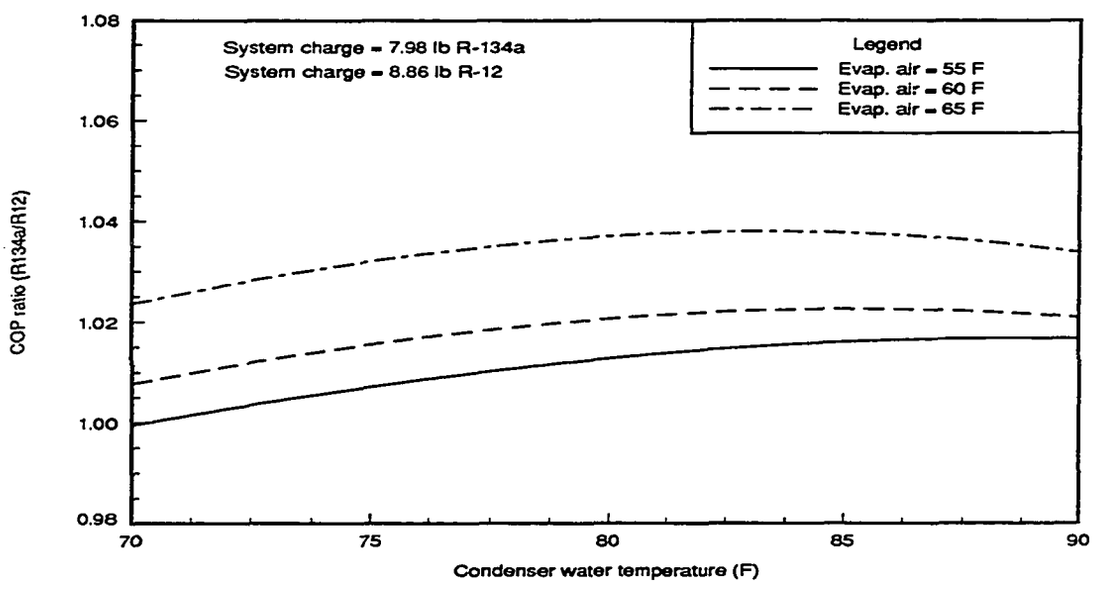

Figure 4.2: COP ratio as a function of operating conditions for a system charge of 7.98 lb of R-134a

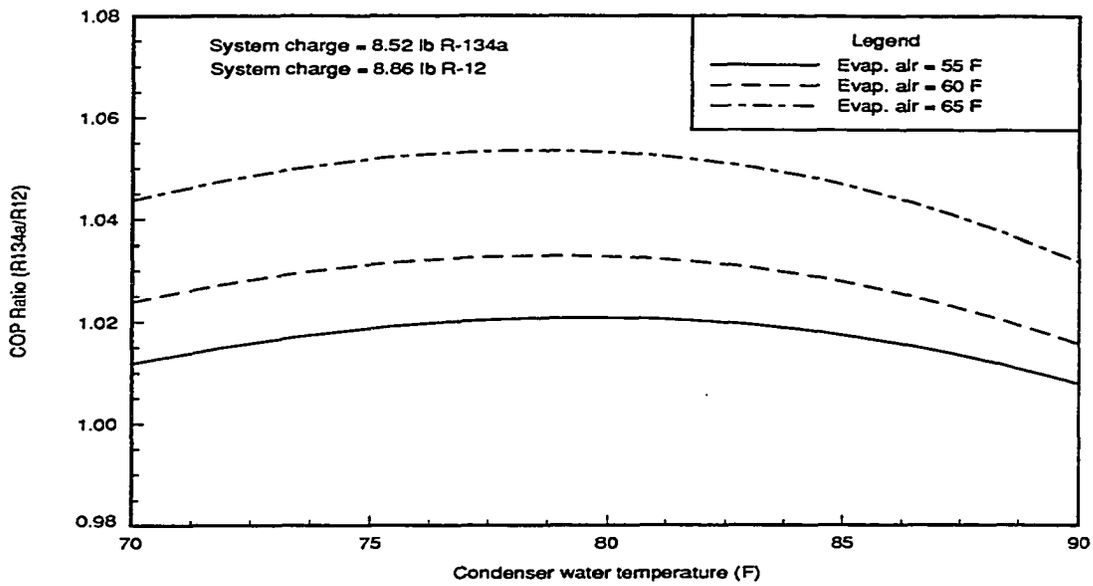

Figure 4.3: COP ratio as a function of operating conditions for a system charge of 8.52 lb of R-134a

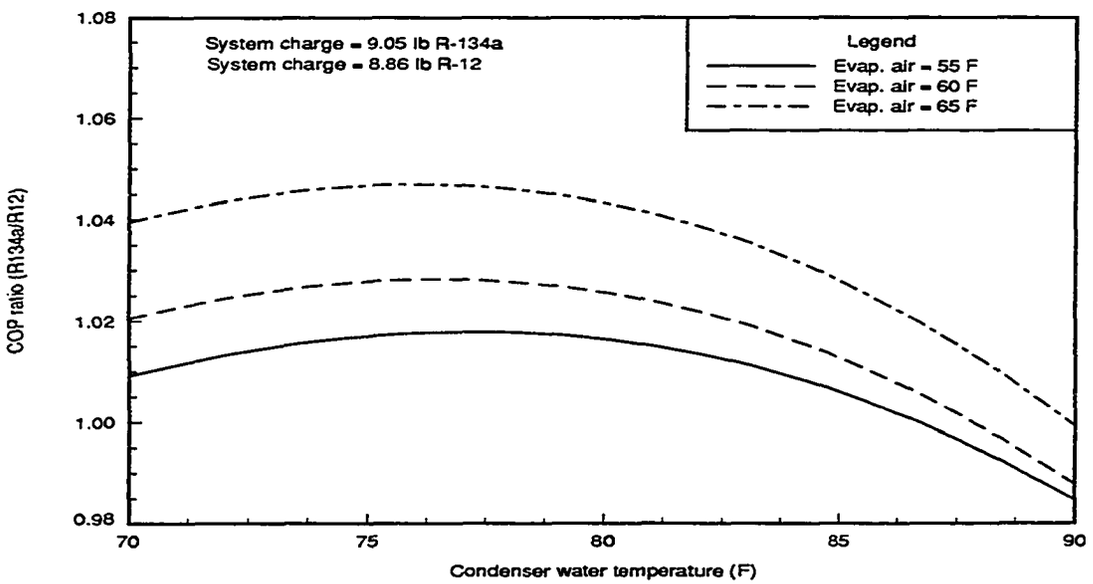

Figure 4.4: COP ratio as a function of operating conditions for a system charge of 9.05 lb of R-134a

Table 4.3: COP ratios of system with 8.52 lb of R-134a

Condenser water (F)	Evaporator air (F) 55	60	65
70.0	1.012	1.024	1.044
75.0	1.019	1.031	1.052
80.0	1.021	1.033	1.053
85.0	1.017	1.028	1.047
90.0	1.008	1.016	1.032

Table 4.4: COP ratios of system with 9.05 lb of R-134a

Condenser water (F)	Evaporator air (F) 55	60	65
70.0	1.009	1.020	1.039
75.0	1.017	1.028	1.047
80.0	1.016	1.026	1.043
85.0	1.006	1.013	1.028
90.0	0.985	0.988	0.999

operating conditions. This is true except at the highest condenser water temperatures where the lower charges showed slightly increased performance. Figure 4.5 shows the curve fits of COP for the different charges superimposed. The evaporator air temperature shown in Figure 4.5 is 60 F. At a charge of 8.52 lb, which is approximately 20% higher than the charge required to produce minimal subcooling, the subcooling varied from 10 to 15°F. At this charge the COP of R-134a varied between 0 to 5% above that of R-12 for the same conditions. The greatest differences occurred at the highest evaporator air temperatures.

Plots of cooling capacity for different refrigerant charges of R-134a are shown in Figures 4.6-4.9. The cooling capacity ratios are also given at the nominal test values for each refrigerant charge in Tables 4.5- 4.8. The same shift in peak values

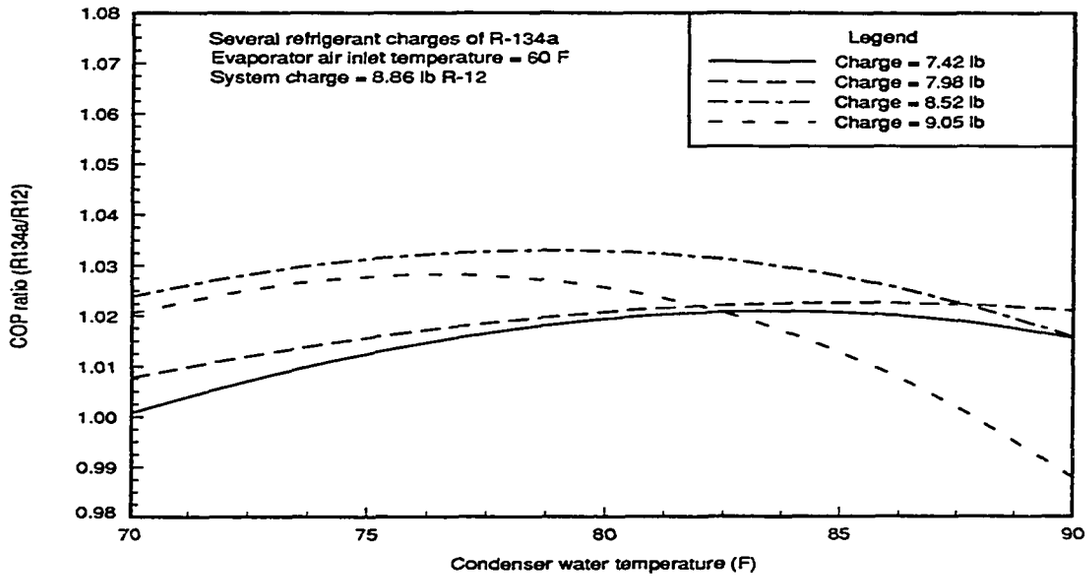

Figure 4.5: COP ratio as a function of operating conditions and system charge of R-134a

that was observed with the COP occurred with capacity. The peak capacity relative to R-12 shifted toward lower condenser water temperatures with increasing charge. The capacity ratios at an evaporator air temperature of 60 F are shown for all the refrigerant charges in Figure 4.10. The greatest differences in performance occurred at the highest evaporator air temperatures. As with COP, a charge of 8.52 lb of R-134a gave the greatest increase in performance over the entire range of conditions however, every other charge showed higher capacities at some condition. For the charge of 8.52 lb of R-134a the ratio of capacities varied between 0.98 and 1.07 with a majority of the curve showing a greater capacity with R-134a.

The increase in COP and cooling capacity of the refrigeration system charged with R-134a suggests that from a performance standpoint, the refrigerant is a good substitute for R-12. Other factors, however, must be considered in choosing a re-

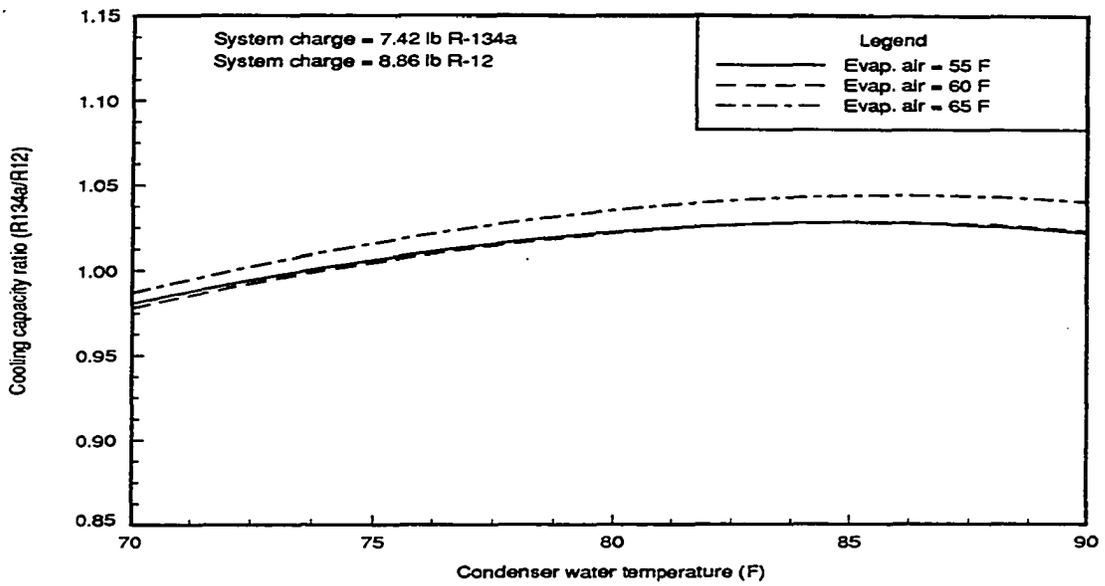

Figure 4.6: Capacity ratio as a function of operating conditions for a system charge of 7.42 lb of R-134a

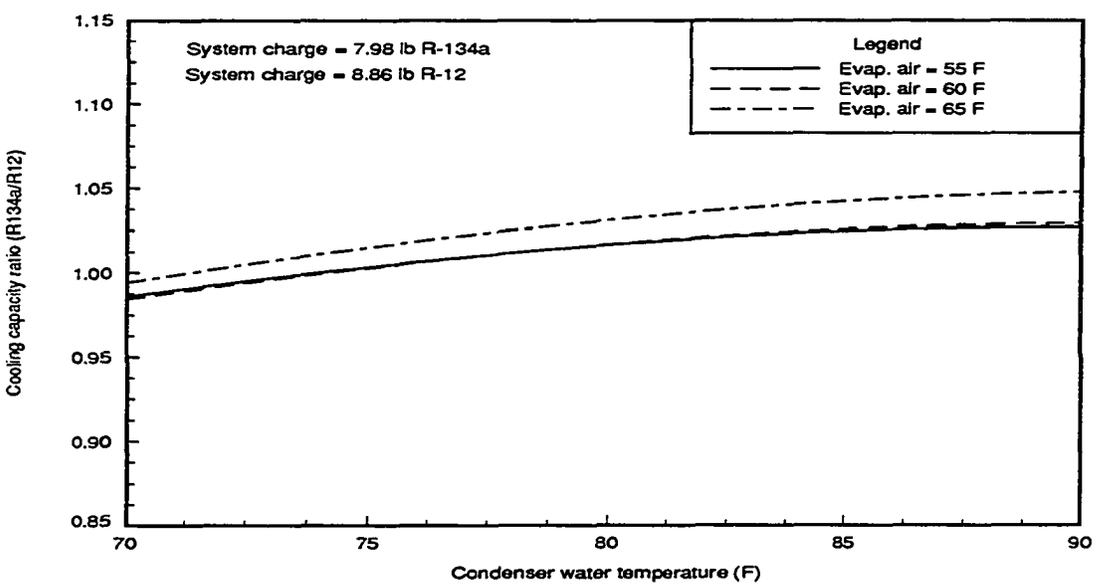

Figure 4.7: Capacity ratio as a function of operating conditions for a system charge of 7.98 lb of R-134a

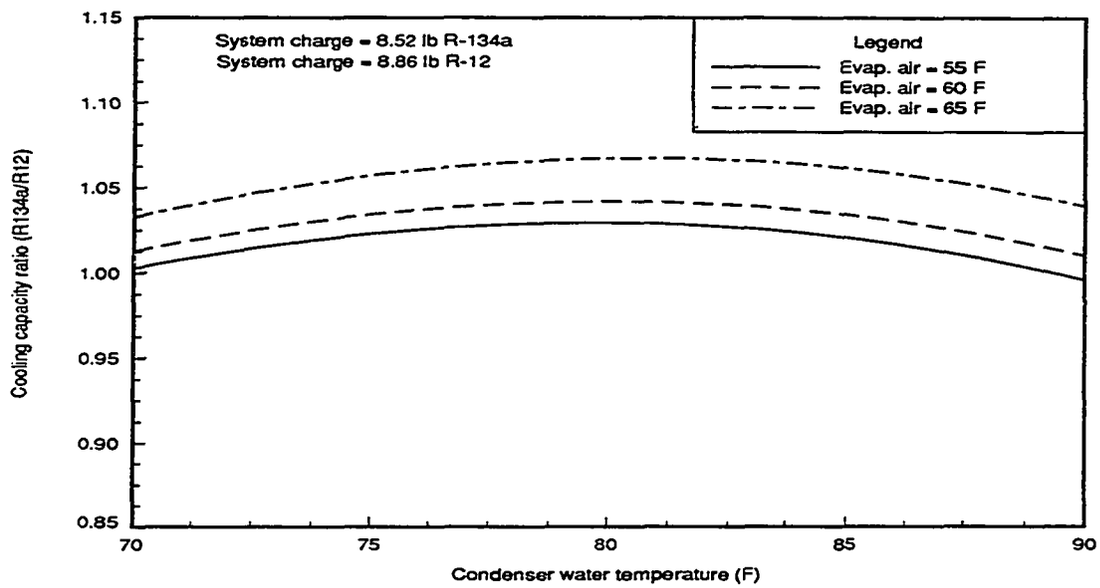

Figure 4.8: Capacity ratio as a function of operating conditions for a system charge of 8.52 lb of R-134a

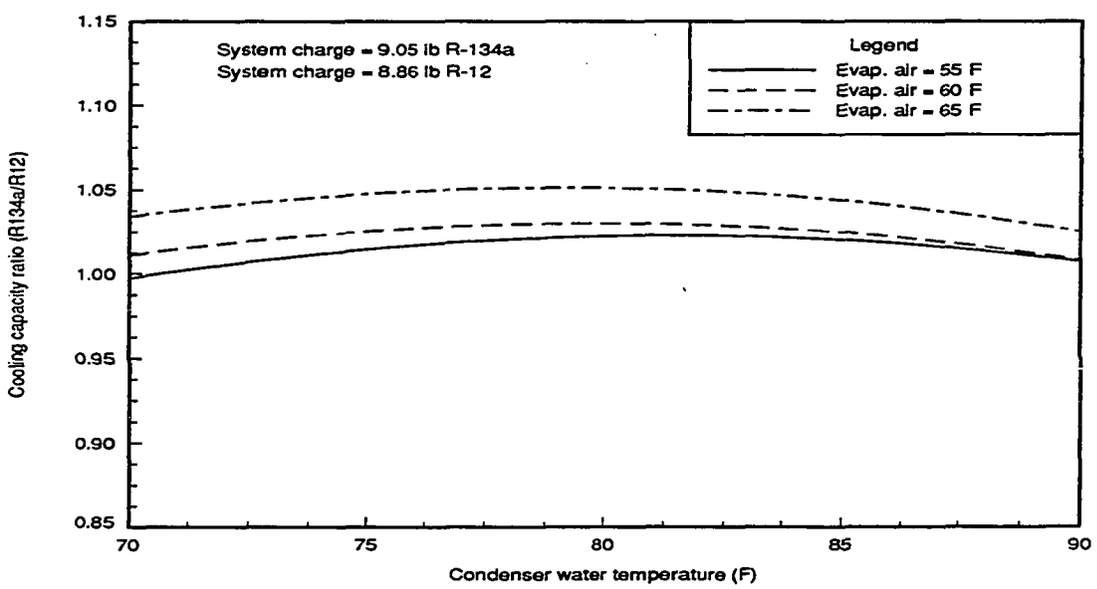

Figure 4.9: Capacity ratio as a function of operating conditions for a system charge of 9.05 lb of R-134a

Table 4.5: Capacity ratios of system with 7.42 lb of R-134a

Condenser water (F)	Evaporator air (F) 55	60	65
70.0	0.980	0.978	0.987
75.0	1.006	1.005	1.016
80.0	1.022	1.022	1.035
85.0	1.028	1.028	1.044
90.0	1.022	1.023	1.040

Table 4.6: Capacity ratios of system with 7.98 lb of R-134a

Condenser water (F)	Evaporator air (F) 55	60	65
70.0	0.986	0.984	0.994
75.0	1.003	1.003	1.015
80.0	1.016	1.017	1.031
85.0	1.025	1.026	1.042
90.0	1.027	1.029	1.048

placement refrigerant. For example, chemical compatibility with lubricants and other system components and performance under other operating conditions. Corr et al. [29] conducted a compressor life-time study considering material compatibility for an R-12 system recharged with R-134a. The results showed an increase in COP and capacity and good system compatibility. The system charge and operating conditions have effects on system performance. Models which are used to compare the performance of R-12 and R-134a must account for these effects if differences in performance are to be predicted.

Table 4.7: Capacity ratios of system with 8.52 lb of R-134a

Condenser water (F)	Evaporator air (F) 55	60	65
70.0	1.003	1.013	1.033
75.0	1.023	1.034	1.057
80.0	1.029	1.042	1.067
85.0	1.021	1.034	1.061
90.0	0.996	1.010	1.039

Table 4.8: Capacity ratios of system with 9.05 lb of R-134a

Condenser water (F)	Evaporator air (F) 55	60	65
70.0	0.997	1.011	1.034
75.0	1.014	1.025	1.048
80.0	1.022	1.030	1.051
85.0	1.020	1.025	1.044
90.0	1.007	1.008	1.025

Comparison Ratios for MP-39

The performance of the refrigeration system charged with MP-39 was very similar to that with R-12. The COP ratios for different operating conditions are shown in Figure 4.11. The COP ratio with MP-39 varied from about 0.99 at the highest condenser water temperature to 1.03 at the lowest condenser water temperature. As with the R-134a data, the relative performance of MP-39 was greater for higher evaporator air temperatures. The COP ratios at the nominal test conditions are also given in Table 4.9. The effect of refrigerant charge was determined to be insignificant for the refrigerant blends. The same system charge (8.86 lb) was used for the two blends tested as was used with R-12.

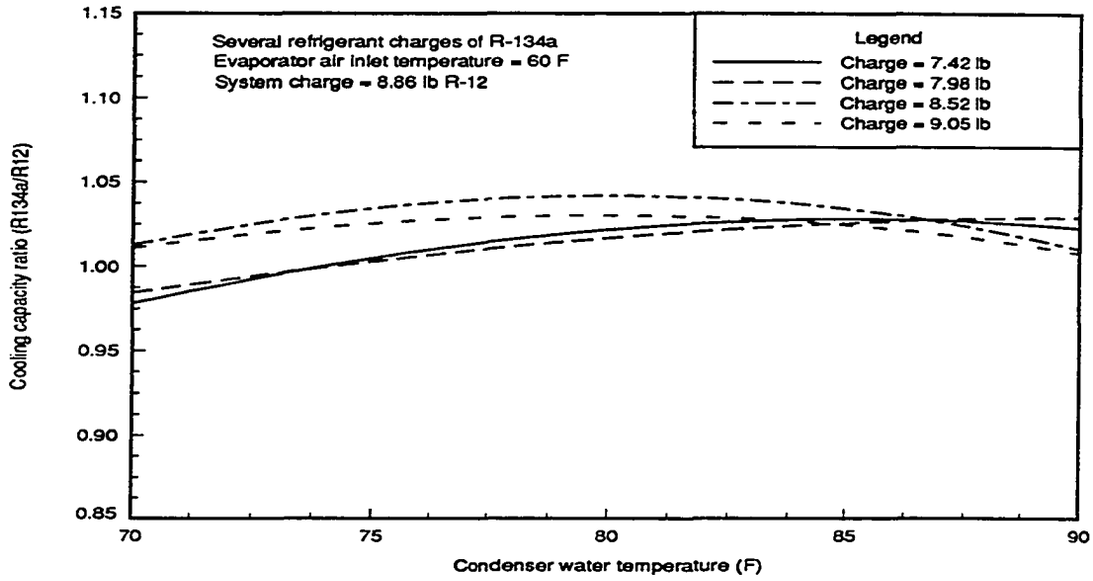

Figure 4.10: Capacity ratio as a function of operating conditions and system charge of R-134a

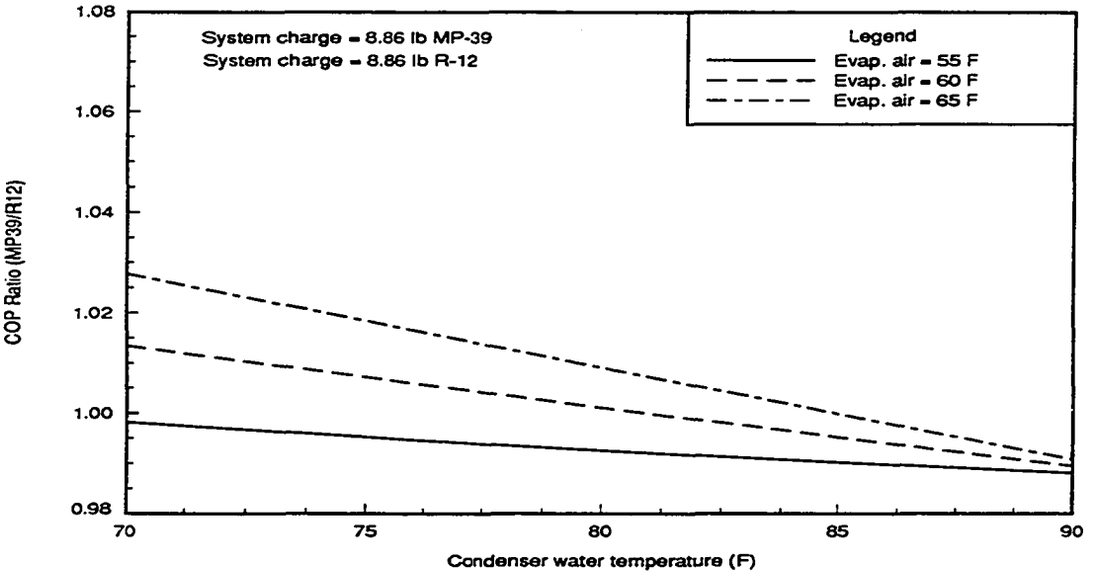

Figure 4.11: COP ratio as a function of operating conditions for MP-39

Table 4.9: COP ratios of system with 8.86 lb of MP-39

Condenser water (F)	Evaporator air (F) 55	60	65
70.0	0.998	1.013	1.028
75.0	0.995	1.007	1.018
80.0	0.993	1.001	1.009
85.0	0.990	0.995	1.000
90.0	0.988	0.989	0.991

Table 4.10: Capacity ratios of system with 8.86 lb of MP-39

Condenser water (F)	Evaporator air (F) 55	60	65
70.0	0.980	1.013	1.042
75.0	0.987	1.012	1.035
80.0	0.993	1.011	1.027
85.0	1.000	1.010	1.018
90.0	1.007	1.008	1.010

The curves of cooling capacity ratio at constant evaporator air temperature for MP-39 are shown in Figure 4.12. The data is presented in tabular form in Table 4.10. The capacity ratio varied from 0.98 at the lowest evaporator air temperature to 1.04 at the highest. The average COP with MP-39 for all the test conditions is slightly greater than with R-12. The refrigerant blend gave comparable system performance over the range of conditions tested.

Comparison Ratios for MP-52

The COP ratios of the refrigerant blend, MP-52, were greater than for MP-39 at all the test conditions. The cooling capacity ratios, however, were about 12% lower.

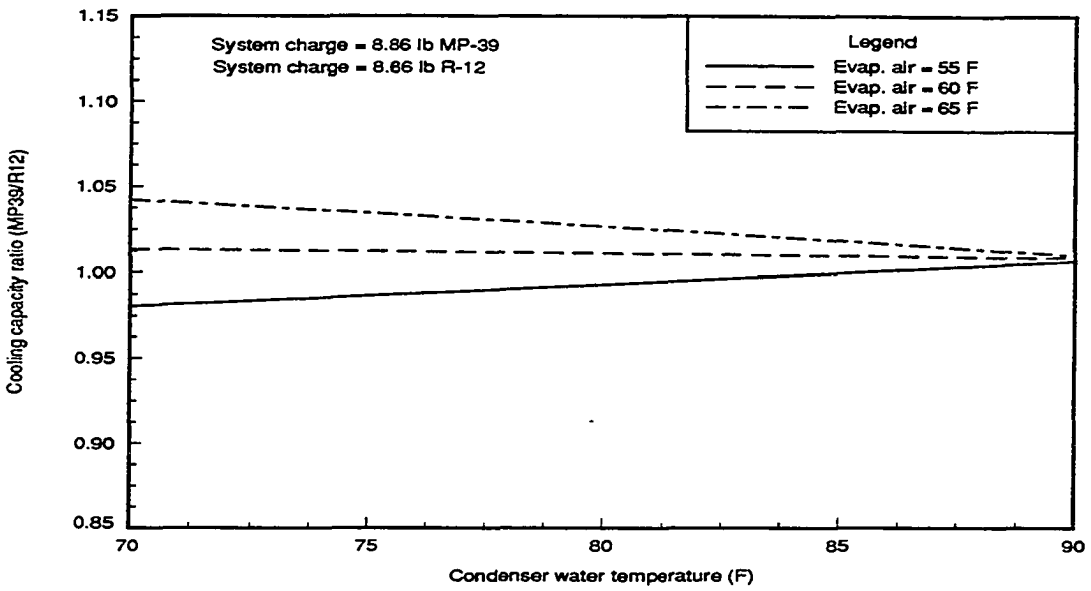

Figure 4.12: Capacity ratio as a function of operating conditions for MP-39

The COP ratios for MP-52 at the nominal evaporator air temperatures are shown in Figure 4.13 and Table 4.11. The COP ratios varied from about 1.00 at the highest condenser water temperature to 1.03 at the lowest. The relative performance of COP was greater with the higher evaporator air temperatures except where little difference was observed at high condenser water temperatures.

Figure 4.14 shows the capacity ratio for MP-52. The ratios are also given in Table 4.12. The average capacity ratio is about 0.87 and is not greatly affected by the operating conditions. The MP-52 blend had the lowest density at the compressor inlet giving it the lowest flow rate. The MP-52 blend also has a lower enthalpy of vaporization than MP-39 at the same pressure. Both of these effects caused the capacity of MP-52 to be lower. The reduced cooling capacity of MP-52 may cause it to be an unsuitable replacement for the operating conditions tested. However,

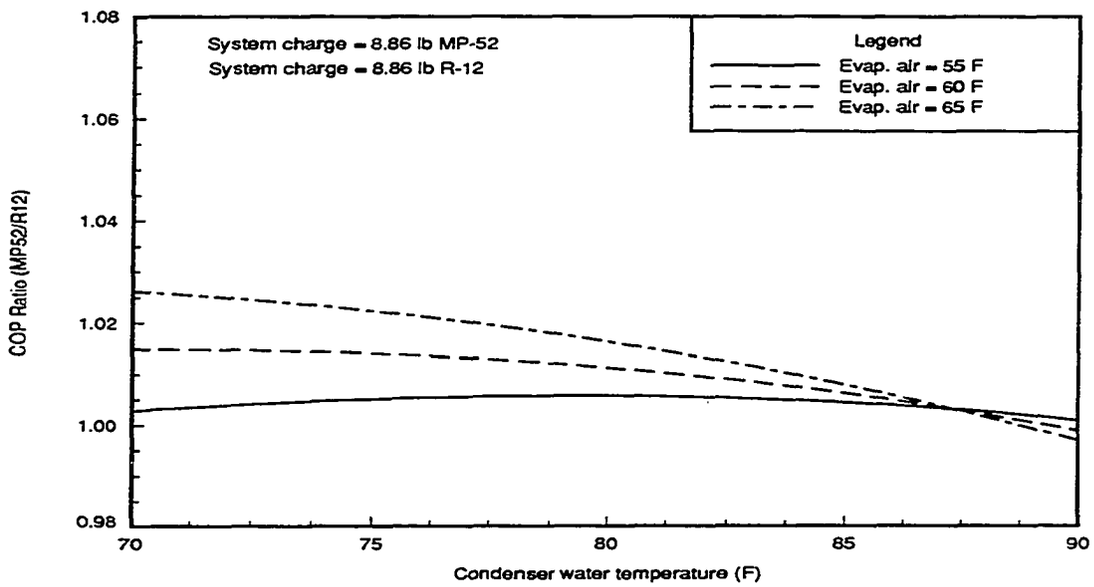

Figure 4.13: COP ratio as a function of operating conditions for MP-52

MP-52 has 36% less R-22 than MP-39 and greater COPs. If an existing system were oversized such that the reduced capacity was not a significant factor, then the MP-52 would serve as an acceptable replacement.

Comparison Ratios for All Refrigerants

The COP ratios for all the refrigerants at each nominal evaporator air temperature are plotted in Figures 4.15 through 4.17. From the standpoint of efficiency R-134a gave the best performance, however all the refrigerants gave acceptable values of COP compared to R-12. The capacity ratios for all the refrigerants are compared in Figures 4.18 through 4.20. Again the performance was greatest with R-134a. The MP-39 blend gave cooling capacities approximately equal to R-134a yet slightly lower in most cases.

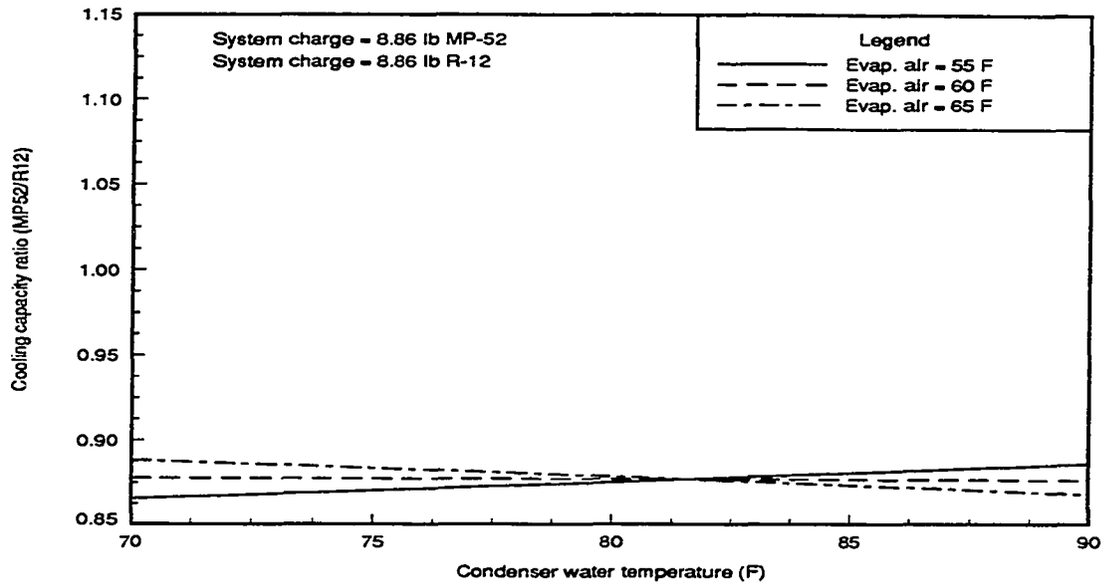

Figure 4.14: Capacity ratio as a function of operating conditions for MP-52

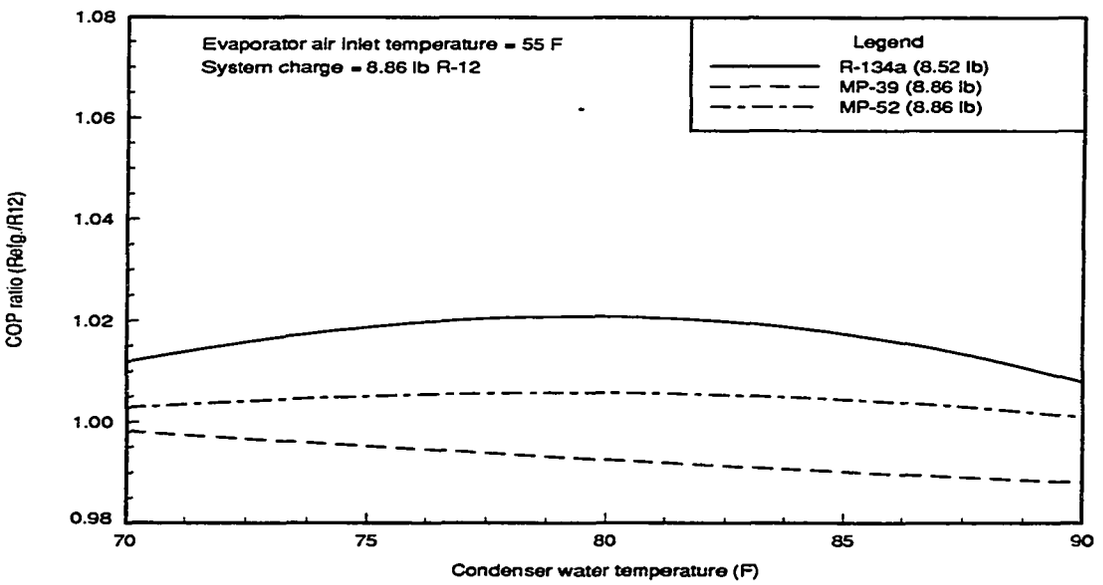

Figure 4.15: Comparison of COP ratios for all refrigerants at an evaporator air temperature of 55 F.

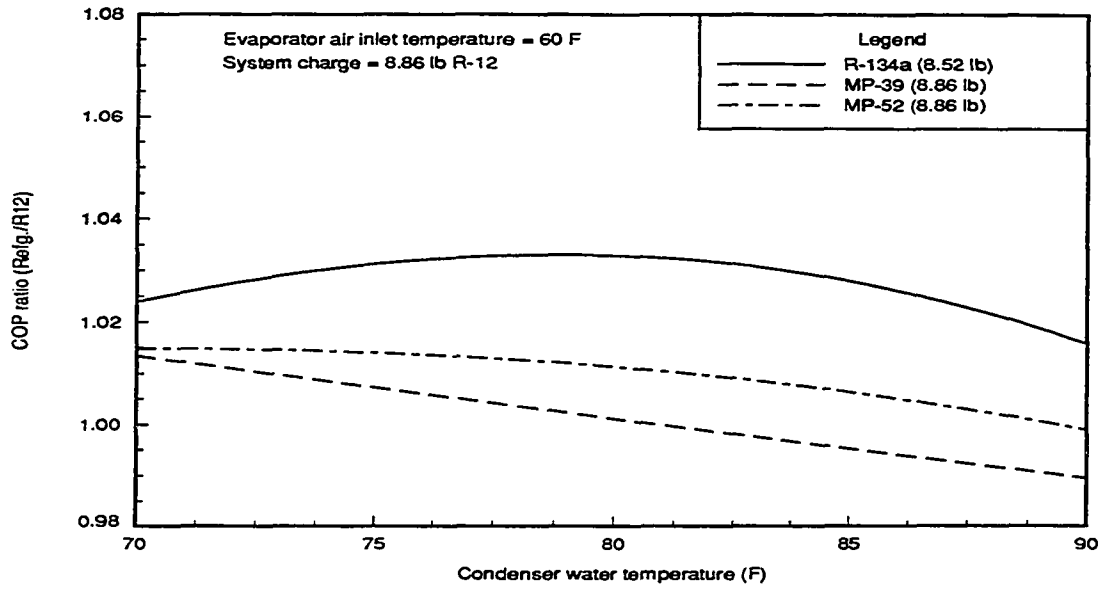

Figure 4.16: Comparison of COP ratios for all refrigerants at an evaporator air temperature of 60 F.

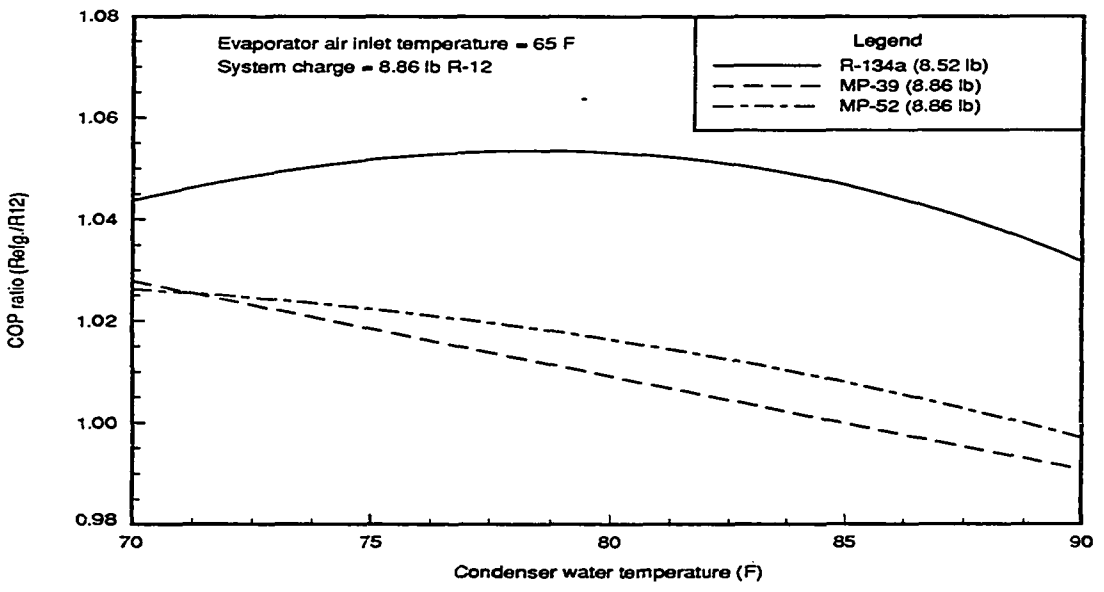

Figure 4.17: Comparison of COP ratios for all refrigerants at an evaporator air temperature of 65 F.

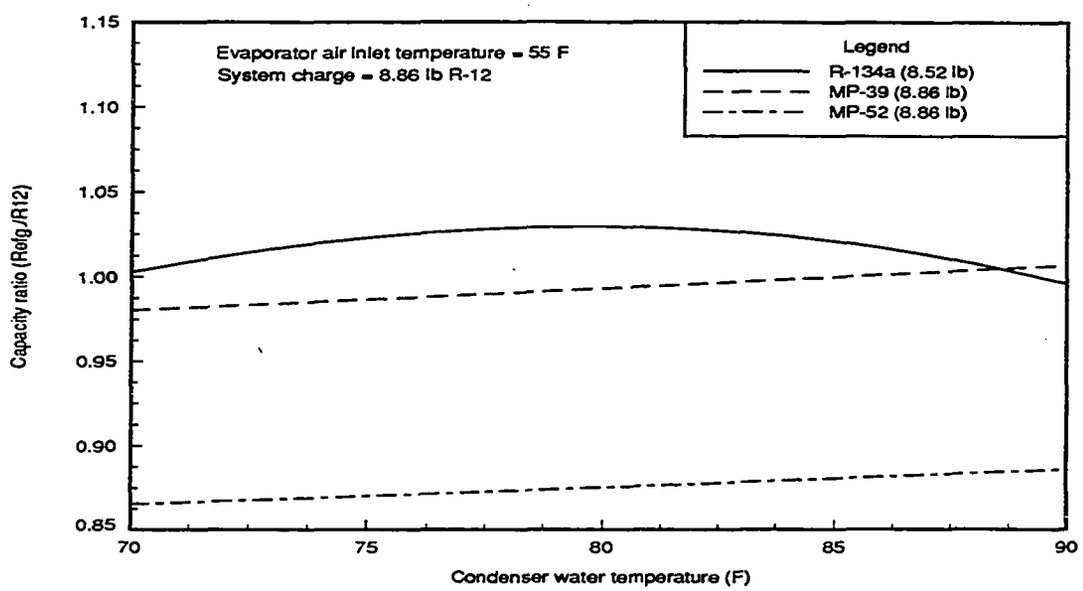

Figure 4.18: Comparison of capacity ratios for all refrigerants at an evaporator air temperature of 55 F.

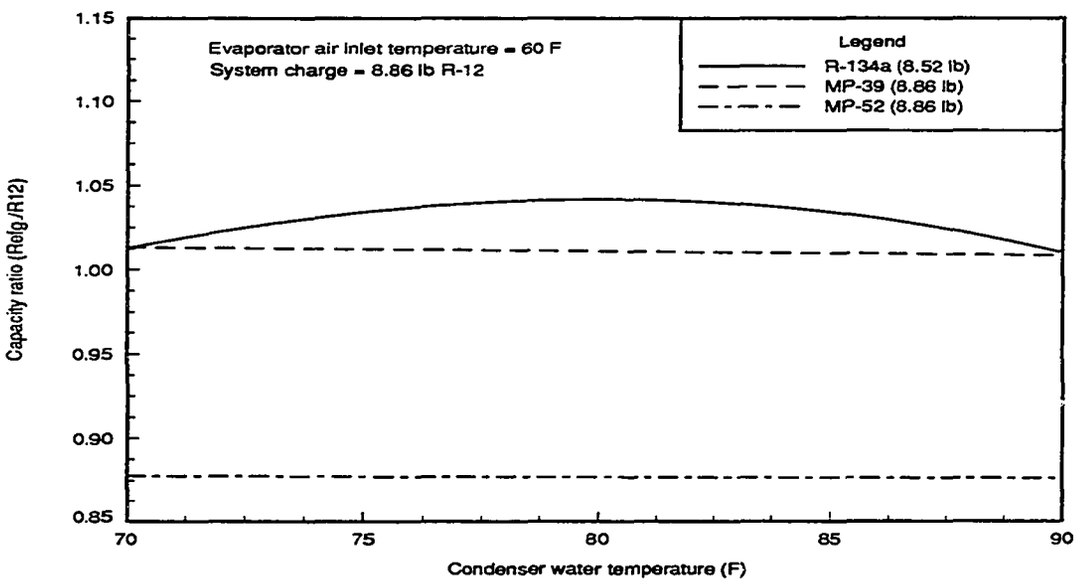

Figure 4.19: Comparison of capacity ratios for all refrigerants at an evaporator air temperature of 60 F.

Table 4.11: COP ratios of system with 8.86 lb of MP-52

Condenser water (F)	Evaporator air (F) 55	60	65
70.0	1.003	1.015	1.026
75.0	1.005	1.014	1.022
80.0	1.006	1.011	1.016
85.0	1.005	1.006	1.008
90.0	1.001	0.999	0.997

Table 4.12: Capacity ratios of system with 8.86 lb of MP-52

Condenser water (F)	Evaporator air (F) 55	60	65
70.0	0.865	0.878	0.888
75.0	0.870	0.877	0.884
80.0	0.875	0.877	0.879
85.0	0.881	0.877	0.873
90.0	0.886	0.876	0.868

Conclusions

The inability to test the refrigerants at repeatable test conditions required the use of curve fits in order to allow comparisons at constant test conditions. The calculation and plots of COP and cooling capacity ratios, relative to R-12 in each case, gives a measure of the acceptability of a refrigerant as a replacement for R-12. Other factors, such as ozone depletion potential, compatibility with materials and lubricants etc., may also effect the choice of an alternative refrigerant.

The COP of all the refrigerants tested had comparable values to the system run with R-12. The system charged with R-134a gave the best performance. The COP with R-134a actually increased relative to R-12 over all operating conditions tested.

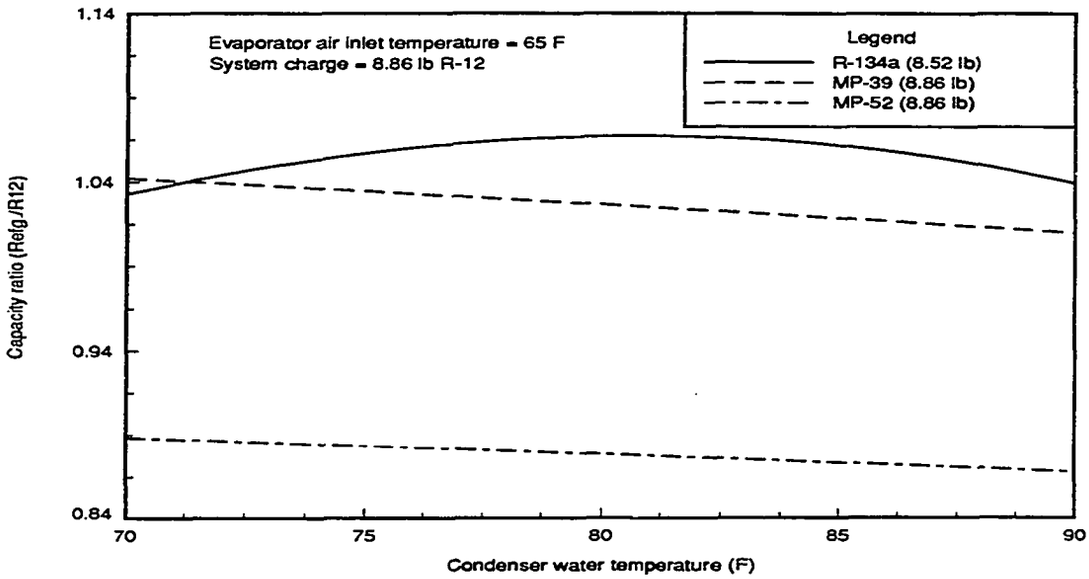

Figure 4.20: Comparison of capacity ratios for all refrigerants at an evaporator air temperature of 65 F.

The maximum increase observed relative to R-12 was about 5%. The blends also showed an increase in COP over most of the test conditions with the MP-52 blend giving slightly higher COPs than MP-39. The maximum increase in COP observed relative to R-12 was about 3%.

The cooling capacity of the system charged with R-134a and MP-39 was slightly higher than for the system charged with R-12. The R-134a gave the greatest increase in capacity up to a maximum of about 7%. The maximum increase in capacity observed with MP-39 was about 4%. The MP-52 gave reduced system capacity over the entire range of operating conditions. The average capacity with MP-52 was about 13% lower than with R-12.

Based on system performance, R-134a is a good replacement for R-12. Both the COP and cooling capacity increased for the system charged with this refrigerant. The

refrigerant blend, MP-39, is also a suitable alternative refrigerant for the conditions tested and would give comparable performance to that of R-12. The refrigerant does, however, contain 52% R-22 which is a HCFC that is being phased out of production because of its ozone depleting potential. The MP-52 blend is suitable if a reduction in cooling capacity can be tolerated. The variation in relative performance with R-12 suggests that the refrigerants may behave quite differently outside of the range of conditions tested.

CHAPTER 5. COMPARISONS OF OTHER SYSTEM VARIABLES

Introduction

The scope of the experimental project undertaken went beyond that of a typical drop-in study where capacity and efficiency are the sole concern. The refrigeration system was carefully instrumented so that a more detailed evaluation of the individual system components could be made. The behavior of all system variables, not just COP and capacity, are of interest in explaining the differences in operation due to changing operating conditions and refrigerants.

The refrigerant temperature and pressure were measured directly at the inlet and exit of each component. The refrigerant mass flow rate was measured at the condenser exit. These variables are affected by the operating conditions and the choice of refrigerant. Systems designed to operate using R-12 may not function well at significantly different temperatures and pressures. A paper by Shiflett and Yokozeki [30] states that lower compressor discharge temperatures are often related to longer compressor life. Comparisons of the system temperatures and pressures of the alternative refrigerants with those of R-12 help determine the appropriateness of the alternative refrigerants. Such comparisons also provide information needed for design and accurate modeling. An understanding of how the refrigerant mass flow rate varies with operating conditions and choice of refrigerant is useful in predicting

the variation in system performance.

Comparison of Refrigerant Temperatures

Temperatures were measured at the condenser inlet and at the inlet and exit of the condenser. The temperature at the exit of the expansion valve was calculated based on the measured pressure and the calculated enthalpy at the valve inlet. It was assumed that the expansion process is isenthalpic. Since the tubing connecting components was insulated, the temperature difference from the exit of one component to inlet of the next was very small.

In order to determine the effects of the operating conditions on the refrigerant temperatures, it is necessary to curve fit the data. This is necessary because both the condenser water temperature and evaporator air temperature varied slightly from the nominal test values. The refrigerant temperature between each component was fit to condenser water and evaporator air temperature using a least squares curve fit. The models used a maximum of four constants to fit the data. Some of the models used a second order term for condenser water temperature giving some curvature with that variable.

Curve fits of refrigerant temperatures for R-12

The compressor inlet temperature curve fit for the system charged with 8.86 lb of R-12 is shown in Figure 5.1. Each line shows the refrigerant temperature for a constant evaporator air temperature. Lines are shown for the three nominal evaporator air temperatures 55, 60 and 65 F. The evaporator air temperature has a much greater effect on the inlet temperature than the condenser water temperature.

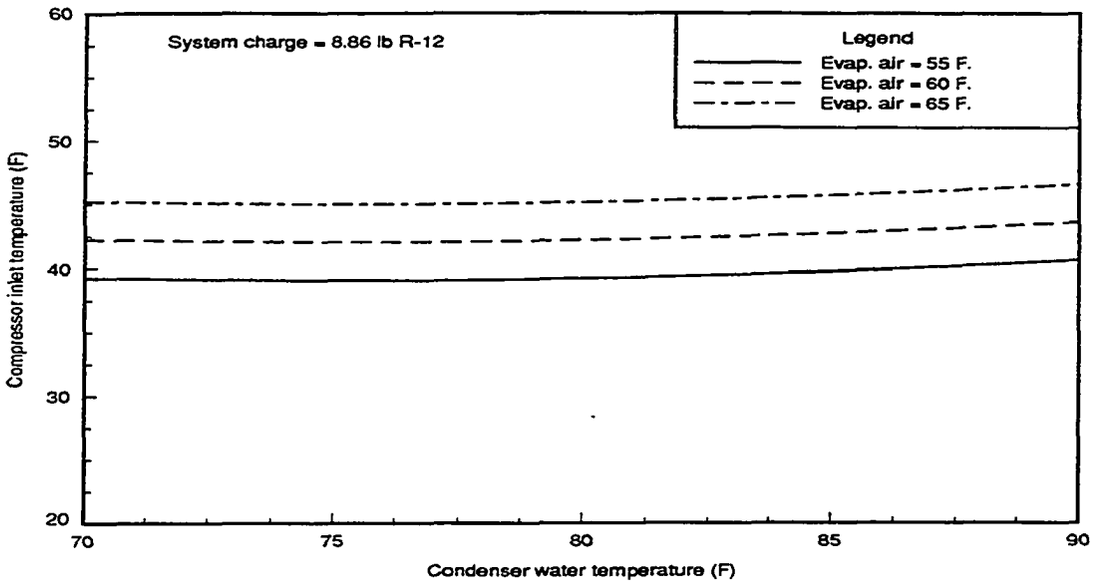

Figure 5.1: Variation in compressor inlet temperature with operating conditions for R-12

The mass flow rate is fairly constant with changes in condenser water temperature, so the heat transfer coefficient and temperature difference in the evaporator are expected to remain constant. This is shown in Figure 5.1 as the lines of constant evaporator air temperature are relatively flat.

The refrigerant temperature at the inlet to the condenser is shown in Figure 5.2. This is the highest temperature in the refrigeration system and may effect compressor performance and the choice of lubricant. In the case of condenser inlet temperature the condenser water temperature has the greatest effect. Since the compressor inlet state is relatively unaffected by changes in water temperature and since the compressor exit pressure increases with increasing water temperature, the condenser inlet temperature increases as observed. The lines of constant evaporator air temperature in Figure 5.2 are inverted compared to those in Figure 5.1. This is because the lower

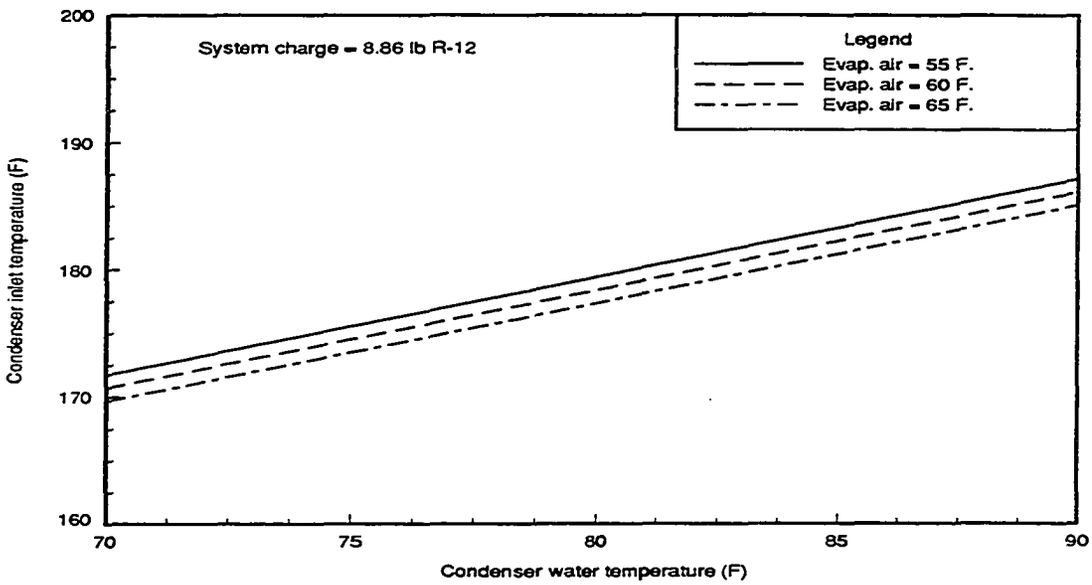

Figure 5.2: Variation in condenser inlet temperature with operating conditions for R-12

flow rate at lower evaporator air temperatures corresponds to a higher pressure ratio. Therefore, the temperatures move in opposite directions.

The condenser exit temperature only varies as a function of condenser water temperature. The curve fit of condenser exit temperature is shown in Figure 5.3. The difference in condenser inlet temperature at the various evaporator air temperatures is offset by the different refrigerant mass flow rates. An increased mass flow rate in the condenser increases the heat transfer coefficient. The temperature difference between the water and refrigerant at the condenser exit is about constant at 2.5 F.

The evaporator inlet temperature, shown in Figure 5.4, is mostly affected by changes in evaporator air temperature. The evaporator inlet and exit temperature are closely related since the pressure drop in the evaporator did not vary significantly and the evaporator exit superheat was held constant. The difference in temperature

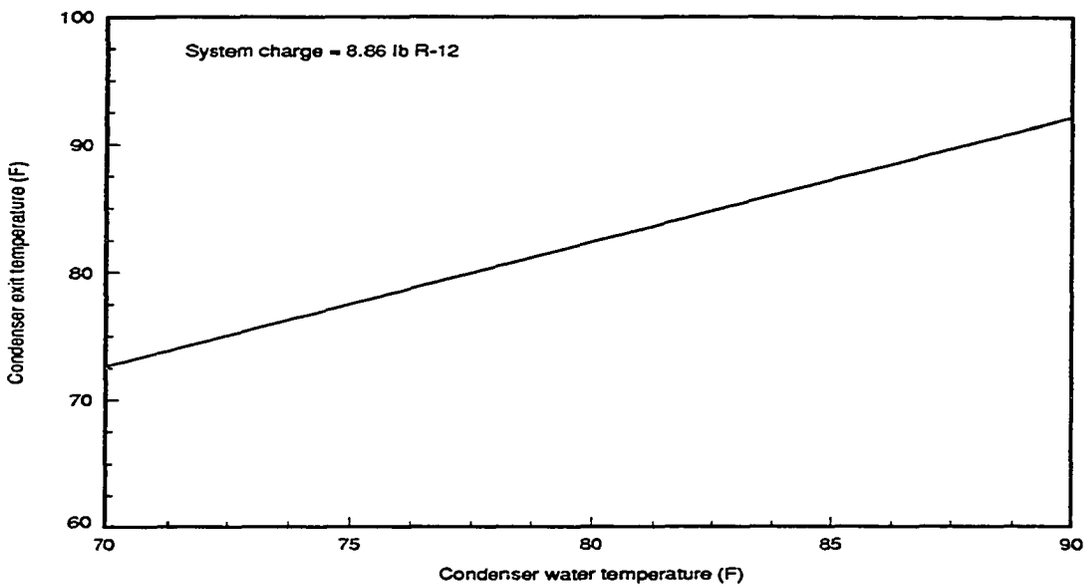

Figure 5.3: Variation in condenser exit temperature with operating conditions for R-12

between the same curves in Figures 5.1 and 5.4 is about constant at 10 F. The difference between this value and the superheat of 13.5 F is due to the pressure drop in the evaporator. The relationship between evaporator inlet and exit temperature difference is different for the blends because of the effects of temperature glide.

Comparisons of refrigerant temperatures with R-12

The refrigerant temperatures between system components for each of the other refrigerants tested were also correlated with operating conditions using least squares curve fits. The difference in refrigerant temperatures compared to R-12 were then calculated as a function of operating conditions for each refrigerant. Plots of these differences show the effects of changes in refrigerant over the range of test conditions. Values above zero correspond to higher temperatures with the specific alternative

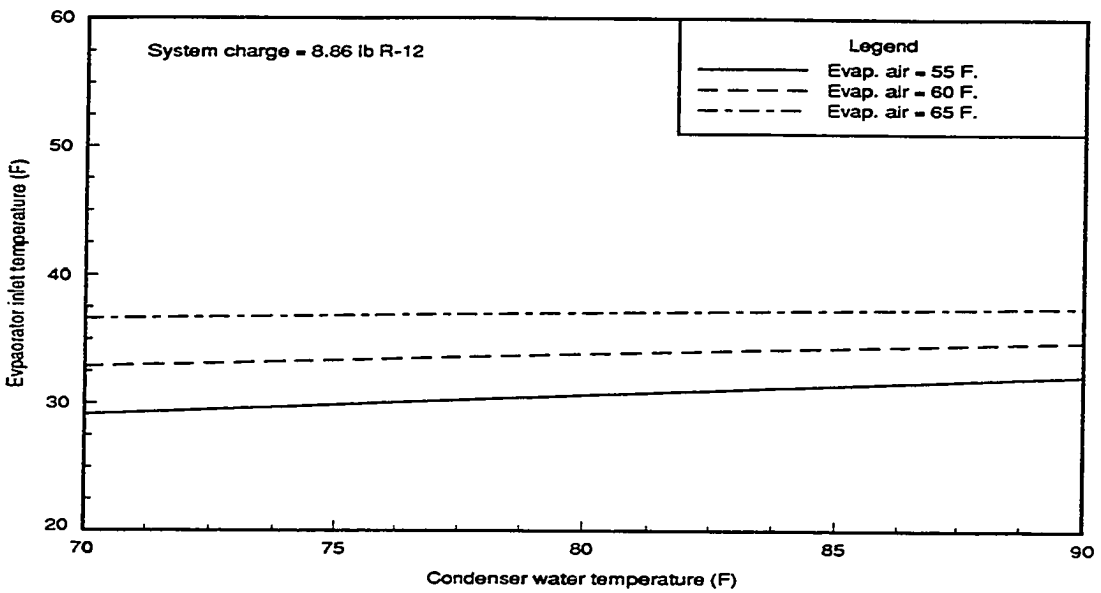

Figure 5.4: Variation in evaporator inlet temperature with operating conditions for R-12

refrigerant than with R-12.

Compressor inlet temperature differences The plot of compressor inlet temperature differences calculated for R-134a is shown in Figure 5.5. The R-134a had slightly higher compressor inlet temperatures than R-12. This corresponds to the lower evaporator pressure drop with R-134a associated with the lower flow rate. The temperature differences for the refrigerant blends, MP-39 and MP-52, are shown in Figures 5.6 and 5.7 respectively. The compressor inlet temperatures were slightly lower than for R-12 with both blends. This is due in part to the difference in temperature profile of the blends associated with temperature glide.

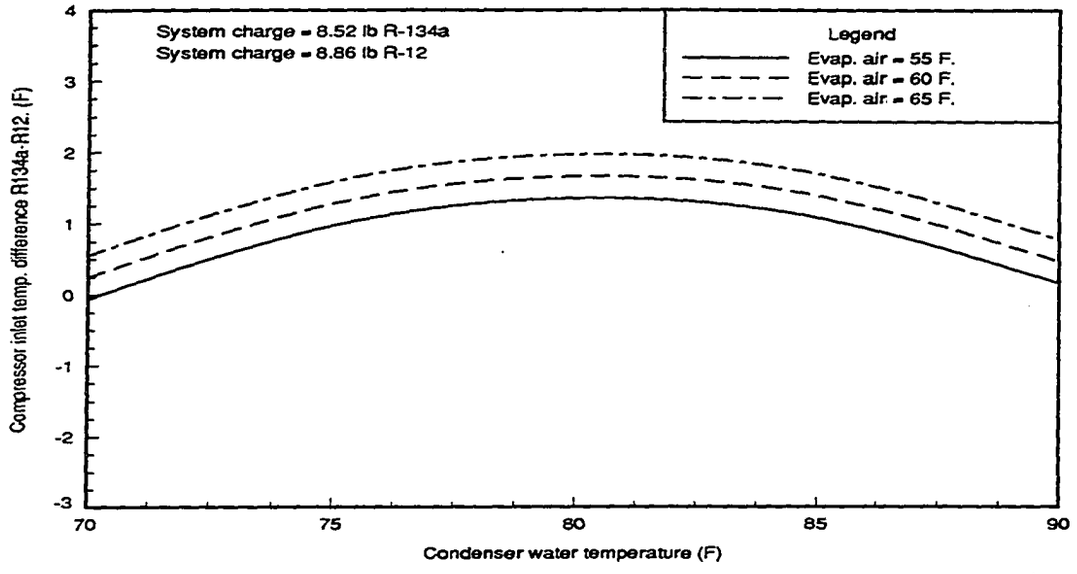

Figure 5.5: Comparison of compressor inlet temperatures with R-134a and R-12

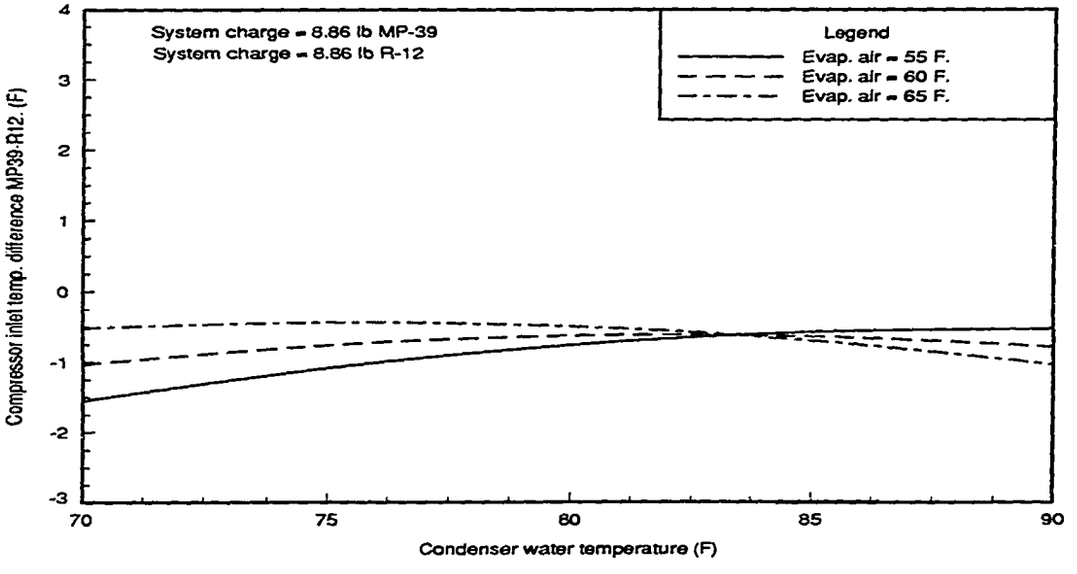

Figure 5.6: Comparison of compressor inlet temperatures with MP-39 and R-12

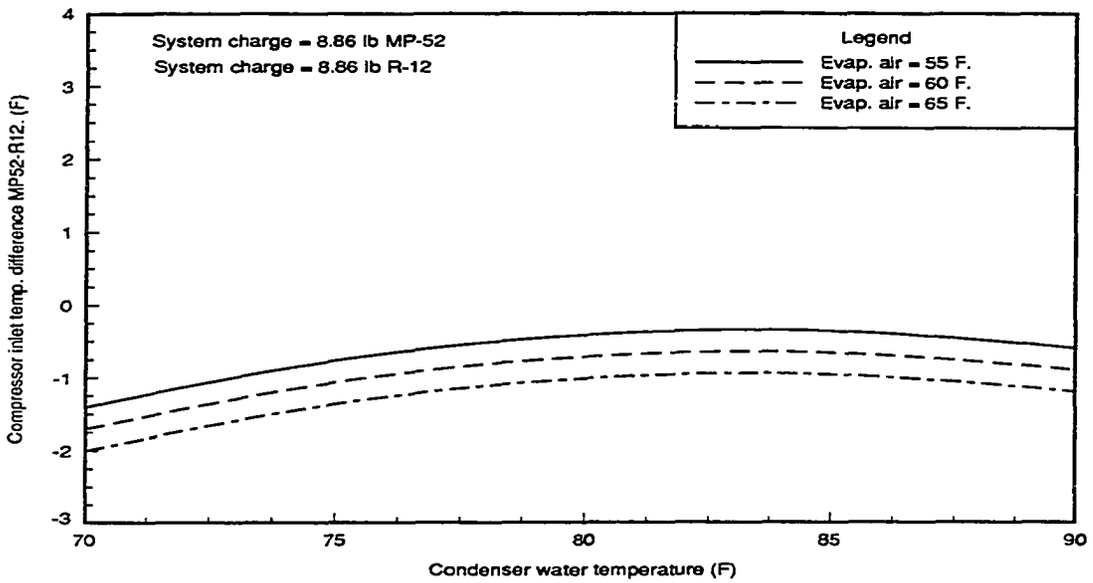

Figure 5.7: Comparison of compressor inlet temperatures with MP-52 and R-12

Condenser inlet temperature difference The temperature differences observed at the condenser inlet were the most significant. The condenser inlet temperature with R-134a was about 13 F cooler than with R-12. A plot of the temperature difference is shown in Figure 5.8. The operating conditions had little effect on this value. The MP-39 operated about 13 F hotter than the R-12. A plot of the difference in condenser inlet temperature for MP-39 is given in Figure 5.9. The difference increased with increasing pressure ratio. There was little difference in temperature for MP-52 as shown in Figure 5.10.

Condenser exit temperature difference All of the refrigerants operated at about the same condenser exit temperature. There was very little temperature difference between the refrigerant and the condenser water at the condenser exit for all

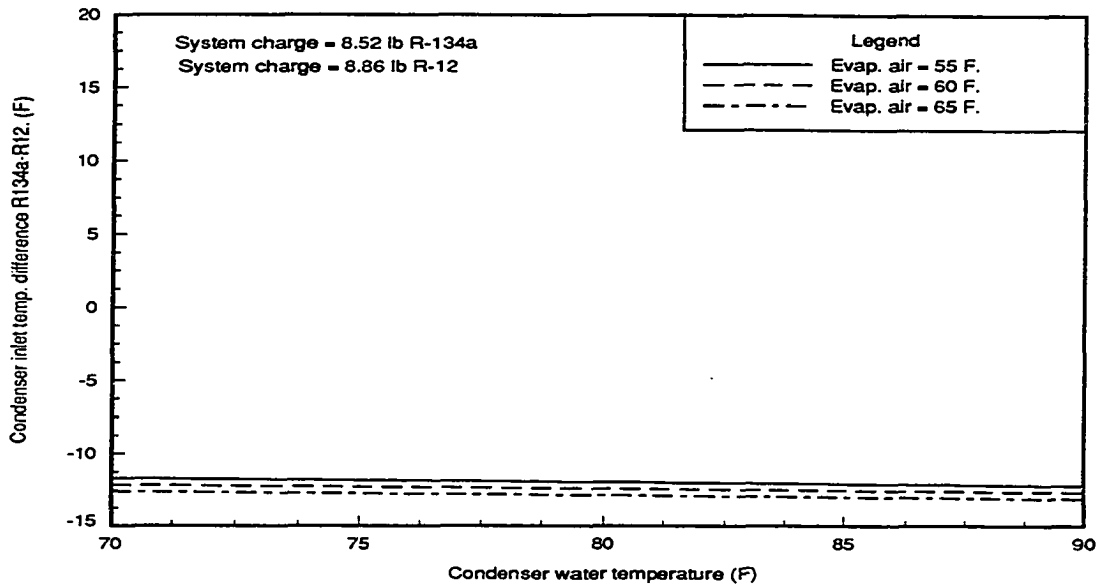

Figure 5.8: Comparison of condenser inlet temperatures with R-134a and R-12

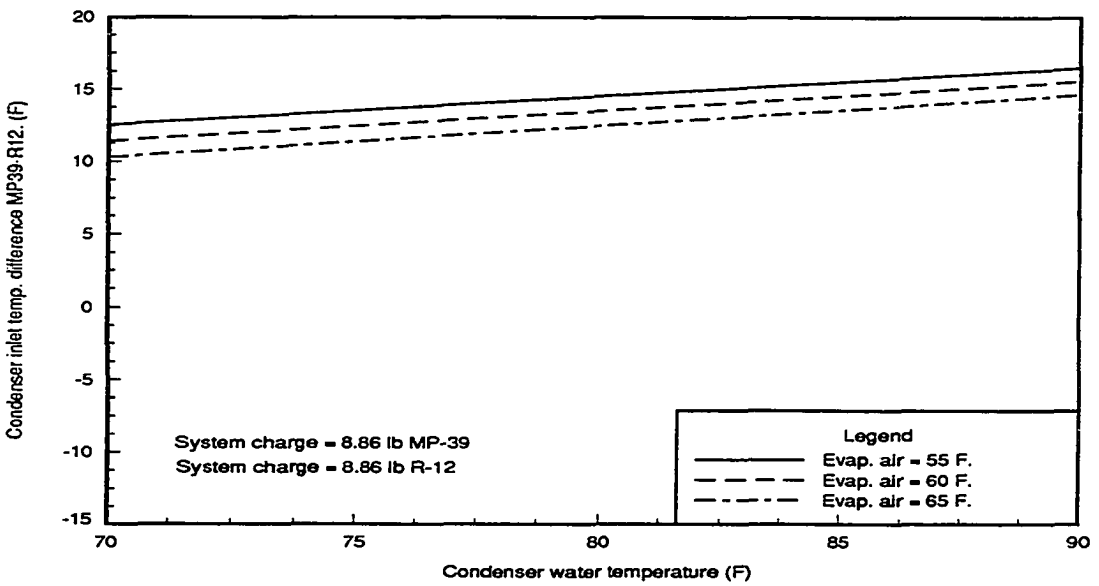

Figure 5.9: Comparison of condenser inlet temperatures with MP-39 and R-12

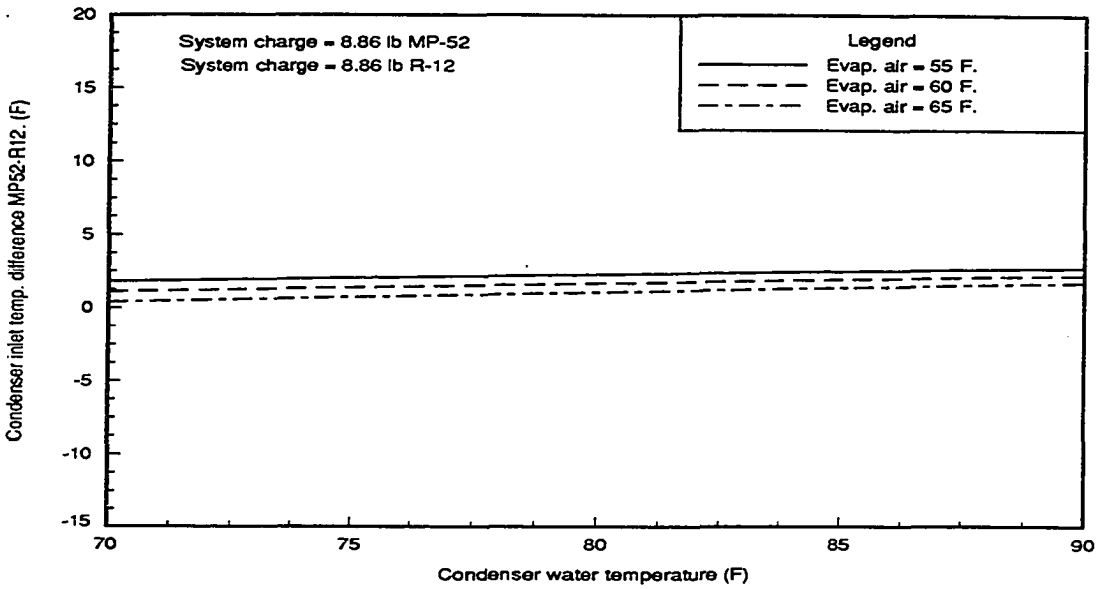

Figure 5.10: Comparison of condenser inlet temperatures with MP-52 and R-12

of the refrigerants. The difference in condenser exit temperatures for the alternative refrigerants are shown in Figure 5.11 for the R-134a and in Figures 5.12 and 5.13 for the blends. All of the alternative refrigerants had lower condenser exit temperatures than the R-12, but the greatest difference was only 1.5 F for R-134a.

Evaporator inlet temperature difference The difference in evaporator temperature difference was very small for the R-134a. A plot of the difference for R-134a is shown in Figure 5.14. The refrigerant blends, however, operated with an evaporator inlet temperature of about 9 to 10 F lower than with R-12. Plots of the difference in evaporator inlet temperature with MP-39 and MP-52 are shown in Figures 5.15 and 5.16 respectively. The lower evaporator inlet temperature of the blends is due to the fact that the two-phase temperature increases with quality at constant

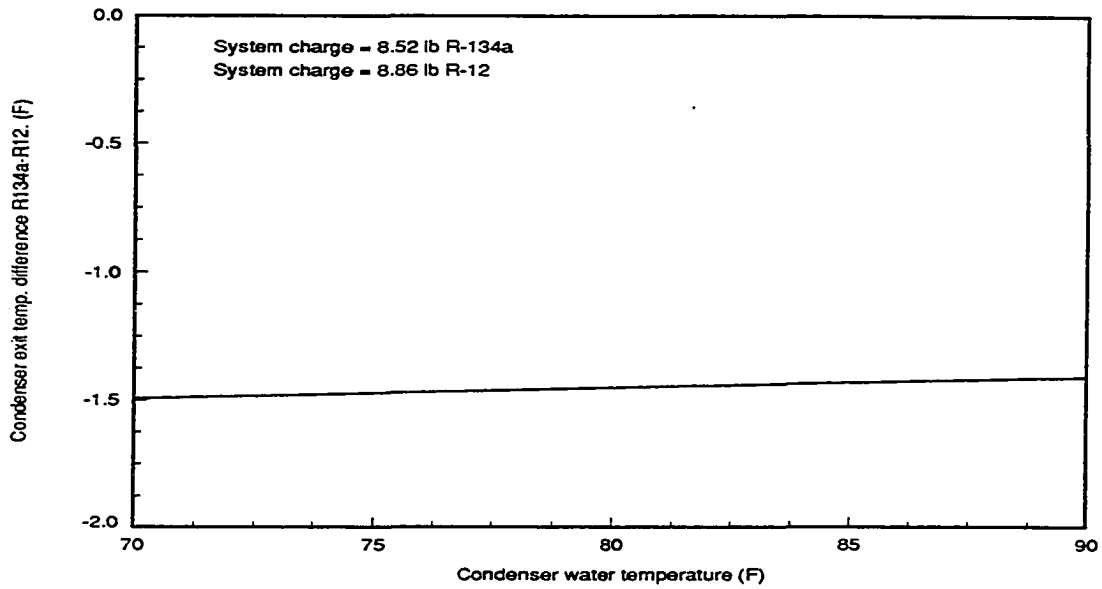

Figure 5.11: Comparison of condenser exit temperatures with R-134a and R-12

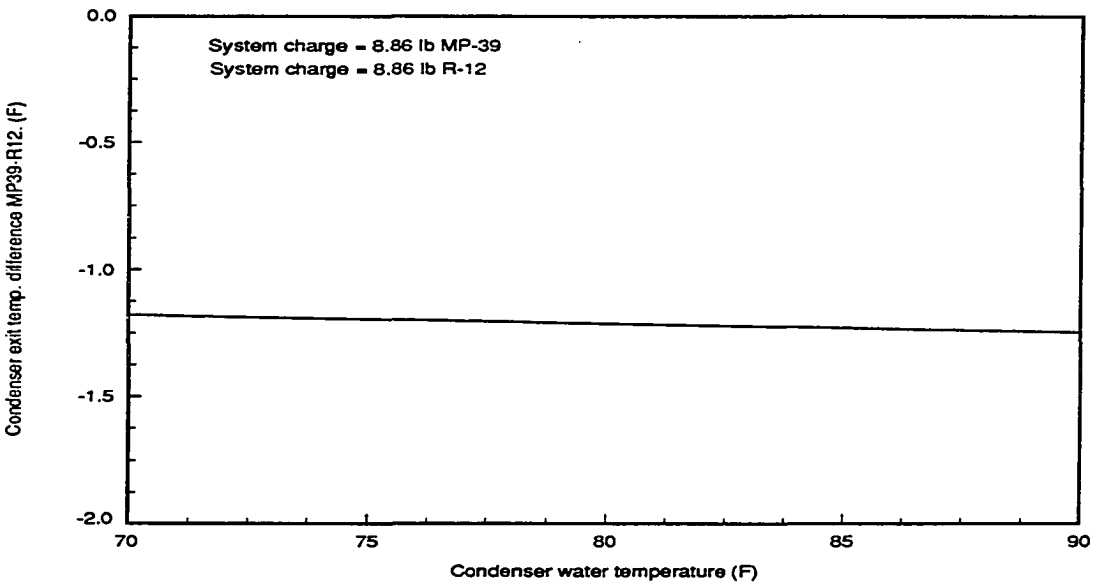

Figure 5.12: Comparison of condenser exit temperatures with MP-39 and R-12

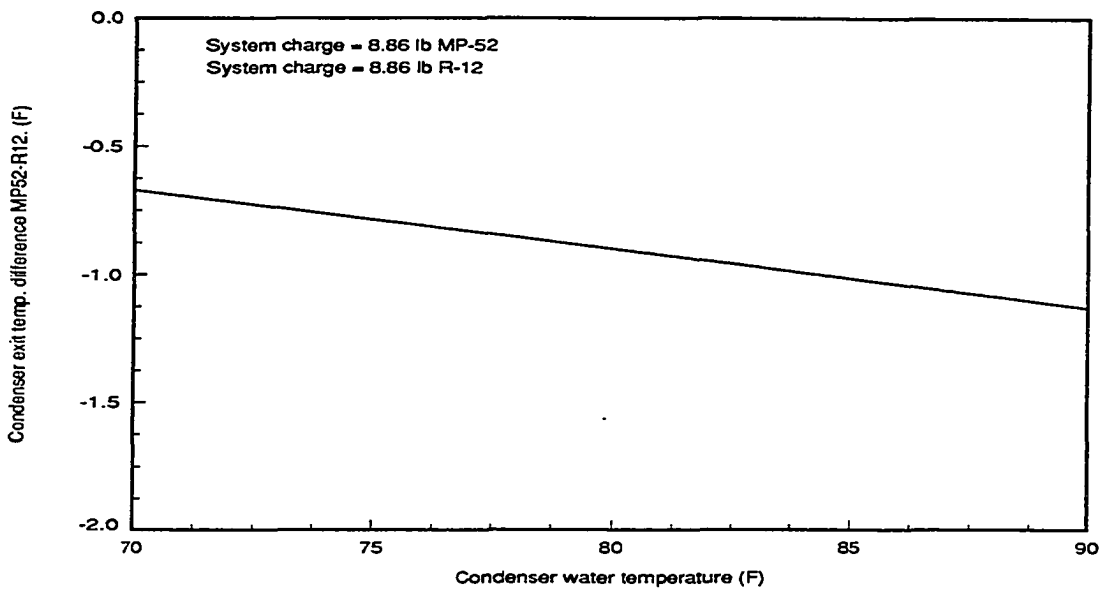

Figure 5.13: Comparison of condenser exit temperatures with MP-52 and R-12

pressure for the blends. This effect, called temperature glide, changes the slope of the two-phase region from a negative slope, due to the effects of pressure drop, to a positive slope. This change in profile makes the evaporator inlet temperature much lower for the blends.

Comparison of Refrigerant Pressures

The absolute pressure was measured at the exit of the condenser and the evaporator. Pressure differences were also measured across the two heat exchanges. These four measurements, recorded at each operating condition, give the pressure between each system component. The pressures at the inlet and exit of the compressor were each fit to evaporator air and condenser water temperature with a least squares curve fit. The pressure ratio, defined as the ratio of compressor inlet to exit pressure, could

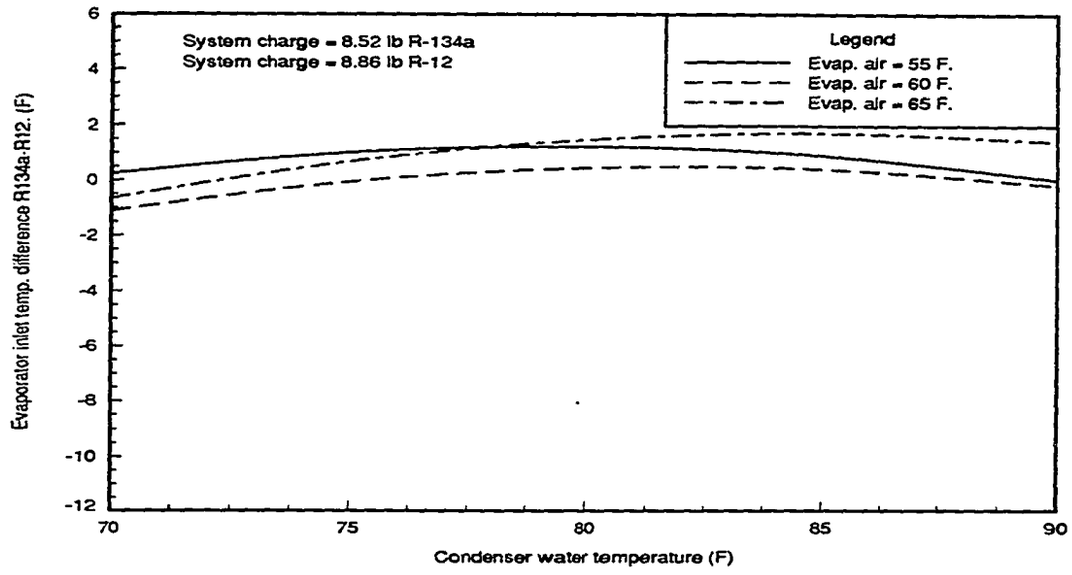

Figure 5.14: Comparison of evaporator inlet temperatures with R-134a and R-12

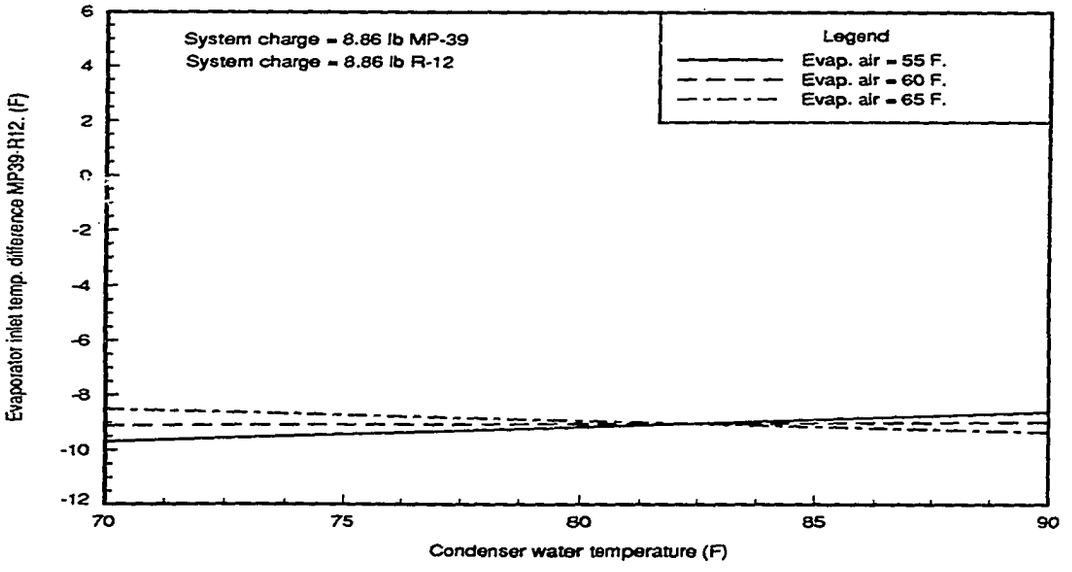

Figure 5.15: Comparison of evaporator inlet temperatures with MP-39 and R-12

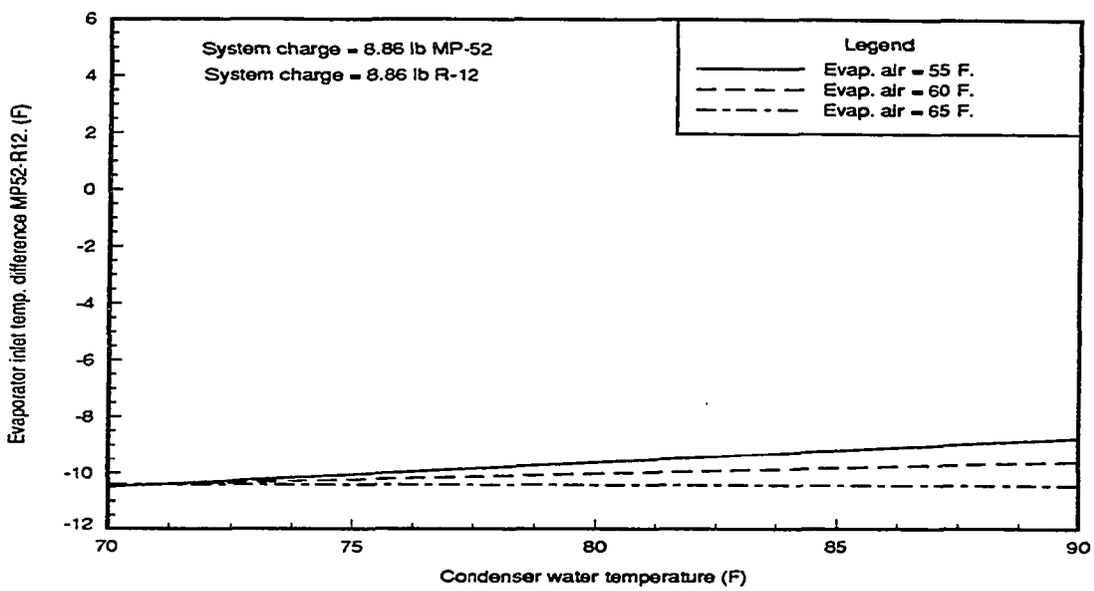

Figure 5.16: Comparison of evaporator inlet temperatures with MP-52 and R-12

then be calculated as a function of operating conditions. The pressures for each refrigerant were fit separately so that the compressor inlet pressure and pressure ratio of each alternative refrigerant could be compared to R-12.

Curve fits of refrigerant pressures for R-12

The compressor inlet pressure for R-12 was fit with a simple polynomial expression with three constants. The evaporator air temperature had a linear effect on pressure and the condenser water had a slight second order effect. The curve fit of compressor inlet pressure is shown in Figure 5.17. The inlet pressure increased primarily with increasing condenser water temperature and slightly with increasing evaporator air temperature. The condenser pressure rises with water temperature because the temperature difference between the two-phase refrigerant and condenser

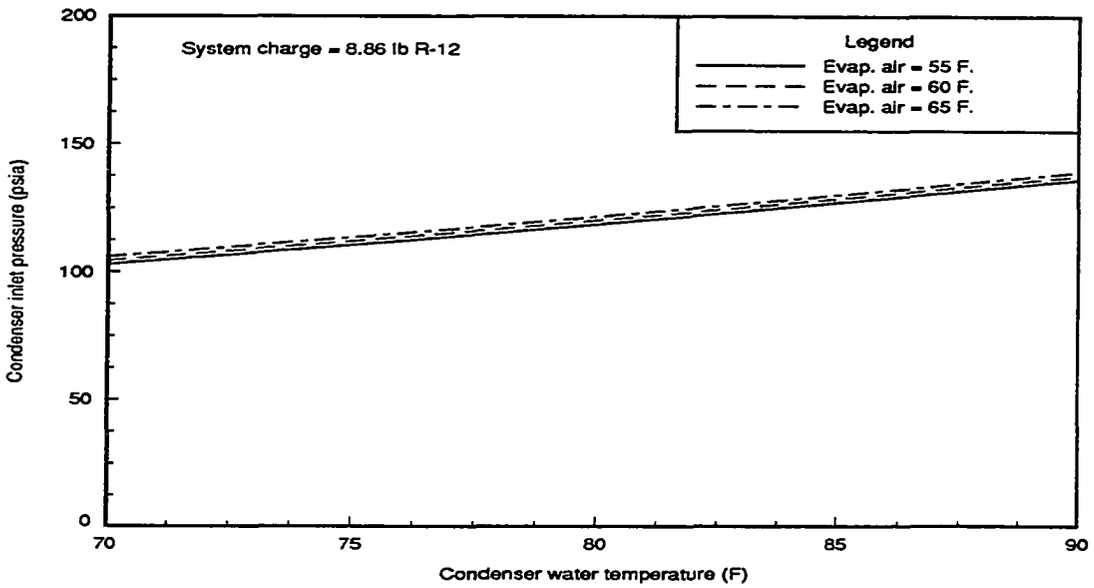

Figure 5.17: Variation in condenser inlet pressure with operating conditions for R-12

water is fairly constant. Increases in condenser saturation temperature correspond to increases in condenser pressure.

The pressure ratio across the compressor is given in Figure 5.18 for R-12. The pressure ratio is primarily affected by changes in condenser water temperature, however the evaporator air temperature also causes a noticeable effect. The effect of water temperature is linear whereas the evaporator air has a second order effect on the pressure ratio. Increasing evaporator air temperature causes a decrease in pressure ratio since the rise in evaporator pressure is proportionally greater than in the condenser. For a constant condenser pressure, changes in evaporator pressure would correspond to exponential changes in pressure ratio. For the range of values tested, this is well represented by a second order polynomial.

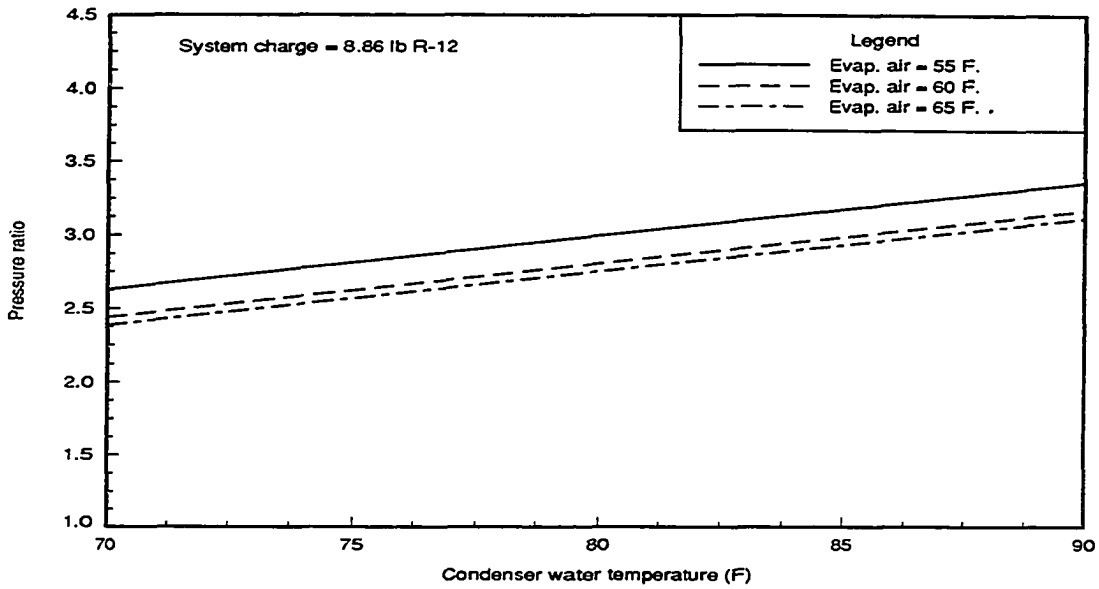

Figure 5.18: Variation in system pressure ratio with operating conditions for R-12

Comparisons of refrigerant pressures with R-12

Ratio of condenser inlet pressures The condenser inlet pressures for each refrigerant were fit to the operating conditions as was done with the R-12 data presented in Figure 5.17. The ratio of the condenser inlet pressure of R-134a to R-12 was calculated at each nominal evaporator air temperature over the range of condenser water temperatures. The plot of these ratios is given for R-134a in Figure 5.19. The condenser inlet pressure with R-134a is about 3 to 7% greater than with R-12. The greatest differences occurred at the higher condenser water temperatures.

The ratio of condenser inlet pressure of MP-39 to R-12 is shown in Figure 5.20. The condenser pressure is much higher for the system charged with MP-39. The condenser inlet pressure is about 18% higher with MP-39 than with R-12 and is fairly independent of the operating conditions. Figure 5.21 shows the same ratio for

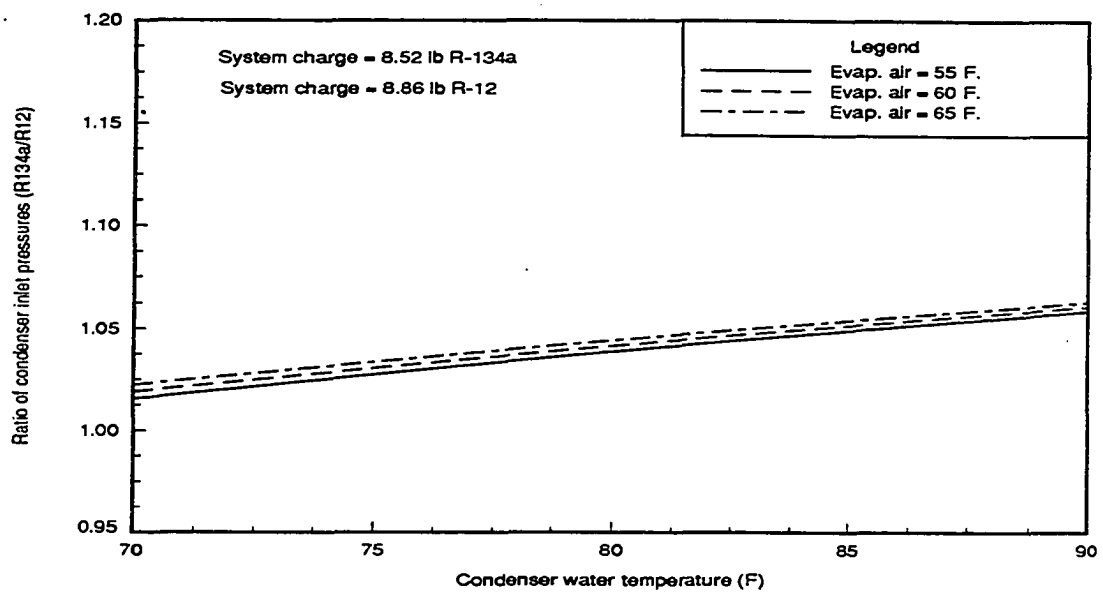

Figure 5.19: Comparison of condenser inlet pressures with R-134a and R-12

MP-52. The condenser inlet pressure for MP-52 is about 3% lower than for R-12 and is also somewhat independent of the operating conditions.

The difference in operating pressures between the refrigerants can be explained in part by examination of the saturation curves of the different refrigerants. The condenser temperature profiles, presented in Chapter 7, show that the temperature difference between the condenser water and the refrigerant at the saturated vapor condition in the condenser is relatively constant for each refrigerant. Since the temperature difference is relatively constant, the ratio of saturation pressures at constant temperature should compare well to the ratios found experimentally. A plot of the saturated vapor line is given in Figure 5.22 for the different refrigerants. The saturated vapor refrigerant temperatures are about 10 F higher than the condenser water inlet temperatures. At these temperatures (80 to 100 F) the refrigerant with the

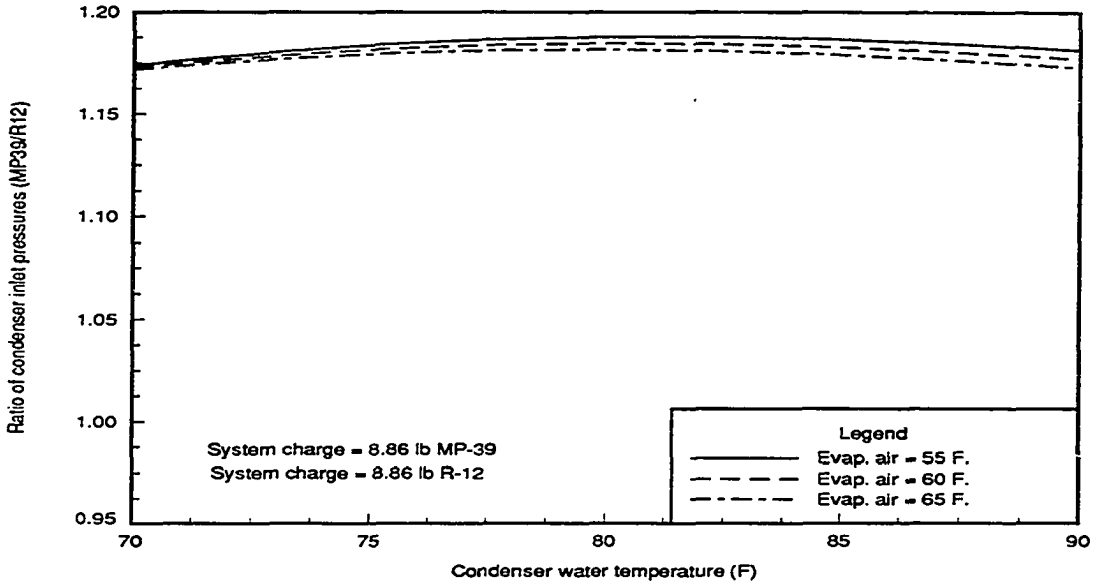

Figure 5.20: Comparison of condenser inlet pressures with MP-39 and R-12

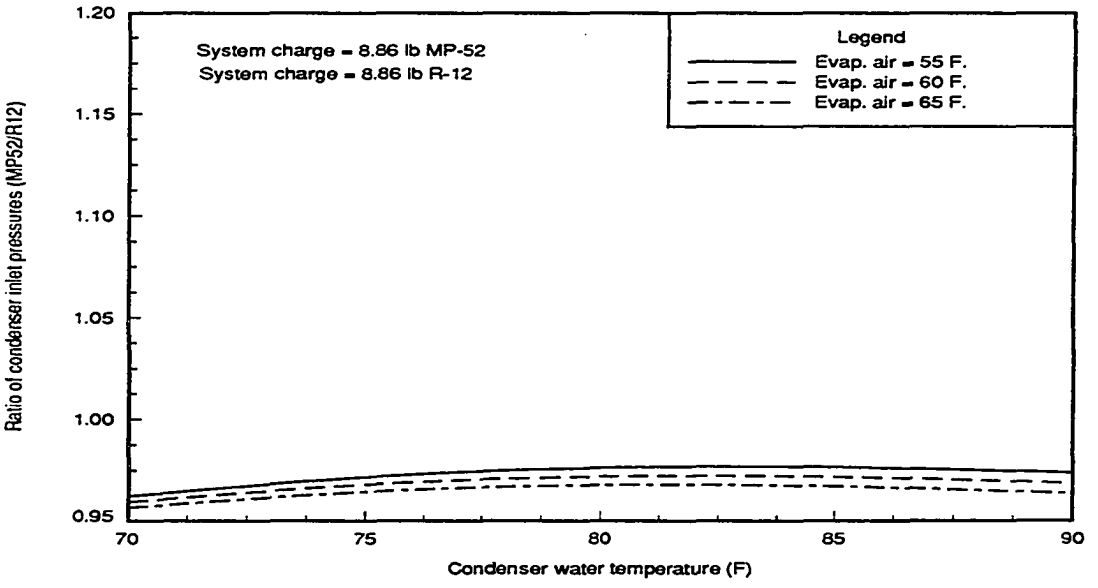

Figure 5.21: Comparison of condenser inlet pressures with MP-52 and R-12

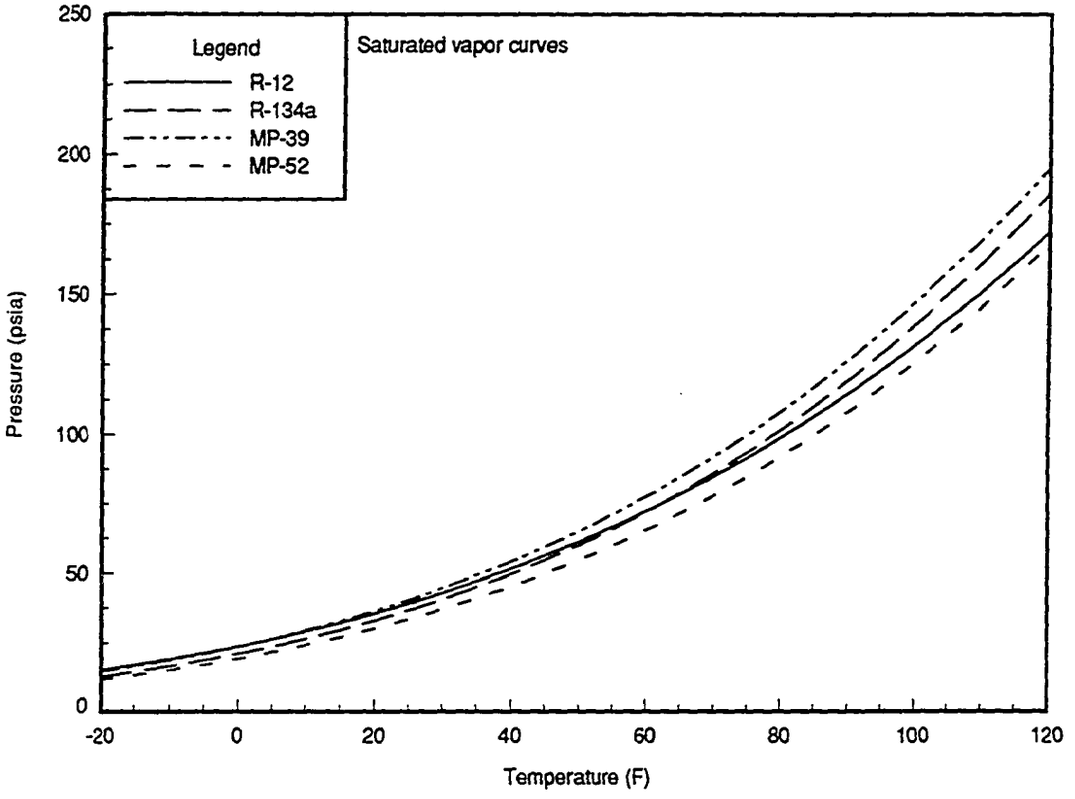

Figure 5.22: Saturated vapor pressure as a function of temperature

lowest pressure is MP-52. The pressures increase with refrigerant in the order: R-12, R-134a and MP-39. This is the same order that was observed in Figures 5.19- 5.21. The relative increase in the pressure of R-134a with increasing water temperature correlates to the increasing distance between the saturation curves of R-134a and R-12.

The saturated liquid curves for the different refrigerants are shown in Figure 5.23. The curves for the pure refrigerants are the same but the blends show higher pressures for the same temperature. This is due to the temperature glide of the blends. The

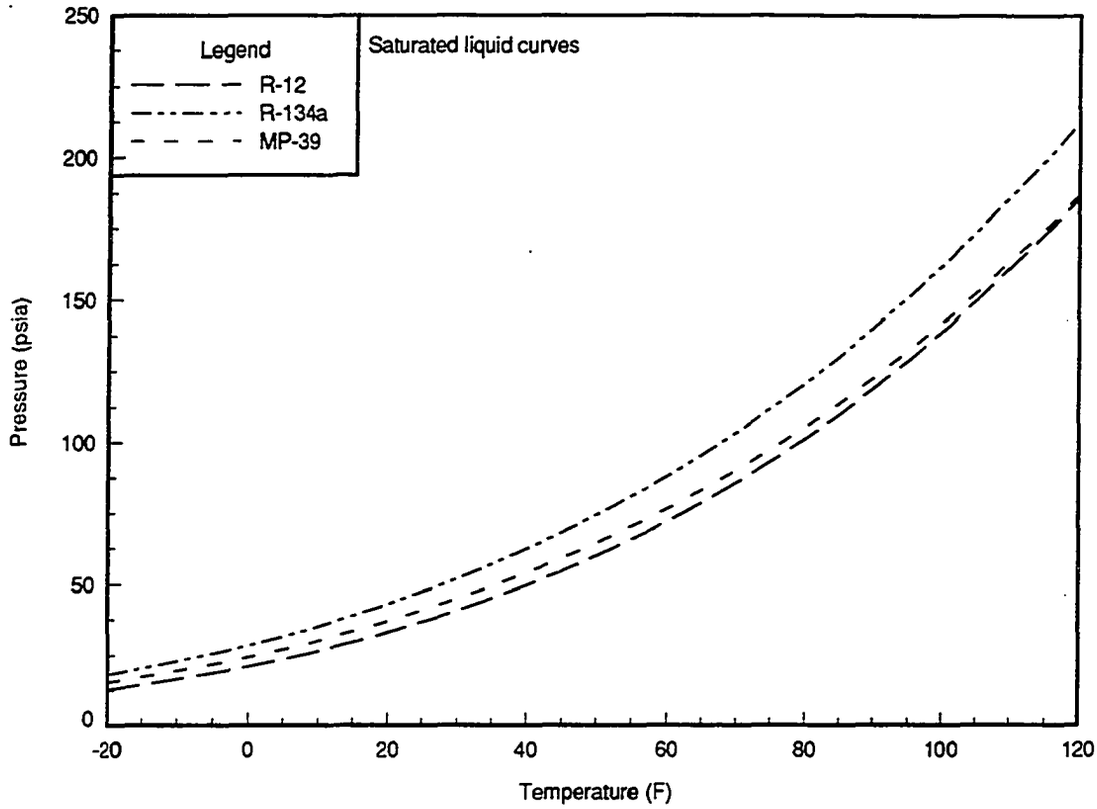

Figure 5.23: Saturated liquid pressure as a function of temperature

difference in temperature between refrigerants at the saturated liquid condition could be estimated from the saturated liquid lines assuming constant pressure drop for the different refrigerants.

Ratio of system pressure ratios The pressure ratios for the three alternative refrigerants studied were all higher than those for R-12. The ratio of system pressure ratios for R-134a is shown in Figure 5.24. The pressure ratios for R-134a are about 5% to 12% higher than with R-12 depending on the operating conditions. The higher pressure ratio observed with R-134a is consistent with the expected performance

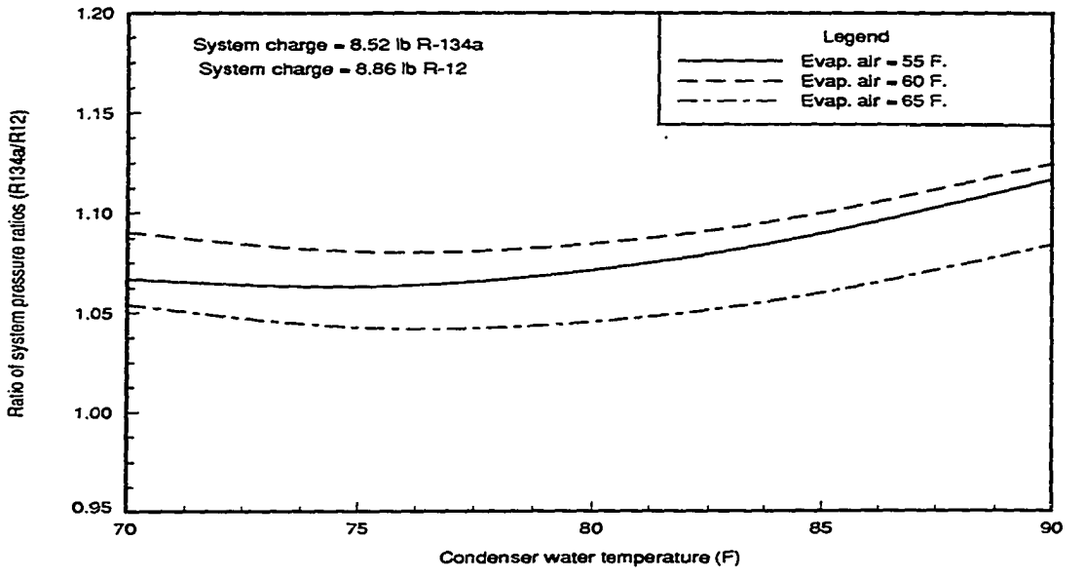

Figure 5.24: Comparison of system pressure ratios with R-134a and R-12

derived from the saturated temperature pressure relationship. The saturation lines for R-134a and R-12 cross at a temperature between the condenser and evaporator temperature. Since the refrigerant saturation temperatures in the evaporator and condenser are approximately equal for R-12 and R-134a, the crossing of the saturation lines translates to a higher pressure ratio for R-134a.

The pressure ratios for the blends varies from about 14% to 18% higher than with R-12 and is slightly greater for MP-39. A plot of the ratio of system pressure ratios for MP-39 is shown in Figure 5.25. A similar plot for MP-52 is given in Figure 5.26. The difference in the saturated vapor temperature between the blends and R-12 is less than 2 F. Therefore, the pressure ratios can be estimated for each refrigerant based on the ratio of pressures at equal temperatures. The pressure ratio of MP-52 should be higher than R-12, as was observed experimentally, since the saturated

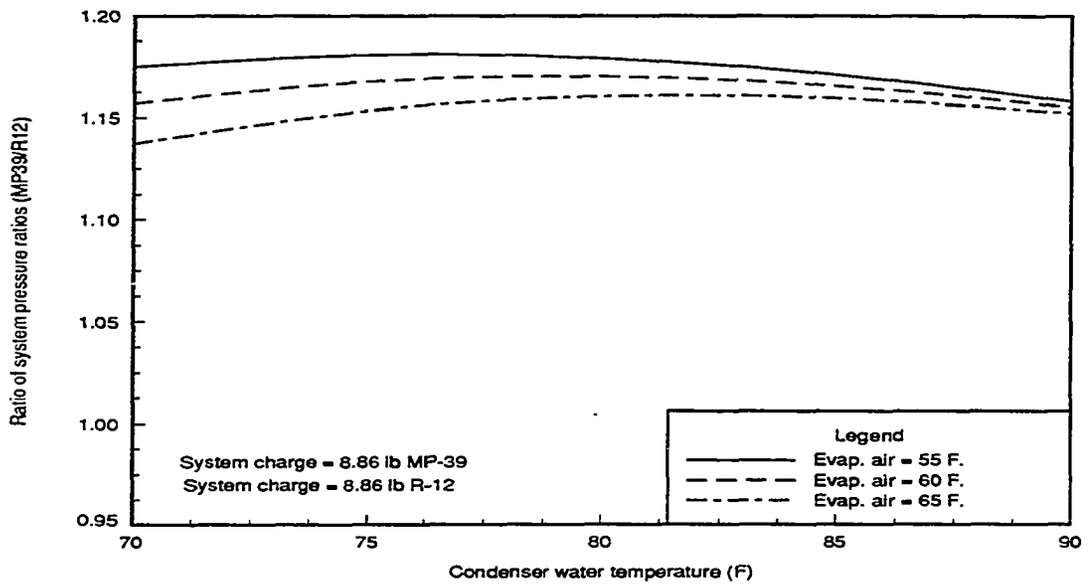

Figure 5.25: Comparison of system pressure ratios with MP-39 and R-12

vapor lines are converging. The pressure ratio of the blend MP-39 is not as easy to predict relative to R-12 since lines of equal pressure ratio should diverge as the R-12 and MP-39 saturation lines do. The lines, however, diverge at a rate greater than what would give equal pressure ratios. Calculation of the pressure ratio assuming equal saturation temperatures predicts a 7% greater pressure ratio for MP-39. This rough estimate of the expected pressure ratio is consistent with the observed values.

Comparison of Refrigerant Mass Flow Rates

The refrigerant mass flow rate was measured with a calibrated coriolis mass flow meter. The refrigerant mass flow rate varied significantly with changes in operating conditions and refrigerant. The data for each refrigerant was fit with a least squares curve fit so that mass flow rate for each refrigerant could be compared at identical

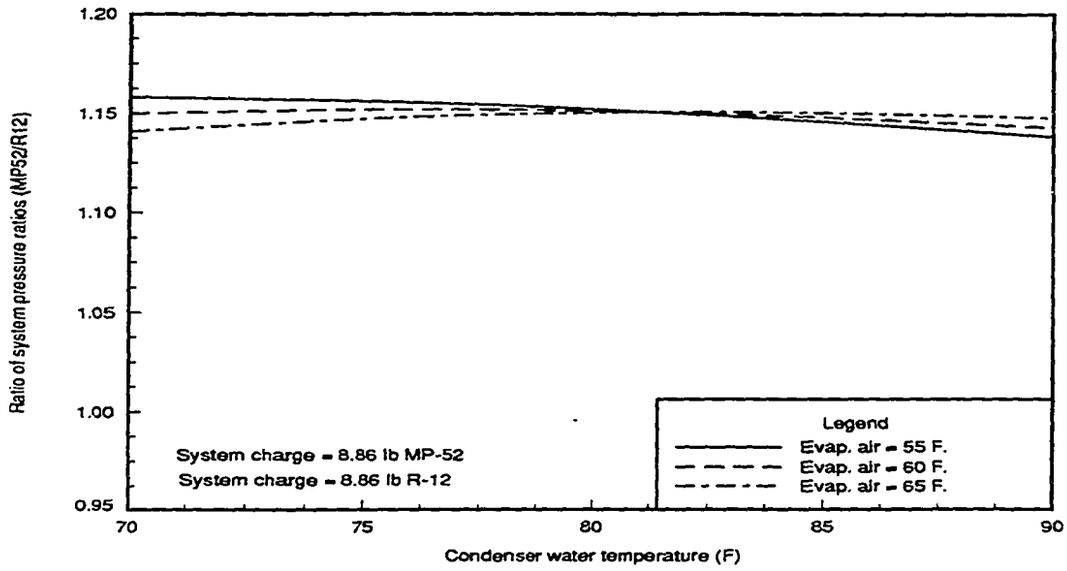

Figure 5.26: Comparison of system pressure ratios with MP-52 and R-12

operating conditions.

Curve fits of refrigerant mass flow rates for R-12

The curve fit of mass flow rate for R-12 showed a slight second order variation with water temperature and an interactive effect of water and air temperature. This translates to evaporator air temperature lines that have slight curvature and which slowly converge with increasing water temperature. A plot of the least squares curve fit for the R-12 data is given in Figure 5.27. Increasing condenser water temperature causes a slight drop in mass flow rate. Increasing evaporator temperature causes a significant increase in mass flow rate.

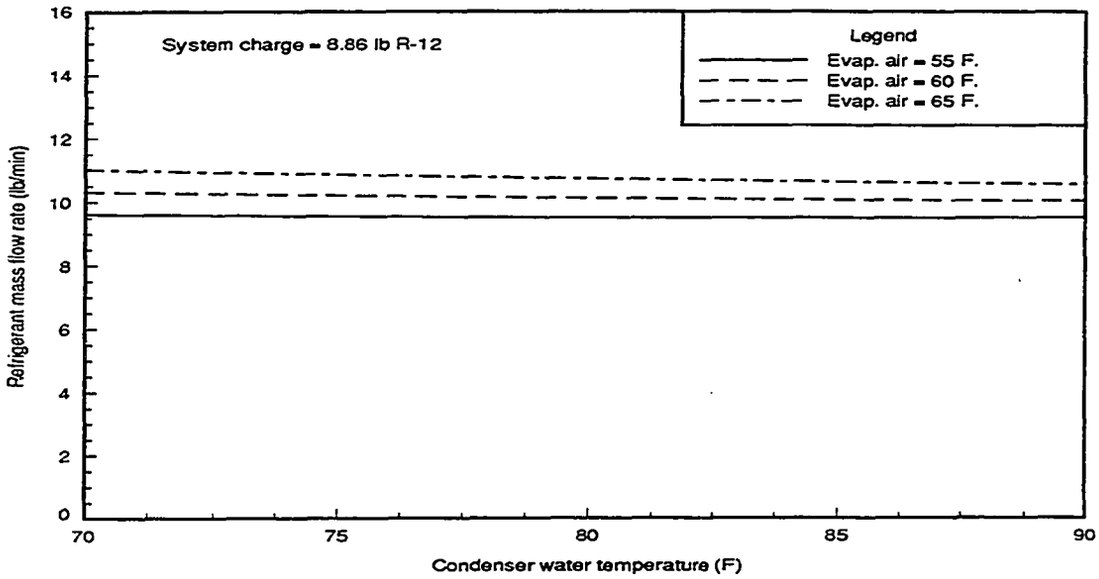

Figure 5.27: Variation in refrigerant mass flow rate with operating conditions for R-12

Comparison with a simple model

The changes observed in refrigerant mass flow with the operating conditions are consistent with the performance of a simple model. Assuming no blow-by or valve leakage during compression the mass flow rate can be calculated as:

$$\dot{m} = (T.V. * \rho_{inlet} - C.V. * \rho_{exit}) * \text{Cycles/min} \tag{5.1}$$

where ρ is the refrigerant density, T.V. is the total cylinder volume and C.V. is the clearance volume. Simply stated, the mass flow per cycle is the difference in mass of refrigerant in the cylinder at the end of the intake and exhaust stroke. The equation for mass flow also assumes that the intake and exhaust valves close exactly at top and bottom dead center. Since the cylinder temperatures and pressures were not measured, it is assumed that the state at the inlet and exit of the compressor shell

represent the refrigerant state in the cylinder at the end of the intake and exhaust stroke. This assumption is probably the most inaccurate since it neglects significant pressure drops in the intake and exhaust valves and ignores the superheating of the refrigerant in the compressor shell and cylinder during the intake stroke. It is reasonable, however, to assume that the data would fit reasonably well to the above form of equation.

The displacement volume per cycle for the compressor is given by the manufacturer as 7.586 in^3. The displacement volume is assumed to be 4% of the displacement volume or 0.303 in^3. The total volume is then 7.889 in^3. The motor speed for the compressor is given as 3450 rpm. The mass flow rate, based on the given assumptions, may then be calculated as:

$$\dot{m} = (7.889 * \rho_{inlet} - 0.303 * \rho_{exit}) * 3450/12^3 \tag{5.2}$$

where the mass flow rate is given in lb/min and the densities are given in lb/ft^3. A plot of the measured mass flow rate versus the calculated mass flow rate is shown in Figure 5.28. All of the refrigerant data is shown including the data taken at different charges. The diagonal line shown in the graph represents the condition of no error between the model and measured values. The model predicted values approximately 40% higher than the measured values. This is consistent with the known error associated with neglecting pressure drops and superheating. Both effects would lower the compressor inlet density, thus giving a lower predicted mass flow rate.

If the constants that are multiplied by each density term are selected such that they minimize the error of the model the data can be fit reasonably well. The constants are then no longer related to the total and clearance volumes. A plot of the measured versus calculated values is shown in Figure 5.29. The adjusted

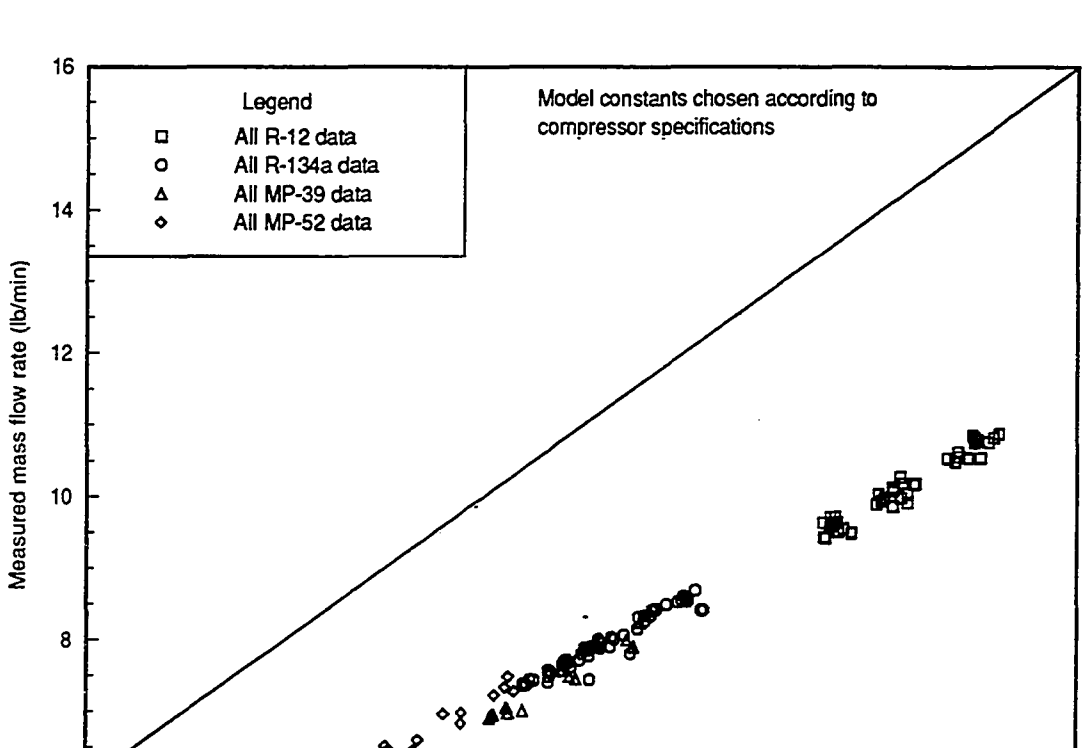

Figure 5.28: Comparison of mass flow rate with model using actual cylinder volumes

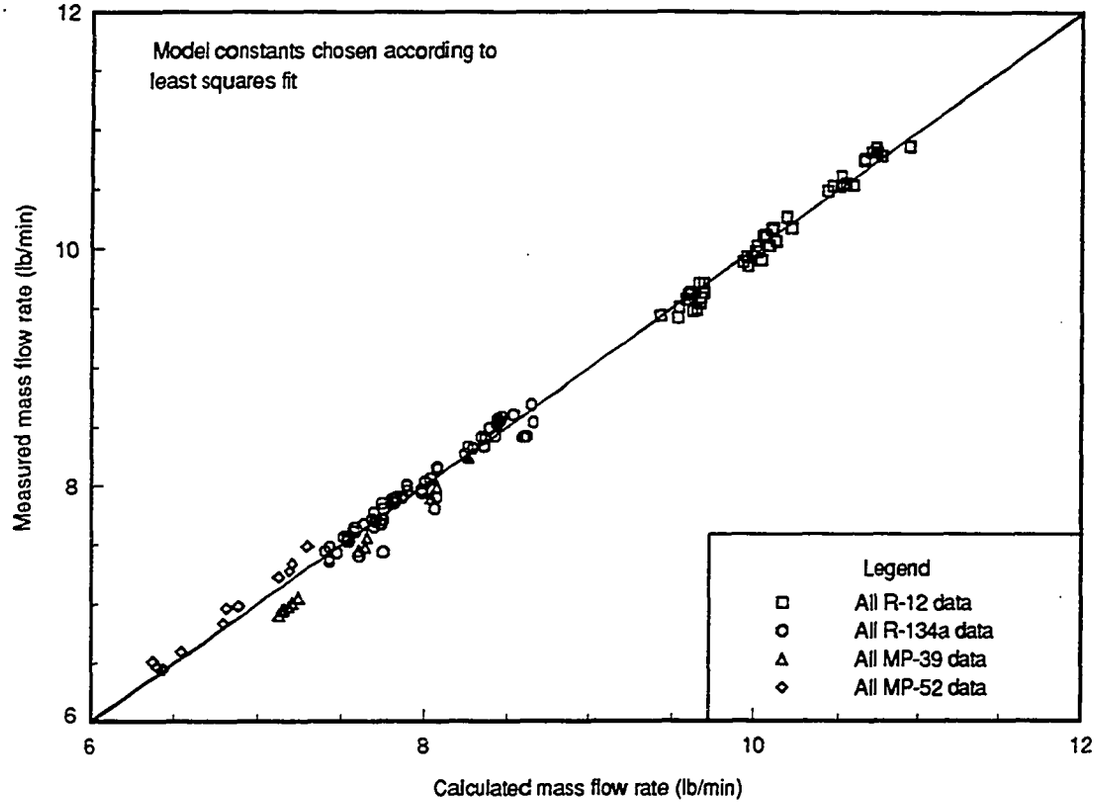

Figure 5.29: Comparison of mass flow rate with model using adjusted cylinder volumes

constants (T.V.=5.75 in^3, C.V.=0.368 in^3) give a model that predicts reasonably well the variation in mass flow rate with changes in operating conditions and refrigerant. If the pressure drop and superheating could be predicted the model would give a much more accurate representation of the data.

The mass flow rate model shows the effect of variations in the compressor inlet and exit state even though the predicted mass flow rate is low. Because the clearance volume is small, percent changes in the inlet density are much more significant than in the exit density. This is consistent with the experimental data for R-12 shown in

Figure 5.27. Changes in the inlet density caused by changes in the evaporator air temperature had the most significant effect on refrigerant mass flow rate.

Comparisons of refrigerant mass flow rates with R-12

The refrigerant mass flow rates with all of the alternative refrigerants are lower than for the system charged with R-12. The ratio of mass flow rates for R-134a are shown in Figure 5.30. The mass flow rate with R-134a was about 20% lower than with R-12. The difference in flow rates decreased with increasing evaporator air temperature. The ratio of mass flow rates for MP-39 is shown in Figure 5.31. The mass flow rate of MP-39 was about 27% lower than with R-12. The lowest refrigerant mass flow rate occurred with MP-52. The mass flow rate with MP-52 was about 32% lower than with R-12. Figure 5.32 shows the ratio of the mass flow rate of MP-52 to R-12. The ratio is fairly constant over the range of operating conditions.

The variation in mass flow rate for the various refrigerants correlates to the variation in saturated vapor density at the compressor inlet temperature. The temperatures at the compressor inlet were fairly constant so a comparison of densities at the same temperature is justified. The saturation curves for the different refrigerants are plotted on temperature specific volume axis in Figure 5.33. At an average saturated vapor temperature of 30 F, the R-12 is shown to have the lowest specific volume or maximum density. This corresponds to the observed maximum refrigerant flow rate with R-12. The curve with the minimum flow rate, MP-52, has the highest saturated vapor specific volume. The differences in flow rates of R-134a and MP-39 are most likely due to differences in specific heats and compressor exit densities.

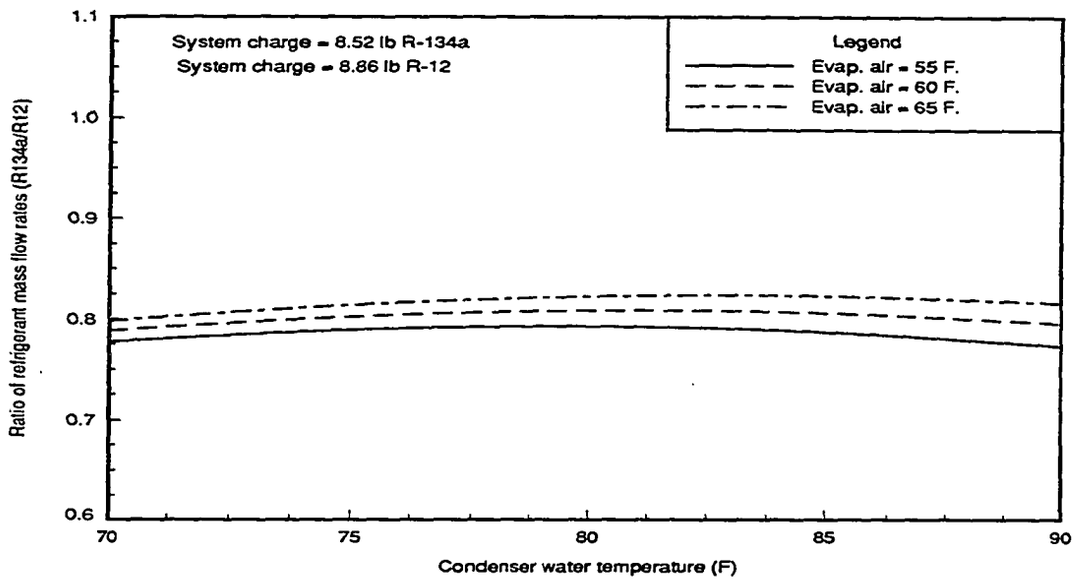

Figure 5.30: Comparison of refrigerant mass flow rates with R-134a and R-12

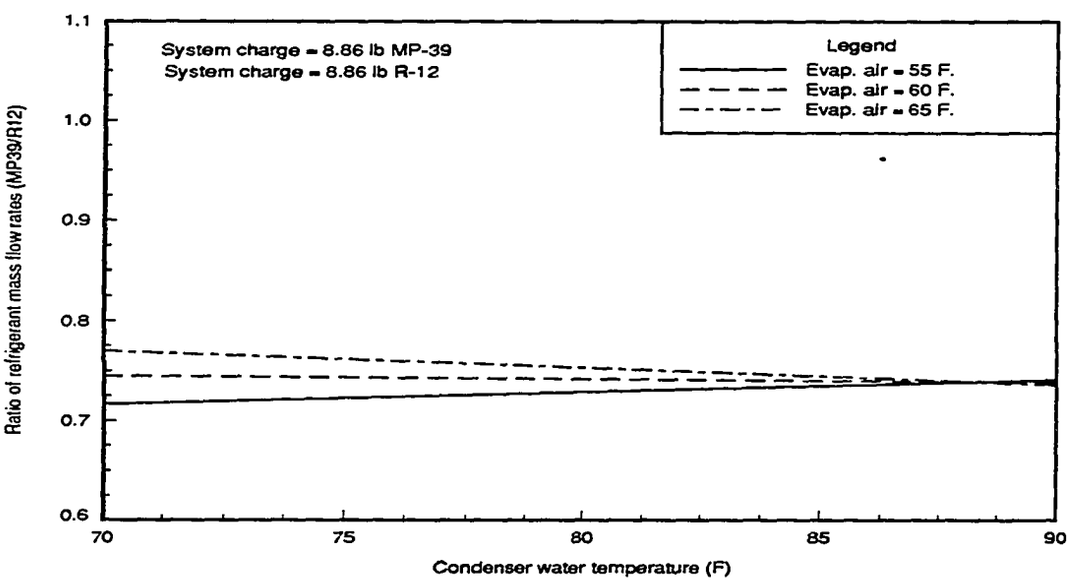

Figure 5.31: Comparison of refrigerant mass flow rates with MP-39 and R-12

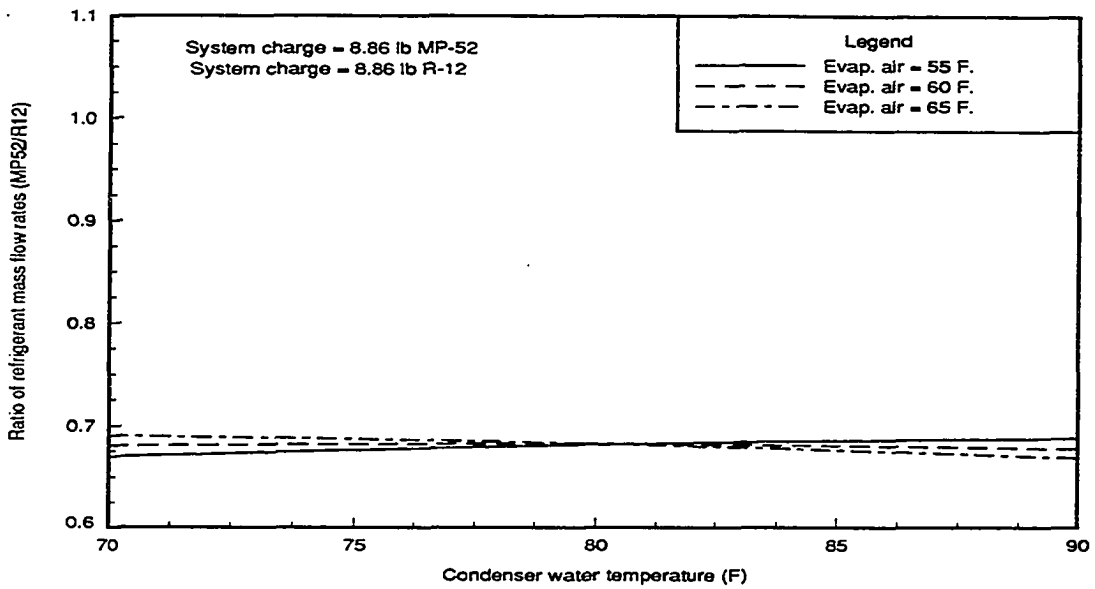

Figure 5.32: Comparison of refrigerant mass flow rates with MP-52 and R-12

Conclusions

The variations in system performance with changes in operating conditions and refrigerant are understood better when the variation in the measured refrigerant properties are understood. The study of the temperatures and pressures at the inlet and exit of components as well as the mass flow rate answered many questions as to why the variations occur. A simple look at the saturation curves explains much of the effect of changes in operating conditions and refrigerants. The expected changes in properties based on simplified models correlated well with the observed changes.

Significant differences were observed in temperature, pressure and mass flow rate for the different refrigerants. An understanding of such differences is essential to the proper modeling and design of systems. Temperature differences of 30 F were observed at the condenser inlet between R-134a and MP-39, with the temperature

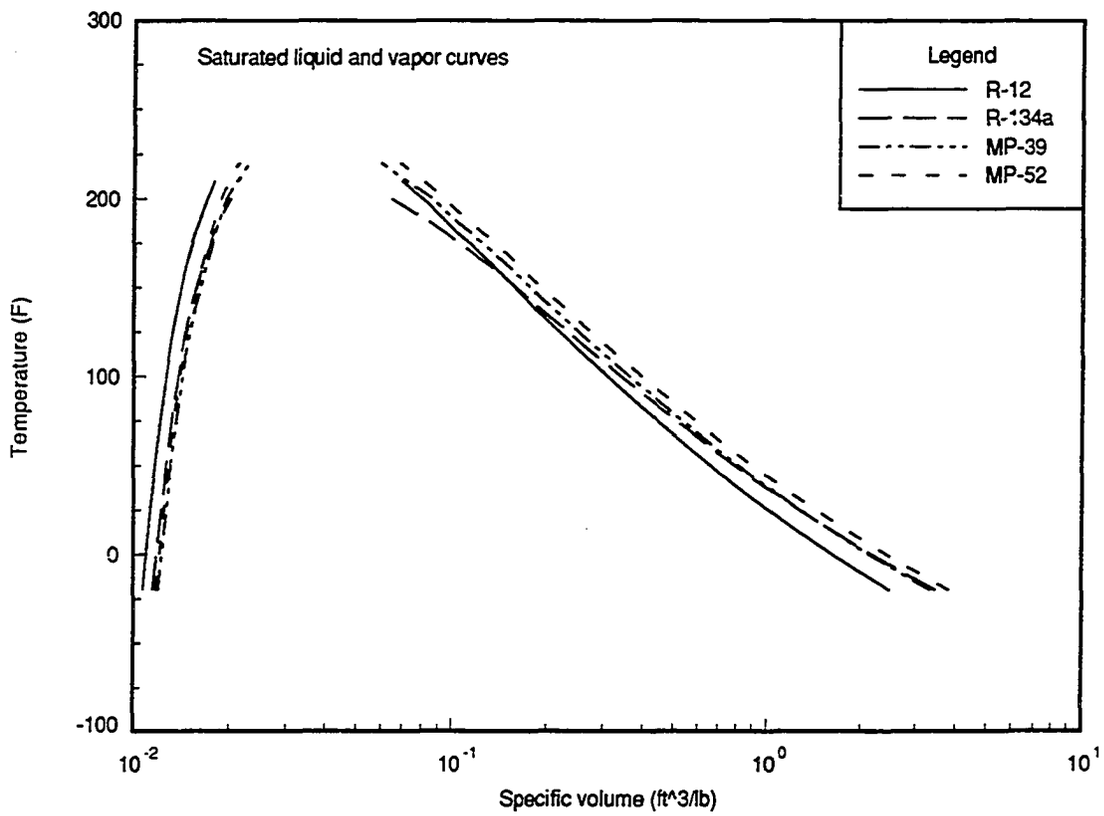

Figure 5.33: Saturated vapor temperature as a function of specific volume

with R-12 falling between these values. The condenser pressure with MP-39 was about 18% higher than with R-12. The pressure ratios with the blends were also significantly higher, 14 to 18%, than with R-12. The mass flow rates of the alternative refrigerants were all lower than with R-12 to a maximum of 33% lower with MP-52. All of these differences in operation with the alternative refrigerants affect system performance. In most cases the differences are predictable and it is assumed that the trends observed are representative of all similar systems.

CHAPTER 6. COMPRESSOR MODELING AND COMPARISON WITH DATA

Compressor Models

The compressor is one of the most complex components of the vapor compression refrigeration system. The experimental set up used a three piston hermetically sealed compressor. An understanding of the operation of the compressor is crucial to a proper understanding of the overall system performance. Compressor modeling is a subject of great interest as it relates to the phase out of CFC's since compressor design and performance is affected by the choice of refrigerant and lubricating oil. Compressor models have been developed that attempt to account for all of the processes occurring within the compressor shell [31]. A paper by Hafner [32] addresses transient effects on compressor performance. Other models simply treat the compressor as a "black box" and try to correlate the performance with inlet and exit conditions.

The two compressor performance models analyzed and compared with the experimental data are based on the concepts of polytropic compression and isentropic efficiency. Models based on specific knowledge of internal processes could not be analyzed since data was only taken at the inlet and exit of the compressor shell. The theory of each model is developed and then is compared to the observed performance.

Polytropic Compression

One method that has been widely proposed for modeling hermetically sealed piston compressors is a polytropic compressor model [33] [10]. This model is based on the assumption that the compression and expansion of the refrigerant within the cylinder follows a polytropic process. A polytropic process is a process that satisfies the following relationship [34]:

$$Pv^n = \text{constant} \tag{6.1}$$

where P is pressure, v is specific volume and n is a constant called the polytropic exponent. If such a relationship holds true, then the polytropic exponent can be determined from the pressure and specific volume at the beginning and end of the process.

$$n = \frac{\log(P_1/P_2)}{\log(v_1/v_2)} \tag{6.2}$$

It is assumed that the polytropic exponent is the same for both compression and expansion. The reason for including the expansion of refrigerant is that there is a small space remaining at the end of the compression stroke called the clearance volume. This volume is normally about 2 to 5% of the total volume measured with the piston at bottom dead center.

The work done by the piston can be calculated from the integral:

$$W = \int F ds \tag{6.3}$$

where F is the force acting on the piston and ds is the differential movement of the piston parallel to the force. The force on the piston is equal to the thermodynamic

pressure of the refrigerant times the piston face area, assuming no measurable pressure gradients in the fluid throughout each cycle and minimal frictional forces. The differential path of the piston, ds, can be described in terms of differential changes in volume, dV, since the piston area is constant. The work for each cycle can then be evaluated as:

$$W = \oint P dV \tag{6.4}$$

An idealized cycle for the compressor is shown in Figure 6.1. The two constant pressure processes shown represent the intake and exhaust portions of the cycle. In an actual compressor these pressures would vary slightly with piston position because of dynamic effects. The other two processes shown assume polytropic compression and expansion represented by a single polytropic exponent. The compressor work for one cycle, given in equation 6.4, is equal to the bounded by the curve shown in Figure 6.1. The same area, and therefore the work per cycle, can be shown mathematically to be equal to the following integral:

$$W = \oint V dP \tag{6.5}$$

Equation 6.5 is easy to evaluate since the two polytropic processes take place with a constant mass. The exhaust and intake portion of the cycle do not affect the integral since it is assumed that these two processes occur at constant pressure. Therefore, the work per cycle may be calculated as:

$$W = \int_1^2 V dP + \int_3^4 V dP \tag{6.6}$$

$$= m_{comp} \int_1^2 v dP + m_{exp} \int_3^4 v dP \tag{6.7}$$

$$= m_{comp} * \frac{n}{n-1}(P_2 v_2 - P_1 v_1) + m_{exp} * \frac{n}{n-1}(P_4 v_4 - P_3 v_3) \tag{6.8}$$

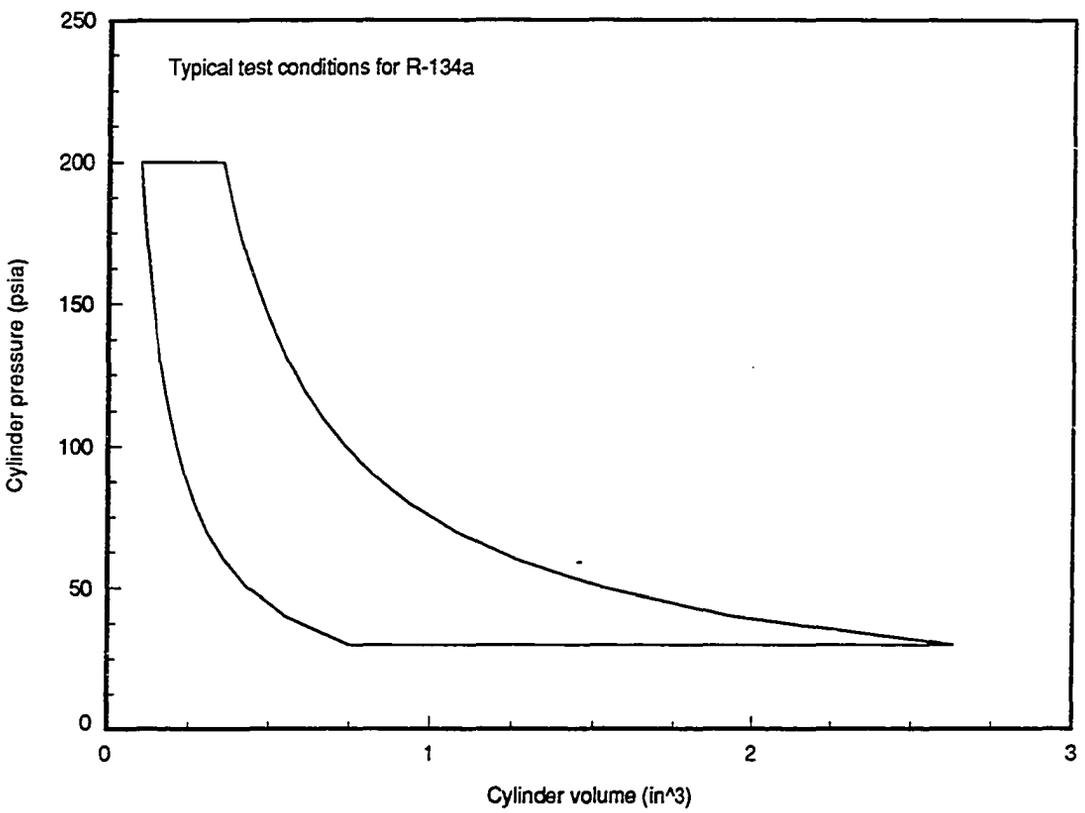

Figure 6.1: Pressure vs. volume for compressor cycle

The mass of the refrigerant during compression and expansion can be defined in terms of the refrigerant density and cylinder volume.

$$m_{comp} = \rho_1 * T.V. \tag{6.9}$$

$$m_{exp} = \rho_3 * C.V. \tag{6.10}$$

The mass delivered by the compressor per cycle is then calculated as:

$$\frac{m}{\text{cycle}} = m_{comp} - m_{exp} \tag{6.11}$$

$$= \rho_1 * T.V. - \rho_3 * C.V. \tag{6.12}$$

Combining the expressions for mass with the expression for work per cycle and noting that $P_1 = P_4$ & $P_2 = P_3$ gives:

$$W = (P_1 * T.V. - P_2 * C.V.) * \frac{n}{n-1} * \left(\left(\frac{P_2}{P_1} \right)^{\frac{n-1}{n}} - 1 \right) \tag{6.13}$$

The work per cycle is then simply a function of the inlet and exit pressure and the polytropic exponent.

The above expression for compressor work per cycle could be used to model the actual performance of a hermetically sealed compressor if certain assumptions are made about pressure drops at the inlet and exit valves of the compressor. As a first guess, it is assumed that the pressure drops across the valves are insignificant. Therefore the measured pressures at the inlet and exit of the compressor shell are used to approximate the cylinder pressures. This will cause the work to be underestimated by some amount as the actual pressure ratio will be somewhat higher. The work calculated by the above expression also assumes 100% mechanical and motor efficiency. The clearance volume was assumed to be equal to 4% of the displacement volume. The displacement volume per revolution and the rotational speed are given

by the compressor manufacturer as 7.586 in^3/rev and 3450 rpm respectively. The compressor power may then be calculated, based on equation 6.13, as:

$$\dot{W} = (P_1 * 1.04 - P_2 * 0.04) * \frac{n}{n-1} * \left(\left(\frac{P_2}{P_1} \right)^{\frac{n-1}{n}} - 1 \right) * \frac{7.586 * 3450}{12 * 778} \qquad (6.14)$$

where the power is in Btu/min and pressure is in psia. The numerator of the last term is the volumetric flow rate in in^3/min.

The set of data for R-12 taken with the new compressor and a system charge of 8.86 lb was fit to the polytropic compressor model shown in equation 6.14. The polytropic exponent (n=8.58) was chosen based on the minimization of the sum of squares of error between the model and actual data. A plot of the measured compressor power versus the value calculated from the compressor model is shown in Figure 6.2. The diagonal line shown in Figure 6.2 represents the condition of zero error between the measured and calculated values. For an accurate model the data should lie along this line. The standard deviation is 28 Btu/min and the range of measured values is only 35 Btu/min. It is clear, from the scatter shown in the plot and the unusually high value of n, that the model is not a useful predictor of compressor power as it is given in equation 6.14.

The above model assumed that all of the power input to the compressor went directly into compressing the refrigerant. Because of frictional effects and motor inefficiencies, some of the input electrical power shows up as heat transfer between the refrigerant and the internal parts of the compressor. A term is added to the compressor work model to account for friction and motor inefficiencies. It is assumed that this term is not directly affected by the operating conditions since the power only varies by about 17% over the range of conditions. The modified model including

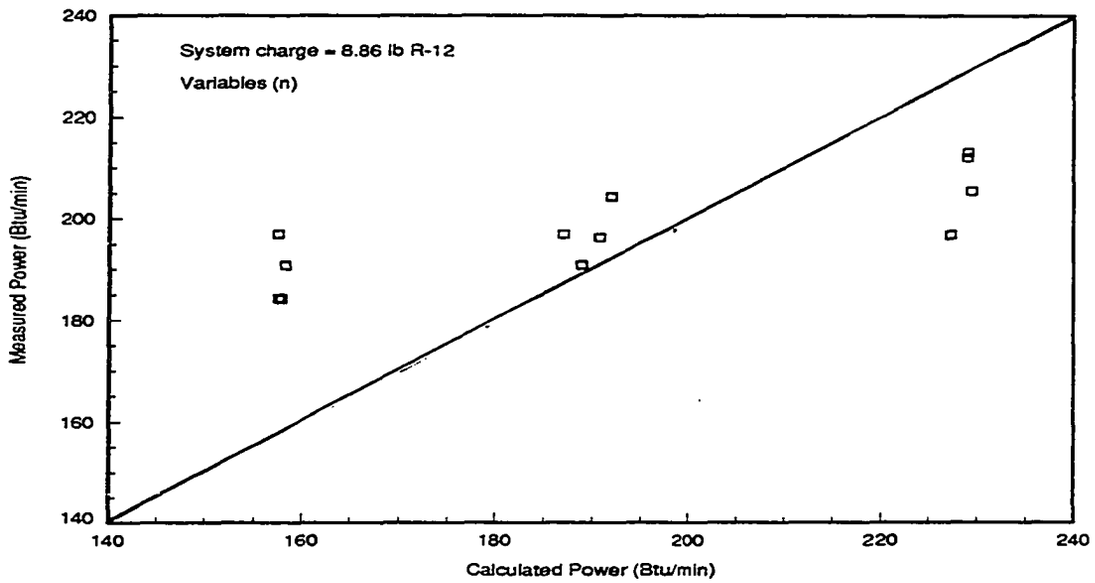

Figure 6.2: Polytropic compressor model (eqn. 6.14) fit with best polytropic exponent

a constant loss term is then given as:

$$\dot{W} = C + (P_1 * 1.04 - P_2 * 0.04) * \frac{n}{n-1} * \left(\left(\frac{P_2}{P_1} \right)^{\frac{n-1}{n}} - 1 \right) * \frac{7.586 * 3450}{12 * 778} \quad (6.15)$$

For the same data as shown in Figure 6.2 the constant C of equation 6.15 is determined to be 108.4 Btu/min. Therefore approximately 50% of the work input to the compressor is accounted for by the polytropic compression process. The remainder of the work input is independent of the operating conditions. The polytropic exponent is determined to be 0.66. A plot of the measured data versus the values calculated with the compressor model is shown in Figure 6.3. The total error for the model which accounts for friction and motor losses is an improvement but the model is still fairly inaccurate in accounting for the measured variation in power.

One of the assumptions made in the original compressor model was that the

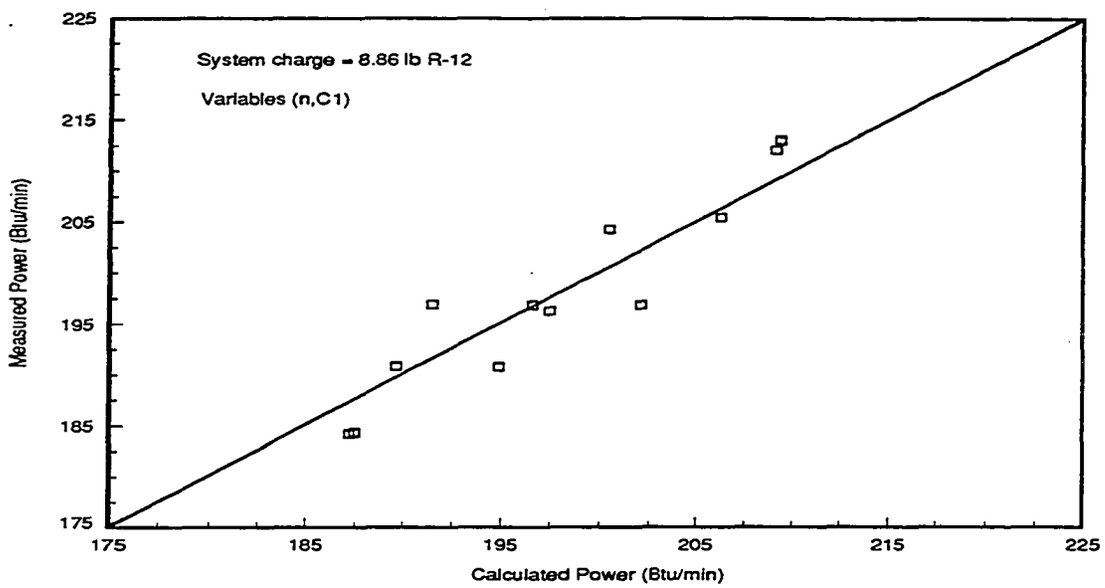

Figure 6.3: Polytropic compressor model (eqn. 6.15) fit with polytropic exponent and constant

pressure drops across the intake and exhaust valves were minimal. If this assumption is not made, then the pressure drop across these valves must be determined since the refrigerant pressures were measured outside of the cylinder. One way to determine these pressure drops is to include another constant in the compressor model. The constants are then determined according to the values that reduce the total sum of squares error. For this model it is assumed that the pressure drops across the intake and exhaust valve are equal. The appropriate compressor model is then given as:

$$\begin{aligned} \dot{W} &= C + ((P_1 - PD) * 1.04 - (P_2 - PD) * 0.04) * \frac{n}{n-1} \\ &* \left(\left(\frac{P_2 - PD}{P_1 - PD} \right)^{\frac{n-1}{n}} - 1 \right) * \frac{7.586 * 3450}{12 * 778} \end{aligned} \tag{6.16}$$

where PD is the assumed pressure drop, in psia, across the compressor valves.

Using the same R-12 data as above, the polytropic exponent is determined to be

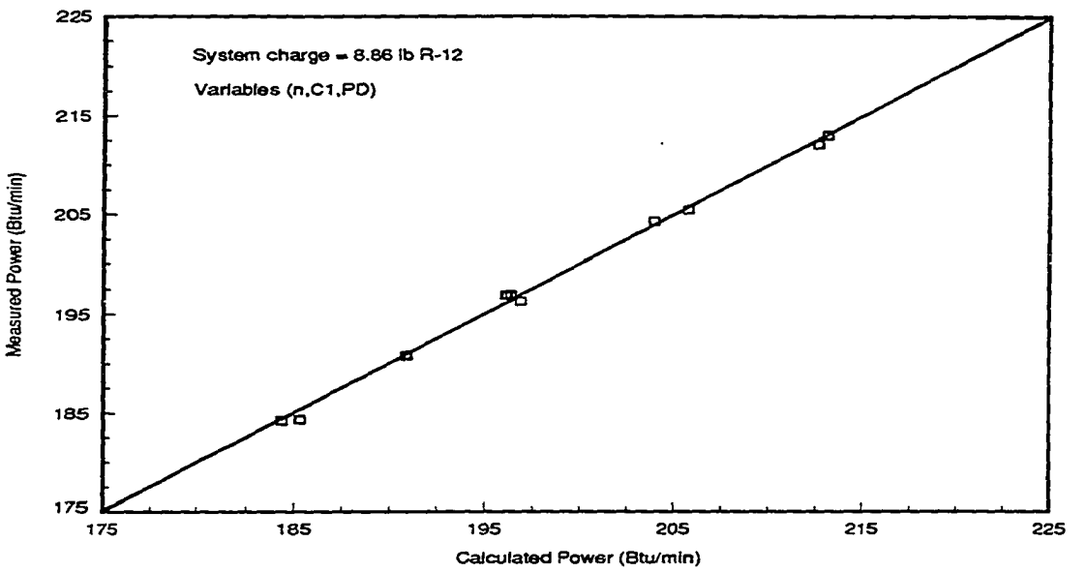

Figure 6.4: Polytropic compressor model (eqn. 6.16) fit with polytropic exponent, constant and pressure drop

1.15. The constant and pressure drop across the valves are found to be 87.5 Btu/lb and 17.6 psia respectively. A plot of the model including pressure drops is shown in Figure 6.4. Most of the data lies along the diagonal line and the standard deviation (S.D.=0.65 Btu/lb) is fairly small. The model represents the measured data well and the constants determined appear to be reasonable. The friction and motor loss term is about 40% of the total input power.

One final refinement to the model could be made by letting the pressure drop across the intake and exhaust valves differ. This is a reasonable modification, since the intake valve is a thin deflection plate and the exhaust valve is held closed by a spring device. The different pressure drops are accounted for with a pressure drop

ratio defined as $PD_{ratio} = PD_{exit} \ / \ PD_{inlet}$. The compressor model is then given as:

$$\dot{W} = C + ((P_1 - PD) * 1.04 - (P_2 - PD * PD_{ratio}) * 0.04) * \frac{n}{n-1} \quad (6.17)$$
$$* \left(\left(\frac{P_2 - PD}{P_1 - PD * PD_{ratio}} \right)^{\frac{n-1}{n}} - 1 \right) * \frac{7.586 * 3450}{12 * 778}$$

From examination of the valves, the exhaust valve will require a greater pressure difference to open than the intake valve. The data for the lowest system charge (7.42 lb) of R-134a are used in the curve fit since this data set represents the largest set of data for any one charge. It is assumed that the pressure drop ratio determined for this data set is representative of all the refrigerant data. The pressure drop ratio was determined to be 3.414 where the least squares error was minimized. A plot of the measured compressor power versus the calculated values from the model is shown in Figure 6.5. The standard deviation (S.D.=0.613 Btu/min) is small compared to the range of values measured.

This model with a pressure drop ratio of 3.414 was then used with the other refrigerant data to determine the other constants. Each data set was fit to the model separately giving a different set of constants for each refrigerant. The constants and standard deviation for each refrigerant are given in Table 6.1. The last row in the table was calculated using the four R-12 data sets representing four system charges and two identical compressors. The measured versus calculated power based on the complete model for each refrigerant is plotted in Figures 6.6-6.9.

The constants for each refrigerant are different, however all of the data are represented with little error by the same form of equation. This gives some validity to the compressor model developed. The usefulness of the model would be enhanced greatly if it could be used to predict system performance. If the values of the constants

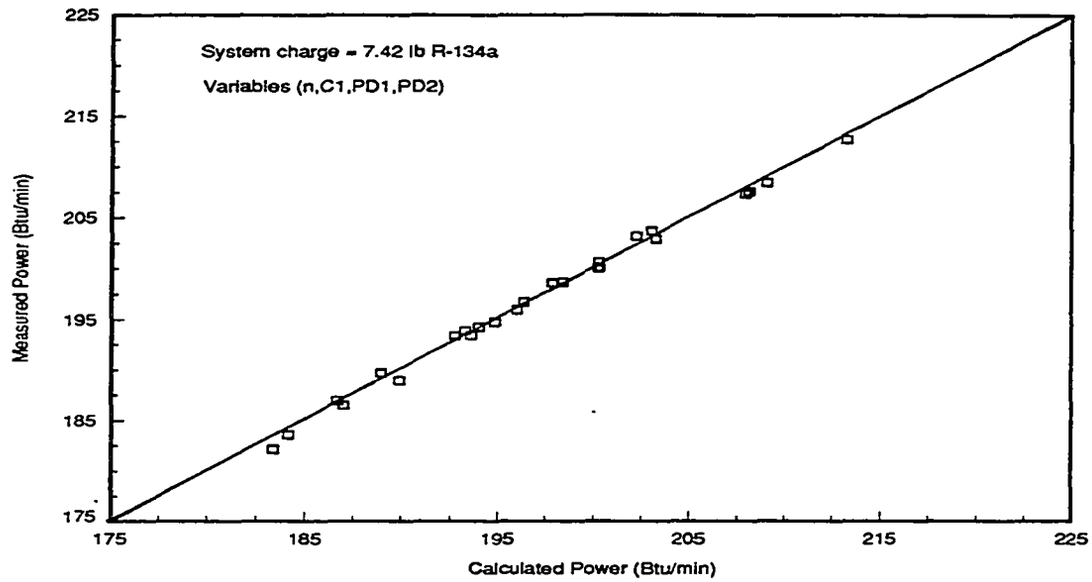

Figure 6.5: Polytropic compressor model (eqn. 6.17) fit with polytropic exponent, constant, pressure drop and pressure drop ratio for R-134a

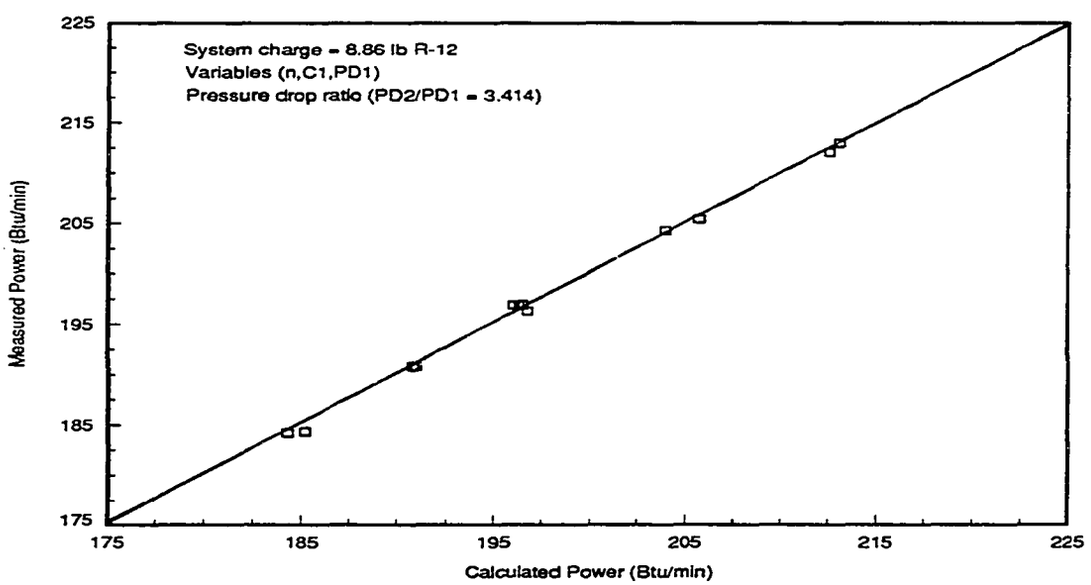

Figure 6.6: Polytropic compressor model (eqn. 6.17) fit with polytropic exponent, constant, pressure drop and pressure drop ratio for R-12

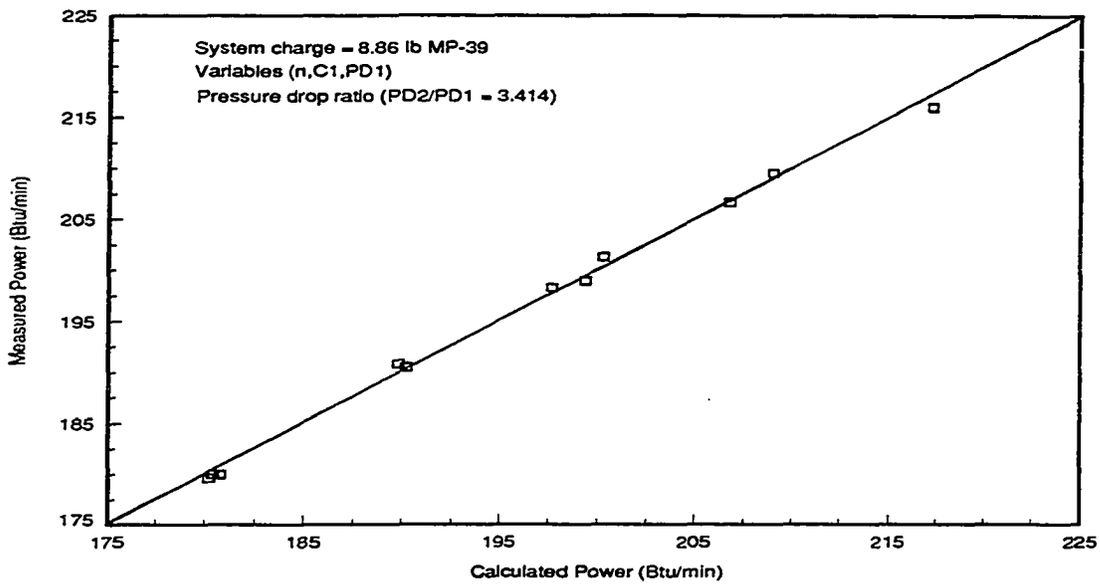

Figure 6.7: Polytropic compressor model (eqn. 6.17) fit with polytropic exponent, constant, pressure drop and pressure drop ratio for MP-39

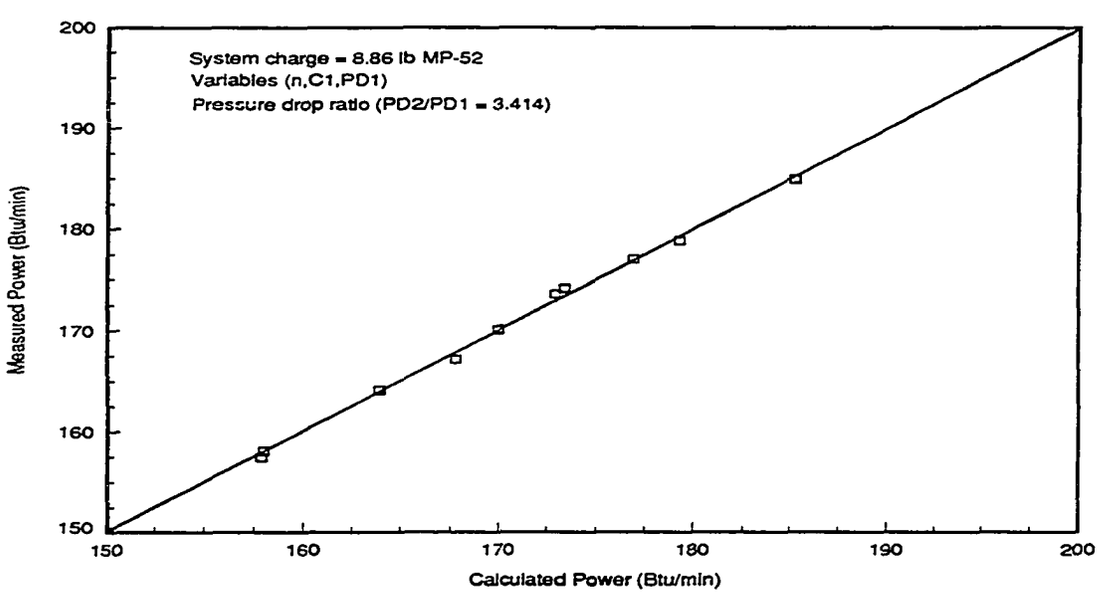

Figure 6.8: Polytropic compressor model (eqn. 6.17) fit with polytropic exponent, constant, pressure drop and pressure drop ratio for MP-52

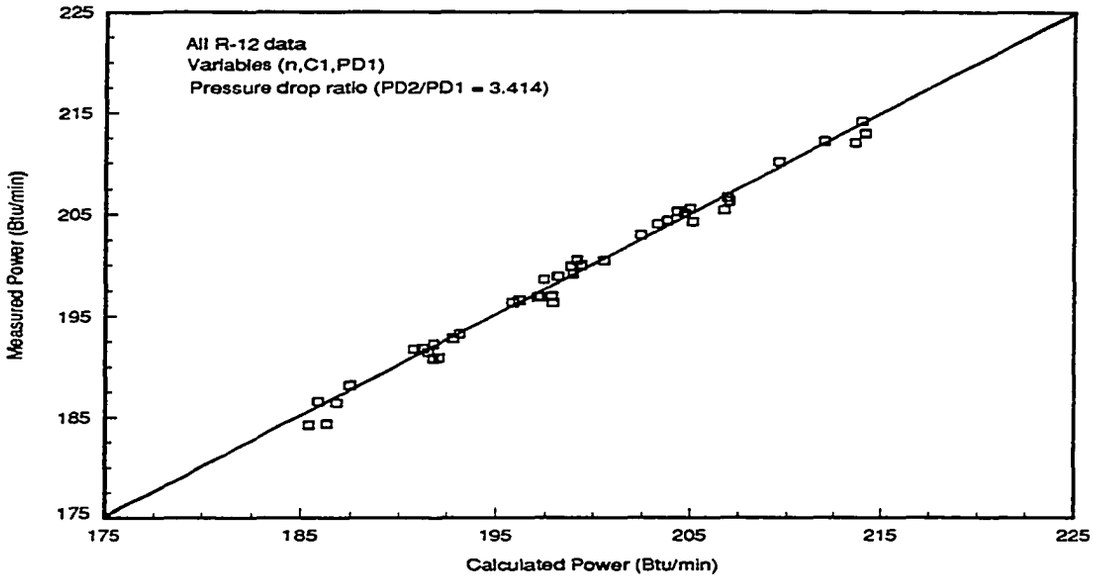

Figure 6.9: Polytropic compressor model (eqn. 6.17) fit with polytropic exponent, constant, pressure drop and pressure drop ratio for all R-12 data

could be related to fluid properties such as specific heats, viscosity, etc., then the performance with other refrigerants could be predicted. An attempt was made to correlate the constants with fluid properties, but no suitable correlations were found. Additional data would be required to give the degrees of freedom required for a model that accounts for both operating conditions and refrigerant type. The constants given in Table 6.1 are useful from the standpoint that they allow some theoretical justification for extrapolating to operating conditions outside of the experimental range of conditions.

A comprehensive model may be constructed using all the data for every refrigerant tested to determine the model constants. When this is done the standard deviation becomes larger than the variability due to changes in operating conditions. The model therefore has little predictive power since the error is so large. The values

Table 6.1: Constants for polytropic compressor model (eqn. 6.17)

Data set	C (Btu/min)	n	P1 (psia)	PD_{ratio}	Std. deviation (Btu/min)
8.86 lb R-12	66.4	1.16	13.0	3.414	0.59
8.79 lb R-134a	77.1	1.06	10.3	3.414	0.61
8.86 lb MP-39	41.2	1.37	12.8	3.414	0.88
8.86 lb MP-52	53.5	1.16	9.3	3.414	0.56
All R-12 data	68.0	1.15	13.1	3.414	0.89

given in Table 6.1 may be varied slightly with little effect on the model. This is shown graphically for all of the R-12 data with a contour plot in Figure 6.10. The axes show the effects of variation in pressure drop and polytropic exponent. The contour lines represent lines of constant standard deviation. The key to the right of the plot gives the standard deviation for the compressor power, in Btu/min. The box located near the center of the plot shows the minimum standard deviation and the corresponding pressure drop and exponent given in Table 6.1. If similar plots were constructed for the other refrigerants, it could be shown that the regions of low standard deviation do not not all overlap in any common point. An additional parameter must be added to the model that accounts for differences in fluid properties.

Isentropic Efficiency

Another common method for determining compressor power is to use an isentropic efficiency. For any real compressor, assuming no heat transfer through the compressor shell, there will be a positive change in entropy from inlet to exit due to irreversibilities. The limiting case where the change in entropy is zero represents a compressor with no irreversibilities, such as friction, temperature gradients, or motor losses. The ratio of enthalpy change for an isentropic compressor to the actual en-

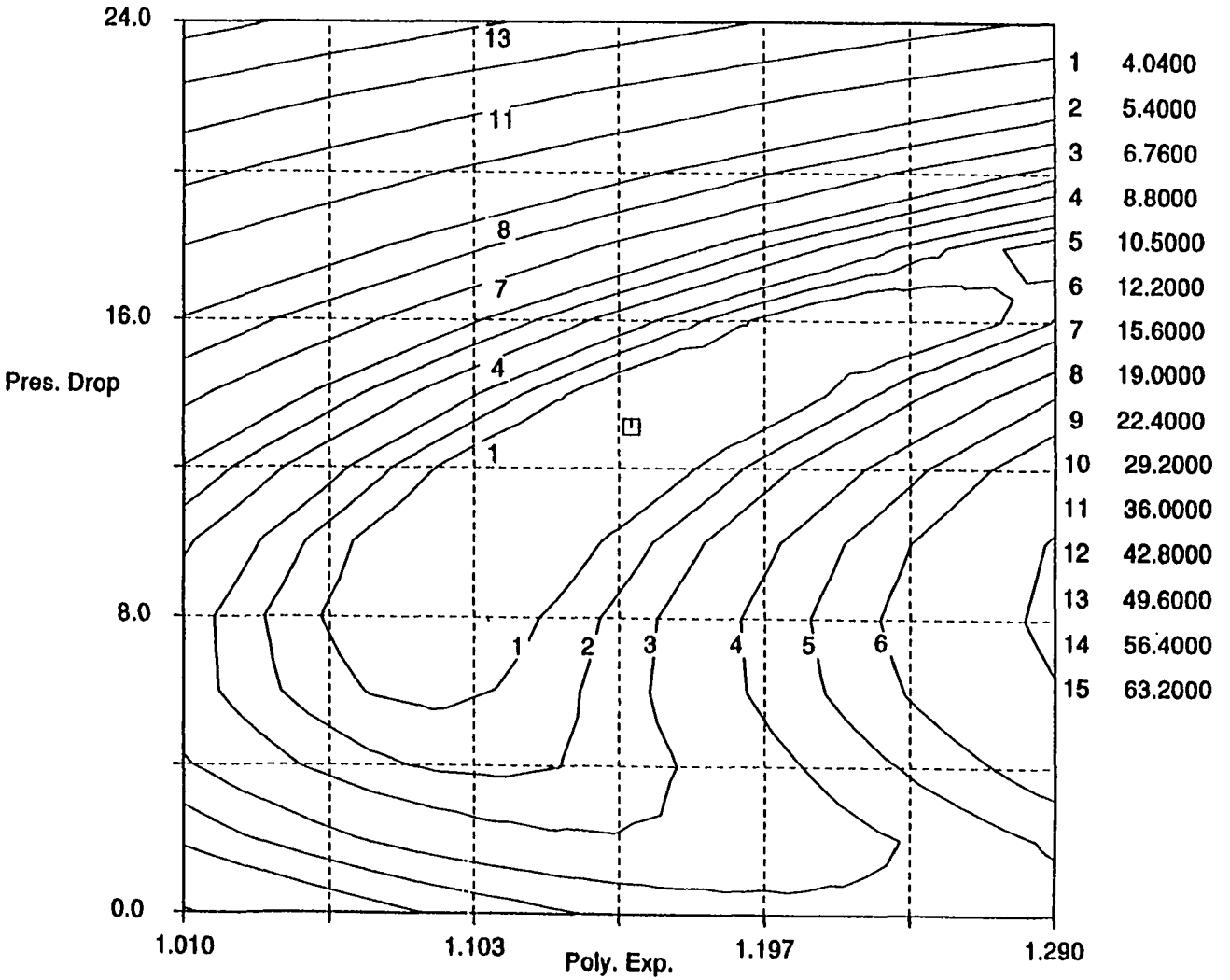

Figure 6.10: Contour plot of standard deviation for polytropic compressor model with all R-12 data

thalpy change is defined as the isentropic efficiency. If the isentropic efficiency were constant, then the compressor power could be calculated from knowledge of the inlet state, the exit pressure, and the refrigerant mass flow rate, as follows:

$$\dot{W} = \dot{m} * \frac{h_{2s} - h_1}{\eta} \tag{6.18}$$

where $\dot{m}$ is the refrigerant mass flow rate, h_{2s} is the enthalpy for isentropic compression, h_1 is the inlet enthalpy and η is the isentropic efficiency. The enthalpy for isentropic compression h_{2s} is calculated at the entropy of the inlet state and the pressure of the exit state.

A key assumption made in the development of equation 6.18 is that there is no heat transfer through the compressor shell. If this were not the case, then isentropic compression would not correspond to an isentropic efficiency of 1. Unless the surface temperature of the compressor shell is known, the entropy transfer through the compressor shell is unknown and the meaning of an isentropic efficiency for the compressor is lost. Figure 6.11 shows the heat transfer rate through the compressor shell for all the data. The heat transfer rate was calculated as the difference in measured power input to the compressor and rate of energy transferred to the refrigerant from compressor inlet to exit as calculated by the product of mass flow rate and enthalpy change. The percent of the energy input that leaves through the compressor shell is less than 10%. It is therefore reasonable to assume that an isentropic efficiency may help predict the performance of the compressor.

The isentropic efficiency for each refrigerant and operating condition was calculated and is plotted in Figure 6.12 versus pressure ratio. The isentropic efficiency varies from 38% to 53%. Use of a constant isentropic efficiency for all operating conditions will not accurately represent the observed changes in performance. The

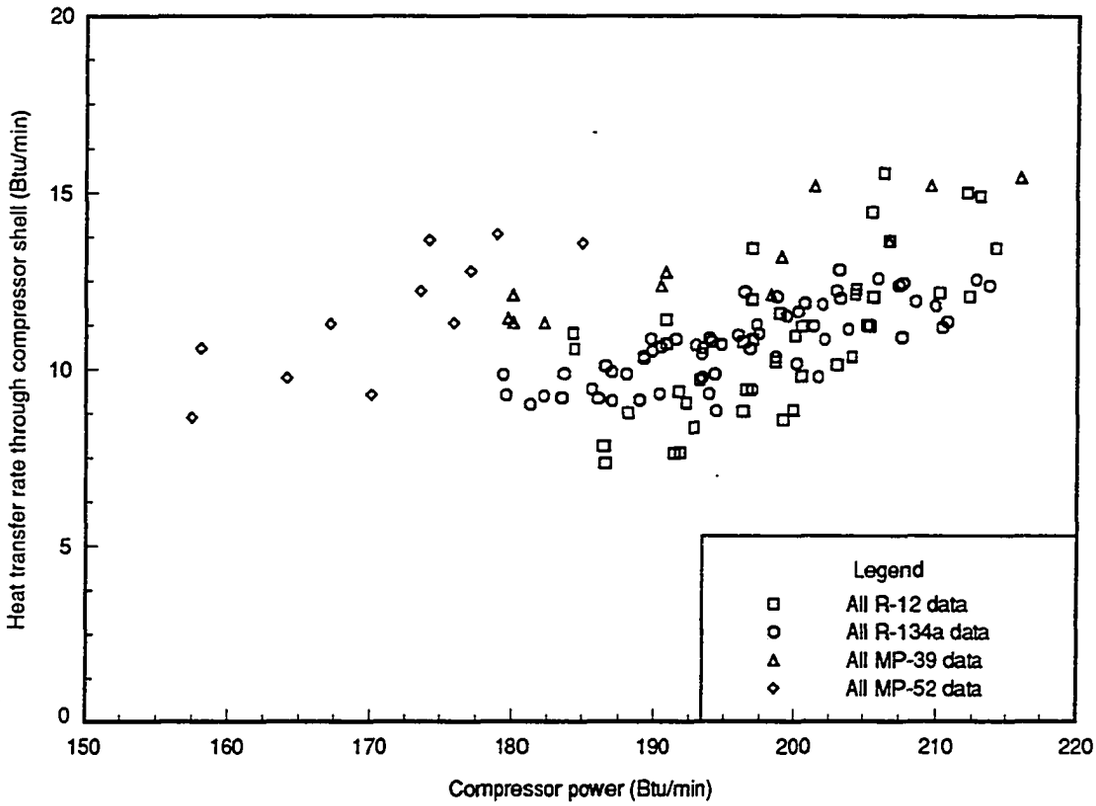

Figure 6.11: Heat transfer through compressor shell for all refrigerants

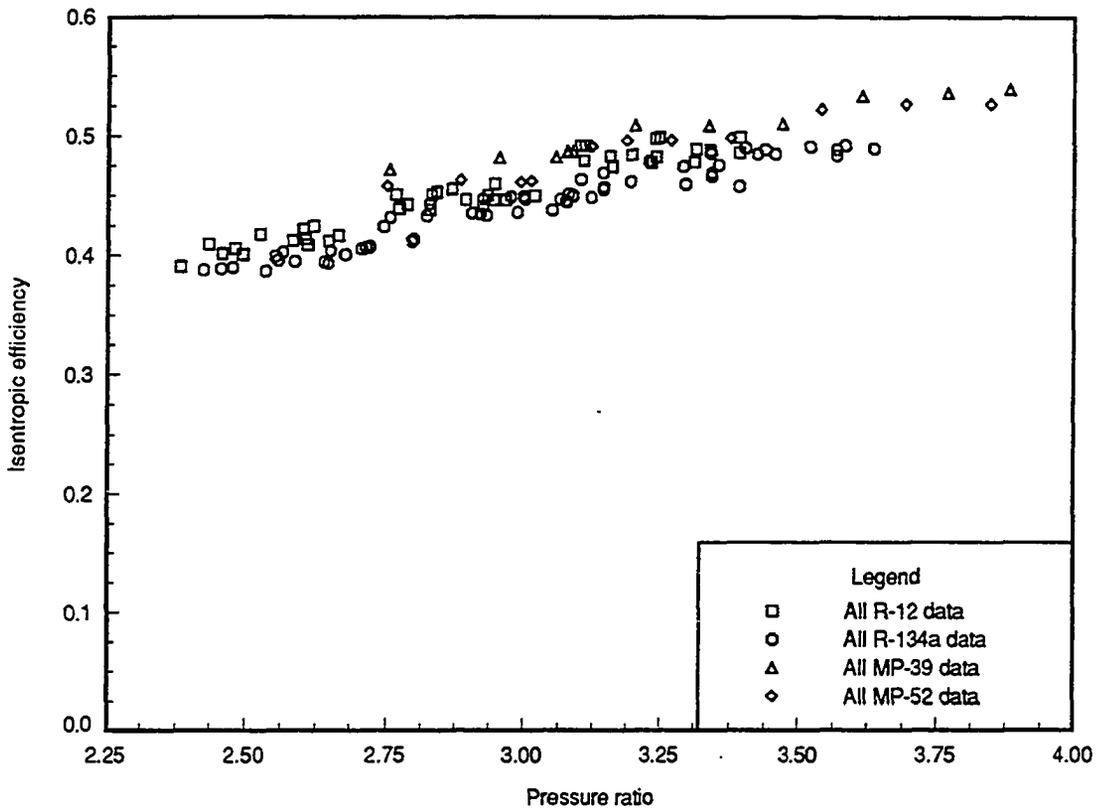

Figure 6.12: Compressor isentropic efficiency as a function of pressure ratio

isentropic efficiency tends to increase with increasing pressure ratio. Even when accounting for this variation, there is still a significant amount of error associated with such a model. The use of an isentropic efficiency is simple but does not adequately represent the small changes observed in compressor performance. Such a model may be useful for design purposes but it will not accurately represent the variation in performance due to different operating conditions or change in refrigerant.

Conclusions

Simple models such as a polytropic compressor model or a model based on the use of an isentropic efficiency are useful in correlating actual compressor data. However, their usefulness in predicting compressor performance of untested refrigerants or well outside the range of test conditions is limited. The constants used in the polytropic model varied from refrigerant to refrigerant and were not correlated to any specific refrigerant property. With more testing, correlations relating these constants to refrigerant properties may be found. Theoretical studies which use a polytropic compressor model or a constant isentropic efficiency and do not take into account variation due to effects of refrigerant properties should be viewed with suspicion.

CHAPTER 7. HEAT EXCHANGER TEMPERATURE PROFILES AND MODELING

Introduction

One of the objectives of the experimental project undertaken was to better understand the performance of the individual system components. The heat exchangers, the evaporator and condenser, are two crucial components of a refrigeration system. The efficiency of the system depends on the effectiveness of the heat exchangers. The heat transfer rate of the two heat exchangers in the refrigeration system is a function of the heat exchanger area, the overall heat transfer coefficient and the temperature difference between the refrigerant and source. This functional relationship is used in both the analysis and design of refrigeration equipment.

A proper understanding of heat exchanger performance is a prerequisite to the development of models that accurately predict system behavior. A detailed analysis of temperature profiles in the two heat exchangers is presented in the present chapter to help explain the effects of changes in operating conditions and refrigerants. In the later half of the chapter, several models are explored and compared to the experimental data. An accurate model of heat exchanger performance is required in order to design exchangers using new refrigerants and to predict the effect of changing refrigerants.

Heat Exchanger Temperature Profiles

The purpose of a heat exchanger is to transfer energy between two fluids. The driving force behind the heat transfer is the local temperature difference between the two interacting fluids. For a given heat exchanger, the two primary means of affecting the heat transfer rate is by increasing the mass flow rate of the fluids or by increasing the temperature difference. The operating conditions, condenser water temperature, evaporator air temperature, mass flow rate and type of refrigerant, affect the heat exchanger temperature profiles in different ways. The effect of each of these variables is presented in detail for both the condenser and evaporator in the following sections.

Calculation of temperature profiles

The instrumentation for the experimental setup was designed to give the temperature and pressure at the inlet and exit of each component of the refrigeration system. Given that the refrigerant can be modeled as a pure simple compressible substance, the temperature and pressure data specifies the thermodynamic state between each component, except at the inlet to the evaporator. For this point, the pressure is measured and the enthalpy is assumed to be the same as the enthalpy at the inlet to the expansion valve. The evaporator and condenser are both evaluated as counterflow heat exchangers. The refrigerant undergoes three processes in the condenser: desuperheating, condensing, and subcooling. In the evaporator, boiling and superheating occur. The heat transfer was broken down into detail representing the above processes with use of the measured inlet and exit temperatures, energy balances, and saturation temperatures.

The data used for determination of the heat exchanger temperature profiles are

the inlet and exit refrigerant temperature and pressure, the inlet and exit air and water temperature and the mass flow rate of each fluid. The total heat transfer rate for each phase can be determined from the refrigerant data. If it is assumed that the pressure drop occurs in the two phase region, then the state of the refrigerant at each saturation state can be determined.

The state at the inlet to the condenser, in the superheated region, is measured. The state, and therefore temperature, at the end of the superheated region is defined by the saturated vapor state at the inlet pressure. The enthalpy change for the superheated region can then be determined. The heat transfer rate for the superheated vapor is calculated as the product of the refrigerant mass flow rate and the corresponding enthalpy change. Assuming steady state operation and no heat loss from the outside of the condenser, the same rate of heat transfer must occur in the condenser water. The temperature change for the water is then calculated from the heat transfer rate. The state at the other end of the two-phase region is defined as the saturated liquid state at the exit pressure. With this method, all of the intermediate temperatures and log mean temperature differences can be determined for each region. The equations used in the condenser temperature profile calculations are given as:

$$\dot{m}_w c_p (T_{w4} - T_{w3}) = \dot{m}_r (h(T_{r1}, P_{r1}) - h_g(P_{r1})) \tag{7.1}$$

$$\dot{m}_w c_p (T_{w3} - T_{w2}) = \dot{m}_r (h_g(P_{r1}) - h_f(P_{r4})) \tag{7.2}$$

$$\dot{m}_w c_p (T_{w2} - T_{w1}) = \dot{m}_r (h_f(P_{r4}) - h(T_{r4}, P_{r4})) \tag{7.3}$$

$$T_{r2} = T_{sat}(P_{r1}) \tag{7.4}$$

$$T_{r3} = T_{sat}(P_{r4}) \tag{7.5}$$

where the subscript w and r stand for condenser water and refrigerant respectively. The subscript 1 corresponds to the fluid inlet condition and the 4 corresponds to the fluid exit condition. The intermediate subscripts refer to the location of the refrigerant saturation conditions. Equations 7.1- 7.3 are the energy balance equations for each region in the condenser. The left side of the equations is the heat transfer rate to the condenser water where the flow is assumed to be incompressible and have constant specific heat.

Temperature profiles for R-12

The temperature profiles for the R-12 data were calculated for the data with a refrigerant charge of 8.86 lb. The data used were taken with the original compressor. The evaporator air temperatures and the condenser water temperatures given on the temperature profile plots represent nominal values only. The nominal values are the desired test conditions. The actual test conditions varied slightly (10 to 15%) since setting these values at exact conditions repeatedly was difficult.

Condenser profiles for constant condenser water temperature The temperature profiles in the condenser showing the effect of changes in evaporator air temperature are given in Figure 7.1. The condenser water inlet temperature was held constant at 80 F for the three profiles shown. The evaporator air temperature was varied from 55 F to 65 F. The temperatures are plotted versus the heat transfer rate rather than versus area. The reason for this is that the relative area of the condenser for each of the three regions could not be measured. The heat transfer rate associated with each region was not directly measured, but can be calculated based

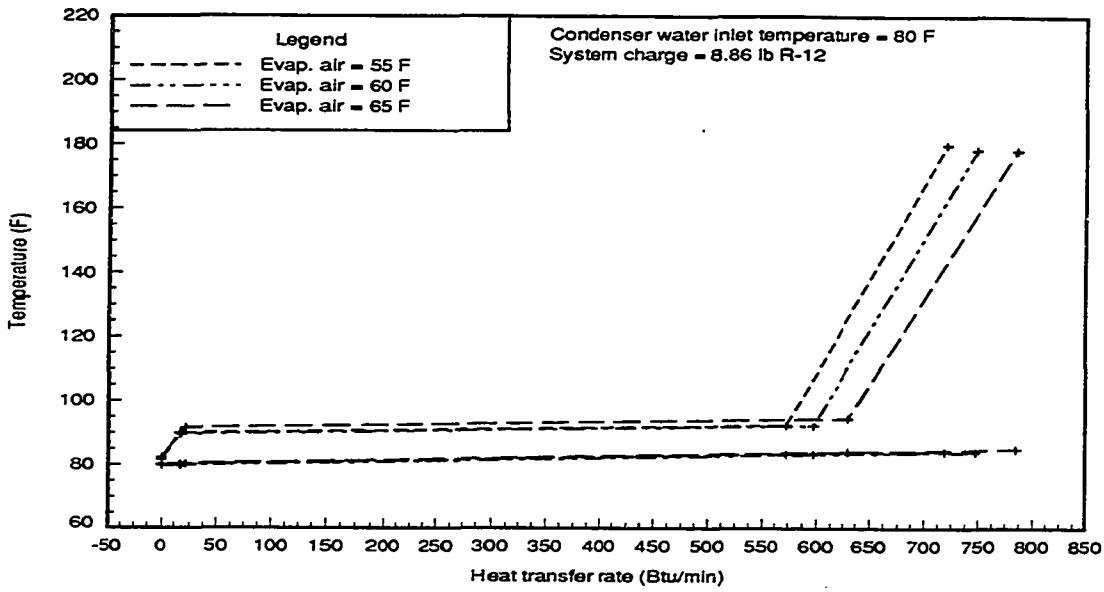

Figure 7.1: Condenser temperature profiles for R-12 showing the effect of varying evaporator temperature

on the enthalpy change and mass flow rate of the refrigerant as noted above. The heat transfer rates shown in the condenser temperature profiles are calculated based on the relative enthalpy of the condenser exit. Assuming a constant specific heat for the condenser water, the bulk water temperature must vary linearly with increasing values of heat transfer rate. Similarly, for constant specific heat of the refrigerant in the subcooled and superheated regions, the temperature profiles are straight lines. If the temperatures were plotted versus condenser position the profiles would not be linear but exponential.

The changes in evaporator air temperature represented in Figure 7.1 show little effect on the condenser water profile except that the total heat transfer rate is increased. This is simply due to the fact that the specific heat, mass flow rate and inlet temperature of the condenser water are each constant. The slight slope of the refrig-

erant temperature profile in the two-phase region is due to the pressure drop in the condenser. The slopes of the temperature profiles in the subcooled and superheated regions decrease slightly for increasing evaporator air temperature because of an associated increase in refrigerant mass flow rate. As the evaporator air temperature rises, the evaporator pressure rises, which increases the density at the compressor inlet. The increase in density causes a rise in mass flow rate. The percent of heat transfer associated with each region is fairly constant for changes in evaporator air temperature. The majority of the heat transfer, about 77%, occurs in the two-phase region.

Evaporator profiles for constant condenser water temperature The temperature profiles for the evaporator with R-12 are shown in Figure 7.2. The temperature profiles for the evaporator were calculated using the same methods used to calculate the condenser temperature profiles. The heat transfer rates shown in the evaporator temperature profiles are based on the relative enthalpy of the evaporator inlet. The refrigerant temperature at the saturated vapor condition is determined using the measured saturation pressure. The corresponding air temperature at this point in the evaporator is determined with an energy balance. The condenser water temperature was held constant at 80 F. The evaporator air temperature was varied from 55 F to 65 F. The upper lines show the evaporator air temperatures and the lower three lines show the refrigerant temperatures. The negative slope of the refrigerant profile in the two-phase region is due to the pressure drop in the evaporator. The mass flow rate increases with evaporator air temperature increasing the total heat transfer rate by affecting the refrigerant side heat transfer coefficient. An increase in

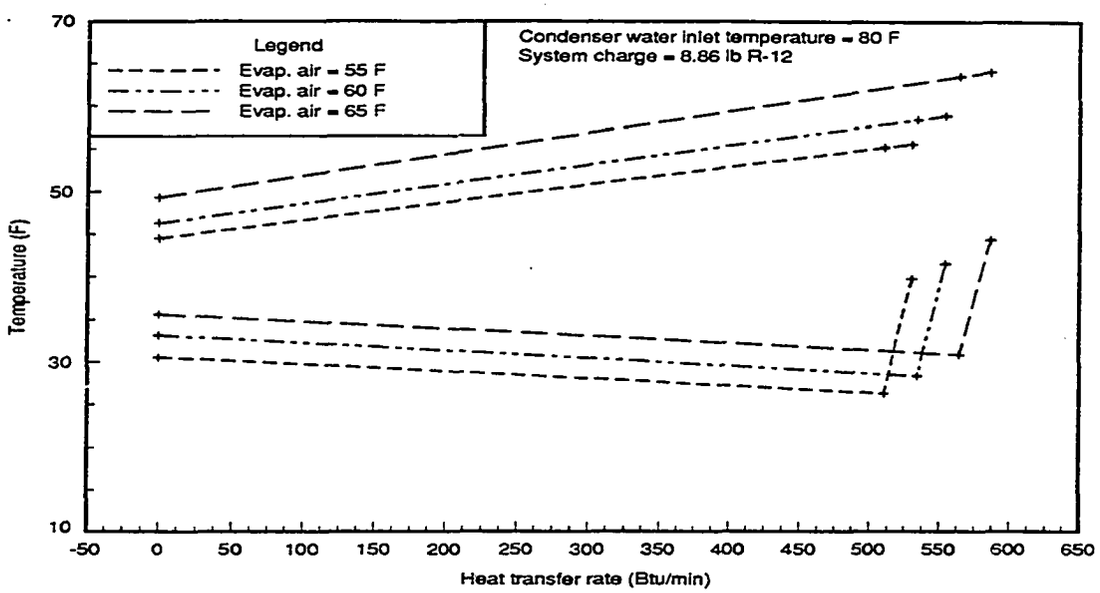

Figure 7.2: Evaporator temperature profiles for R-12 showing the effect of varying evaporator temperature

the evaporator air temperature causes the refrigerant temperature to increase. The majority of the heat transfer occurs in the two-phase region. Only about 4% of the heat transfer occurs in the superheated region. The percent of heat transfer associated with each region is fairly constant for changes in evaporator air temperature.

Condenser profiles for constant evaporator air temperature Figure 7.3 shows the condenser temperature profiles for changes in the condenser water temperature. The evaporator air inlet temperature was held constant at 60 F. The slope of the water temperature profiles are constant. An increase in condenser water temperature causes a rise in every point of the refrigerant temperature profile. The refrigerant mass flow rate decreases with increasing condenser water temperature increasing the slope of the temperature profile in the superheated and subcooled regions. The pos-

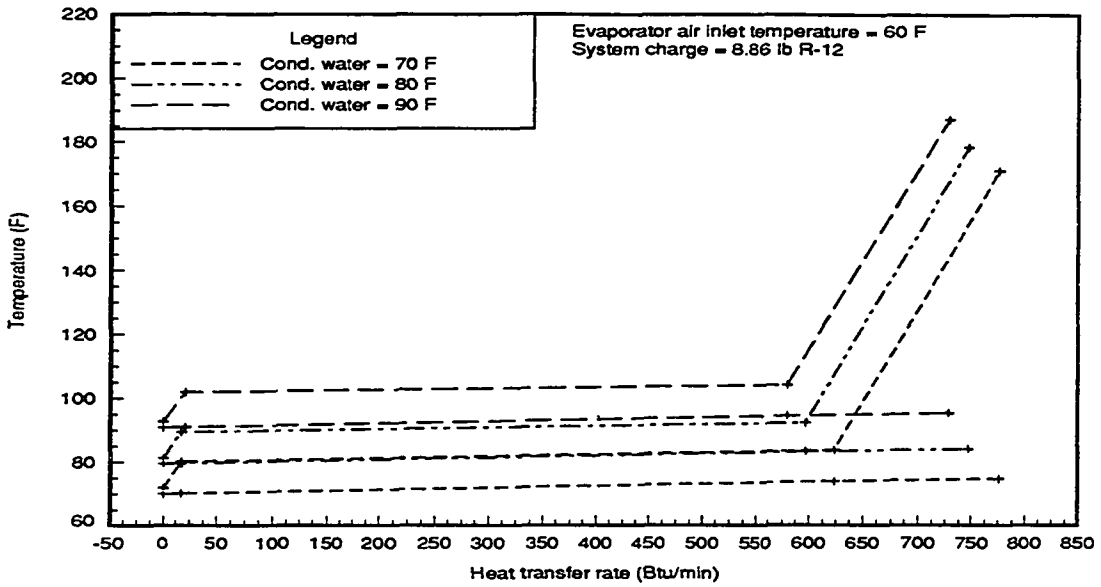

Figure 7.3: Condenser temperature profiles for R-12 showing the effect of varying condenser temperature

itive slope in the two-phase region is due to the pressure drop in the condenser. The percent of heat transfer that occurs in the two-phase region decreases slightly, about 2.5%, for the increase in evaporator air temperature. The percent of heat transfer for both of the other regions increases.

Evaporator profiles for constant evaporator air temperature For a constant evaporator air inlet temperature, a change in condenser water temperature has little effect on the temperature profile of the evaporator. Figure 7.4 shows this effect for the R-12 data. The evaporator air temperature is help constant at 60 F. The upper three lines are the evaporator air temperature profiles. The lower lines are the refrigerant temperature profiles. An increase in condenser water temperature causes a decrease in the total heat transfer rate. The percent of heat transfer associated

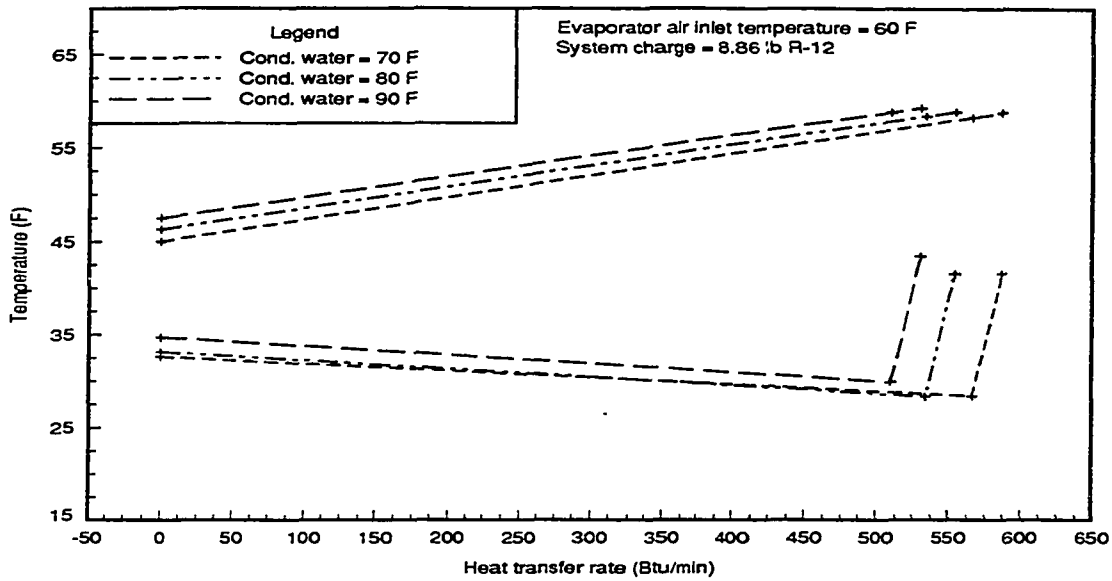

Figure 7.4: Evaporator temperature profiles for R-12 showing the effect of varying condenser temperature

with the superheated region, about 4%, increases about 12% for the 20 F rise in condenser water temperature.

Temperature profiles for R-134a.

The temperature profiles for the R-134a data are very similar to those for the R-12 data. The same four plots as given in Figures 7.1-7.4 are given in Figures 7.5-7.8 except the refrigerant has been changed to R-134a. In Figure 7.5, showing the temperature profiles for the condenser, the temperature difference for the two-phase region is about the same as for the R-12 data. The average temperature difference for the superheated region, however is much smaller for the R-134a data. The percent of heat transfer associated with each region in the evaporator and condenser is approximately the same as with the R-12 data. The total heat transfer rate, however,

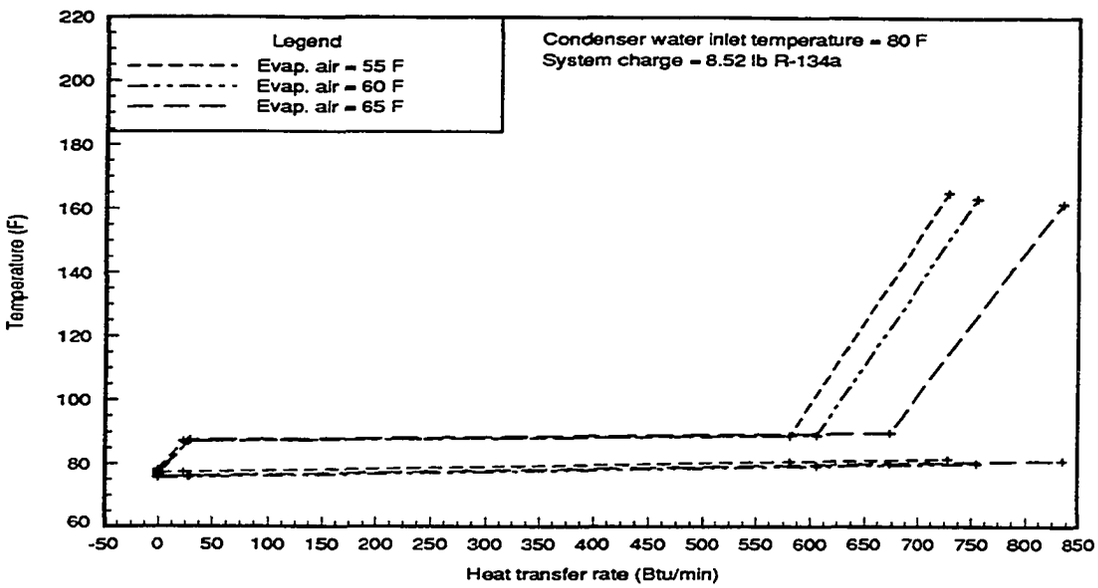

Figure 7.5: Condenser temperature profiles for R-134a showing the effect of varying evaporator temperature

in both the evaporator and condenser are higher with the R-134a data.

Temperature profiles for MP-39

The temperature profiles for the condenser with the refrigerant blend MP-39 are shown in Figure 7.9. This Figure shows the effect of varying the evaporator air temperature. The two-phase region has a more pronounced positive slope than the pure refrigerants because of the temperature glide in the condenser. Part of the slope is due to the pressure drop in the condenser and part is due to the decrease in saturation temperature associated with the changing composition of the liquid phase as the refrigerant condenses. The percent of heat transfer that occurs in each phase remains relatively constant for changes in the evaporator air temperature. The percent associated with the two-phase region is about 78% which is slightly higher

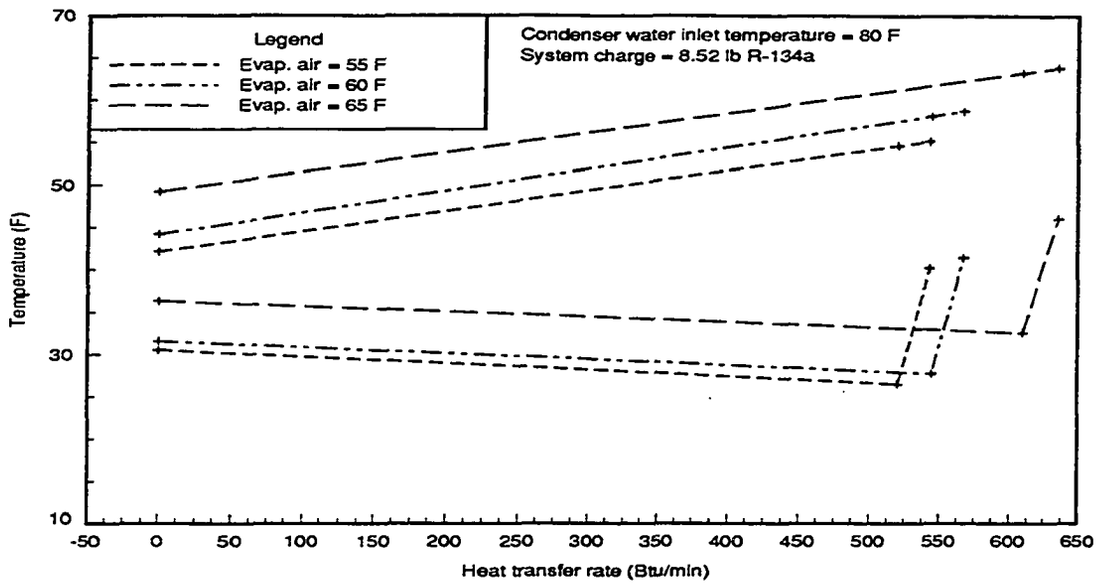

Figure 7.6: Evaporator temperature profiles for R-134a showing the effect of varying evaporator temperature

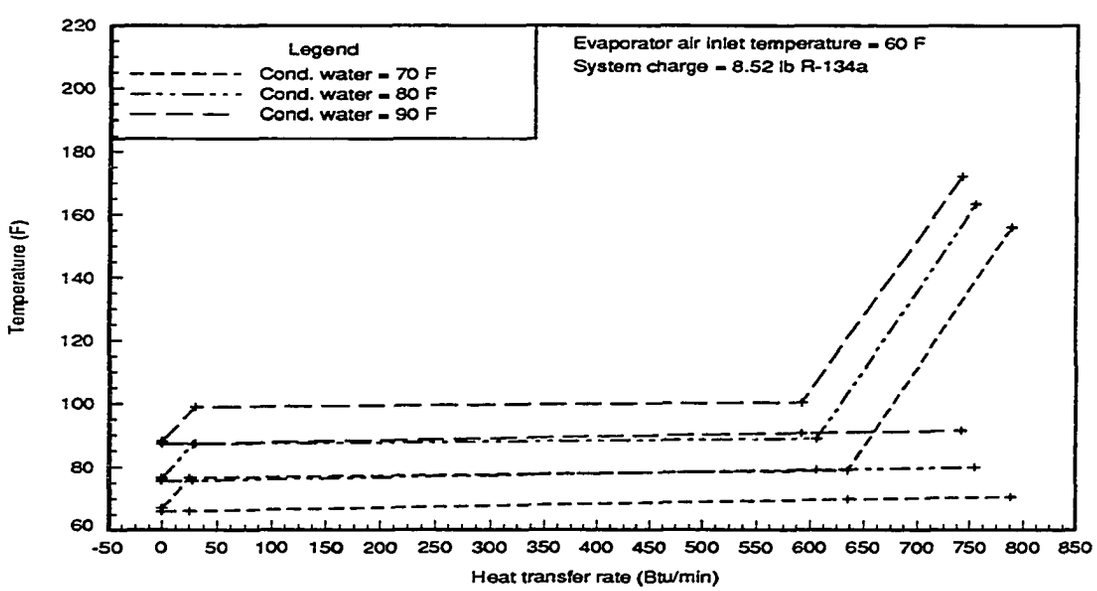

Figure 7.7: Condenser temperature profiles for R-134a showing the effect of varying condenser temperature

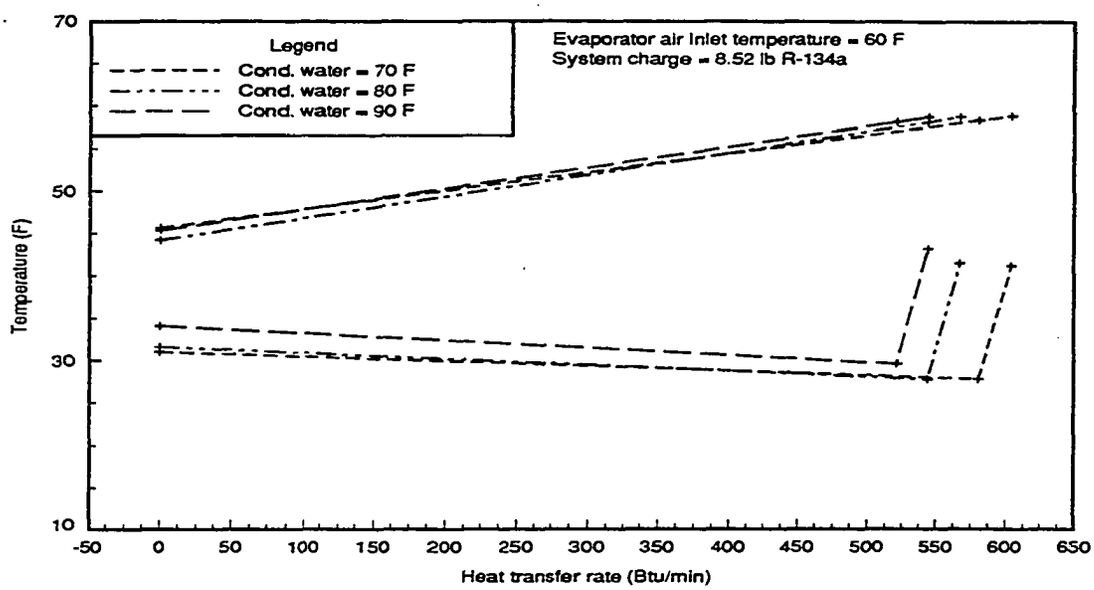

Figure 7.8: Evaporator temperature profiles for R-134a showing the effect of varying condenser temperature

than for the pure refrigerants.

As the refrigerant boils in the evaporator, the composition of the liquid refrigerant changes and the boiling temperature increase. This effect is called temperature glide. The temperature glide in the evaporator has a great effect on the temperature profile. Figure 7.10 shows the temperature profiles for the evaporator with several different evaporator air temperatures. The effect of the pressure drop in the evaporator is to lower the saturation temperature. This effect is offset by the effect of the temperature glide to give a positive slope in the two-phase region. The percent of heat transfer that occurs in the two-phase region is about the same as for the pure refrigerants.

The effect of varying the condenser water temperature is shown in Figures 7.11 and 7.12. For both the evaporator and condenser, the percent of heat transfer asso-

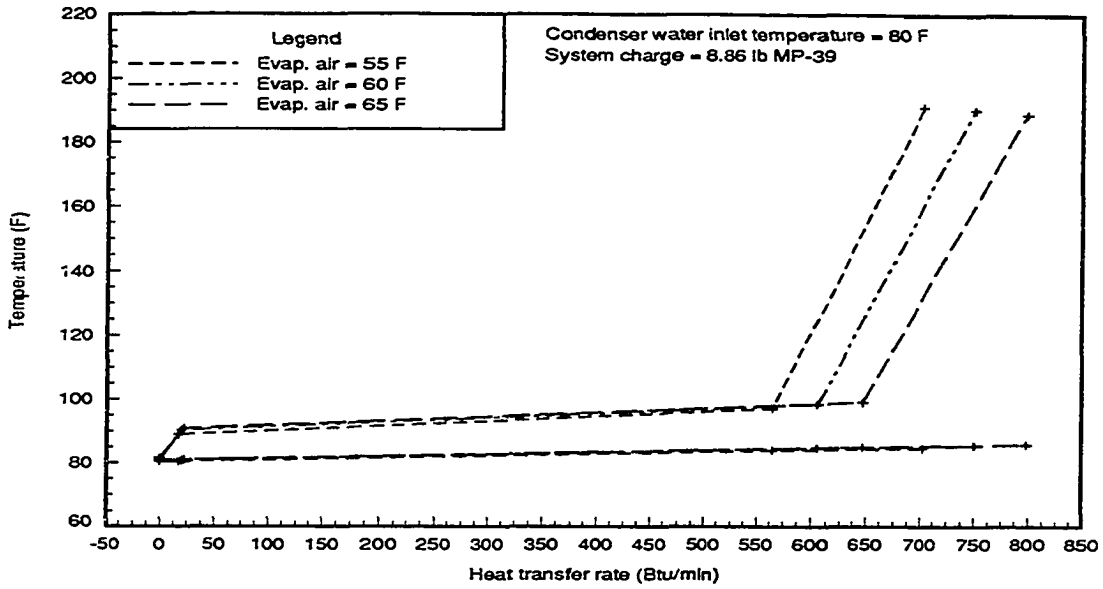

Figure 7.9: Condenser temperature profiles for MP-39 showing the effect of varying evaporator temperature

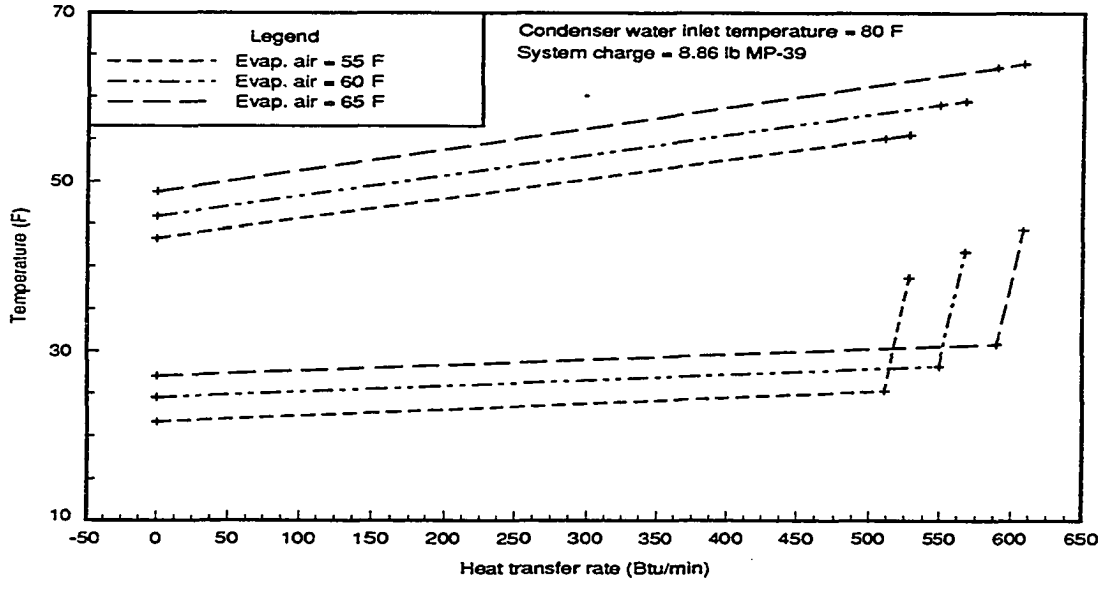

Figure 7.10: Evaporator temperature profiles for MP-39 showing the effect of varying evaporator temperature

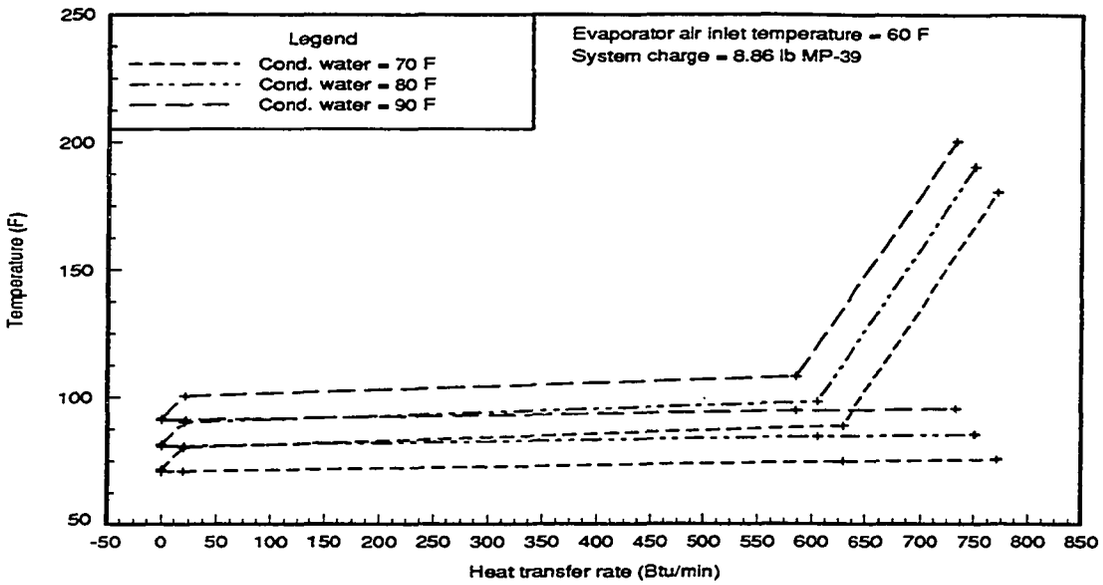

Figure 7.11: Condenser temperature profiles for MP-39 showing the effect of varying condenser temperature

ciated with the two-phase region decreases with increasing condenser water temperature. The effects of temperature glide are also evident in the two figures.

Temperature profiles for MP-52

The second refrigerant blend tested, MP-52, has a lower percentage of R-22 and gives temperature profiles similar to those of MP-39. However, the temperature glide has a more pronounced effect and the total heat transfer rate is lower. The temperature profiles are shown in Figures 7.13-7.16. The percent of heat transfer associated with the two-phase region in the condenser is about 4.5% greater for MP-52 than for the other refrigerants. This difference was not observed in the evaporator.

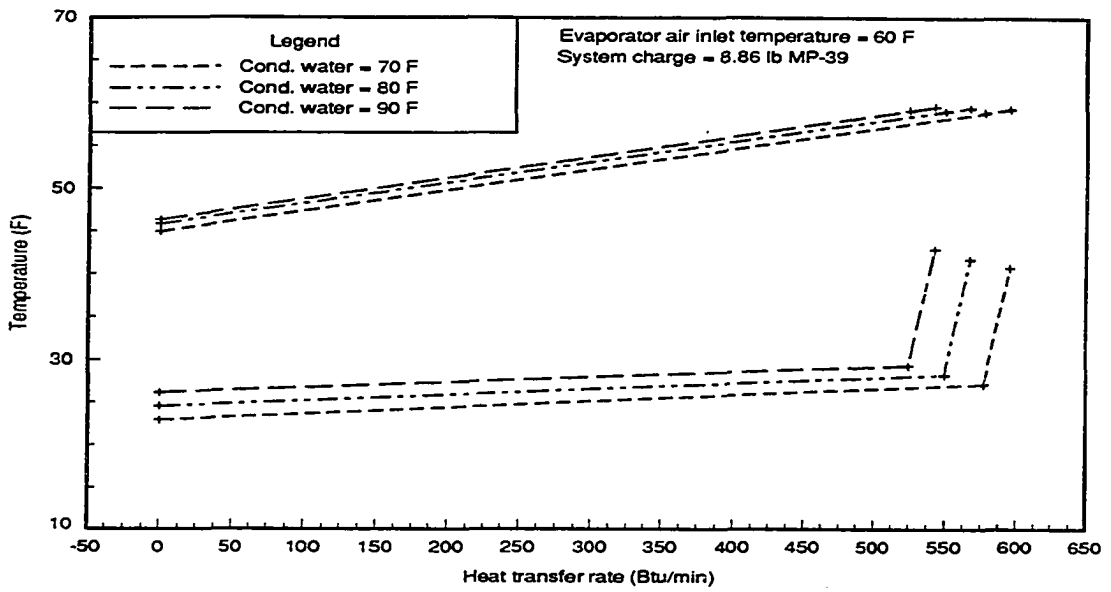

Figure 7.12: Evaporator temperature profiles for MP-39 showing the effect of varying condenser temperature

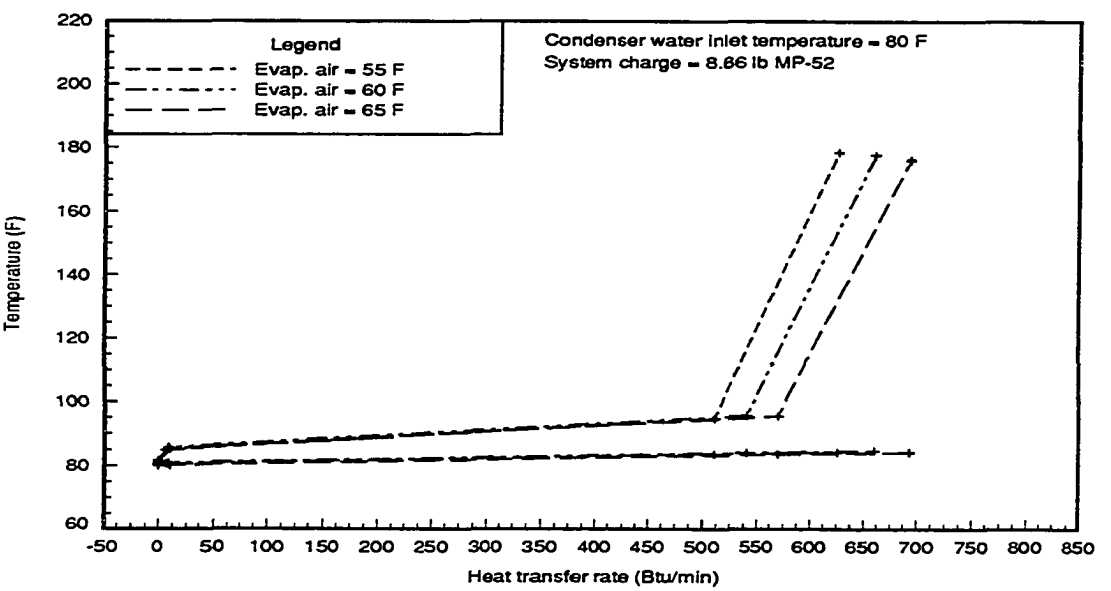

Figure 7.13: Condenser temperature profiles for MP-52 showing the effect of varying evaporator temperature

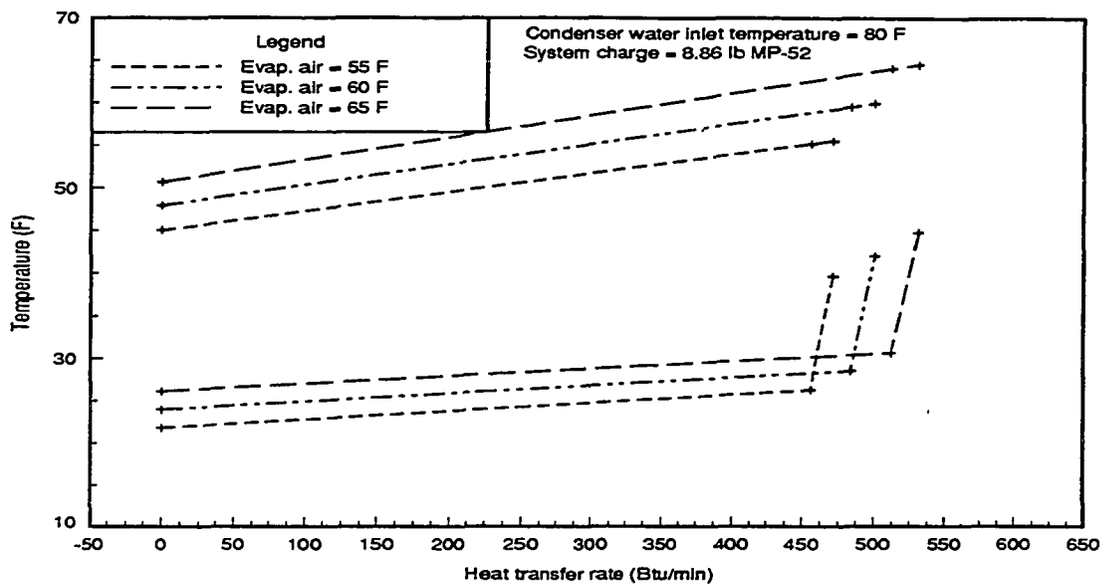

Figure 7.14: Evaporator temperature profiles for MP-52 showing the effect of varying evaporator temperature

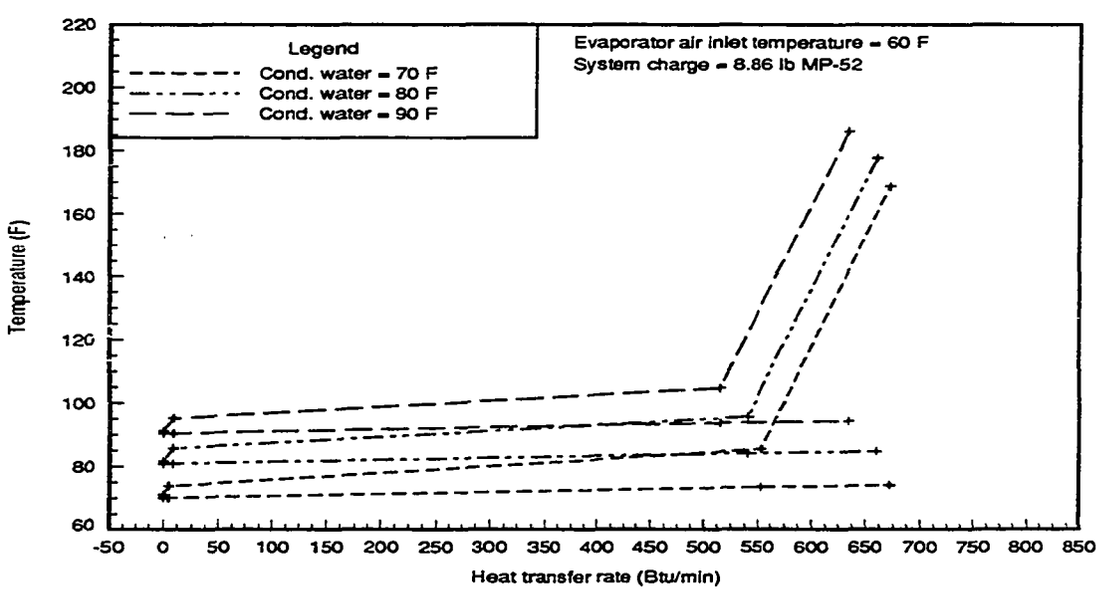

Figure 7.15: Condenser temperature profiles for MP-52 showing the effect of varying condenser temperature

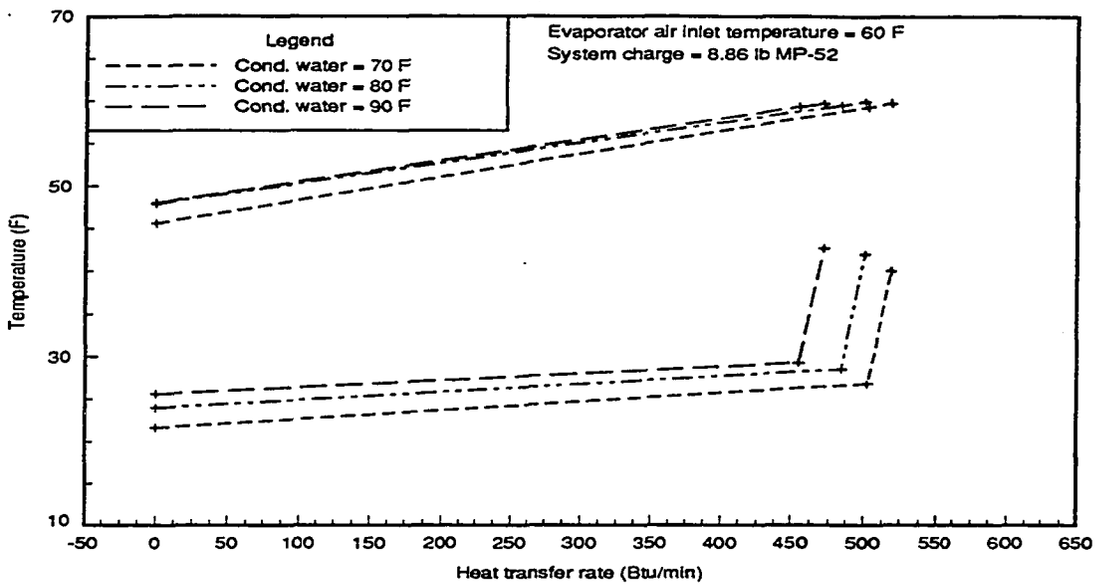

Figure 7.16: Evaporator temperature profiles for MP-52 showing the effect of varying condenser temperature

Heat Exchanger Modeling and Comparison With Data

The local heat transfer coefficient and temperature difference in heat exchangers has been correlated by numerous researchers. The overall performance of the heat exchanger is then determined by integration over the entire area of the heat exchanger. It is also common to evaluate heat exchangers with regard to their overall performance, which greatly simplifies the governing equations [35]. One such approach uses a log mean temperature difference. This approach is analyzed and compared to the experimental data, in the following sections.

Log mean temperature difference

Both of the heat exchangers used in the experiment could be classified as counter flow heat exchangers. That is that the two fluids flow counter to one another and the inlet temperature of one fluid may approach the exit temperature of the other fluid. The local heat transfer rate between fluids is a function of the temperature difference and the rate of change in temperature of each fluid is a function of the heat transfer rate. Therefore, the temperature profile of each fluid is non-linear with position along the heat exchanger. Combining the energy equation and the definition of the overall heat transfer coefficient and integrating gives:

$$\int_1^2 \frac{d(T_1 - T_2)}{(T_1 - T_2)} = \int_1^2 U * \left(\frac{1}{(\dot{m} * c_p)_1} + \frac{1}{(\dot{m} * c_p)_2} \right) dA \tag{7.6}$$

The overall heat transfer coefficient (U) and the specific heats are assumed to be constants, simplifying the right hand integral. The temperature profile is therefore exponential and the appropriate average temperature difference is defined in [36] as the log mean temperature difference (ΔT_{lm}).

$$\Delta T_{lm} = \frac{\Delta T_2 - \Delta T_1}{ln(\Delta T_2 / \Delta T_1)} \tag{7.7}$$

where ΔT_1 and ΔT_2 are the inlet and exit temperature differences between the refrigerant and the other fluid.

Since the overall heat transfer coefficient (U) and the specific heats were assumed to be constant in the development of the expression for ΔT_{lm} it would be inaccurate to use this expression for several different refrigerant phases. It should, however, represent the exchanger over each phase of the refrigerant. Three phases exist in the condenser. The refrigerant is subcooled liquid over a small portion at the exit of

the condenser. A larger portion at the inlet of the condenser contains superheated vapor. The balance of the condenser area, which constitutes a majority of the total area, is filled with a two-phase mixture of saturated liquid and vapor. The heat transfer rate for each of these regions can be related to the heat transfer coefficient and temperature difference with the LMTD method. The expression for the heat transfer rate is given as [36]:

$$q = U * A * \Delta T_{lm} \tag{7.8}$$

Therefore the total heat transfer rate for the condenser is given as:

$$q = q_{\text{subcooled}} + q_{\text{two-phase}} + q_{\text{superheated}} \tag{7.9}$$

The log mean temperature difference can be calculated for each region in the heat exchangers using the temperature profiles developed previously. Once the temperature profiles have been established the temperature differences at the inlet and exit of each region may be determined. These values are then used in equation 7.7 to calculate the log mean temperature difference.

A model for the heat exchanger may be developed if some assumptions are made about the overall heat transfer coefficient. One assumption that could be made is that there is a linear relationship between UA values for each phase. Such a relationship would be of the form:

$$(UA)_1 = (UA)_2/C2 = (UA)_3/C3 \tag{7.10}$$

The total heat transfer rate is then defined as:

$$q = UA_1 * (\Delta T_{lm1} + \Delta T_{lm2}/C2 + \Delta T_{lm3}/C3) \tag{7.11}$$

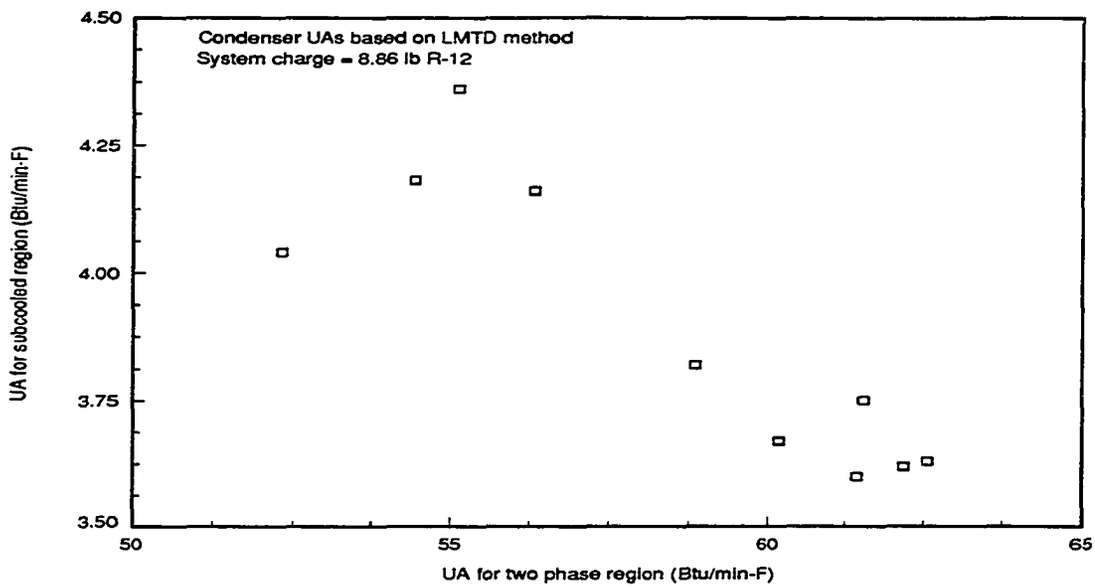

Figure 7.17: UA values for the subcooled and two-phase region of the condenser

A plot of UA values for each region of the heat exchangers shows that the relationship assumed for the UA values is not accurate. Figure 7.17 is a plot of the UA value for the subcooled region versus the UA value for the two-phase region. If the relationship given in equation 7.10 were valid, then the data would lie along a straight line and the slope would give the value of the constant. The line should also have a positive slope and pass through the origin. Comparisons of other experimentally derived UA values for the R-12 data are shown in Figures 7.18 and 7.19. These figures also show that the relationship given by equation 7.10 is not an accurate representation of the data. Since the areas of each region were not measured, the overall heat transfer coefficient of each phase can not be determined from the experimental data.

Another reasonable assumption that could be made about the heat exchanger data is that the relative areas occupied by each region remain a constant. If such an

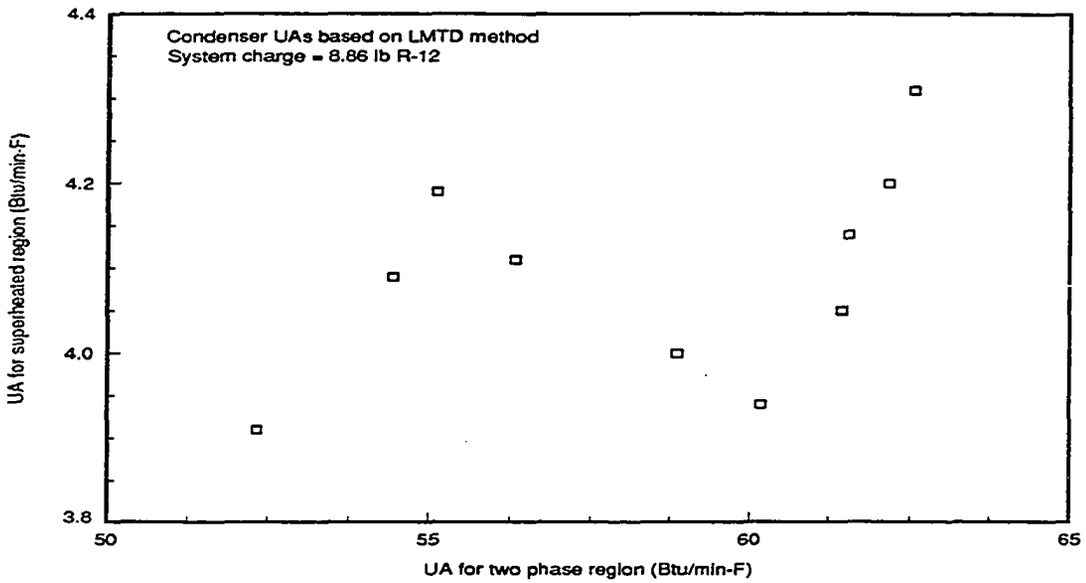

Figure 7.18: UA values for the superheated and two-phase region of the condenser

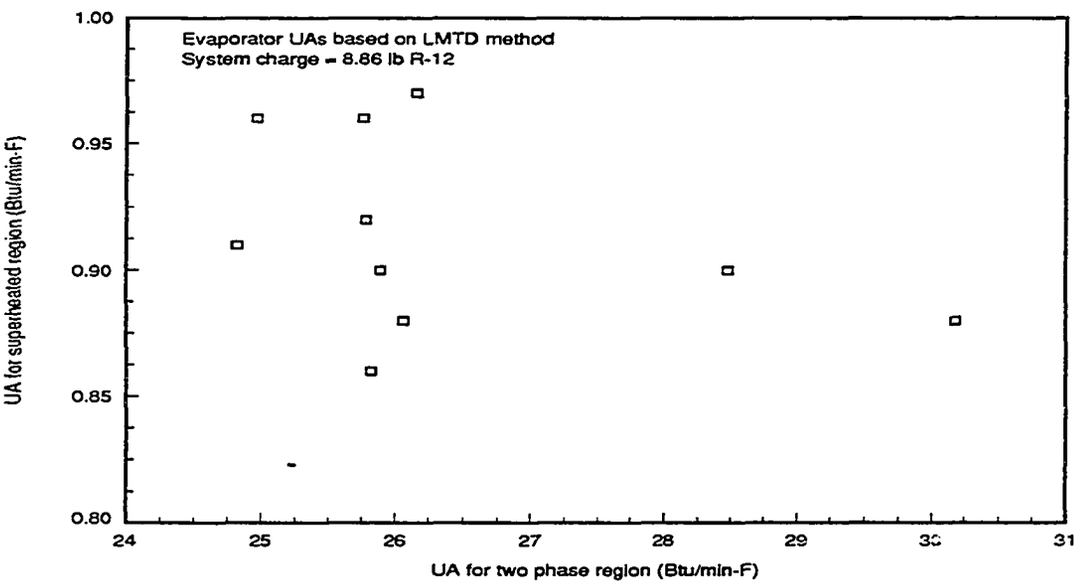

Figure 7.19: UA values for the superheated and two-phase region of the evaporator

assumption is made then the overall heat transfer coefficients for each region would be related by the following expression. This assumption is made for the heat exchanger model used in a simulation program (CYCLE11) developed at the National Institute of Standards [10].

$$(U)_1 = (U)_2/C2 = (U)_3/C3 \tag{7.12}$$

The relationship between UA values, however, would be the same as that given in equation 7.10. Since that relationship was shown to be false it follows that such a model does not represent the data well.

The problem with the previous model is most likely related to the assumption of constant relative areas rather than with with errors associated with equation 7.12. The variation in relative areas is evident from plots of UA values with refrigerant mass flow rates. Such a plot for the condenser data with the R-12 data is shown in Figure 7.20. The UA values for the evaporator are shown in Figure 7.21. The variable with the greatest effect on the overall heat transfer coefficient is the refrigerant mass flow rate. Other variables affecting this value, such as viscosity and thermal conductivity, are relatively constant over the entire range of test conditions. Therefore, there should be a simple relationship between the U values of each region and the mass flow rate. It is clear from Figures 7.20 and 7.21 that such a relationship does not exist. The conclusion that can be drawn is that the relative areas for each phase of heat transfer are significantly effected by the operating conditions.

Overall heat transfer coefficient

A final approach used to try to correlate the heat exchanger data is based on the assumption that the total heat transfer may be related to an overall heat transfer

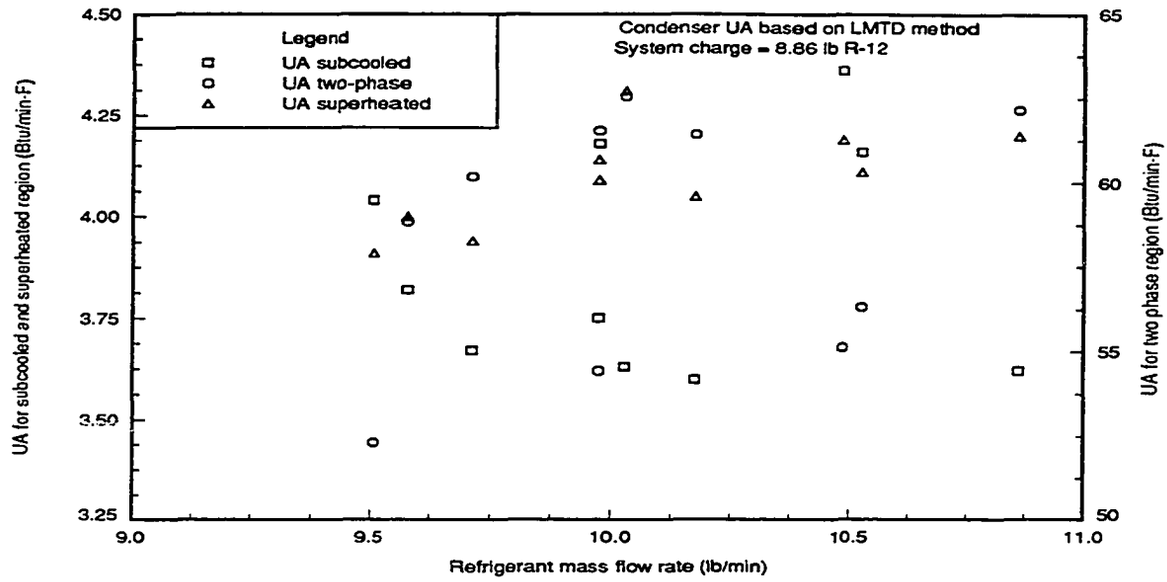

Figure 7.20: UA values for the condenser plotted verses refrigerant mass flow rate

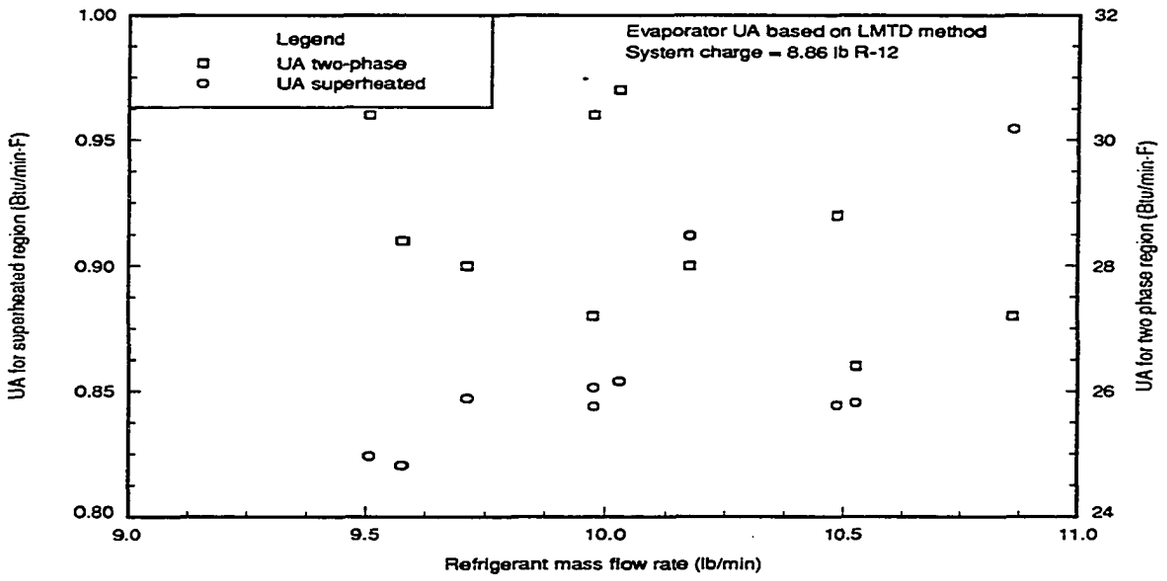

Figure 7.21: UA values for the evaporator plotted verses refrigerant mass flow rate

coefficient and a representative temperature difference. Such a model is represented simply as:

$$q = UA * \Delta T \tag{7.13}$$

The overall heat transfer coefficient varies over the range of test conditions so an accurate model must account for that variation. The total area of the heat exchanger was constant for all of the data collected since none of the equipment was changed during the testing. A representative temperature difference must be chosen for use in equation 7.13. One choice would be to use a weighted average of the log mean temperature differences. However, the relative areas are unknown and are effected by the operating conditions. Another approach would be to use the maximum and minimum temperatures in the exchanger. For the condenser this would be the difference between the refrigerant inlet temperature and the water inlet temperature.

The overall heat transfer coefficient in the condenser is a function of several variables. The U value, based on the inside tube area, is calculated as:

$$U = \frac{1}{\frac{1}{h_{in}} + \frac{r_{in} * ln(r_{out}/r_{in})}{k} + \frac{r_{in}}{r_{out} * h_{out}}} \tag{7.14}$$

where h_{in} and h_{out} are the inside and outside heat transfer coefficients, respectively, k is the thermal conductivity of the tube wall, and r_{in} and r_{cut} represent the inside and outside tube radius, respectively. The last two terms in the denominator of equation 7.14 are constant for all the test conditions since the condenser water flow rate was held constant and any temperature effects are small. The overall heat transfer coefficient can then be calculated as:

$$U = \frac{1}{\frac{1}{h_{in}} + C} \tag{7.15}$$

The inside heat transfer coefficient, on the refrigerant side, might then be related to the flow rate and refrigerant properties by the Dittus-Boelter equation [37] given as:

$$Nu_D = 0.023 * Re^{0.8} * Pr^{0.3} \tag{7.16}$$

where Nu, Re, and Pr are the Nusselt, Reynolds and Prandtl number respectively. The heat transfer coefficient (h) is related to the Nusselt number by the following expression:

$$Nu_D = \frac{h * D}{k} \tag{7.17}$$

Making use of the definitions of the Reynolds and Prandtl number gives an expression for the heat transfer coefficient in terms of several refrigerant properties.

$$h_{in} = C\frac{\dot{m}^{0.8} C_p^{0.3} k^{0.7}}{\mu^{0.7}} \tag{7.18}$$

where C is a constant. This assumes that the heat transfer coefficient of each phase is related to the same form of equation. Finally the overall heat transfer coefficient can be expressed as:

$$U = \frac{C_1}{\frac{\mu^{0.7}}{\dot{m}^{0.8} C_p^{0.3} k^{0.7}} + C_2} \tag{7.19}$$

For a set of data where the same refrigerant is used, the mass flow rate is the only term of equation 7.19 which varies significantly. Therefore, for each set of refrigerant data the UA value based on the above model should correlate to the experimental values of $q/\Delta T$. That is:

$$\frac{q}{\Delta T} = \frac{C_1}{\frac{1}{\dot{m}^{0.8}} + C_2} \tag{7.20}$$

where the constant C_1 includes the heat exchanger area. This model was used to fit the overall UA values for the data sets of the four refrigerants tested. The measured

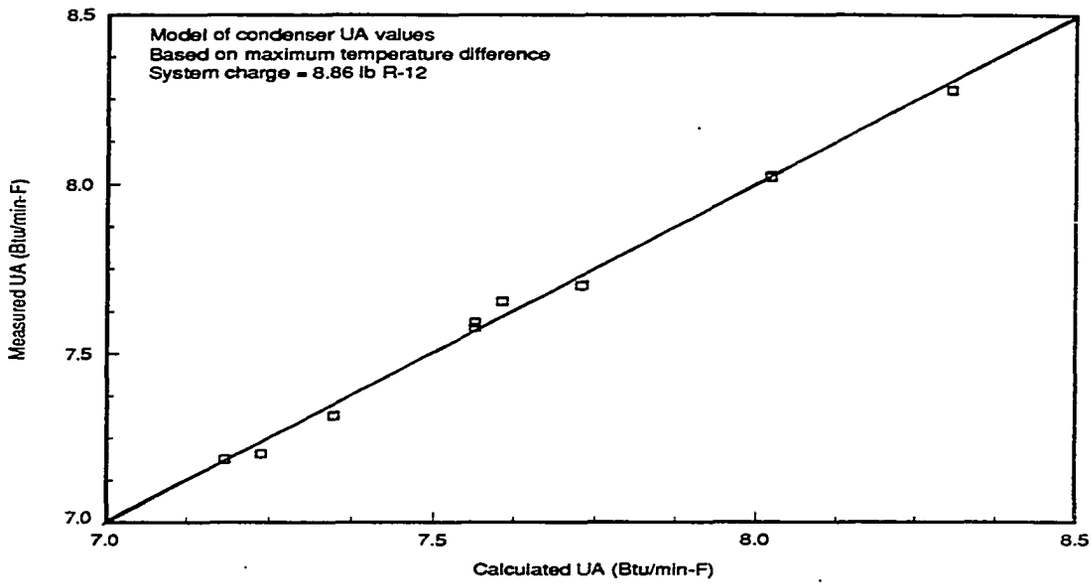

Figure 7.22: Comparison of measured and calculated overall UA values with R-12

versus calculated UA values for R-12 are shown in Figure 7.22. The standard deviation is very small compared to the range of values. Similar plots for the other three refrigerants are shown in Figures 7.23 through 7.25. For all of the refrigerants the error is fairly small. The coefficients for the curve fit and values of standard deviation are given in Table 7.1.

The coefficients of Table 7.1 are different for each refrigerant because the thermal conductivity, specific heat and viscosity of the refrigerants are different. Including these parameters may allow for a heat exchanger correlation that takes into account the effect of the refrigerants properties and the mass flow rate of the refrigerant. Built into the coefficients of Table 7.1 are the outside heat transfer coefficient and the wall resistance. The magnitude of these resistances are particular to the equipment and operating conditions of the non-refrigerant side of the exchanger. The model could

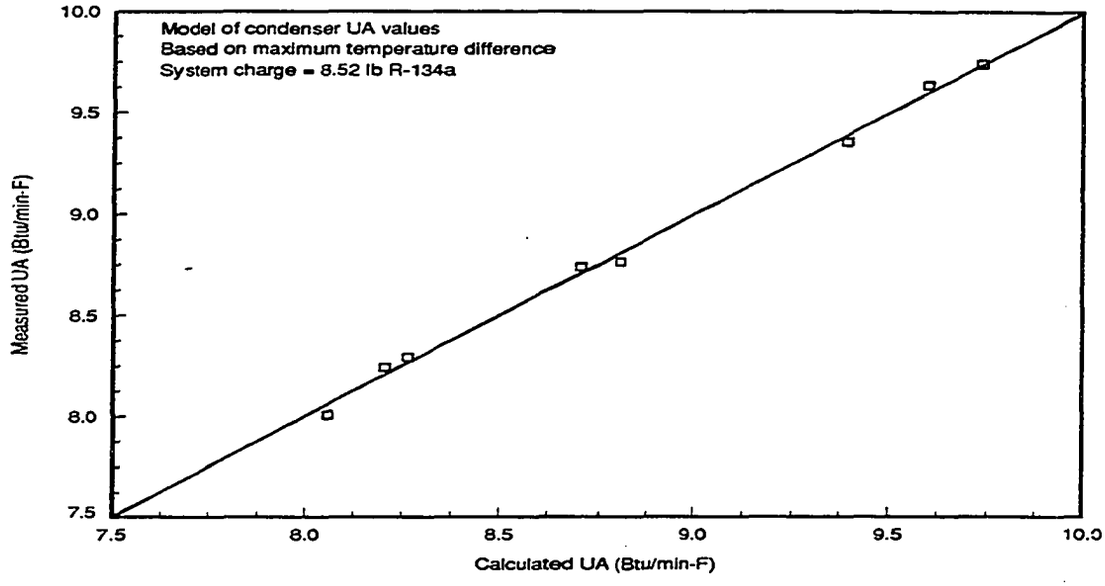

Figure 7.23: Comparison of measured and calculated overall UA values with R-134a

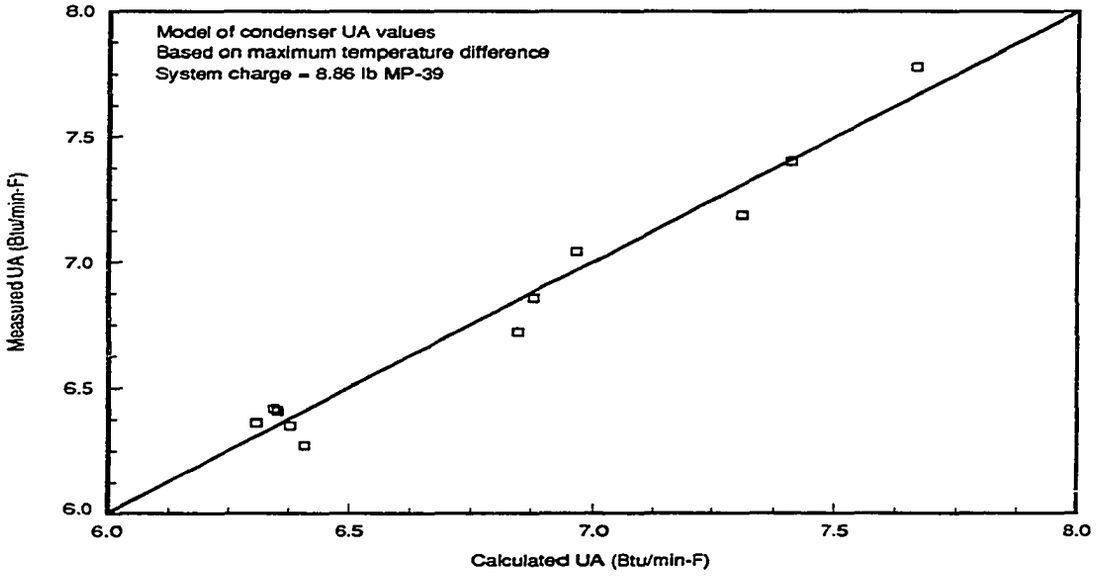

Figure 7.24: Comparison of measured and calculated overall UA values with MP-39

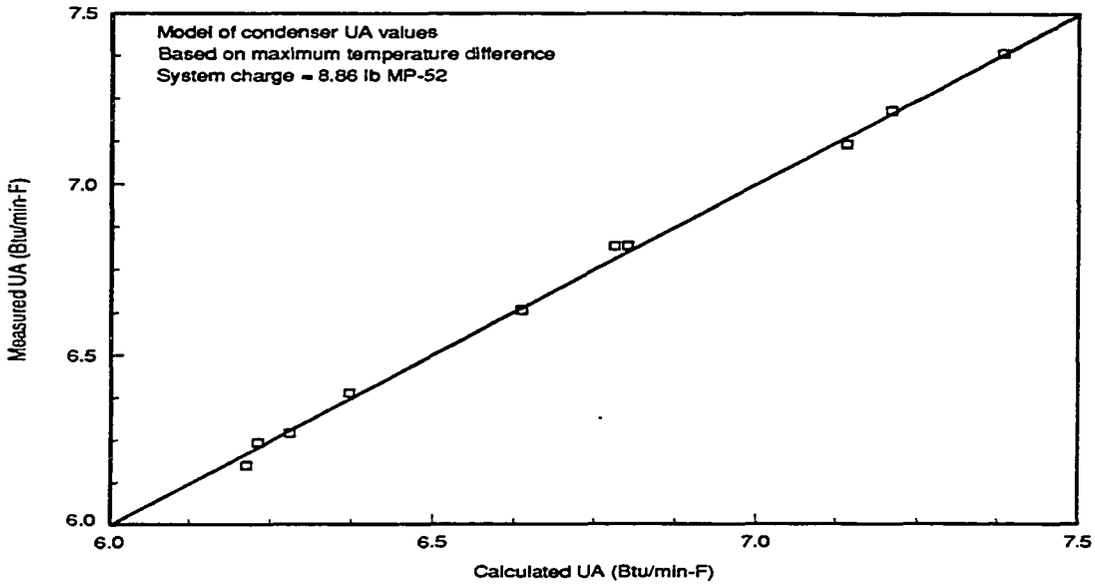

Figure 7.25: Comparison of measured and calculated overall UA values with MP-52

be improved by choosing a temperature difference that is more representative of the average temperature difference in the exchanger. Several attempts were made to do this, however none gave better results than using the maximum temperature difference as done above.

Conclusions

The temperature profiles for all the refrigerant data have many similarities making the prospect of modeling heat exchanger performance a more obtainable goal. There are, however, many differences in the temperature profiles. It is clear that to neglect the effects of operating conditions or the effects of using different refrigerants will give inaccurate results. The temperature glides associated with the refrigerant blends had the most pronounced effect on the nature of the temperature profiles. In

Table 7.1: Constants for heat exchanger model

Data set	C_1	C_2	Std. deviation (Btu/min-F)
8.86 lb R-12	0.885	-0.0418	0.033
8.79 lb R-134a	1.17	-0.0568	0.041
8.86 lb MP-39	0.997	-0.0550	0.096
8.86 lb MP-52	0.991	-0.0655	0.023

the evaporator, the temperature decreased with increasing quality due to pressure drops for the pure refrigerants. This effect was offset with the blends due to temperature glide, to give an increase in temperature with increasing quality. Such a change in the nature of the temperature profiles will certainly have an effect on the heat exchanger and system performance.

Modeling the heat transfer in the heat exchangers is difficult since the areas associated with different regions (subcooled, two-phase and superheated) are unknown. The assumption, that a linear relationship exists between UA values for the different regions, is not justified based on the experimental data presented here. It was shown that the relative areas of each region of heat transfer are affected by the operating conditions. Therefore, it is inaccurate to assume a constant area associated with each region. Using an overall heat transfer coefficient that varied refrigerant flow rate, based on the Dittus-Boelter equation, gave good results. The data for each refrigerant was correlated with little error using the maximum temperature difference in the exchanger. An expression that would accurately model the heat exchangers for all refrigerants was proposed, but would require further study.

CHAPTER 8. CONCLUSIONS

The vapor compression refrigeration test equipment was successfully used to compare the performance of alternative refrigerants. Several variables significant to system performance, namely the evaporator air temperature, condenser water temperature, and refrigerant charge were varied over wide ranges of values. Three alternative refrigerants (R-134a, MP-39, and MP-52) were tested as well as R-12 in over 100 independent tests. These tests provided a data base in which comparisons of performance between refrigerants could be made at any number of conditions.

The control of evaporator air and condenser water temperatures was such that these temperatures could not be set at the exact test conditions. Therefore, comparisons between refrigerants necessitated the use of curve fits which correlated system performance with operating conditions. The data for each refrigerant charge was well represented by second-order polynomials with far fewer constants than data points. The error associated with the curve fits was very small, and this allowed for valid comparisons between refrigerants whose performance was very nearly the same.

Many similarities were observed in performance with the different refrigerants. The performance in general followed that of simple thermodynamic models. The following conclusions are based on the similarities found in the experimental data with the different refrigerants.

- The COP is affected almost equally by a change in either evaporator air temperature or condenser water temperature, whereas the capacity is much more affected by the evaporator air temperature.

- The correlations of COP and capacity with condenser water temperature were approximately linear.

- Condenser water flow rate and evaporator superheat were shown to have an insignificant effect on system performance compared to other parameters.

- With the exception of R-134, the system performance was not significantly affected by changes in system charge. In all cases the effects of charge were smaller than the effects of the other parameters.

The ratios of COPs and cooling capacities of each alternative refrigerant compared to R-12 were shown to be affected by the choice of test conditions and charge. Therefore, variation in operating conditions was indeed necessary to provide accurate comparisons. In general, however, the COPs were similar for all of the refrigerants tested. The R-134a at an optimum charge had higher COPs than R-12 at every operating condition, up to a maximum of 5% higher. The refrigerant blends showed slightly greater values of COP than R-12 under certain conditions, up to a maximum of 3% greater. The cooling capacity was slightly greater with R-134a and MP-39 than with R-12. A maximum increase of 7% over R-12 was observed with R-134a. The MP-52 gave a cooling capacity of about 13% less than with R-12.

The refrigerant temperatures, pressures, and mass flow rates were shown to be significantly different for the various refrigerants. Such differences help explain the variation observed in system performance. Differences of 30 F were observed at the

condenser inlet for two of the refrigerants under the same operating conditions. The mass flow rates were all lower than that of R-12 to a maximum of 33% lower. The relationships between temperatures, pressures, and flow rates are helpful in developing more accurate system models and in the area of design.

Models of the compressor and heat exchangers were examined and compared to the experimental data. The models were useful in correlating data, but their usefulness in predicting performance with other refrigerants or test conditions is limited. More sophisticated models need to be developed which take into account the effects of the different refrigerant properties. Assumptions such as constant isentropic efficiency for a compressor or constant overall heat transfer coefficients for the heat exchangers were shown to be inappropriate.

The environment may be greatly affected by the choices made regarding the use of refrigerants. Each of the alternative refrigerants tested all show some conditions where it would be an acceptable alternative to R-12. The delicate balances at play in our environment and the serious consequences related to upsetting them is a call to responsible engineering. Continued development of new refrigerants, more accurate models, and experimental testing is necessary in order to address these concerns.

BIBLIOGRAPHY

[1] Kurylo, M. J. "The chemistry of stratospheric ozone: its response to natural and anthropogenic influences." *International Journal of Refrigeration 13* (1990): 62-73.

[2] Kuijpers, L.J.M. "UNEP assessment of the Montreal Protocol: Refrigeration within the framework of the technology review." *International Journal of Refrigeration 13* (1990): 95-99.

[3] Jung, D. S., and R. Radermacher. "Prediction of heat transfer coefficients of various refrigerants during evaporation." *ASHRAE Transactions 97* (1991): 48-53.

[4] Sisgel, R., and J. R. Howell. *Thermal Radiation Heat Transfer,* 3rd ed., New York: Hemisphere Publishing Corporation, 1981.

[5] Fischer, S. J., P. D. Fairchild, and P. J. Hughes. "Global warming implications of replacing CFCs." *ASHRAE Journal* (April 1992): 14-19.

[6] Vineyard, E. A. "The alternative refrigerant dilemma for refrigerator-freezers: Truth or consequences." *ASHRAE Transactions 97* (1991): 955-960.

[7] Vineyard, E. A., J. R. Sand, and W. A. Miller. "Refrigerator-freezer energy testing with alternative refrigerants." *ASHRAE Transactions 95* (1989): 295-299.

[8] Sand, J. R., E. A. Vineyard, and R. J. Nowak. "Experimental performance of ozone-safe alternative refrigerants." *ASHRAE Transactions 96* (1990): 173-182.

[9] Linton, J.W., W.K. Snelson, and P.F. Hearty. "Effect of condenser liquid subcooling on system performance for refrigerants CFC-12, HFC-134a, and HFC-152a." *ASHRAE Transactions 98* (1992): 160-166.

[10] Domanski, P. A., M. O. McLinden. "A simplified cycle simulation model for the performance rating of refrigerants and refrigerant mixtures " *International Journal of Refrigeration 15* (1992): 81-88.

[11] Devotta, S., and S. Gopichand. "Comparative assessment of HFC134a and some refrigerants as alternatives to CFC12." *International Journal of Refrigeration 15* (1992): 112-118.

[12] Petersson, B., H. Thorsell. "Comparison of the refrigerants HFC 134a and CFC 12." *International Journal of Refrigeration 13* (1990): 176-180.

[13] Muir, E. B. "Commercial refrigeration and CFCs." *International Journal of Refrigeration 13* (1990): 106-112.

[14] Kopko, W. L. "Beyond CFCs: Extending the search for new refrigerants." *International Journal of Refrigeration 13* (1990): 79-85.

[15] Didion, D. A., D. B. Bivens. "Role of refrigerant mixtures as alternatives to CFCs." *International Journal of Refrigeration 13* (1990): 163-175.

[16] Bare, J. C., C. L. Gage, R. Radermacher, and D. Jung. "Simulation of nonazeotropic refrigerant mixtures for use in a dual-circuit refrigerator/freezer with countercurrent heat exchangers." *ASHRAE Transactions 97* (1991): 447-454.

[17] Galloway, J. E., and V. W. Goldschmidt. "Air-to-air heat pump performance with three different nonazeotropic refrigerant mixtures." *ASHRAE Transactions 97* (1991): 296-303.

[18] Boot, J. L. "Overview of alternatives to CFCs for domestic refrigerators and freezers." *International Journal of Refrigeration 13* (1990): 100-105.

[19] Spauschus, Hans O. "Compatibility requirements for CFC alternatives." *International Journal of Refrigeration 13* (1990): 73-78.

[20] Downing, R. C. "Refrigerant equations." *ASHRAE Transactions 80* (1974): 158-168.

[21] Wilson, D. P., and R. S. Basu. "Thermodynamic properties of a new stratospherically safe working fluid, refrigerant 134a." *ASHRAE Transactions 94* (1988): 2095-2118.

[22] Morrison, G., and M. O. McLinden. "Application of a hard sphere equation of state to refrigerants and refrigerant mixtures." *N.B.S. Technical Note 1218*, Washington, DC, 1986.

[23] *NIST Thermodynamic Properties of Refrigerants and Refrigerant Mixtures Database (REFPROP).* Gaithersburg, MD. (1990)

[24] Taylor, J. R. *An Introduction to Error Analysis,* Mill Valley, California: University Science Books, 1980.

[25] Damasceno, G. S., P. A. Domanski, S. Rooke, and V. W. Goldschmidt. "Refrigerant charge effects on heat pump performance." *ASHRAE Transactions 97* (1991): 304-310.

[26] Farzad, M., and D. L. O'Neal. "System performance characteristics of an air conditioner over a range of charging conditions." *International Journal of Refrigeration 14* (1991): 321-328.

[27] Eckels, S. J., and M. B. Pate. "An experimental comparison of evaporation and condensation heat transfer coefficients for HFC-134a and CFC-12." *International Journal of Refrigeration 14* (1991): 70-77.

[28] Ott, L. *An Introduction to Statistical Methods and Data Analysis,* 3rd ed., Boston: PWS-Kent Publishing Co., 1988.

[29] Corr, S., T. W. Dekleva, and A. L. Savage. "Retrofitting large refrigeration systems with R-134a." *ASHRAE Journal* (February 1993): 29-33.

[30] Shiflett M. B., and A. Yokozeki. "Near azeotropic refrigerants as alternatives for R-502." *ASHRAE Journal* (February 1993): 24-27.

[31] McGovern, J. A. "Utilization of Volumetric displacement in reciprocating compressors." *Proceedings of the 1990: USNC/IIR-Purdue Refrigeration Conference* (1990): 254-263.

[32] Hafner, J., B. Gaspersic. "Dynamic modeling of reciprocating compressor." *Proceedings of the 1990: USNC/IIR-Purdue Refrigeration Conference* (1990): 216-221.

[33] Berlinck, E. C., C. A. T. Uriu, T. B. Herbas and J. A. R. Parise. "Performance analysis of domestic heat pump units running on CFC substitutes." *Proceedings of the 1992: USNC/IIR-Purdue Refrigeration Conference* (1992): 693-702.

[34] Moran, M. J., and H. S. Shapiro. *Fundamentals of Engineering Thermodynamics,* 2nd ed., New York: John Wiley and Sons, 1992.

[35] Eckels, S. J., and M. B. Pate. "Evaporation and condensation of HCFC-134a and CFC-12 in a smooth tube and a micro-fin tube." *ASHRAE Transactions 97* (1991): 71-81.

[36] Incropera, F. P., and D. P. DeWitt. *Fundamentals of Heat and Mass Transfer,* 3rd ed., New York: John Wiley and Sons, 1990.

[37] Dittus, F. W., and L. M. K. Boelter. University of California Publications on Engineering, Vol 2, p. 443. Berkeley, California, 1930.